Homogeneous Hydrogenation and Photochemistry as Tools in Pharmaceutical Process Development

Youssef Shaalan

Initiation of studies: October 2017

DECLARATION

This thesis is the result of the author's original research and is submitted for the partial fulfilment of a Ph.D. degree. It has been composed by the author and has not been previously submitted for examination which has led to the award of a degree. All sources of information are acknowledged by means of references.

Signed: Date:

ACKNOWLEDGEMENTS

Firstly, I would like to thank my supervisors, Lee Boulton and Craig Jamieson for being a constant source of inspiration, guidance and encouragement. Working with you both has been a privilege and has undoubtedly given me a much deeper understanding of Chemistry.

It has been an honour partaking in the GSK/Strathclyde Collaborative PhD Programme and I am very grateful to Harry Kelly and William Kerr for granting me a position and their constant support. GSK and the University of Strathclyde have been wonderful places to work, and among many others I would like to thank:

Everyone in 2G121 including Luke Whitaker, Chloe Markham, Stephen Lovelock, Umanti Patel and John Leahy for the friendly working atmosphere;

Lee Edwards for mentoring me in exploring photochemical transformations;

Gemma Cook and Kayleigh Mercer for training and useful advice with using photochemical equipment;

Richard Horan for adding great enthusiasm to problem sessions and for putting forward critical and thought-provoking questions;

Katherine Wheelhouse, Martin Woods, Katherine Priestley, Enertitz Fernandez-Puertas for sharing their knowledge and experiences around hydrogenation reactions;

Colin Edge, Janelle Steves, Doo-Hyun Kwon for running and helping with interpretation of quantum mechanical calculations;

Tom Atherton, Anne-Sophie Bretonnet, Simon Watson, Sean Lynn, Steve Richards, Richard Upton, Jasmine Green, Omar Rahman, Craig Irving, Alan Kennedy, Tran Pham, Adrian Bateman, Helen Taylor and Patricia Keating for outstanding support and coming up with creative solutions around all analytical and spectroscopic matters;

Glynn Williams, Chris McKay, Spence Calvert, John Rose and Nick Yarwood for advice, discussions and operation of DART flow reactors;

Simon Bate, Daniel Tray, Sandra Harling for sharing their knowledge and passion on statistical interpretations of data and advice with experimental design;

Jennifer Clark, Jennifer Duffy, Genna Mowat, Kirsty Milne, and Chris Riley for onboarding me and being so accommodating during my secondment in Glasgow;

Andrea Malley, Abby Mullord, Dawn Peel, Terri Davidson, Laura Patterson, Ruth Telfer, Benson Amukpo and Saito Gon for ensuring smooth running of the “behind the scenes” work.

Lastly, I would like to thank my family, and in particular my parents, Laila El-Kady and Mohamed Shaalan for their unconditional love and support. It is to them that this thesis is dedicated.

ABSTRACT

Ruthenium catalysed ester reductions using hydrogen have become increasingly industrially relevant as a means of accessing primary alcohols, while avoiding the need for pyrophoric and wasteful metal hydride-based reducing agents. A catalytic system was identified capable of reducing esters under mild conditions accessible in general purpose pressure vessels more likely encountered within the pharmaceutical industry (< 10 bar of hydrogen pressure). Process understanding was obtained using an experimental design approach which was used to rationalise and suppress the formation of impurities. Mechanistic insight was also gathered using time-course experimentation and *in situ* monitoring.

A number of substrates, more representative of the types of molecules encountered in a pharmaceutical environment were tested in the reaction. Selected substrates were scaled-up in batch and in a bespoke CSTR flow reactor to furnish relevant pharmaceutical intermediates. These processes compared favourably to existing metal hydride mediated processes, both in the reduction of waste and number of unit operations. The resulting alcohols were then further elaborated to generate more advanced intermediates.

Photochemical transformations are another increasingly useful technology being employed within the pharmaceutical industry as a tool to enable novel disconnections, though these can be challenging to scale. The second part of this thesis examines the photochemical bromination of two substrates. Further optimisations are performed on the benzylic bromination of ethyl 4-methylbenzoate to intensify the process. Simplification of the work-up and isolation procedures compared to a previous process were also studied. Scale-up was performed in a plug-flow reactor as well as a prototype photochemical DART flow reactor. The results from this experimentation have been used to inform the design of a next-generation prototype reactor.

TABLE OF CONTENTS

ABBREVIATIONS

HFIP	1,1,1,3,3,3-hexafluoro-2-propanol
TEMPO	2,2,6,6-tetramethylpiperidinyloxy
IBX	2-iodoxybenzoic acid
2-MeTHF	2-methyltetrahydrofuran
IPA	2-propanol
acac	acetylacetonate
API	active pharmaceutical ingredient
ANOVA	analysis of variance
Ar	aryl
PNP	bis(2-(diphenylphosphaneyl)ethyl)amine
BGS	British geological survey
br.	broad
br. s	broad singlet
BHT	Butylated hydroxytoluene
cat.	catalytic
CSTR	continuous stirred tank reactor
DFT	density functional theory
DoE	design of experiment
DX-10	Design-Expert 10
DCM	dichloromethane
DIBAL	diisobutylaluminium hydride
d	doublet
ESI	electrospray ionsiation
eq.	equivalents
EtOAc	ethyl acetate
EMA	European Medicines Agency
e.g.	example
FDA	Food and Drug Administration
GC	gas chromatography
Hz	hertz
HPLC	high performance liquid chromatography
HRMS	high resolution mass spectrometry
h	hours
ICP-MS	inductively coupled plasma mass spectrometry
IR	infra red
KF	Karl Fischer
kcal	kilocalorie
LCMS	liquid chromatography mass spectrometry
LAH	lithium aluminium hydride
MS	mass spectrometry

M. pt.	melting point
mL	millilitres
mmol	millimoles
min	minutes
M	molar (mol/L)
mol	moles
nm	nanometer
NBS	*N*-bromosuccinimide
NDA	new drug application
NHC	*N*-heterocyclic carbene
N	normality
NMR	nuclear magnetic resonance
nOe	nuclear Overhauser effect
OVAT	one variable at a time
ppm	parts per million
PPAR	peroxisome proliferator activated receptor
Ph	phenyl
PMI	process mass intensity
q	quartet
quint.	quintet
R&D	research and development
t_R	retention time
rpm	revolutions per minute
rt	room temperature
SMEAH	sodium bis(2-methoxyethoxy)aluminium hydride
SMD	solvation model based on density
SM	starting material
Temp.	temperature
TBME	*tert*-butyl methyl ether
THF	tetrahydrofuran
TMS	tetramethylsilane
TLC	thin layer chromatography
t	triplet
TOF	turnover frequency
TON	turnover number
UV	ultraviolet

1 CATALYTIC REDUCTION OF ESTERS

1.1 INTRODUCTION

1.1.1 Reduction of Esters in Organic Chemistry

The reduction of esters to primary alcohols is one of the most fundamental functional group interconversions in organic chemistry.[1] Indeed the importance of this is evident throughout work in academia and industry alike. In Nicolaou's total synthesis of the anticancer drug Paclitaxel (Taxol), LAH was used to reduce γ-lactone (**1.1**) to diol (**1.2**) **(Scheme 1)**.[2] On a somewhat larger scale, the formation of the pharmaceutical building block, 3-(*R*)-3-amino-1-butanol (**1.3**) has been effected by reduction of the corresponding methyl ester (**1.4**) using $NaBH_4$. This key building block is used *en route* to Dolutegravir (Tivicay), an oral HIV integrase inhibitor with sales totaling > $5 billion in 2017 **(Scheme 1)**.[3, 4]

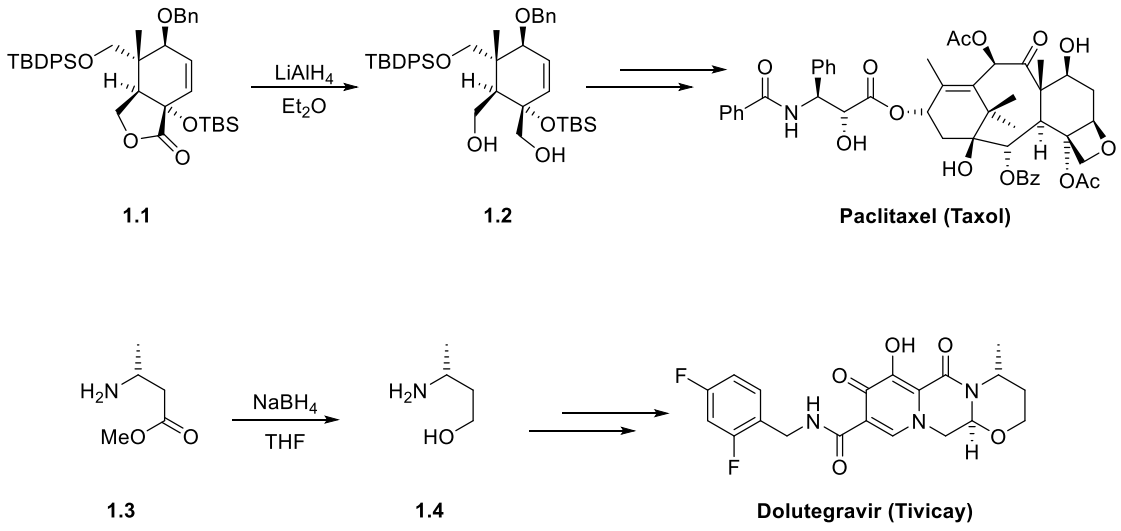

Scheme 1 *Examples of ester reductions on intermediates leading to biologically active molecules.*

The reductions of esters to alcohols, as with many other functional group interconversions, are often considered to be non-strategic, as these often do not directly contribute to forming key bonds present in the final target.[5] This has led to the emergence of the concept of "redox economy", whereby the number of changes to oxidation states are as far as possible kept to a minimum.[6] The preference is to have the correct oxidation states present in the starting materials, or to introduce these *via* strategic redox reactions. However, due to the complexity and challenging nature of natural products and many drug candidates, these are frequently difficult to avoid. Furthermore, many esters are available on large scale from natural precursors. The possibility of converting these into value-added products and building blocks thus also provides incentive for developing efficient methods for such transformations.[7, 8]

This is particularly true in the context of process chemistry, wherein the synthesis of a desired target is to be scaled-up. In addition to running reactions in larger vessels, other considerations including yield, purity, robustness, cost and environmental impact must be taken into account.[9] This review will take aspects of process chemistry into account and give examples related to the pharmaceutical industry where possible.

It should be noted that reductions are generally preferred over oxidations on large scale as the former have fewer safety and toxicity concerns associated with the reagents themselves and the resulting waste streams.[1] Accordingly, the bulk of this review will be focused on reduction. In the case of non-oxidation reactions, unwanted exotherms and the possibility of fires are avoided by running reactions in the absence of any oxidants, for example, by running reactions under an atmosphere of nitrogen.[10] In the case of oxidation reactions, however, fuel, oxidant and energy are typically all present, thus leading to additional safety concerns. Oxidations typically run on laboratory scale, such as the Swern oxidation,[11] are undesirable for scale up, due the requirement for low temperatures and the stoichiometric generation of dimethyl sulfide. Hypervalent iodine-based reagents, such as IBX[12] and Dess-Martin periodinane[13] are operable at room temperature, but are expensive and have a high molecular weight leading to low mass efficiency. While TEMPO-bleach[14] oxidations are cheaper to operate, they suffer from being biphasic and thus require additional engineering considerations when scaling up, and can result in the formation of chlorinated side-products.[10]

1.1.2 Stoichiometric Methods for Reducing Esters to Alcohols

The earliest recorded methodology for the chemical reduction of esters to primary alcohols was reported by Bouveault and Blanc in 1903 (**Scheme 2**).[15-18] This dissolving metal reduction involved heating an ester with sodium metal in ethanol at reflux.

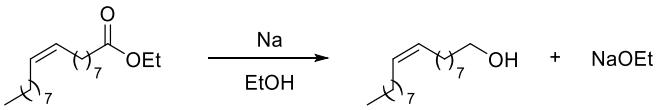

Scheme 2 *Reduction of ethyl oleate with the conditions developed by Bouveault and Blanc.*

The sodium metal serves as a single electron transfer reagent, while the ethanol acts as a proton donor. As such, the proposed mechanism involves formation of radical anionic species (**Scheme 3**).[19]

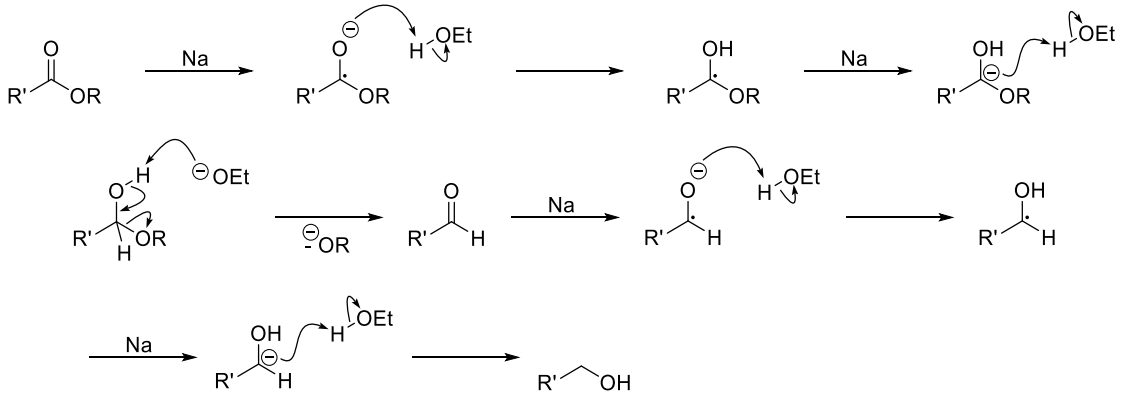

Scheme 3 *Proposed mechanism for Bouveault-Blanc reduction.*[19]

As a consequence of this radical pathway, reactivity other than ester reduction could be observed in certain cases. In an example by Glattfeld and Mochel, unexpected loss of a methoxy group during the reduction of ethyl ester (**1.5**) was observed in addition to reduction of the ethyl ester (**Scheme 4**).[20]

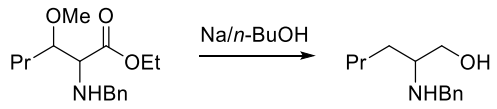

1.5 **1.6**

Scheme 4 *Concomitant loss of methoxide and ester reduction.*[20]

In another example reported by Cossy and co-workers, reduction of δ,ε-unsaturated ester (**1.7**) resulted in formation of a transient ketyl radical which was trapped by the pendant alkene to afford a new 5-membered ring (**Scheme 5**).[21] Notably, this adaptation of the Bouveault-Blanc reduction employed liquid ammonia as the solvent, rather than the more commonly employed alcoholic solvents.

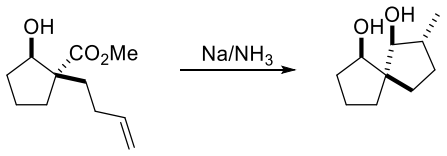

1.7 **1.8**

Scheme 5 *Concomitant ester reduction and cyclisation.*[21]

More recent work on the Bouveault-Blanc reduction has focussed on making the reaction conditions milder and more robust. Bodnar and Vogt demonstrated that using sodium adsorbed onto silica gel allows for reactions to be run at lower temperatures, as well as being cheaper compared to a more typical aluminium-based reducing agent.[22] Procter and co-workers showed that a sodium dispersion could be used instead of sodium metal as a less pyrophoric alternative.[23] In spite of these developments, the Bouveault-Blanc reduction has largely fallen out of common use, both on preparative and large-scales due to the risk of foaming and fire, as well as the capricious nature of the reaction in certain cases.[24] The related dissolving metal reductions used for reducing aromatic rings, namely the Benkeser reduction[25] and the Birch reduction[26] are by contrast still routinely employed.

The most widely reported method described for the reduction of esters is achieved using a variety of nucleophilic hydride reagents including (diisobutylaluminium hydride) DIBAL and lithium aluminium hydride (LAH) **(Figure 1)**.[27] The relatively weak Al-H bond is strongly polarised towards the hydrogen atom. Consequently, these types of reagents are very competent at reducing a plethora of polar functional groups.

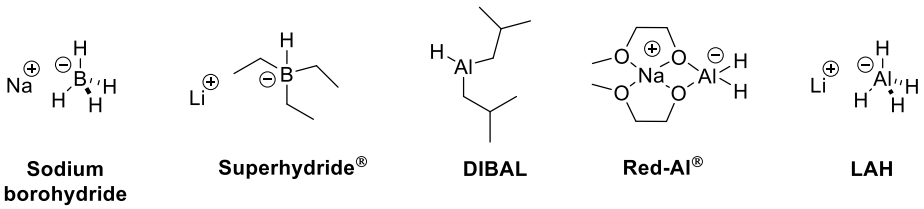

Figure 1 *Commercially available nucleophilic hydride reagents used for reducing esters.*

Indeed, these reagents have proven to be reliable in a wide range of scenarios,[28,29] and their introduction provided a safer and more robust method of achieving ester reductions in a variety of different contexts compared to the Bouveault-Blanc reduction.

Some examples of these types of reagents being used in process development in the pharmaceutical industry are described and discussed below.

Guo and co-workers at GSK reduced diester (**1.9**) to diol (**1.10**) using LAH *en route* to PPARpan agonist (**1.11**) (**Scheme 6**).[30]

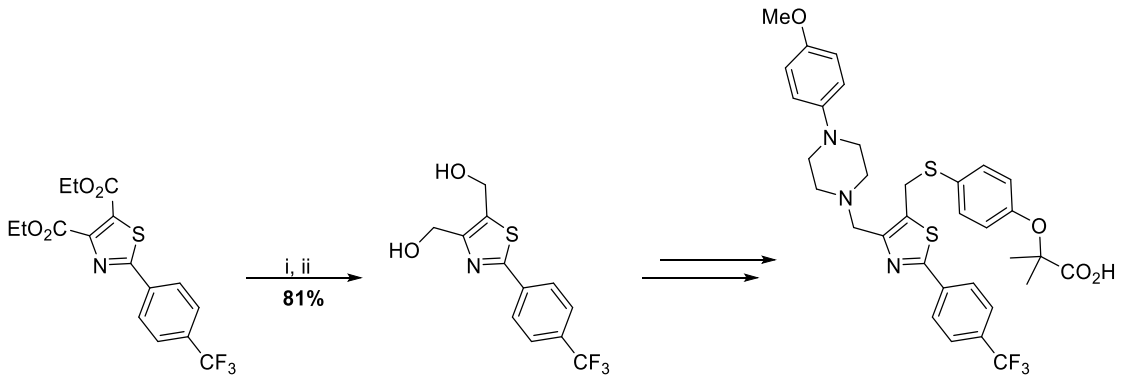

1.9 1.6 kg **1.10** **1.11**

Reagents and conditions; (i) LAH, THF, – 15 °C; (ii) H_2SO_4, H_2O.

Scheme 6 *LAH reduction described by Guo and co-workers.*[30]

Diester (**1.9**) was added as a solution in THF to a solution of LAH in THF in a controlled manner to ensure the reaction temperature did not exceed –15 °C, as mono- and bis-desfluoro side-products were observed at higher temperatures. These desfluoro impurities were found to track through the synthesis, and as such it was pertinent that their formation was suppressed. This allowed for formation of the required diol (**1.10**) in good yield, which was isolated as a solid and taken through the subsequent chemistry stages.

While LAH is a strong, indiscriminate reducing agent, milder, more selective reducing agents are also routinely employed, as shown in the example below. Rozema and co-workers at Abbott Laboratories effected reduction of menthol ester (**1.12**) to diol (**1.13**) using sodium borohydride *en route* to a novel farnesyl transferase inhibitor (**1.14**). Doing so selectively removed the chiral auxiliary, while leaving the aromatic nitrile intact. The use of stronger reducing agents such as lithium borohydride resulted in concomitant reduction of both the ester and the nitrile functionality (**Scheme 7**).[31]

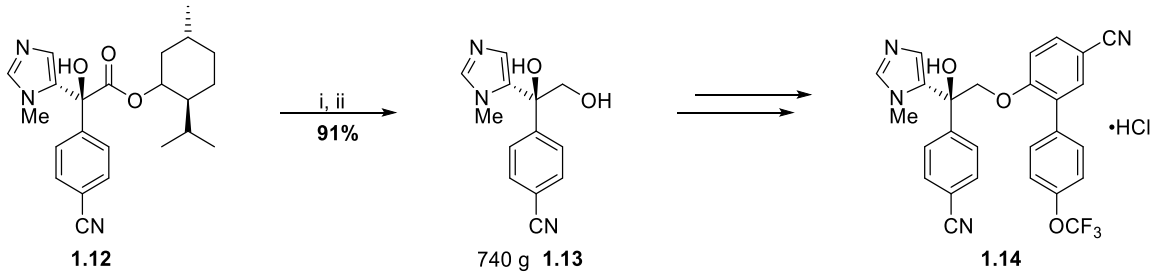

1.12 740 g **1.13** **1.14**

Reagents and conditions; (i) $NaBH_4$, THF/MeOH (5:1), 40-60 °C; (ii) citric acid, H_2O.

Scheme 7 *Reduction of menthol ester (**1.12**) as described by Rozema and co-workers.*[31]

Classically, sodium borohydride is regarded as being a mild reducing agent, reducing esters only slowly in the presence of more reactive functional groups such as ketones or aldehydes.[27] Sodium borohydride is however not an uncommon reagent used for the reduction of esters, particularly in the context of process development,[1] both by itself as shown above and in combination with other additives such as $ZnCl_2$.[32] Though heating is typically needed when used by itself to achieve acceptable reaction rates, sodium borohydride has some advantages over other reducing agents such as being operable in methanol and having a less problematic reaction work-up, in addition to the increased selectivity.

Aside from the chemoselectivity demonstrated in the above example, nucleophilic hydride reagents may also be used to selectively effect partial reductions of esters to aldehydes. This transformation is challenging as the product aldehyde is inherently more reactive than the ester starting material, and as such it can be difficult to prevent over-reduction. For this very reason, partial reduction of esters is infrequently encountered within process development.[1] The same overall transformation is more commonly achieved by means of a two-step process, namely full reduction to the alcohol, followed by selective oxidation to the aldehyde oxidation level.[1]

Abe and co-workers at Eisai reported the synthesis of Aricept (**1.17**), an oral medication for treatment of Alzheimer's disease.[33] Aldehyde (**1.16**) was initially furnished *via* a Wittig coupling of ketone (**1.15**) to generate an enol ether which was subsequently hydrolysed (**Scheme 8**). For the purposes of manufacturing, this was deemed too expensive and wasteful, prompting the search for a new route.

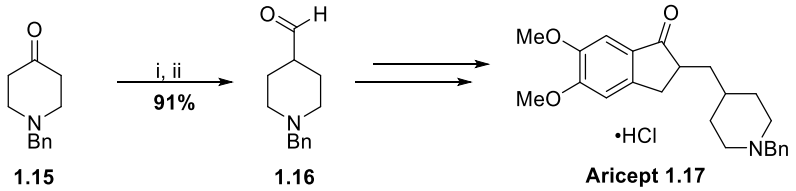

Reagents and conditions; (i) $MeOCH_2PPh_3Cl$, KO*t*-Bu; (ii) $HCl_{(aq.)}$.

Scheme 8 *Previous route to Aricept as reported by Abe and co-workers.*[33]

It was determined that accessing aldehyde (**1.16**) by partial reduction of ethyl isonipecotate (**1.18**) would offer significant cost savings. DIBAL was investigated as a possible reducing agent, but it was found that cryogenic conditions were required to suppress over-reduction to the alcohol, which presented issues for large scale production. The authors then describe a novel modification of Red-Al with pyrrolidine and KO*t*-Bu. The resulting reagent which they name Red-ALP is reported as a general reagent for the selective reduction of esters to aldehydes at temperatures just below ambient (**Scheme 9**).

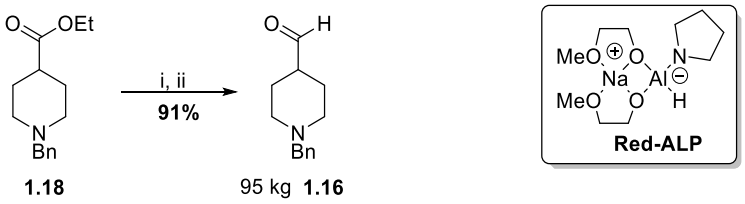

Reagents and conditions; (i) Red-ALP, KO*t*-Bu, TBME, <15 °C; (ii) $NaOH_{(aq.)}$.

Scheme 9 *Formation of aldehyde (**1.16**) by partial reduction of ethyl isonipecotate (**1.18**).*[33]

The optimised reaction conditions allowed for aldehyde (**1.16**) to be furnished in good yield on large scale, with very little over-reduction to the alcohol taking place, and significantly improved ease of operation compared to the use of DIBAL.

To date, nucleophilic hydride reagents have remained the standard method to reduce carbonyl-containing compounds, including esters. While these reagents are indeed reliable, even on scale as shown in the examples above, they also have a number of disadvantages

associated with them. LAH and Superhydride are pyrophoric, requiring careful handling and the use of anhydrous solvents. Additionally, the aqueous quench required when working reaction mixtures up is both exothermic, and rapidly generates hydrogen gas.[1] The issue however, which is common to all nucleophilic hydride reagents is poor atom economy. The concept of atom economy, first highlighted by Trost,[34] is a measure of the efficiency of a reaction, taking into account all atoms involved and the desired products produced (**Equation 1**).

$$Atom\ economy = \frac{molecular\ mass\ of\ desired\ product}{molecular\ mass\ of\ all\ reactants} \times 100\%$$

Equation 1 *Formula for calculating atom economy.*

As such, catalytic reactions exhibit higher atom economies than stoichiometric reactions. Sodium borohydride, in addition to being a stoichiometric reagent, contains 11 wt% hydrogen, while Red-Al, a less pyrophoric alternative to LAH,[35] contains just 1 wt% hydrogen. Furthermore, $NaBH_4$ and LAH rarely donate four equivalents of hydride, despite their molecular formulae suggesting this to be possible. As a result, an excess of these nucleophilic hydride reagents is typically used in practice.

The disadvantage of atom economy as a green metric is that neither yield nor solvent are taken into account, both of which affect the amount of waste generated and become increasingly important on large scale. Consequently, process mass intensity (PMI) is the preferred metric used to determine the relative efficiency of a process (**Equation 2**).[36]

$$Process\ mass\ intensity = \frac{total\ mass\ in\ a\ process\ or\ process\ step}{mass\ of\ product}$$

Equation 2 *Formula for calculating process mass intensity.*

PMI bears the advantage of taking into account all solvents and reagents, including those used in the work-up procedure to give a better overall indication of how much material is

needed to generate a specific quantity of product. In the context of aluminium-based reductions, the work-up typically involves a quench followed by several aqueous extractions, all of which significantly add to the overall PMI. Furthermore, the waste generated within such reactions would typically be dilute aluminium containing aqueous waste.[37] These generally require off-site disposal, and may in some cases have to be transported long distances.

Another approach to reducing esters involves using a silane as the stoichiometric reducing agent. This was first demonstrated by Buchwald and co-workers[38] as a two step process: first hydrosilylation of the ester using triethoxysilane, followed by hydrolysis of the resulting silyl protected alcohols (**Table 1**). The authors noted that substoichiometric quantities of titanocene dichloride and *n*-butyllithium were required for the reaction to proceed.

Reagents and conditions; (i) 5 mol% Cp_2TiCl_2, 10 mol% *n*-BuLi, triethoxysilane, THF, – 78 °C; (ii) 1 M NaOH.

Entry	Ester	Product	Yield/%
1	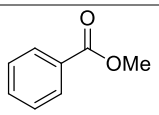	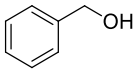	93
2	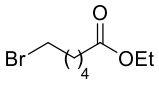	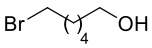	78
3	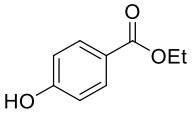	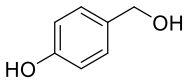	88
4	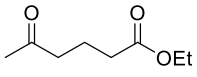	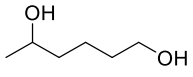	78
5	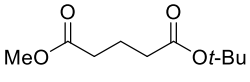	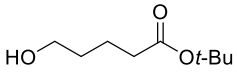	87

Table 1 *Reduction of esters using triethoxysilane demonstrated by Buchwald and co-workers.[38]*

This method proved to be versatile and also showed some interesting selectivity in certain cases. An ethyl ester was successfully reduced in the presence of a primary alkyl bromide (**entry 2**). In another example, a methyl ester was selectively reduced in the presence of a *tert*-butyl ester (**entry 5**). While the authors suggested this as a possible alternative to aluminium-based reducing agents, the requirement for cryogenic conditions is unfavourable, and the authors also noted that in cases where additional *n*-BuLi was added, formation of SiH_4 would cause the appearance of a flame. They suggested the use of the liquid polymer, polymethylhydrosiloxane (PHMS), a commodity material, as a possible alternative to by-pass this risk.

This approach was then further developed by Mimoun at the flavours & fragrances company Firmenich.[39] In addition to employing non-pyrophoric and inexpensive PHMS, the use of titanocene dichloride and *n*-BuLi was replaced with substoichiometric zinc bis(2-ethylhexanoate) and sodium borohydride (**Table 2**).

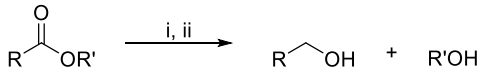

Reagents and conditions; (i) 2 mol% zinc bis(2-ethylhexanoate), 2 mol% sodium borohydride, PMHS, diisopropyl ether, 70 °C; (ii) NaOH, MeOH.

Entry	Ester	Product	Yield/%
1	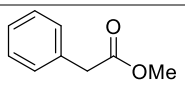	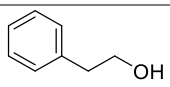	91
2	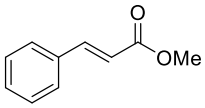	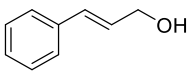	90
3	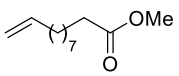	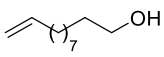	94
4	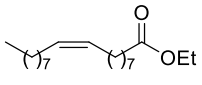	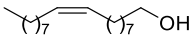	94

Table 2 *Reduction of esters using PMHS demonstrated by Mimoun.*[39]

The conditions developed were demonstrated on a number of different simple esters, in addition to aldehydes, ketones and epoxides. While no detailed mechanistic studies were conducted, it was suggested that formation of zinc hydride complexes and pentaco-ordinated hydridosilicates were responsible for the observed reactivity. Of particular interest was the selectivity of the reaction towards internal and terminal alkenes, as well as alkenes conjugated into esters as a means of generating unsaturated alcohols as value-added products. Following this, the reaction was applied to a variety of naturally occurring triglycerides to afford glycerol and linear alcohols (**Table 3**).

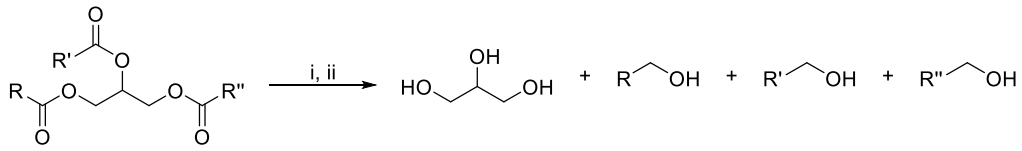

Reagents and conditions; (i) 4 mol% zinc bis(2-ethylhexanoate), 4 mol% sodium borohydride, PMHS, diisopropyl ether, 70 °C; (ii) NaOH, MeOH.

Entry	Oil	Yield/%
1	triolein	95
2	coconut	94
3	cocoa butter	92
4	palm kernel	78
5	peanut	94
6	sunflower	81
7	linseed	75
8	jojoba	95

Table 3 *Reduction of triglycerides using PMHS.*[39]

In addition to being a high-yielding process, this methodology had the additional advantage of being capable of directly reducing triglycerides. This is to be contrasted with catalytic hydrogenation of these fatty esters using hydrogen gas and heterogeneous copper chromite catalysts,[40, 41] which in addition to causing concomitant reduction or isomerisation of any alkene functionality, also require prior transesterification to give the corresponding fatty acid methyl esters (FAMEs).

The author noted the increased safety from avoiding the use of pyrophoric LAH, or molten sodium metal as in the Bouveault-Blanc reduction. Further to this, the reaction could conveniently be operated in a multipurpose reactor as opposed to the specialised high temperature and pressure equipment typically required to operate heterogeneous ester hydrogenations over copper chromite catalysts. While this methodology shows some clear advantages compared to the use of aluminium-based reducing agents both in terms of selectivity and operational ease, it suffers from generating large silicon-containing waste streams. In the examples where triglycerides were being reduced, 7 equivalents of PMHS were employed relative to each equivalent of triglyceride. The issue is further exacerbated by the fact that PMHS contains only ~2 wt% hydrogen. Consequently scaling this up to commercial manufacturing would generate very large waste streams and unfavourably high PMI values.

A further example of a PMHS mediated ester reduction was described by Depré and co-workers at Johnson and Johnson. Tens of kilograms of lactol (**1.20**) were required as part of a project on Selective Estrogen Receptor Modulators (**Scheme 10**).[42]

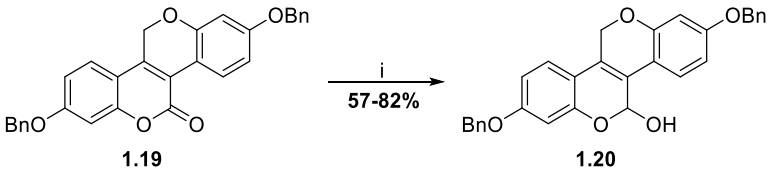

1.19 **1.20**

Reagents and conditions; (i) DIBAL, DCM.

Scheme 10 *DIBAL mediated reduction of lactone (**1.19**) to lactol (**1.20**).*

Reduction of lactone (**1.19**) to lactol (**1.20**) was successfully achieved using DIBAL in DCM. Though the product lactol could be furnished in acceptable yield and purity, large volumes of DCM were required owing to poor solubility, thus leading to large waste streams of a problematic solvent. Furthermore, very precise quantities of DIBAL had to be added to avoid over-reduction to diol (**1.21**) and ether (**1.22**) (**Figure 2**). In addition to this, residual aluminium salts from the DIBAL reduction were found to complicate later synthetic manipulation by causing decomposition.

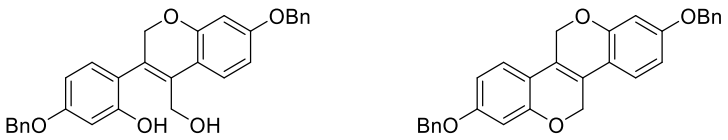

1.21 **1.22**

Figure 2 *Side-products from over-reduction.*

After screening a variety of different reductive conditions, it was established that a PMHS/titanocene mediated reduction was particularly advantageous, as over-reduction to the diol would not occur, even when an excess of the PMHS was employed. Before this approach could be scaled-up, a number of concerns were required to be addressed. An induction period was observed during which catalyst activation took place, which was followed by rapid generation of hydrogen gas. Furthermore, the aqueous quench resulted in large amounts of hydrogen gas being formed along with a nonfilterable gel consisting of a polymeric siloxane side-product. It was determined that by performing catalyst activation prior to addition of lactone (**1.19**) at 90 – 100 °C, the induction period could be eliminated, such that the rate of reaction was controlled by the rate at which the PMHS was dosed into the reaction mixture. Following this, lactone (**1.19**) was added to the reaction mixture, at which point the reduction to the lactol took place. Running the reaction at 45 – 50 °C was essential to ensure a homogeneous reaction mixture and full consumption of the starting material. During the quench, addition of Dicalite allowed the polysiloxane to be filtered off as a hard powder (**Scheme 11**).

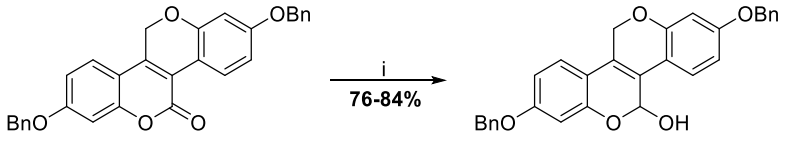

1.19 26 kg **1.20**

Reagents and conditions; (i) titanocene (5 mol%), PMHS (5 eq.), THF, 45-50 °C; (ii) TBAF, Dicalite, THF/H_2O.

Scheme 11 *Optimised conditions for reduction of lactone (**1.19**) to lactol (**1.20**).*

This approach was concluded to be safe after thermodynamic studies and was successfully scaled to afford 26 kg of lactol (**1.20**). In addition to increased yield, purity and reduction of the total waste effluent owing to less solvent usage, this approach also simplified the subsequent chemistry stages, as the presence of the problematic aluminium salts was eliminated.

In summary, nucleophilic metal hydrides are reliable and often high yielding reagents for effecting the reduction of esters. While these have successfully been demonstrated on scale, these reagents remain problematic and non-preferred due to safety concerns with their pyrophoric nature, the complicated quench and work-up procedure which typically involves liberation of large quantities of hydrogen gas, as well as the stoichiometric generation of waste, which can require specialised and costly disposal. Titanocene/PMHS mediated ester reductions do address some of the safety concerns of aluminium-based reducing agents, though they still suffer from generating large volumes of waste. Consequently, catalytic alternatives to existing reduction processes are highly beneficial and have been subject to increasing amounts of research.

1.1.3 Heterogeneous Catalytic Reduction

Hydrogen is the most atom efficient reducing agent and has the additional advantages of being relatively cheap, sustainable and readily available.[43] The hydrogen molecule itself consists of two hydrogen atoms covalently bound by a pair of electrons. This may be represented by one of the simplest molecular orbital schemes, in which there is a strongly bonding molecular orbital (MO) which contains the electron pair, as well as a strongly anti-bonding MO which is left unfilled (**Figure 3**).[44]

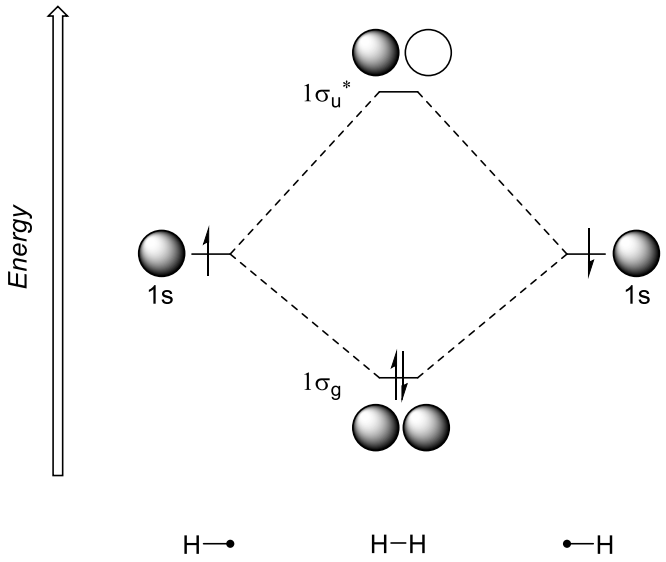

Figure 3 *Molecular orbital diagram of dihydrogen.*

Consequently, the H-H bond is relatively strong, with a bond enthalpy of 104 kcal mol^{-1} and thus requires catalysis in order to react with unsaturated compounds under mild conditions.[45,46,47] Only transition metal catalysts will be examined here, although frustrated Lewis pairs also show promise to heterolytically cleave hydrogen for the purposes of reduction under relatively mild, metal-free conditions.[48]

Early examples of heterogeneous catalytic hydrogenation include the work reported by von Wilde in 1874, whereby acetylene was reduced in the presence of hydrogen and platinum black.[49] Nobel Laureate, Sabatier, later demonstrated the reduction of various unsaturated organic species including ethene in 1897[50] and benzene in 1901[51] using finely divided nickel to catalyse these transformations (**Scheme 12**). Large industrial applications of such hydrogenations include the reduction of vegetable oils in the production of margarine,[52, 53] and reduction of benzene to cyclohexane, a precursor to adipic acid which is used extensively in the polymer industry for production of nylon.[54]

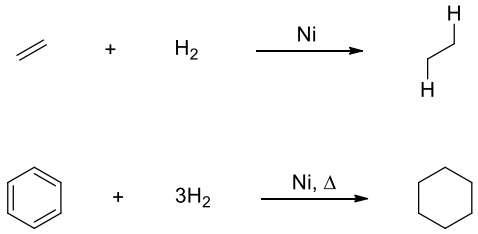

Scheme 12 *Reduction of ethene and benzene using hydrogen and nickel reported by Sabatier and co-workers.*[50, 51]

Activation of hydrogen takes place by adsorption of hydrogen atoms onto the surface of the metal. This is believed initially to occur *via* an interaction between the H-H σ-bond and the metal surface. Eventually, this leads to dissociation of the H-H bond to give hydrogen atoms bound to the surface of the metal (**Figure 4**).[52] This process proceeds *via* a low energy transition barrier, and has been demonstrated to take place at temperatures as low as –236 °C in the case of palladium.[55]

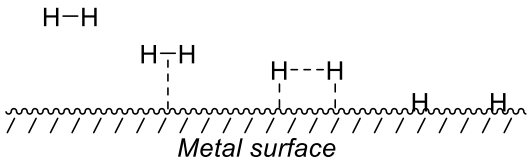

Figure 4 *Adsorption of hydrogen atoms onto metal surface.*

The mechanism of heterogeneous metal-catalysed reductions of alkenes in particular has been extensively studied, which is widely accepted to proceed *via* the Horiuti-Polanyi mechanism, first proposed in 1934 (**Figure 5**).[56] This also involves initial adsorption of the alkene substrate to the metal surface, however, utilising the π-bond in this instance. Following this, hydrogen migration to the *β*-carbon takes place to form the first C-H σ-bond. Studies have revealed this step to be highly reversible, as evidenced by deuterium-hydrogen exchange taking place when such reactions are performed using D_2. The final step, which is rate-determining involves the irreversible reductive elimination of the partially hydrogenated substrate and a hydrogen atom to afford the fully saturated alkane. This is then subsequently released from the metal surface in an entropically favourable process.[52]

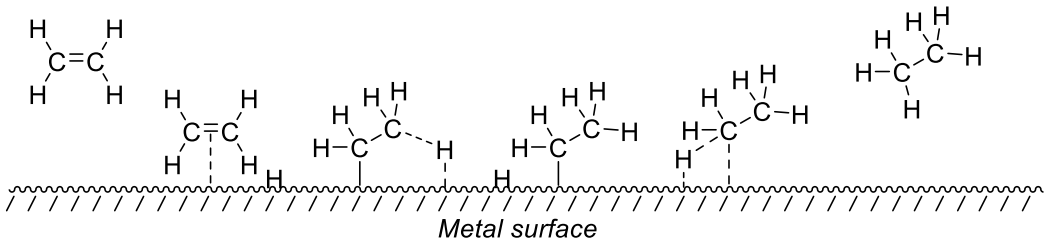

Figure 5 *Reduction of ethene via the Horiuti-Polanyi mechanism.*[56]

Applying catalytic reductions to esters later also gained interest as a means of converting naturally available feedstocks into value added products on large scale. Pioneering work by Adkins in the 1930s established heterogeneous copper chromite catalysts as being most suited for this purpose, as these catalysts afford product alcohols in good yields, possess good durability and are readily scalable.[40] These catalysts are prepared by thermal decomposition of copper ammonium chromate to give an approximately equimolar combination of CuO and $CuCr_2O_4$.[41] Barium is often included as an additive as it is known to make the resulting catalyst more resistant to deactivation. The reactions themselves require very forcing conditions in order for acceptable reaction rates to be attained, as well as to shift the equilibrium toward the alcohol and maximise the yield. Typically temperatures in excess of 200 °C, and pressures between 275 and 400 bar are employed depending on the nature of the substrate in order to favour product formation.[57] As a consequence of these high temperatures, reactions may typically be run solvent-free, as both the substrates and product tend to be liquids under these elevated temperatures, making these significantly more efficient than the Bouveault-Blanc reduction, the reaction this catalytic alternative was designed to replace. The issue with such forcing conditions, aside from being energy intensive, is the lack of selectivity towards functional groups. Reductions of alkenes, aromatic rings and benzylic alcohols would typically take place, in addition to reduction of the ester itself (**Scheme 13**).

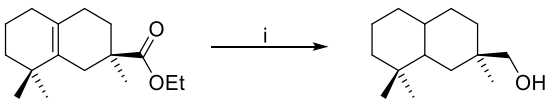

Reagents and conditions; (i) Raney nickel or copper chromite, H_2.

Scheme 13 *Concomitant alkene and ester reduction under heterogeneous hydrogenation conditions.*[58]

Furthermore, the presence of halogen or sulfur atoms in organic compounds would typically result in their removal by hydrogenolysis followed by catalyst deactivation, while the presence of acid, base or water would also induce deactivation by reduction of the catalyst to form copper metal. The need for specialist equipment for reactions to be run and the limited functional group tolerance dictates that this reaction is most suited for high-volume chemical processes, such as those used in the bulk chemical industry. These processes have since largely remained unchanged, and as such this technology is mature and well understood.[59] One of the typical applications of such a process is the reduction of fatty acid methyl esters (FAMEs) derived from naturally occurring triglycerides, such as those discussed previously (**Table 3**). The key difference is that in contrast to the PMHS/titanocene mediated reduction, only saturated alcohols are obtained in this case. Prior transesterification and separation of glycerol is necessary in such a process, as the reaction conditions degrade this valuable side-product. Indeed, other common side-products from heterogeneous ester reductions are hydrocarbons formed as a result of over-reduction.[59] The product alcohols from these reductions have found applications within many industries including fragrances, pharmaceuticals, detergents, emulsifiers and lubricants.[60]

An issue highlighted with the use of copper chromite catalysts is the formation of hexavalent chromium during the process of manufacturing the catalyst itself. This has been identified as a safety issue[61] and has been the basis of research conducted to find a chromium-free alternative, which still retains the activity and durability of the copper chromite catalysts. A heterogeneous Cu-Fe-Al catalyst reported by Hattori and co-workers suggest this as a promising alternative. In particular, their findings show that the incorporation of Fe has a promoting effect close to that of chromium, while the presence of Al improves the durability of the resulting catalyst. Following extensive characterisation work and kinetic studies, the Cu-Fe-Al catalyst was tested by reduction of methyl esters derived from coconut oil in a

slurry-bed reactor continuously for 20 days. During this time, no loss of activity was observed, and the product distribution obtained was almost the same as that typically seen with copper chromite catalysts. The level of productivity achieved equated to formation of 35 000 tons/per annum of alcohol, and was suggested to be a suitable, less toxic alternative.[61]

The possibility of effecting selective reductions with a heterogeneous catalyst has also been investigated. In particular, zinc chromium oxide, while a less efficient catalyst than copper chromite, requiring both higher temperatures (300 °C) and catalyst loadings, has been demonstrated to reduce esters, while only partially reducing alkenes, to give unsaturated alcohols (**Figure 6**).[62]

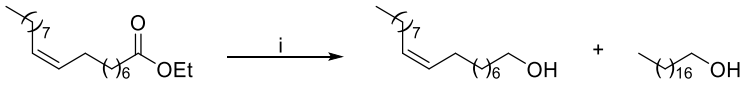

Reagents and conditions; (i) zinc chromium oxide, H_2.

Figure 6 *Catalytic reduction of ethyl oleate to give a mixture of saturated and unsaturated alcohols.*[62]

The usefulness of such a process is limited due to the difficulty of separating the saturated and unsaturated alcohols.

More recently there have been other developments in reducing both esters and carboxylic acids using heterogeneous catalytic hydrogenation through identifying milder catalytic systems. In particular emphasis has been placed on exploiting bifunctional catalysts for this purpose, and typically involves additional use of promoters including Sn, Zn or Ge.[60] It is thought that the presence of these Lewis acidic promoters in close proximity to the transition metal gives rise to synergistic effects and enhanced activity compared to either metal individually.[63] Despite some of the advances made in this field, the conditions still remain relatively forcing, and access to milder conditions is being increasingly achieved by means of homogeneous catalysis.[8]

In summary, hetereogeneous catalytic ester reductions are of significant industrial importance, and are used extensively on very large scale for reduction of methyl esters derived from naturally occurring triglycerides. Due however to the high pressures and temperatures required, these are less well suited for more highly functionalised molecules,

as these have a tendency either to be reduced, or to poison the catalyst. Furthermore, operation requires specialist high pressure equipment and high capital investment. Based on all of the above, catalytic heterogeneous ester hydrogenation has not had significant uptake for comparatively lower volume applications, such as within the pharmaceutical industry and where multipurpose plant vessels are typically encountered.

1.1.4 Homogeneous Catalytic Reduction of Esters

1.1.4.1 Initial Contributions

Homogeneous hydrogenation has the advantage of typically being operable under milder conditions compared to those required for heterogeneous hydrogenations. Homogeneous hydrogenation of alkenes with $RuCl_3$ was initially reported by Halpern, Harrod, and James.[64] Subsequently, hydrogenation of alkenes with a rhodium-based homogeneous complex was reported by Wilkinson and co-workers.[65] Significant work was also conducted by Noyori and co-workers in the field of asymmetric hydrogenation of ketones starting in the 1980s.[66] These reductions typically employ chiral bisphosphine/bisamine ruthenium complexes and have found a plethora of industrial applications.[67, 68] Developments in homogeneous ester reductions, in contrast, have been comparatively slower, owing to the inherent lower electrophilicity of esters compared with ketones due to a variety of stablising interactions at play (**Figure 7**).

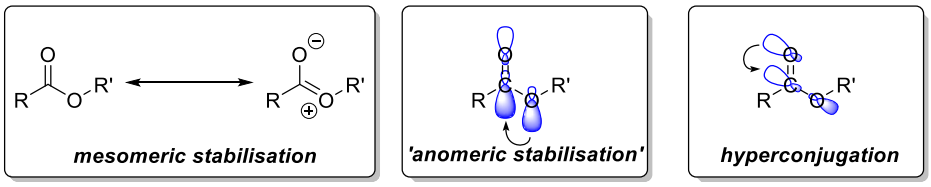

Figure 7 *Stabilising stereoelectronic interactions contributing to reduced electrophilicity of esters when compared to ketones.*

Early work in the field of homogeneous ester reductions was reported in 1981, when Grey and co-workers[69] disclosed an anionic phosphine-ruthenate complex, which was capable of reducing aldehydes, ketones and esters to alcohols under conditions significantly milder compared to conditions typically employed in heterogeneous ester reductions (**Scheme 14**). This system was, however only capable of reacting with particularly reactive esters, including methyl trifluoroacetate and dimethyl oxalate. Unactivated esters, which did not bear α-electron withdrawing groups, such as methyl acetate, in contrast underwent only limited conversion, while methyl benzoate did not react under these conditions. This limitation therefore prevented this methodology from finding wider application. Nevertheless, this was the first reported example of homogeneous catalytic ester reduction.

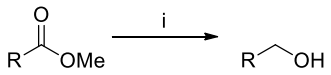

R = CF_3, CO_2Me

Reagents and conditions; (i) 0.3 mol% $K_2[Ru_2(PPh_3)_3(PPh_2)H_4]\cdot 2C_6H_{14}O_3$, 6.2 bar H_2, toluene, 90 °C, 20 h.

Scheme 14 *First example of homogeneous catalytic ester reduction by Grey and co-workers.[69]*

Following the work from Grey, efforts in this field were relativity scarce until the contributions made by Teunissen and Elsevier in 1998 (**Scheme 15**).[70] The ruthenium catalyst (**1.23**) reported was generated *in situ* from $Ru(acac)_3$ and $MeC(CH_2PPh_2)_3$ (triphos) to generate a facially coordinated complex which was found to be effective for the partial reduction of the activated ester dimethyl phthalate to phthalide. In order to achieve reduction of unactivated esters such as benzyl benzoate and methyl palmitate, triethylamine was required as a promoter, and switching from methanol to the fluorinated solvent, HFIP, was found to be particularly beneficial for activity. The reason behind the beneficial role of HFIP is not fully understood, though the increased acidity and ability to hydrogen bond either to the substrate or catalyst are possibilities.[71] Subsequent studies have indeed shown related Ru(triphos)(hydride) complex to form a strong hydrogen bond to HFIP, which also exists in equilibrium with a nonclassical η^2-H_2 complex.[72]

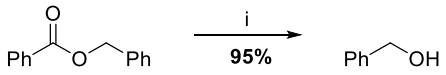

Reagents and conditions; (i) 0.05 mol% $Ru(acac)_3$, $MeC(CH_2PPh_2)_3$, 9 mol% NEt_3, 85 bar H_2, HFIP, 120 °C, 16 h.

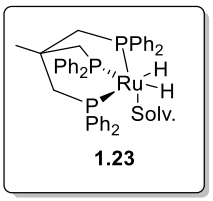

1.23

Scheme 15 *Example of catalytic reduction of unactivated esters by Teunissen and Elsevier.*[70]

As with the work reported by Grey and co-workers, significantly lower temperatures and hydrogen pressures were required to operate the reaction compared to conditions used for heterogeneous hydrogenations, though significantly more forcing compared to conditions required for more typical homogeneous hydrogenations. Consequently, benzene rings were not reduced under these conditions, with the reduction of benzyl benzoate giving high yields of benzyl alcohol. More easily reducible functional groups, in contrast, were not preserved, as was evident during reduction of dimethyl maleate which afforded butanediol with concomitant reduction of the alkene group (**Scheme 16**).

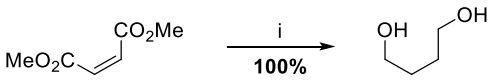

Reagents and conditions; (i) 0.01 mol% $Ru(acac)_3$, $MeC(CH_2PPh_2)_3$, 19 mol% NEt_3, 85 bar H_2, HFIP, 120 °C, 16 h.

Scheme 16 *Simultaneous reduction of both esters and conjugated alkene.*

This approach suggested that with further development, such transformations could become more broadly applicable. Further research into Ru(triphos) catalytic systems was performed by Leitner, Klankermayer and co-workers (**Scheme 17**).[73]

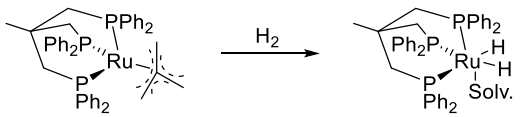

1.24 **1.23**

Scheme 17 *Formation of active hydrogenation catalyst.*

They reported the use of the pre-catalyst, Ru(triphos)(tri-methylene methane) (**1.24**), which could be activated in the presence of hydrogen to give facially coordinated ruthenium-hydride complex (**1.23**). As with the catalytic system reported by Teunissen and Elsevier, relatively forcing conditions were employed, though an increased scope of esters and lactones were converted to their corresponding alcohols in high yields (**Table 4**).

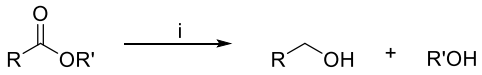

Reagents and conditions; (i) 1 mol% [Ru(triphos)(trimethylenemethane)], 50 bar H_2, dioxane, 140 °C, 16 h.

Entry	Substrate	Product	Yield/%
1	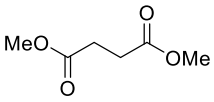	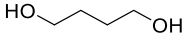	99
2	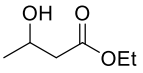	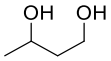	95
3	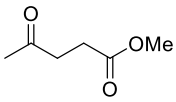	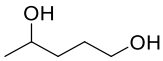	99
4	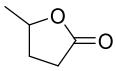	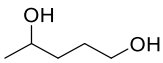	99

Table 4 *Reduction of esters reported by Leitner and Klankermayer.*[73]

By increasing the temperature, the catalyst was also found to be effective in reducing carboxylic acids, carboxylic anhydrides and imides. Furthermore, elevated temperatures and addition of bistriflimidic acid allowed for successful reduction of amides and ureas to amines.

The catalytic cycle of the reaction was investigated my means of DFT calculations, and a proposed cycle is depicted below (**Figure 8**).

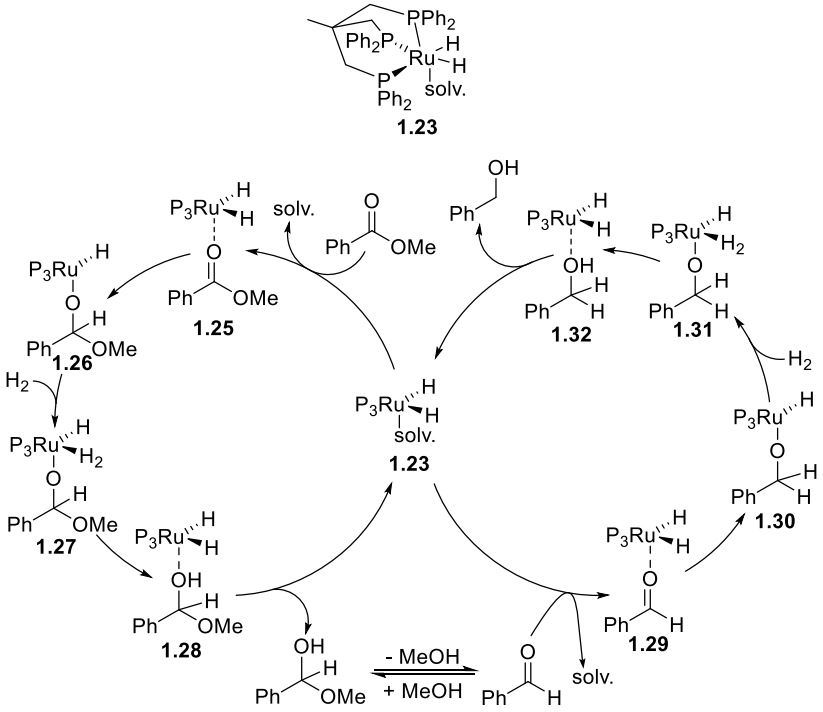

Figure 8 *Catalytic cycle for ester reduction mediated by Ru(triphos) complex.*[73]

After formation of the active catalytic species (**1.23**) bearing two hydride ligands, initial reduction takes place to form a hemiacetal intermediate (**1.26**). This hemiacetal decomplexes from the metal, and eliminates an alcohol (methanol in the case of methyl esters) to afford an aldehyde. This in turn binds to ruthenium (**1.29**) and is further reduced to the alcohol oxidation level (**1.30**). It is noteworthy that this particular catalytic cycle follows an inner-sphere pathway, one in which the substrate is directly bound to the metal centre. Furthermore, the key role of the triphos ligand is to stabilise the ruthenium centre and impose facial geometry, but is otherwise a "redox-innocent" ligand, which does not directly partake in the catalytic cycle.

Ru(triphos)-based catalytic systems have since found numerous other applications, including depolymerisation of polyesters,[74] reduction of CO_2 to methanol[75] and transfer hydrogenation of amides to amines.[76] Indeed, triphos has as a result been described as a privileged ligand,[77] one which is applicable to multiple different catalytic processes. Access to milder conditions, however, has since been enabled by redox non-innocent ligands. These ligands participate in the activation of hydrogen and subsequent delivery to the target molecule.

The next major breakthrough in this field came from the highly influential work conducted by Milstein and co-workers, wherein a unique Ru pincer complex (**1.33**) bearing a redox active ligand could reversibly bind to dihydrogen to afford complex (**1.34**), a process which was accompanied by aromatisation of the pyridyl ring (**Scheme 18**). This complex (**1.33**) was initially found to effectively catalyse acceptorless dehydrogenative coupling of alcohols to afford an ester.[78] Consequently, the microscopic reverse process, ester hydrogenation was also investigated by applying pressurised hydrogen gas.[79]

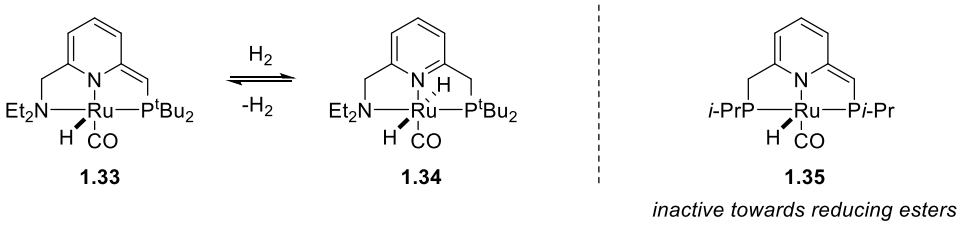

Scheme 18 *Milstein's Ru-PNN complex (**1.33**) reversibly binding to dihydrogen to give an aromatised complex (**1.34**)*[79]

Of particular note was the ability of this complex to facilitate reduction of a variety of both aliphatic and aromatic esters (**Table 5**)[79] without the need for additives, and benefitted from working under relatively low pressures of hydrogen (5.4 bar). Indeed, following this initial report, Milstein's catalyst (**1.33**) has since become commercially available.

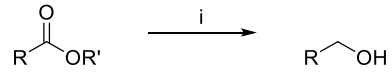

Reagents and conditions; (i) 1 mol% (**1.33**), 5.4 bar H_2, dioxane, 115 °C, 4-24 h.

Entry	Ester	Product	Yield/%
1	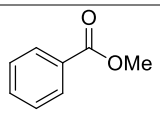	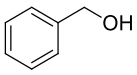	97
2	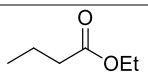	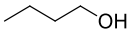	98
3			86
4	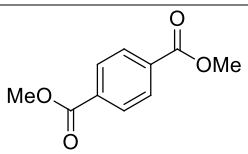	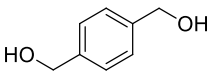	97
5	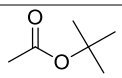		11

Table 5 *Catalytic reduction of a variety of esters using Ru-PNN complex (**1.33**) reported by Milstein.*[79]

An issue with this methodology was the need for relatively high temperatures. Furthermore, an analogous symmetrical Ru-PNP complex (**1.35**) was synthesised bearing an additional phosphine in place of the tertiary amine, however, this proved to be less efficient at reducing esters. Milstein argued that the less strongly bound amine was crucial, as its increased lability created a free site for the ester to coordinate to, a process which only takes place at elevated temperatures, and used this as evidence to point towards an inner-sphere mechanism being in operation. Subsequent work conducted by Chianese and co-workers, however, revealed an unexpected dehydroalkylative process to take place prior to reduction of the ester itself (**Scheme 19**).[80] Time-course experiments observed an initial induction period during which evolution of ethane gas took place.

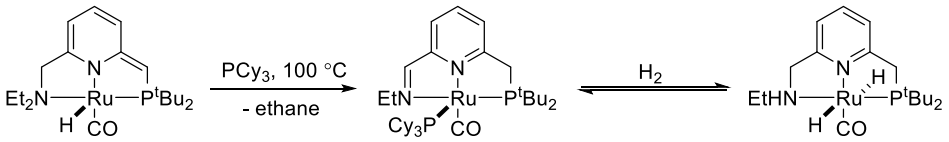

Scheme 19 *Dehydroalkylative process allowing formation of catalytically active complex.*

Closer analysis of this phenomenon revealed formation of Ru-PNN imine complex (**1.36**). This complex was also capable of reversibly binding to hydrogen to give complex (**1.37**) bearing a secondary amine. Perhaps most remarkably, this catalyst was capable of reducing esters at room temperature rather than the elevated temperatures previously required. The mechanistic implication of these experiments was that hemilability is not a condition for designing efficient catalysts as was initially postulated as the reaction proceeds *via* an outer-sphere. Rather, the NH functionality was crucial, and until this active catalyst forms, no consumption of the substrate ester would take place. A similar complex (**1.38**) has since also been demonstrated to reduce amides at room temperature by Milstein and co-workers (**Table 6**).[81]

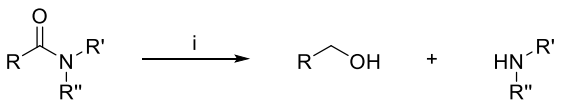

Reagents and conditions; (i) 0.5 mol% Ru complex (**1.38**), 2 mol% KO*t*-Bu, 10 bar H_2, THF, rt, 68 h.

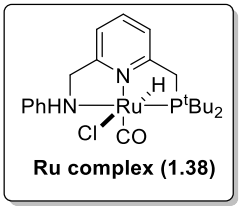

Ru complex (1.38)

Entry	Ester	Products	Yield (alcohol)/%	Yield (amine)/%
1	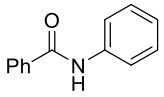	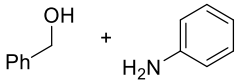	91	93
2	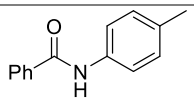	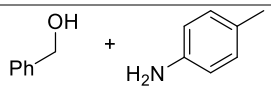	97	98
3	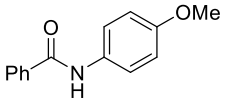	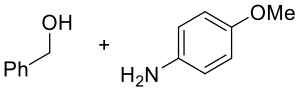	92	92

Table 6 *Reduction of amides at room temperature reported by Milstein and co-workers.*[81]

The key issue with these complexes are their highly air sensitive nature, requiring a glove-box for handling. A broad range of other catalysts based on ruthenium and base metals including manganese have also since been reported.[82]

1.1.4.2 Homogeneous Ester Reductions in Industry

Following the work performed by Milstein and co-workers, the number of reports concerning homogeneous ester reductions has risen exponentially. As such, this review will not attempt to discuss all examples, but will focus in particular on those cases which have been relevant in an industrial setting. Other interesting contributions have been discussed in a number of other published reviews. [60, 83-87]

Various groups have investigated the possibility of employing Noyori catalysts for the reduction of esters. Being inherently less reactive when compared to ketones, the reaction was promoted by employing aprotic solvents (including THF or toluene) rather than the alcoholic solvents (*i*-PrOH, MeOH) typically used for ketone reduction, as well as addition of

strong alkoxide bases. Interestingly, chiral ligands have been used in the context of ester reductions, although no chiral centres are being generated in this case (**Figure 9**).[68]

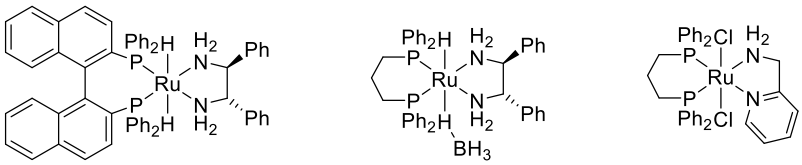

Firmenich, 2008
Bergens, 2009

Takasago, 2008

Clarke, 2012

Figure 9 *Examples of ester hydrogenation catalysts with scaffolds reminiscent of Noyori hydrogenation catalysts.*[88-92]

Firmenich, and other companies in the flavours & fragrances industry including Takasago International Corporation and Givaudan have been innovators in this field, driven in particular by the need to minimise waste generated by processes including metal hydride and PMHS/titanocene mediated reductions.[68] This approach has allowed for more selective processes to be developed compared to heterogeneous hydrogenations.

An important drive in the flavour & fragrances industry is the cost of intermediates and feed stocks, as well as the ability to rapidly increase scale. Typically within homogeneous hydrogenations a trade-off between pressure and catalyst loading is made. In the context of the flavours & fragrances industry, low catalyst loadings take precedence, partly as the necessary equipment and expertise for high-pressure hydrogenations are available, and partly as a means of driving down the cost contribution from the catalyst itself in order to make such processes economically viable. This is particularly pertinent given that these are large volume processes, where small changes in catalyst loading may lead to large overall savings over the lifetime of a particular product.

Saudan and co-workers synthesized a series of Ru complexes, inspired by Noyori catalysts, and eventually synthesised achiral variants.[93] Two examples in particular showed good activity across a broad range of substrates, namely Ru(PNPN)Cl_2 (**1.39**) and Ru(dppea)$_2Cl_2$ (**1.40**) (**Figure 10**). Substoichiometric alkoxide base such as NaOMe was also necessary to generate the active form of the catalyst in each case.

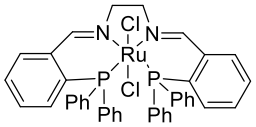

Ru(PNPN)Cl_2 **1.39**

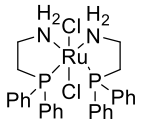

Ru(dppea)Cl_2 **1.40**

Figure 10 *Ester hydrogenation catalysts reported by Saudan and co-workers.*[93]

Ru(PNPN)Cl_2 (**1.39**) showed good chemoselectivity, and was capable of reducing esters while leaving unconjugated alkenes intact (**Table 7, entries 3-4**). By contrast, conjugated alkenes were predominantly reduced to the saturated alcohol (**Table 7, entry 5**). In addition, the catalyst proved to be effective at much lower loadings (0.05 mol%) giving a TON as high as 2000.

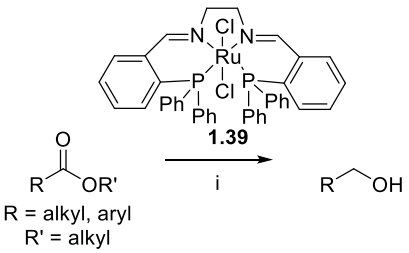

Reagents and conditions; (i) 0.05 mol% (**1.39**), 5-10 mol% NaOMe, 50 bar H_2, THF, 100 °C, 2.5-4 h.

Entry	Ester	Product	Unsat:Sat.	Yield/%
1	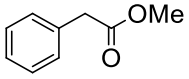	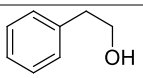	n/a	83
2	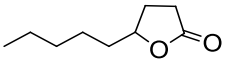	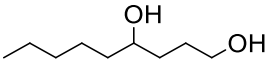	n/a	87
3	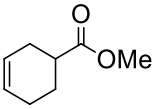	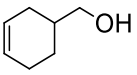	98:2	88
4	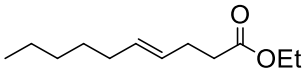	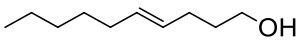	99:1	92
5	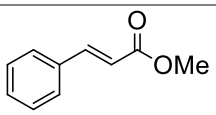	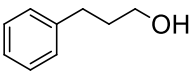	12:88	77

Table 7 *Reduction of a variety of esters using cataylst (**1.39**) reported by Saudan and co-workers.*[93]

As with Noyori catalysts, the reaction was suggested to occur *via* an outer-sphere mechanism. This was evident as an NH group (either present in the catalyst, or formed under the reaction conditions) was required for good activity.

Conservation of terminal alkenes was also found to be challenging as they are easily reducible. 9-decenol (Rosalva™) was a target of particular interest for its rosy-floral aldehydic scent as a fragrance ingredient. Optimisation was carried out using hydrogenation catalyst (**1.39**) at Givaudan. This eventually led to a process in which high levels of chemoselectivity were observed (**Scheme 20**).

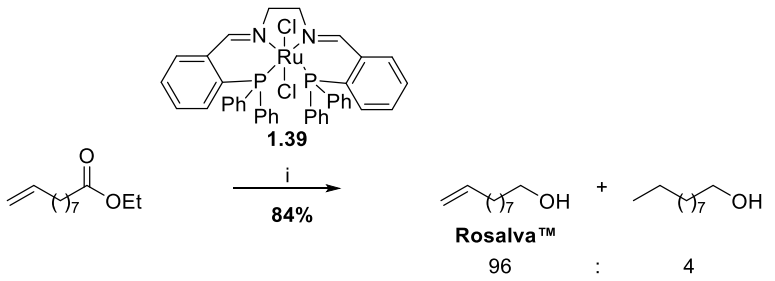

Reagents and conditions; (i) 0.01 mol% (**1.39**), 10 mol% KOMe, 50 bar H_2, THF, 80 °C, 5 h.

Scheme 20 *Reduction of ethyl decenoate to 9-decenol, a fragrance ingredient.*[94]

Furthermore, modification of the catalyst by prior treatment with $NaBH_4$ in analogy to work previously reported by Noyori and co-workers[95] generated a complex capable of catalysing reductions under base-free conditions. This allowed for reductions of esters sensitive to base, and esters bearing α-chiral centres to be reduced with minimal racemisation. This was demonstrated on Boc-L-alanine methyl ester (**1.42**) to generate the corresponding chiral amino alcohol (**1.43**) by Kuriyama and co-workers (**Scheme 21**).

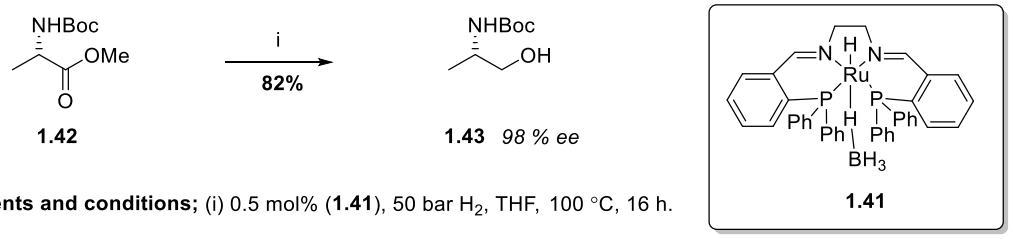

Reagents and conditions; (i) 0.5 mol% (**1.41**), 50 bar H_2, THF, 100 °C, 16 h.

Scheme 21 *Reduction of Boc-L-alanine methyl ester (**1.42**) under base-free conditions.*[96]

In another development, Ru-MACHO (**1.44**), and Ru-MACHO-BH (**1.45**), ruthenium complexes bearing PNP pincer ligands were developed at Takasago by Kuriyama and co-workers[97, 98] specifically to reduce esters on large scale (**Figure 11**). Ligand design moved away from adapted Noyori-type ligands to systems dedicated towards ester hydrogenation. This was also the first ester hydrogenation catalyst to be widely commericalised. Interestingly, unlike the aforementioned catalysts, Ru-MACHO (**1.44**) is resistant to MeOH. This is advantageous not only from being able to use MeOH as the solvent, but also makes the catalyst less prone to deactivation by alcohols produced as the stoichiometric side-products

during the reduction of esters. Ru-MACHO-BH (**1.45**) is obtained by treating Ru-MACHO (**1.45**) with sodium borohydride and has the added advantage of being capable of catalytically reducing esters under base-free conditions. A variety of industrial applications have been found for Ru-MACHO (**1.44**), some of which are described below.

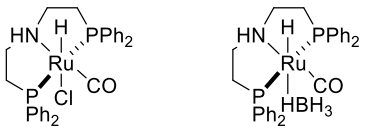

1.44 **1.45**

Figure 11 *Ru-MACHO (**1.44**) and Ru-MACHO-BH (**1.45**).*

The catalytic reduction of methyl trifluoroacetate (**1.46**) using catalytic Ru-MACHO (**1.44**) was reported by Otsuka and co-workers at Central Glass company (**Scheme 22**).[99, 100]

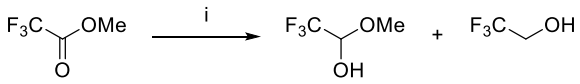

1.46 **1.47** **1.48**

Reagents and conditions; (i) Ru-MACHO , NaOMe, 10-20 bar H_2, MeOH, 40 °C.

Scheme 22 *Catalytic reduction of methyl trifluoroacetate (**1.46**).*

By tuning the conditions, either the alcohol (**1.48**) or hemiacetal (**1.47**) could be selectively formed in good yields. As such this was developed into a process for the production of trifluoromethyl acetaldehyde, a compound which finds applications in pharmaceutical products.[101]

In another example, this catalyst system was demonstrated by performing a multi-ton reduction of methyl (*R*)-lactate (**1.49**) to (*R*)-1,2-propanediol (**1.50**) (**Scheme 23**). The conditions had to be optimised to run the reaction at near room temperature in order to prevent erosion of the optical purity.[97]

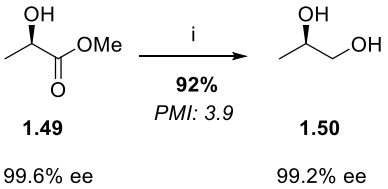

Reagents and conditions; (i) Methyl (*R*)-lactate (2200 kg, 21133 mol), Ru-MACHO (**1.44**) (6.4 kg, 10.6 mol, 0.05 mol%), NaOMe (28% in MeOH, 51.0 kg, 256 mol,1.2 mol%), 40-42 bar H_2, MeOH, 26-28 °C, 12 h.

Scheme 23 *Large scale reduction of methyl (R)-lactate (**1.49**) using Ru-MACHO (**1.44**).*

Industrial production of (*R*)-1,2-propanediol (**1.50**) by asymmetric reduction of hydroxyacetone was well established, but could not furnish the product in sufficiently high optical purity for the purposes of pharmaceutical intermediates where enantiomeric excesses greater than 99% are typically required. Though the enantiomeric excess could be upgraded by derivatisation and recrystallisation, this approach added to the lead-time and reduced the overall efficiency of the synthesis. As such an alternative approach was taken by starting with methyl (*R*)-lactate (**1.49**), available in bulk from natural feedstocks in greater than 99% ee, and reducing this while maintaining stereochemical integrity. The authors also note the operational ease and significantly reduced waste stream which resulted from developing this approach over using aluminium-based reducing agents.

This chiral building block finds applications in pharmaceutical products such as levofloxacin, a broad spectrum antibiotic with sales reaching US$1.6 billion in 2009[101, 102] and tenofovir a marketed drug used to treat patients with chronic hepatitis B and for HIV/AIDS prevention (**Figure 12**).[103]

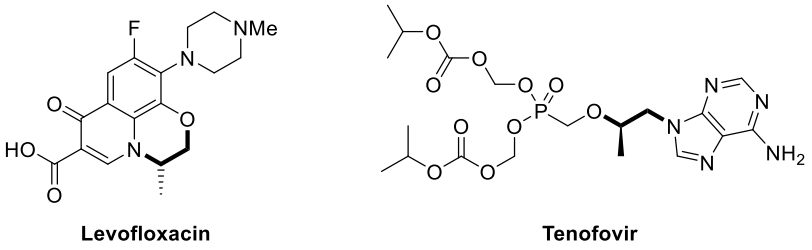

Figure 12 *Commercial drugs requiring non-racemic 1,2-propanediol (**1.50**) as building block.*

In 2016, Kayaki and co-workers[104] from Takasago disclosed another analogue of Ru-MACHO (**1.44**) bearing a carbene ligand in place of the CO ligand, Ru(PNP)Cl_2(NHC) (**1.51**) (**Scheme 24**).

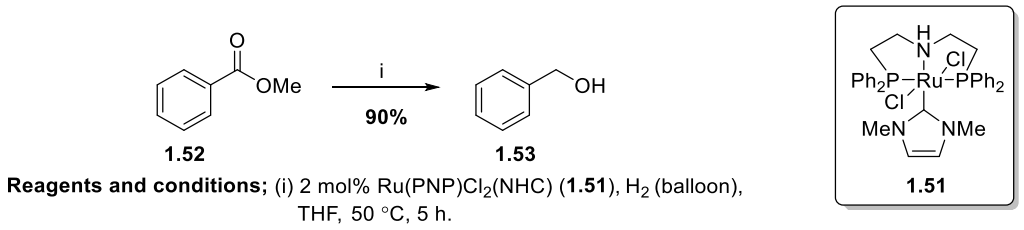

Reagents and conditions; (i) 2 mol% Ru(PNP)Cl_2(NHC) (**1.51**), H_2 (balloon), THF, 50 °C, 5 h.

Scheme 24 *Catalytic reduction of esters under a balloon of hydrogen reported by Kayaki and co-workers.*[104]

The authors reasoned that the presence of the CO ligand in Ru-MACHO (**1.44**) was in place to stabilise the complex, but that the π-backbonding from the ruthenium centre results in decreased hydride nucleophilicity and thus necessitated more forcing conditions. In light of this, they replaced the CO ligand for a strongly σ-donating NHC ligand. The resulting complex (**1.51**) was capable of reducing esters under particularly mild conditions, specifically under 1 atmosphere of hydrogen. This methodology is particularly attractive for operation within the pharmaceutical industry, where multi-purpose hydrogenation vessels typically have a maximum pressure rating of 10 bar.[105] This argument however also suggests that this may lead to decreased stability of the complex when compared to Ru-MACHO (**1.44**), and indeed the conditions reported did employ significantly higher catalyst loadings when compared to Ru-MACHO (**1.44**). No comment was made by the authors on whether treatment of this complex with sodium borohyride results in a complex capable of base-free ester reductions analogous to Ru-MACHO-BH (**1.45**).

While these catalysts have been specifically developed for the purpose of catalytic ester reductions, various groups have published work in which these catalysts have been successfully applied to effect a variety of other transformations including dehydrogenative ester formation,[106] amide synthesis,[107] amide and lactam reductions,[85, 108] cyclopropanations,[109] cross coupling of secondary alcohols[110] and N-methylation of anilines[111] to name a few.

Since the disclosure of Ru-MACHO (**1.44**) a range of other ruthenium-based catalysts bearing tridentate ligands containing phosphorus, sulfur, nitrogen and carbenes have been reported by numerous other groups, and this has become a common motif within the field of homogeneous ester reductions.[80, 106, 112] The majority of these catalysts are operable under similar conditions and possess similar substrate scopes and limitations. Direct comparison of these catalysts based on available data within the patent and academic literature is, however, not trivial due to the differences in conditions employed, extent to which reactions have been optimised and other miscellaneous variables including purity of substrates and catalysts.

Gusev and co-workers investigated a series of ruthenium- and osmium-based catalysts for the purpose of ester reductions.[113-116] The most successful example, Ru-SNS (**1.54**) utilizes an SNS ligand in contrast to the PNP ligand seen on Ru-MACHO (**1.44**) (**Figure 13**).[112, 117]

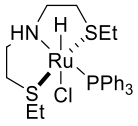

1.54

Figure 13 *Ru-SNS (**1.54**) catalyst reported by Gusev and co-workers.[112]*

It was reasoned that this would allow for hydrogenation catalysts to be accessed in a more practical and cost-effective manner owing to sulfur being both cheaper and less susceptible to oxidative degradation. Catalytic hydrogenation reactions were performed with THF or toluene as the solvent, rather than methanol as in the case of Ru-MACHO (**1.44**). Good activity was demonstrated for a variety of different substrates with low catalyst loadings. Remarkably, neat ethyl acetate underwent 95% conversion at a substrate/catalyst ratio of 40,000. This Ru-SNS catalyst (**1.54**) has since also been commercialised by Johnson Matthey. Applicability of this catalyst towards the pharmaceutical industry was demonstrated, whereby gem-difluoro ester (**1.55**), a compound reported in a medicinal chemistry patent published by Vertex was reduced to the corresponding alcohol (**1.56**).[118] Compared to a process employing stoichiometric hydride reagents,[119] the catalytic reduction offered a 72% reduction in the PMI (**Scheme 25**).

Previous process:

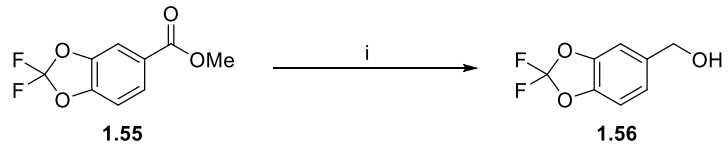

1.55 **1.56**

Reagents and conditions; (i) $NaBH_4$ or $LiAlH_4$, then quench and aqueous extraction.

	PMI
LAH process	91
Catalytic process	26
% Δ PMI	**–72%**

Catalytic process:

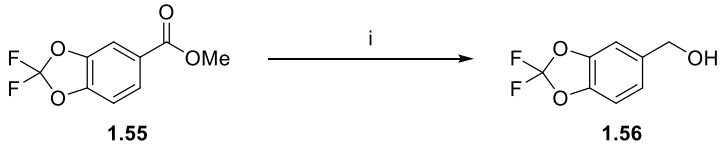

1.55 **1.56**

Reagents and conditions; (i) Ru-SNS (**1.54**), NaOEt, 30 bar H_2, THF, 40 °C, 16 h.

Scheme 25 *Comparison of stoichiometric and catalytic ester reduction processes.*[118]

The flavours & fragrances company, Givaudan have also reported their own hydrogenation catalyst (**1.57**) bearing and unsymmetrical SNP ligand.[120] As with the catalysts reported by Firmenich, the priority in their catalyst design was low catalyst loadings and good selectivity towards reducing esters in the presence of alkenes.

Of particular interest was the reduction of sclareolide (**1.58**) (itself derived from sclareol, a compound present in clary sage oil) to sclareodiol (**1.59**).[68] This is then subjected to acid mediated cyclisation to afford ambroxide (**1.60**), a valuable fragrance ingredient used to provide an amber note to perfumes. As naturally occurring ambroxide (**1.60**) found in ambergris which itself is secreted from whales is no longer used for this purpose, the need for a scalable and efficient chemical synthesis was necessary.[121] Catalytic reduction of sclareolide (**1.58**) to sclareodiol (**1.59**) was achieved in very high yields with catalyst loadings as low as 25 ppm (**Scheme 26**). This impressively low catalyst loading is pertinent in achieving a low cost of goods, as well as reducing the burden of the resulting waste streams.

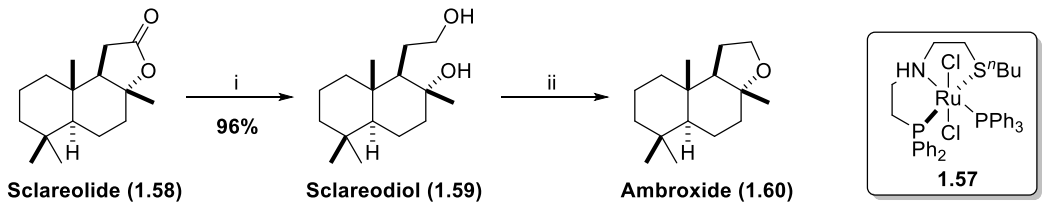

Sclareolide (1.58) **Sclareodiol (1.59)** **Ambroxide (1.60)**

Reagents and conditions; (i) 0.0025 mol% (**1.57**), H_2 (50 bar), toluene, 100 °C, 16 h;
(ii) acid mediated cyclisation.

Scheme 26 *Catalytic reduction of sclareolide (**1.58**) to sclareodiol (**1.59**) en route to ambroxide (**1.60**).*

1.1.4.3 Base Metal Catalysed Homogeneous Ester Hydrogenations

In an attempt to move away from catalysts based on precious metals, iron complex (**1.61**) reported simultaneously by Guan[122] and Beller[123] was reported to reduce a variety of esters under base-free conditions (**Table 8**).

Reagents and conditions; (i) 1 mol% Fe-PNP (**1.61**), 30 bar H_2, THF, 120 °C, 19 h.

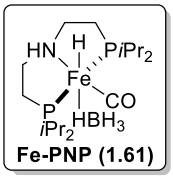

Entry	Ester	Product	Yield/%
1			89
2	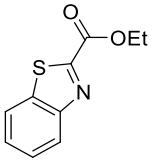	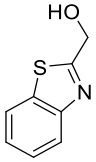	63
3	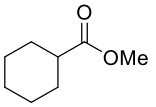	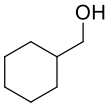	92
4	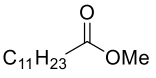	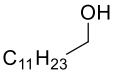	97
5	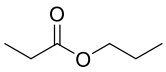		68

***Table 8** Fe-PNP complex (**1.61**) reported by Beller and co-workers.[123]*

As with the synthesis of Ru-MACHO-BH (**1.45**), this complex is generated by displacement of chloride ligands using sodium borohydride. Due to the sensitivity of the complex (**1.61**), synthesis and storage of the catalyst requires use of a glove-box and higher catalyst loadings were required when compared to precious metal counterparts such as Ru-MACHO (**1.44**).

Nonetheless, Fe-PNP (**1.61**) was demonstrated to effect the desired reduction under base free conditions. This point was highlighted by Guan and co-workers[8] who reasoned that the more robust ruthenium catalysts are currently more suited for industrial applications, though possible future directions of this field may see precious metals being replaced with cheaper and more abundant ones. Indeed, increased efforts have been put into base metal catalysis in order to discover novel catalytic activity.[124] From the perspective of the pharmaceutical industry, iron, in addition to low price and high availability also has the additional advantage of not being subject to the same tight limits as ruthenium due to its lower toxicity and is therefore of less concern in the manufacture of APIs.[125]

In relation to this, a study conducted by the British Geological Survey (BGS) ranked iron as having a relatively low supply risk index of 5.2 compared with the platinum group elements which have a higher supply risk index of 7.6 (1 representing a very low risk and 10 representing a very high risk). Their assessment was based on a number of factors including the rates of recycling and political stability of major producing countries.[126] Accordingly, avoiding the use of higher risk elements within a process in favour of low risk elements is desirable. Catalysis does, however, only represent a small proportion of the total consumption of ruthenium, and its high recyclability does mitigate this risk to an extent.

Continuing on the theme of using metals that are abundant in the Earth's crust, extensive studies using manganese-based catalysts has also been performed by Clarke and co-workers.[127]

In particular, it was demonstrated that using manganese catalyst (**1.62**), potassium carbonate was sufficient to promote catalytic activity (**Table 9**).[128] This is to be contrasted with the more usual strong alkoxide bases which are employed. In addition to the lower cost of goods, this approach has the advantage of suppressing racemisation of base-labile substrates, even at elevated temperatures.

Reagents and conditions; (i) 1 mol% Mn-PNN (**1.62**), 50 bar H_2, K_2CO_3, IPA, 50-110°C, 16 h.

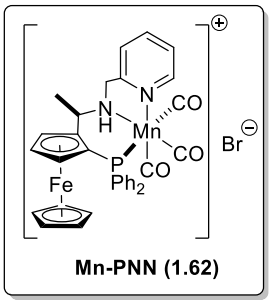

Mn-PNN (1.62)

Entry	Ester	Product	Δee/%	Yield/%
1	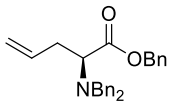	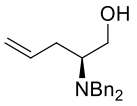	0	76
2	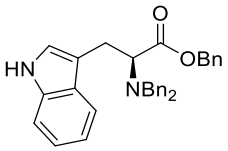	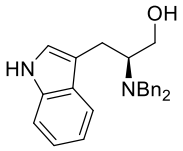	0	92
3	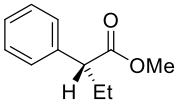	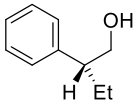	2	90
4	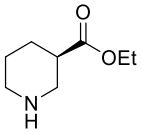	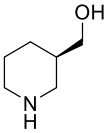	0	83

Table 9 *Catalytic reduction of optically active esters using a catalytic Mn-PNN (**1.62**) reported by Clarke and co-workers.*[128]

Other base-metal catalysts explored for the purpose of homogeneous ester reductions include examples based on cobalt,[129, 130] however, in the interests of brevity these will not be discussed further.

1.1.4.4 Mechanistic Considerations

A catalytic cycle for the reduction of methyl trifluoroacetate using Ru-MACHO (**1.44**) as the catalyst has been proposed by Dub and Ikariya[45, 100] (**Figure 14**). Calculations were performed using continuum methanol reaction field DFT analysis with the SMD (solvation model based

on density) of the hydrogenation of methyl trifluoroacetate. Methylating the NH unit of Ru-MACHO (**1.44**) results in near complete loss of catalytic activity,[98, 131] suggesting that this reduction also proceeds *via* an outer-sphere mechanism. Notably, this catalytic cycle does not involve formal cleavage of the N-H bond, but rather assists the reaction by means of formation of a strong hydrogen bonding interaction to the carbonyl oxygen.[101, 132, 133] Experimental evidence also confirmed activation of molecular hydrogen being accelerated by the presence of an alcohol acting as a proton shuttle compared to direct activation of hydrogen *via* a 4-membered transition state.[134, 135]

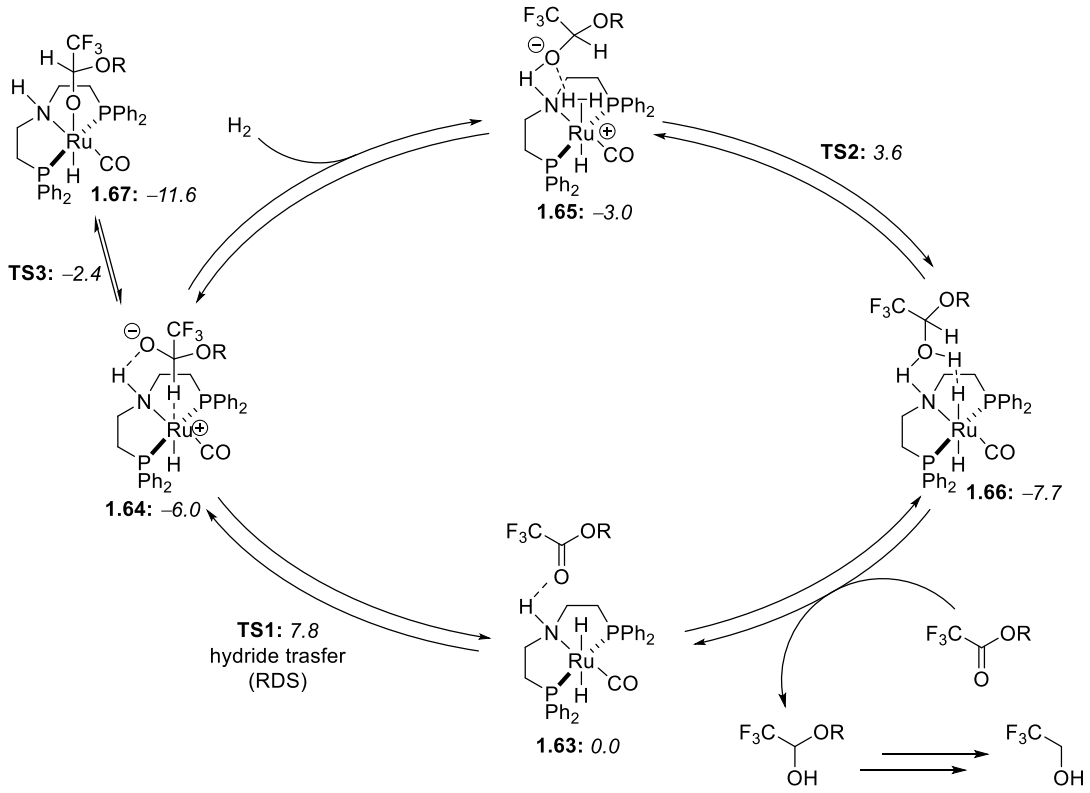

Figure 14 *Proposed catalytic cycle for the reduction of ester with Ru-MACHO (**1.44**). Free energies ($\Delta G°_{298K}$, kcal mol^{-1}) are calibrated relative to **1.63**.*

1.63 is formed from Ru-MACHO (**1.44**) after net addition of hydrogen and loss of HCl (promoted by the presence of NaOMe[136]). Though the catalytic cycle only depicts formation of a hemiacetal, this is able to eliminate to give the corresponding aldehyde, which itself is then reduced to give the alcohol. Due to the structural similarities between Ru-MACHO (**1.44**)

and Ru(PNP)Cl_2(NHC) (**1.51**), it is anticipated that the two follow a similar mechanistic pathway, albeit with different energy levels. As such the rate-determining step in this mechanism will later be revisited as a means of assessing how novel catalytic structures may perform.

1.1.5 Extension to Flow

Industrially, a longer-term goal is to investigate the possibility of transferring hydrogenations into flow reactors. The clear benefit of flow chemistry over traditional batch chemistry is the increased energy and mass transfer efficiency, which in turn leads to increased safety.[137] Though the reaction inventory is typically low in the context of flow chemistry, reactions are run continuously and may be run in parallel, and hence are more readily scalable. GSK has set ambitious sustainability goals which include having a net zero impact on climate, and net positive impact on nature by 2030. As part of realising these targets, reduction of waste, carbon emissions and water usage all play a critical role. Leveraging catalysis and enabling technologies such as continuous processing are as such preferred platforms that bring GSK as an organisation closer to achieving these goals.

Gas-liquid reactions have previously been demonstrated by Khan and co-workers in a segmented flow reactor.[138, 139] These operate by passing alternating “slugs” of liquid and gas phases through the reaction tubing (**Figure 15**). This allows for increased contact between the gas and liquid phases, which leads to increased reaction rates.

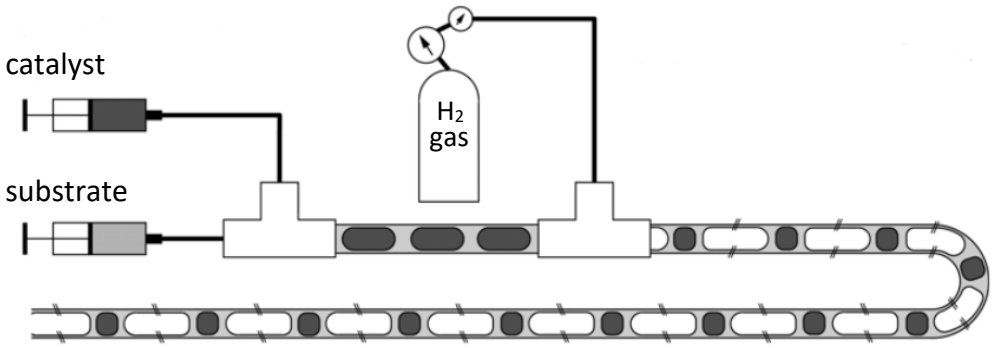

Figure 15 *Possible setup of segmented flow reactor.*[139, 140]

Aside from the advantage of increased reaction rate, this approach also allows measurement of the intrinsic reaction kinetics. Flow reactors of this nature, however, typically require homogeneous liquid phases and no solids to be present in order to avoid blockages.

The reduction of 2,2-difluoro-2-phenylacetate (**1.68**), an intermediate *en route* to a β-2-adrenergic receptor agonist (**1.70**) has previously been achieved using Ru-MACHO (**1.44**) under 20 bar of hydrogen enabled by use of a continuous flow reactor in the laboratory of Kappe and co-workers (**Scheme 27**).[141]

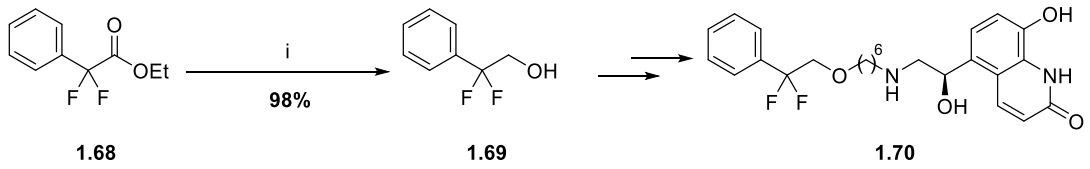

1.68 **1.69** **1.70**

Reagents and conditions; (i) Ru-MACHO (**1.44**) (0.065 mol%), NaOMe in MeOH (20 mol%), 20 bar H_2, MeOH, 60 °C, 70 min residence time, 6 hour run.

Scheme 27 *Reduction of 2,2-difluoro-2-phenylacetate (**1.68**) en route to API (**1.70**).*[141]

Initial screening work was performed in a batch autoclave. The optimised conditions transferred well into the segmented flow reactor by virtue of the relatively short reaction times required. Furthermore, the reaction solvent, methanol, allowed for formation of a homogeneous solution and no clogging or fouling was reported. Compared to LAH and $NaBH_4$ processes, an improved safety profile was noted due to the need of a quench being obviated,

as well as a significantly improved PMI. By running the reaction in flow through a stainless steel coil, 20 bar of hydrogen was readily attainable and the reaction benefited from superior gas-liquid contact provided by the segmented flow regime. The authors also note that 3.3 equivalents of hydrogen were supplied to the reaction. Compared to the 2 eq. of hydrogen theoretically required, this resulted in lower excesses of hydrogen being used compared to a typical batch process. High yields of product were obtained as well as a consistent composition of the product stream as was observed by in-line ^{19}F NMR. Excellent yields were obtained provided fresh methanol was used, with a 6 hour run furnishing 13.7 g of the product alcohol.

1.1.6 Summary of Literature

In summary, the area of catalytic ester hydrogenation has gained increased attention from both academic groups and various sectors of the chemical industry. Significant advancements have been made allowing these catalysts to operate broader substrate scopes under milder conditions. Catalytic ester reductions are at the point of gaining widespread industrial acceptance. This is clear from the increasing number of publications and patents which have been granted in this field.

Having stated this, further improvements will however be necessary in order to enable more widespread adoption of these catalysts, particularly within the pharmaceutical industry where the reduction of esters has remained for a long time a challenging transformation. At present, the majority of substrates examined are alkyl and aryl hydrocarbons, with very little other functionality. As such, it is instructive and essential that this transformation is demonstrated on more drug-like molecules and intermediates.[142] This will of course present additional challenges, as drug molecules are generally significantly more complex in comparison to the model substrates examined previously, or the bulk chemicals of interest to the flavour & fragrance industry.

Additionally, both low pressure and catalyst loading will be required in order to make these operationally more accessible within the pharmaceutical arena. Furthermore, the comparison of catalysts based on published data is non-trivial due to the different conditions employed, differing grades of reagents used and extent to which reactions have been optimised. There is however a strong drive to deliver such a catalyst, as processes involving molecular hydrogen are inherently desirable as a means of reducing the generation of waste and as a means of bringing companies such as GSK closer to achieving their sustainability goals.

1.2 AIMS AND OBJECTIVES

From consideration of all of the emerging studies discussed in the previous section, it is evident that catalytic hydrogenation of ester precursors is an important transformation in the context of the pharmaceutical industry. Accordingly, it is pertinent to undertake a systematic evaluation of such systems to fully understand their application and limitations when applied in a Chemical Development setting.

The initial goal of this investigation is to synthesise a palette of both known and novel hydrogenation catalysts, including $Ru(PNP)Cl_2(NHC)$ (**1.51**), and use these systems to demonstrate, initially, the catalytic reduction of simple esters (e.g. methyl benzoate (**1.52**)) under practical reaction conditions involving pressures below 10 bar. Following this, an optimised set of conditions and process understanding should be developed through use of high throughput screening and statistical design of experiments (DoE).

Furthermore, mechanistic insight and understanding of the reaction kinetics is to be generated using Process Analytical Technologies (PAT), and used to inform the feasibility of using continuous processing as an alternative method of running reactions.

Improved understanding of the functional group tolerances is also to be investigated, with a focus on substrates and functionality frequently encountered within pharmaceutical R&D. Once this has been achieved, the amenability of the reaction to scale-up is to be examined. The resulting processes will be compared with existing processing using traditional reduction methods. The longer-term goal of this investigation would be to examine running reductions in a continuous flow set-up. This would potentially bring a number of benefits including increased safety and ease of scale-up and accessibility, ultimately providing new knowledge and insight on the applicability of these catalyst systems in process research and development.

1.3 Results and Discussion

1.3.1 Computational Analysis of Transition Barrier

Prior to commencing experimental work, computational studies were conducted, in which the proposed rate determining step of the reduction of methyl trifluoroacetate (**1.46**) was examined as a function of different ligand substitutions (**Figure 16**). The aim was to obtain a preliminary indication of the feasibility of pursuing the synthesis of novel catalytically active complexes by comparing the TS barrier for systems proposed for synthesis with an established catalyst. The transition state investigated was analogous to that described by Dub, Ikariya and co-workers with the SMD methanol solvent model.[100] Investigation of tridentate SNS-type ligands was of particular interest, as prior work by Gusev and co-workers had demonstrated Ru-SNS complexes to provide superior activity compared with Ru-PNP analogues.

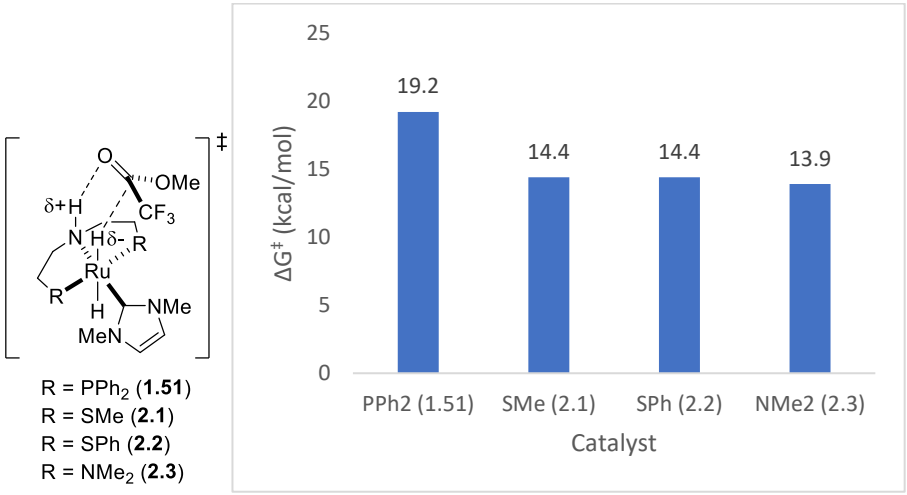

Figure 16 *Results from computational analysis examining TS barriers as a function of ligand substitution; calculations performed by Doo-Hyun Kwon (GSK).*

Interestingly, the results suggest that replacing the PNP ligand for SNS ligands results in a lowered energetic barrier (ΔG = 14.4 kcal/mol), and thus potentially more efficient catalysts. While an *in situ* synthesis of a Ru-SNS complex bearing a carbene ligand has previously been

suggested,[106] no subsequent characterisation was conducted to confirm whether such a complex had indeed been formed. Synthesising and examining such a complex as a well-defined species may offer improved catalytic activity. Also interestingly, introduction of a NNN ligand bearing methyl groups was suggested to lower the energetic barrier even further (ΔG = 13.9 kcal/mol), though to the best of our knowledge, no such complex has previously been reported.

Based on these results, the aim was to synthesise the known Ru(PNP)Cl_2(NHC) (**1.51**), in addition to novel Ru(SNS) catalysts (**2.1** and **2.2**) and Ru(NNN) catalyst (**2.3**) and to examine whether increased catalytic performance is indeed provided (**Scheme 28**).

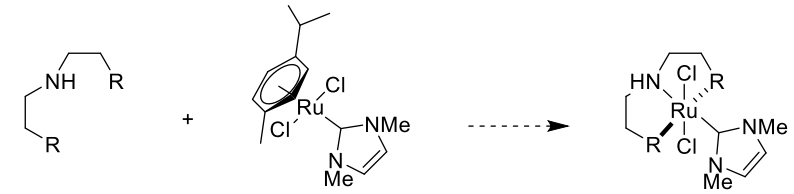

R = PPh_2 (**2.4**)
R = SEt (**2.5**)
R = SPh (**2.6**)
R = NMe_2 (**2.7**)

2.8

R = PPh_2 (**1.51**)
R = SEt (**2.1**)
R = SPh (**2.2**)
R = NMe_2 (**2.3**)

Scheme 28 *Proposed synthesis route of ruthenium catalysts bearing tridentate ligands and N-heterocyclic carbene ligand.*

1.3.2 Synthesis of Tridentate Ligands

With target complexes identified from the computational work above, attention then turned to the synthetic approaches to these systems, and these are outlined below with the initial focus on the preparation of the requisite ligands.

While bis(2-(diphenylphosphino)ethyl)amine hydrochloride (**2.4·HCl**) is commercially available, it was decided to synthesise this starting from alkyl dihalide (**2.8**) and diphenylphosphine (**Scheme 29**). Having familiarity with this process, particularly in relation to ambient stability would be advantageous, particularly when progressing with synthesis of non-commercially available analogues.

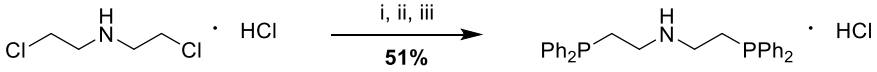

2.8·HCl **2.4·HCl**

Reagents and conditions; (i) KO*t*-Bu, THF; (ii) $PHPh_2$, reflux; (iii) $HCl_{(aq)}$.

Scheme 29 *Synthesis of bis(2-(diphenylphosphino)ethyl)amine hydrochloride (**2.4·HCl**).*

The procedure followed was adapted from literature,[143] and proceeded smoothly, albeit in modest yield (51%). While the free-base of PNP (**2.4**) is a highly viscous oil, the hydrochloride salt of PNP (**2.4·HCl**) is a crystalline solid. This allowed for both convenient purification by recrystallisation from acetonitrile, as well as facilitating long-term storage of this important intermediate.

The next step was to synthesise a series of SNS ligands. A SNS ligand bearing ethyl groups (**2.5**) was synthesised according to the procedure described by Schörgenhumer (**Scheme 30**).[1]

2.8·HCl **2.5** **2.9**

Reagents and conditions; (i) NaOH, MeOH; (ii) EtSH.

Scheme 30 *Synthesis of bis(2-(ethylthio)ethyl)amine (**2.5**).*

The desired product was obtained, but several impurities including the mono-alkylated product (**2.9**) and unreacted starting material (**2.8**) were also present. The reaction mixture was suspended in heptane and passed through basic alumina as suggested in the literature procedure, which removed some, but not all impurities. Neutral alumina was also tested but this proved to be inferior. Furthermore, the thiol reagent was not effectively purged, leading to the product being highly malodorous.

In order to make this reaction amenable to scale-up, chromatographic purifications were avoided. The crude product was treated with aqueous hydrochloric acid to generate the

corresponding hydrochloride salt (**2.5·HCl**), an off-white powder as opposed to a yellow oil (**Scheme 31**).

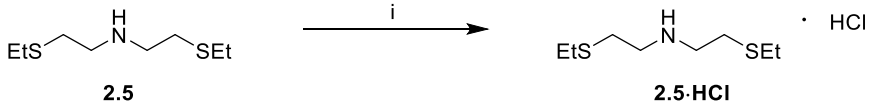

Reagents and conditions; (i) $HCl_{(aq)}$.

Scheme 31 *Synthesis of bis(2-(ethylthio)ethyl)amine hydrochloride (**2.5·HCl**).*

This salt (**2.5·HCl**) was found to be sparingly soluble in toluene at room temperature, but highly soluble in boiling toluene. As such the product (**2.5·HCl**) was recrystallised from toluene and washed with heptane. In addition to the improved purity profile, this approach also facilitated handling and storage. The heptane washes removed any remaining traces of unreacted ethanethiol giving product free of any odour. The starting material, bis(2-chloroethyl)amine (**2.8·HCl**), however did not purge under these conditions and tracked through the process. This was overcome using a larger excess of ethanethiol and extending reaction times and thereby ensuring complete consumption of the starting material (**2.8**).

This approach was found to be generally applicable to generate three related SNS ligands in multi-gram quantities (**Scheme 32**).

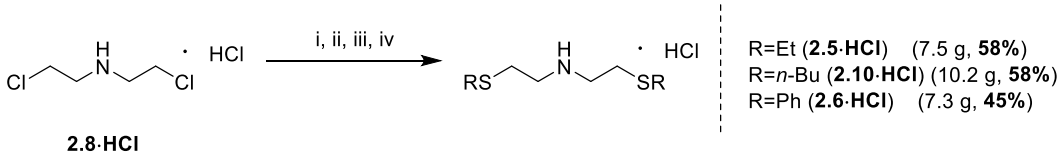

Reagents and conditions; (i) NaOH, MeOH; (ii) RSH; (iii) HCl(aq); (iv) toluene recrystallisation.

Scheme 32 *Synthesis of SNS ligands.*

Having generated a sufficient quantity of the ligands of interest, these could now be bound to ruthenium to afford the desired catalysts on large scale if necessary.

1.3.3 Synthesis of Ruthenium Catalysts

With a focused set of PNP and SNS ligands successfully generated, the following step was used to generate a series of hydrogenation catalysts, starting with hydrogenation catalyst (**1.51**) previously reported by Kayaki (**Scheme 33**).[104]

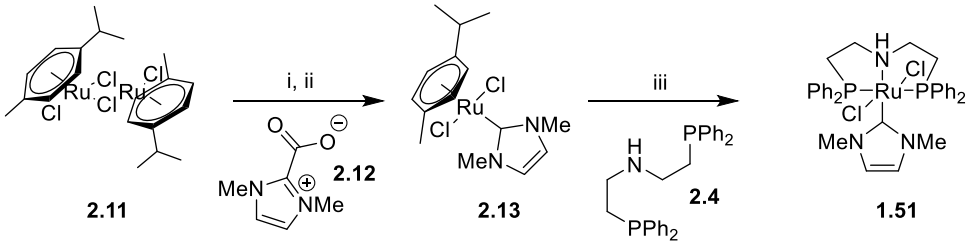

Reagents and conditions; (i) NHC precursor (**2.12**), THF, reflux; (ii) IPA reflux; (iii) PNP (**2.4**), EtOH.

Scheme 33 *Synthesis of hydrogenation catalyst (**1.51**) as described by Kayaki and co-workers.*[104]

The preparation of Ru(*p*-cymene)Cl_2(NHC) (**1.51**) starting from commercially available dichloro(*p*-cymene)ruthenium(II) dimer (**2.11**) was initially attempted (**Table 10**). Despite appearing to be a relatively simple transformation, it proved to be more challenging than expected. Due to the sensitive nature of these compounds, reactions were kept free of oxygen, and anhydrous solvents were used. Initially, the procedure was followed as described by Kayaki (**Table 10, entry 1**),[104] but only trace amounts of product were isolated. The low mass recovery prompted further investigation. The supernatant solution was concentrated and analysed by ^{1}H NMR, which revealed additional product to be present as well as numerous unidentified side products.

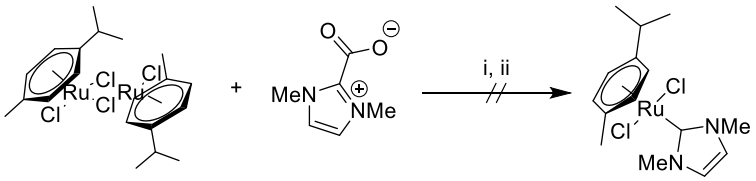

2.11 **2.12** **2.13**

Reagents and conditions; (i) THF, reflux, 4 h; (ii) IPA, reflux, 10 mins.

Entry	Modifications to procedure	Outcome
1	Literature procedure followed	Traces of product (**2.13**) isolated
2	Reaction run for 16 h	Complex mixture obtained
3	Addition of IPA omitted	Complex mixture obtained

Table 10 *Attempted formation of Ru(p-cymene)Cl_2(NHC) (**2.13**).*

Further analysis revealed that the reaction had not gone to completion, and thus the reaction was run overnight (**Table 10, entry 2**). This, however, did not appear to improve the outcome, and again a complex mixture was obtained. Finally, the role of adding IPA was scrutinised. While the reaction mixture itself was a suspension in THF, addition of IPA appeared to cause all the contents to dissolve and turn from red to black. It was suggested that the IPA could indeed be causing undesired side reactions and possibly be contributing to the low mass recovery. Consequently, the reaction was reattempted, with the addition of IPA omitted (**Table 10, entry 3**). While this did lead to a mass recovery commensurate with what was expected, analysis of this also showed it to be a complex mixture, containing the desired product (**2.13**).

Having failed to obtain Ru(*p*-cymene)Cl_2(NHC) (**2.13**) in acceptable yield, and with no obvious method to purify the complex mixtures obtained, an alternative method to generate the desired complex was therefore sought. This resulted in considering the use of NHC complexes of silver(I) in place of 1,3-dimethylimidazolium-2-carboxylate (**2.12**) as the carbene transfer reagent. These reagents are commonly used, as they offer a number of advantages, including ease of preparation, stability towards both air and moisture, and the ability to undergo transmetallations even at room temperature.[144]

Though not commercially available, Ag(NHC) complex (**2.15**) is conveniently formed in one step. Following a literature procedure,[145] 1,3-dimethylimidazolium iodide (**2.14**) was deprotonated using silver(I) oxide as a base (**Scheme 34**) to afford Ag(NHC) complex (**2.15**).

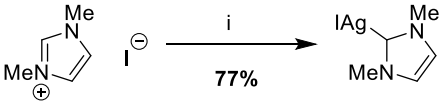

2.14 **2.15**

Reagents and conditions; (i) Ag_2O, CH_2Cl_2, 55 °C.

Scheme 34 *Preparation of Ag(NHC) complex (**2.15**).*

The reaction proceeded to give the desired product (**2.15**) in good yield. Its remarkable stability was further demonstrated as the Ag(NHC) complex (**2.15**) was recrystallized from hot DMSO without the requirement for an inert atmosphere. This procedure was easily scalable to 17 g with an additional hot filtration being necessary to remove unreacted silver(I) oxide.

With the silver carbene transfer reagent (**2.15**) in hand, the next stage was to demonstrate its applicability towards the desired transmetallation. Following a literature procedure,[146] ruthenium dimer (**2.11**) and Ag(NHC) complex (**2.15**) were combined and stirred at room temperature (**Scheme 35**). The AgI generated as a side-product was easily removed by filtration under an atmosphere of nitrogen.

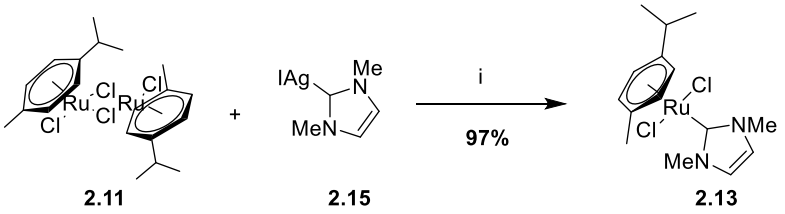

2.11 **2.15** **2.13**

Reagents and conditions; (i) CH_2Cl_2, rt.

Scheme 35 *Preparation of Ru(p-cymene)Cl_2(NHC) complex (**2.13**).*

Pleasingly, the reaction proceeded to give analytically pure product (**2.13**) in high yield, without the requirement for further purification.

Having prepared the Ru(*p*-cymene)Cl_2(NHC) complex (**2.13**), the final stage required substitution of the *p*-cymene ligand with a series of tridentate ligands. In the first instance bis(2-(diphenylphosphino)ethyl)amine (**2.4**) was examined. The literature procedure suggested stirring the hydrochloride salt of the PNP ligand (**2.4·HCl**) in toluene and aqueous sodium hydroxide to generate the free-base.[104] It was determined, however, that the crystalline PNP·HCl (**2.4·HCl**) only dissolved in toluene after continuous sonication for 1 h. Thus after the same procedure was repeated using a variety of common solvents, it was found that dichloromethane promoted must faster dissolution of the salt. The disappearance of the 2H singlet at δ_H 9.92 ppm (corresponding to the NH_2 of the protonated ammonium salt) and appearance of a broad 1H singlet at around δ_H 1.4 ppm (corresponding to the NH of the free amine) in the ^{1}H NMR confirmed that the free-base had been formed.

Heating ruthenium complex (**2.13**) with the free-base PNP ligand (**2.4**) in ethanol smoothly afforded the desired product, provided that particular care was taken in ensuring equimolar stoichiometry **(Scheme 36)**.

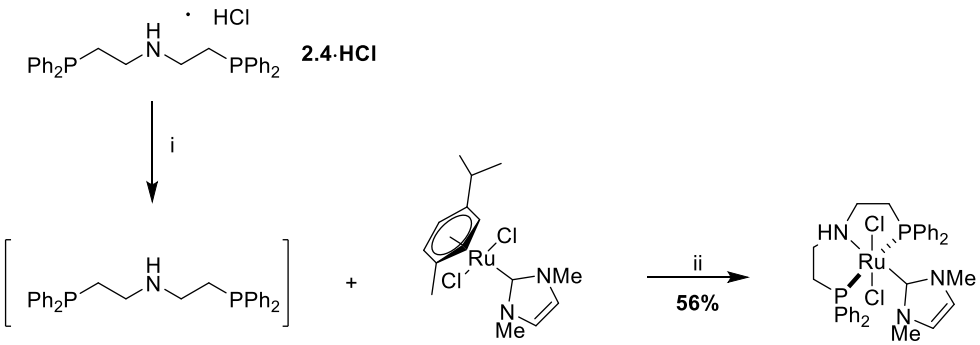

Reagents and conditions; (i) $NaOH_{(aq)}$, CH_2Cl_2; (ii) EtOH, 80 °C.

Scheme 36 *Ligation of PNP ligand (**2.4**) to ruthenium centre to afford ruthenium complex (**1.51**).*

The product (**1.51**) was washed with heptane and ethyl acetate to ensure complete removal of *p*-cymene, the stoichiometric side-product. The reaction itself was also conveniently monitored by ^{31}P{^{1}H} NMR. Disappearance of the signal at δ_P –21 ppm and appearance of a new signal at δ_P 43 ppm indicated the reaction had gone to completion (**Figure 17**).

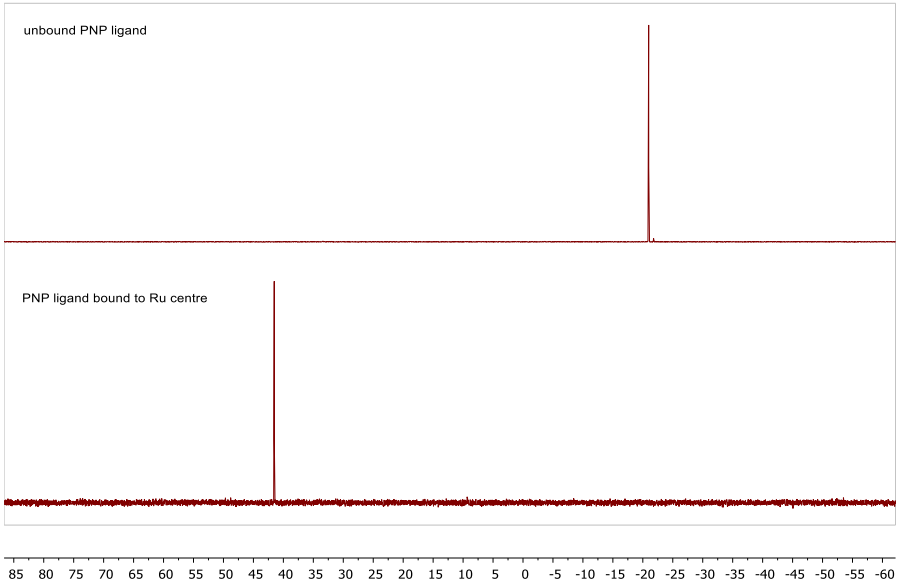

Figure 17 *Comparison of ^{31}P chemical shift of bound and unbound PNP ligand (**2.4**).*

This large difference in chemical shift between the unbound ligand and the ligand coordinated to the ruthenium centre is typically observed in complexes of this type.[147] This suggests strong sigma donation from the phosphorus atom into the ruthenium centre to be taking place.

In contrast to silver(I) carbene complex (**2.15**), and Ru(*p*-cymene)Cl_2(NHC) (**2.13**), the two methyl groups in Ru(PNP)Cl_2(NHC) (**1.51**) gave rise to different signals in the ^1H NMR. This suggests that in the solution state, Ru(PNP)Cl_2(NHC) (**1.51**) is not as symmetrical as inferred from their structures. It should also be noted that Ru(*p*-cymene)Cl_2(NHC) (**2.13**) and Ru(PNP)Cl_2(NHC) (**1.51**) are relatively stable to air as dry isolated solids and exist as orange and yellow powders, respectively. When dissolved however, any exposure of the solution to air results in rapid degradation of the complexes, as evident from the accompanying colour change to black. This approach for generating Ru(PNP)Cl_2(NHC) (**1.51**) was shown to be scalable and was used to generate gram quantities of the catalyst through employing this modified method.

Following on from this, the aim was to bind SNS ligands to a ruthenium centre using a similar approach as used above to generate a series of novel complexes (**Scheme 37**).[1]

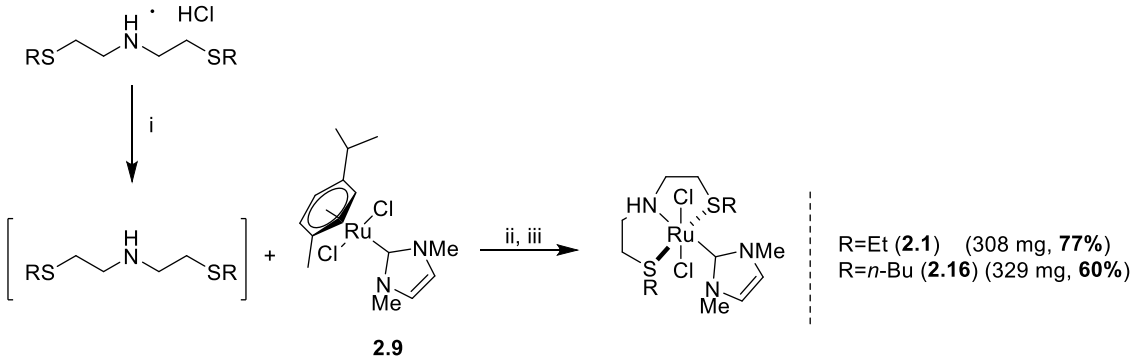

2.9

Reagents and conditions; (i) $NaOH_{(aq)}$, CH_2Cl_2; (ii) EtOH, 70 °C; (iii) heptane washes.

Scheme 37 *Ligation of SNS ligands to ruthenium to afford corresponding complexes.*

This approach proved to be effective for the diEtSNS (**2.5**) and di*n*-BuSNS (**2.10**) ligands where full consumption of starting material was observed. The desired products were precipitated out of solution by addition of heptane, and the liquid phase containing excess SNS ligand and the side-product *p*-cymene was removed using a filtered cannula. Further heptane washes and careful drying under vacuum afforded the desired products as air-stable, free-flowing powders in moderate to good yield and good purity by ^{1}H and ^{13}C NMR.

Binding of the diPhSNS ligand (**2.6**) to ruthenium in contrast was a more challenging task. Multiple attempts were made using varying quantities of diPhSNS (**2.6**) (**Table 11**), mostly unsuccessfully. The primary issue stemmed from reactions not going to completion, presumably due to the increased steric bulk around the sulfur atoms – a surprise given this was not an issue with the seemingly sterically more congested PNP ligand (**2.4**). This led to complications as the starting material and product complexes are not readily separable from each other. In contrast to the diEtSNS (**2.5**) and di*n*-BuSNS (**2.10**) ligands, a significant excess of the diPhSNS ligand (**2.6**) was required for reactions to reach acceptable conversions. Addition of 4 equivalents of ligand (**2.6**) and stirring the reaction for 3 days resulted in the highest yield (41%) of complex (**2.2**) and good purity by ^{1}H and ^{13}C NMR. Addition of heptane induced precipitation of the product, while excess ligand remained in solution, thereby allowing for convenient separation of the product, again using a filtered cannula.

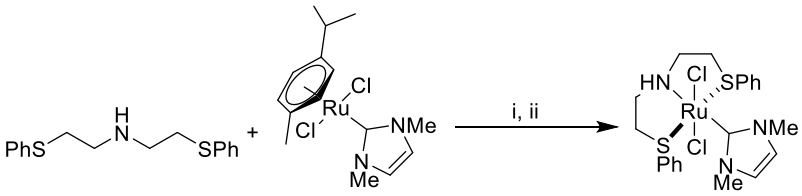

2.6 **2.13** **2.2**

Reagents and conditions; (i) EtOH, 70 °C; (ii) heptane washes.

Method employed	Outcome
1.0 eq. of diPhSNS ligand (**2.6**) added	mixture of SM (**2.13**) and product (**2.2**)
1.5 eq. of diPhSNS ligand (**2.6**) added	mixture of SM (**2.13**) and product (**2.2**)
3.0 eq. of diPhSNS ligand (**2.6**) added	< 40% yield (impurities present)
4.0 eq. of diPhSNS ligand (**2.6**) *added*	*41% isolated product* (**2.2**)

Table 11 *Optimisation of formation of Ru(diPhSNS)Cl₂(NHC) (**2.2**)*

Unlike in Ru(PNP)Cl_2(NHC) (**1.51**), the two methyl groups on the carbene ligand of Ru(diEtSNS)Cl_2(NHC) (**2.1**) gave rise to one broad singlet as opposed to two sharper singlets. This prompted further investigation using VT NMR experiments (**Figure 18**). When cooled down to 0 °C, the carbene ligand on Ru(diEtSNS)Cl_2(NHC) (**2.1**) gave two distinct signals, and when heated to 50 °C, the broad singlet sharpened.

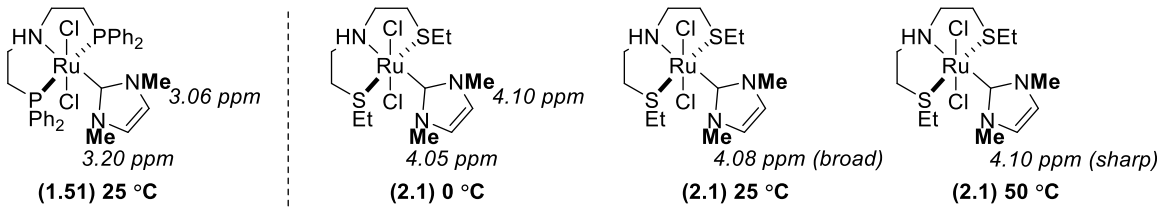

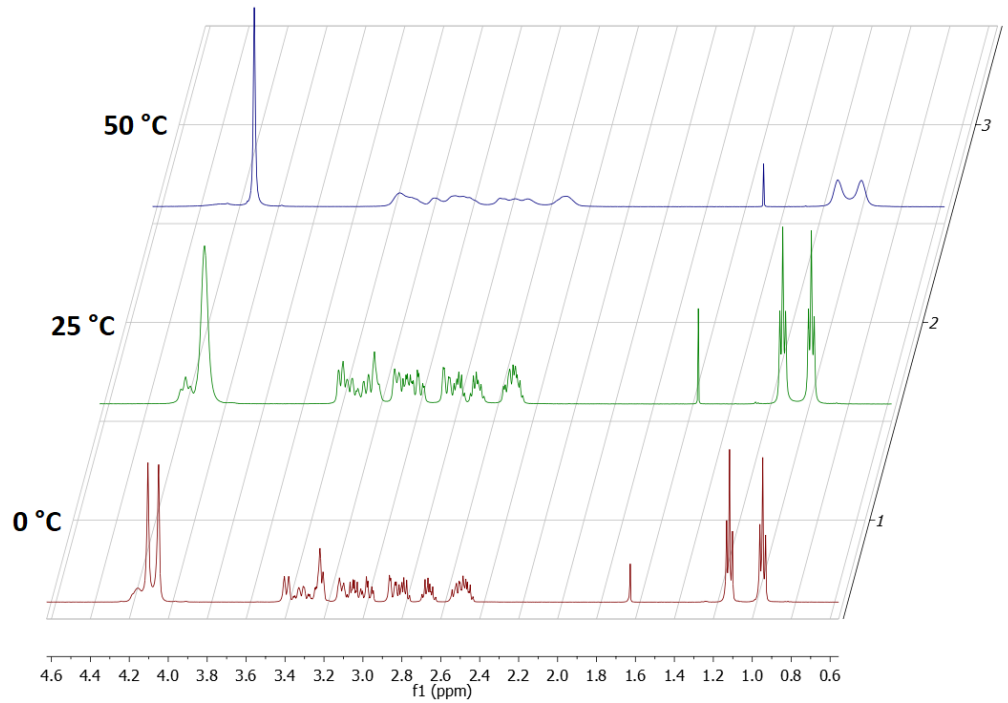

Figure 18 *Variable temperature NMR experiment performed on Ru(diEtSNS)Cl$_2$(NHC) (**2.1**).*

Meridional geometry of the ligand around the ruthenium centre was also confirmed by means of an X-ray crystal structure (**Figure 19**). Crystals suitable for X-ray diffraction were obtained by allowing slow diffusion of heptane into a solution of the complex (**2.1**) dissolved in DCM under a nitrogen atmosphere.

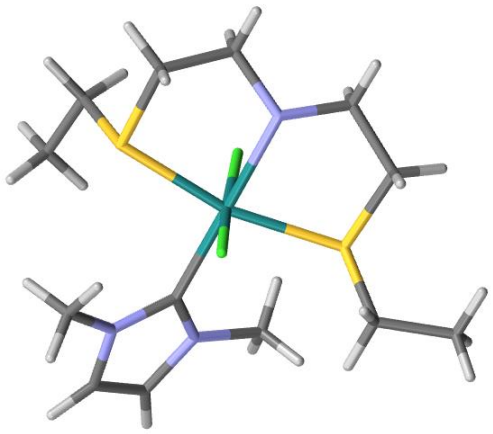

Figure 19 *X-ray crystal structure of Ru(diEtSNS)Cl$_2$(NHC) (**2.1**).*

The synthesis of Ru(NNN) (**2.3**) was also of particular interest as the computational studies predicted this to provide the lowest energy transition barrier with respect to ester reduction reactions. NNN (**2.7**) ligand which is commercially available (an added benefit to this class) was heated with ruthenium complex (**2.13**) in ethanol (**Table 12**).

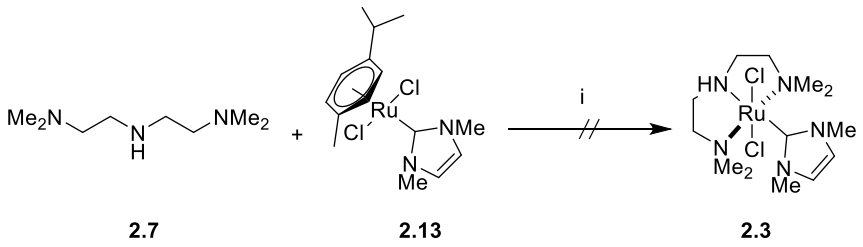

2.7 **2.13** **2.3**

Reagents and conditions; (i) EtOH, 70 °C.

Method employed	Outcome
1.2 eq. of NNN ligand (**2.7**) added	complex mixture containing starting material
2.8 eq. of NNN ligand (**2.7**) added	complex mixture containing starting material
4.9 eq. of NNN ligand (**2.7**) added	complex mixture containing starting material

Table 12 *Attempted synthesis of Ru(NNN) complex (**2.3**).*

No clean conversion was observed in any of these experiments. During the third attempt the mixture was initially left to stir at room temperature at which point mainly starting material was observed, as was clear by the aromatic protons on the *p*-cymene ligand. The mixture was gradually heated, at which point new peaks started to form suggesting some kind of ligation process was taking place, though the presence of starting material (**2.13**) was still noted. Addition of heptane did not, however, cause any precipitation as was the case with the Ru(SNS) series. The mixture was concentrated to dryness, however, analysis of the residue showed an intractable mixture. Consequently, this approach was not pursued further.

Future work in accessing Ru(NNN) complex (**2.3**) would require investigation around the apparent reluctance of NNN ligand (**2.7**) to bind to ruthenium by substitution of *p*-cymene. This could be addressed by investigation of alternative solvents to run this reaction in. Higher boiling solvents such as 1-butanol or toluene may allow reactions to be heated sufficiently to allow the desired substitution process to take place.

1.3.4 Synthesis of Modified Catalyst (2.17)

Previous reports have shown that Ru-MACHO-BH (**1.45**), a modified version of Ru-MACHO (**1.44**) is capable of performing base-free ester reductions (**Scheme 38**)[98] This is an attractive prospect as it simplifies both the reaction setup and subsequent work-up. Additionally, this also allows for substrates prone to racemisation under basic conditions to be reduced.

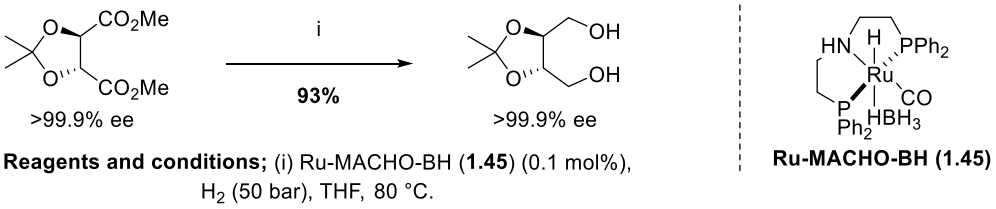

Scheme 38 *Base-free reduction of chiral diester using Ru-MACHO-BH (**1.45**).*

The key shortcoming of Ru-MACHO-BH (**1.45**), however, is the need for high pressures of hydrogen gas (50 bar). In this case the possibility of synthesising a modified version of Ru(PNP)Cl_2(NHC) (**1.51**) which would retain the ability to perform reductions at low pressures of hydrogen, but also to do so without requiring the addition of base was envisaged (**Scheme 39**).

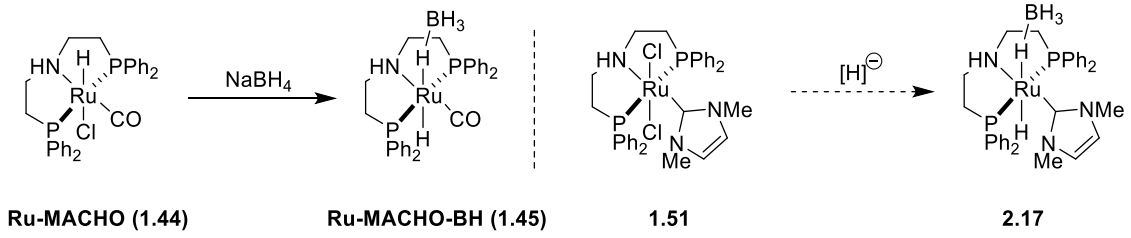

Scheme 39 *Generation of modifed catalysts by reduction using metal hydride reagents.*

Ru-MACHO-BH (**1.45**) is obtained through subjecting Ru-MACHO (**1.44**) to treatment with sodium borohydride. The aim was to treat Ru(PNP)Cl_2(NHC) (**1.51**) with sodium borohydride

in an analogous manner to displace the chloride ligands. Initially this was attempted with sodium borohydride in ethanol (**Figure 20**).

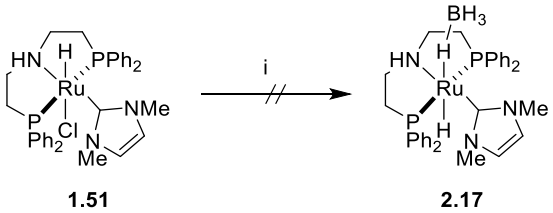

Reagents and conditions; (i) $NaBH_4$, EtOH, rt.

Figure 20 *Subjection of Ru(PNP)Cl$_2$(NHC) (**1.51**) to sodium borohydride in ethanol.*

This however did not give the desired product (**2.17**), as was evident by the lack of metal hydride signals within the ^{1}H NMR spectrum. It was thought that the high basicity of the Ru-H bond may result in reactivity with the ethanol solvent. As such, the solvent was changed to THF, an aprotic solvent. The reducing agent, sodium borohydride was also replaced with lithium borohydride (**Scheme 40**).

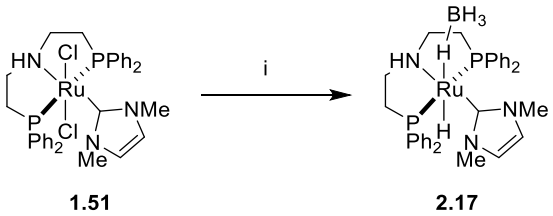

Reagents and conditions; (i) $LiBH_4$, THF, rt.

Scheme 40 *Subjection of Ru(PNP)Cl$_2$(NHC) (**1.51**) to lithium borohydride in THF.*

It was reasoned that lithium chloride, the by-product of the reaction having a higher lattice enthalpy than sodium chloride would provide a stronger driving force for the reaction. The reaction was initially set up in an NMR tube using an excess of lithium borohydride. The diagnostic hydride signal was observed as a triplet at –16.06 ppm, suggesting that the desired reaction had taken place (**Scheme 41**).

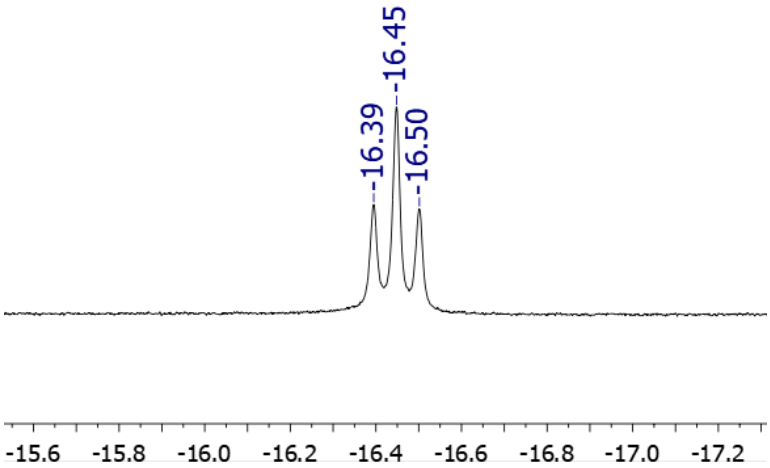

Scheme 41 *Diagnostic signal present in ^{1}H NMR spectrum suggesting successful formation of modified catalyst (**2.17**).*

Encouraged by these results, the reaction was performed on a larger scale. Attempts were then made to isolate the desired ruthenium hydride complex (**2.17**) by removal of the solvent. Doing so, however, led to decomposition of the complex. It was thus thought that the complex (**2.17**) could be generated *in situ* and used to reduce an ester. The complex (**2.17**) was generated and in a glove box the complex was added to a vessel containing methyl 2-naphthoate (**2.18**) in 2-MeTHF. The mixture was then transferred into a hydrogenation vessel and subjected to hydrogen and heated (**Scheme 42**).

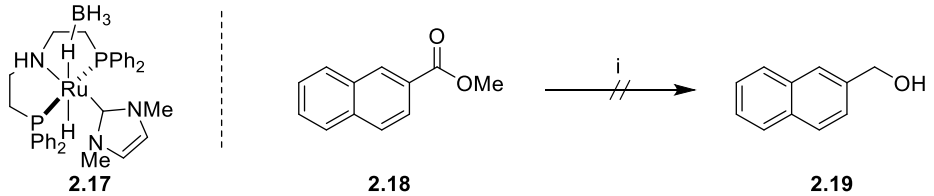

2.17 **2.18** **2.19**

Reagents and conditions; (i) 2 mol% **2.17**, H_2 (5 barg), THF, 45 °C.

Scheme 42 *Treatment of methyl 2-naphthoate (**2.18**) with modified catalyst (**2.17**) and hydrogen.*

No ester reduction was observed under these conditions. It was postulated that the BH_4 moiety may not have dissociated, and more forcing conditions were required. As such, the reaction mixture was heated to 90 °C. This too, however, did not lead to any measured gas-uptake or reduction of the ester. At this stage it became clear that while the possibility of base-free reductions using mild hydrogen pressures may not be ruled out, this would likely not bring the benefit of a simplified setup as was initially anticipated. As such, this approach was not pursued further as it is likely not to be compatible for applications in a Chemical Development setting.

1.3.5 *In situ* Generation of Catalytically Active Species (2.20)

The catalytically active complex in the case of related hydrogenation catalysts is typically shown to be a ruthenium dihydride complex.[45, 148] However, this has not been formally reported in the case of Ru(PNP)Cl_2(NHC) (**1.51**). Preparation of such a complex would be of interest as a means of gaining mechanistic insight into the process. Accordingly, the complex (**2.20**) was prepared in an NMR tube by mixing the pre-catalyst, Ru(PNP)Cl_2(NHC) (**1.51**) with potassium *tert*-butoxide and deuterated THF, and exposing this to hydrogen using a balloon and a septum (**Scheme 43**).

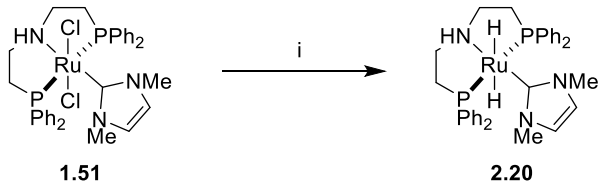

1.51 **2.20**

Reagents and conditions; (i) hydrogen (balloon), KO*t*-Bu, THF-d_8.

Scheme 43 *Formation of ruthenium dihydride complex (**2.20**).*

A single new compound could be observed by ^{31}P NMR provided great care was taken to exclude ingress of oxygen. The ^{1}H NMR also strongly suggested the complex (**2.20**) above to have been formed as evident by the presence of two hydridic peaks [δ = –7.33 (td, *J* = 21.0, 9.5 Hz), –7.71 (td, *J* = 21.0, 9.5 Hz)] (**Figure 21**). Both the chemical shift values as well as the

coupling constants were comparable to those of related ruthenium complexes previously reported.[148]

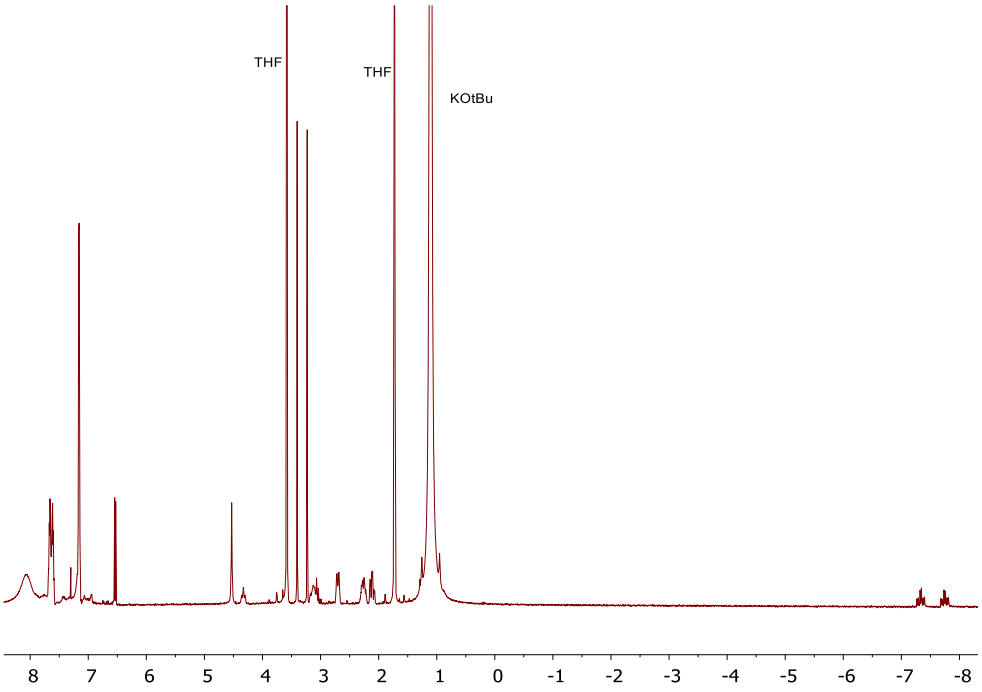

Figure 21 *^{1}H NMR spectrum of ruthenium dihydride complex (**2.20**).*

Due, however, to the highly air sensitive nature of this, isolation and further characterisation was unfeasible. Exposure to even small quantities of air resulted in an increase to more than 10 different signals as determined by ^{31}P NMR (**Figure 22**)

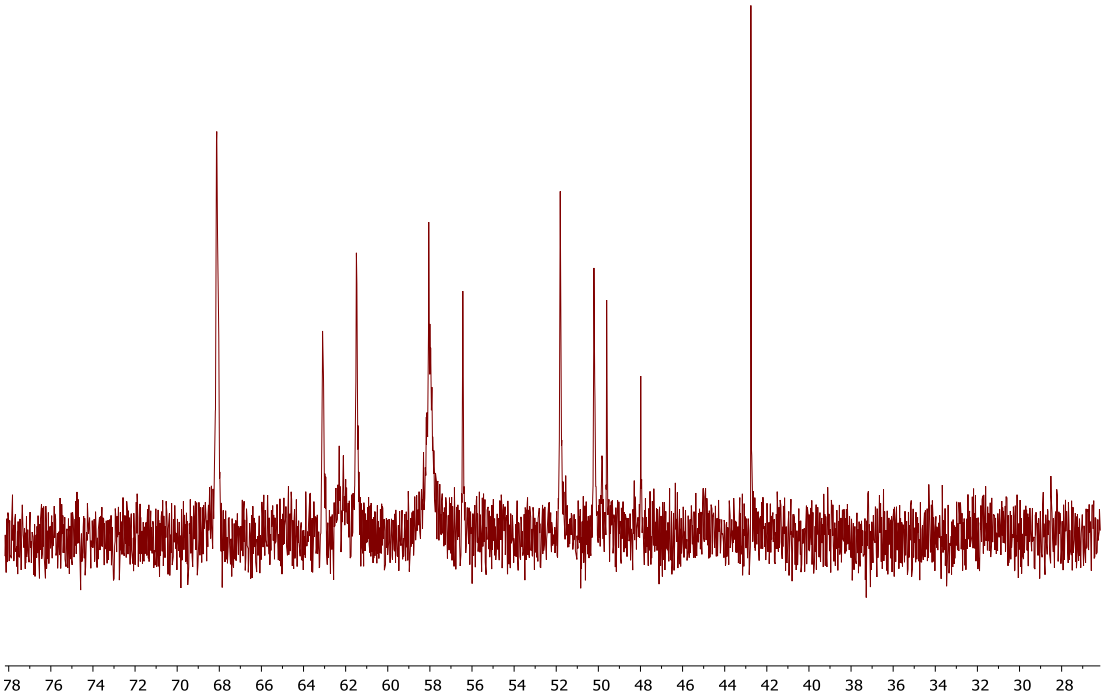

Figure 22 *^{31}P NMR spectrum of mixture of hydride containing species following isolation efforts.*

This result strongly suggests that conversion of Ru(PNP)Cl_2(NHC) (**1.51**) to dihydride complex (**2.20**) is an important transformation in order to achieve catalytic activity. The data also stresses the importance of rigorous purging cycles to be performed, as the presence of oxygen has been shown to result in rapid degradation of dihydride complex (**2.20**) to an intractable, poorly defined mixture.

In summary, four ruthenium complexes (**1.51, 2.1, 2.2** and **2.16**) have been successfully synthesised, including three novel Ru(SNS) complexes (**2.1, 2.2** and **2.16**). It has also been demonstrated that subjecting Ru(PNP)Cl_2(NHC) (**1.51**) to hydrogen and base results in the formation of a ruthenium hydride complex (**2.20**) which is likely the catalytically active species.[45] Attempts to generate a complex pre-reduced with borohydride (**2.17**) initially showed promise, and appeared to be stable in solution. This approach was ultimately abandoned, however, due to instability of the complex in addition to the lack of activity with respect to catalytic ester reductions in the absence of base.

1.3.6 Catalytic Reduction of Methyl Benzoate (1.52)

With Ru(PNP)Cl_2(NHC) (**1.51**) in hand the next stage was to attempt to reproduce the work previously reported[104] by reducing methyl benzoate (**1.52**) to benzyl alcohol (**1.53**) using a balloon of hydrogen (**Scheme 44**). Initial experiments delivered highly variable results, with differing levels of conversion observed and in some cases no product formation detected at all. Reactions were also particularly prone to stalling when air was inadvertently introduced into the Schlenk flask, as would be expected with air sensitive metal complexes of this class.

1.52 **1.53**

Reagents and conditions; (i) 2.6 mol% Ru(PNP)Cl_2(NHC) (**1.51**), 20 mol% KO*t*-Bu, H_2 (balloon), THF, 50 °C.

Scheme 44 *Reduction of methyl benzoate using Ru(PNP)Cl_2(NHC) (**1.51**).*

In one particular example, a higher catalyst loading of 2.6 mol% was used and the reaction proceeded smoothly to completion. After working up and purifying the mixture by flash column chromatography, pure benzyl alcohol (**1.53**) was obtained, albeit in modest yield (31%). This is markedly lower than the 90% yield previously reported[104] and may be in part due to formation of various side-products being formed (likely benzyl benzoate based on previous reports, though not formally characterised in this instance) and in part due to mechanical losses of the relatively volatile product, benzyl alcohol (**1.53**). Despite this discrepancy, it was established that the reduction of methyl benzoate (**1.52**) under an atmosphere of hydrogen is indeed achievable in our own hands.

1.3.7 Catalytic Reduction of Methyl 2-Naphthoate (2.18)

With this proof of principle in hand, the decision was made to move away from using a Schlenk flask and a balloon to run hydrogenation reactions. While operationally simple, the

disadvantage of this approach was the lack of control over the pressure of hydrogen being applied, and the difficulty in monitoring the progress of the reaction. Thus it was decided to perform subsequent reductions in a Biotage Endeavor, a multi-vessel reactor capable of controlling temperature, pressure and stirring while simultaneously measuring gas uptake, thus allowing us to infer the progress of the reaction (**Figure 23**).

Figure 23 *Biotage Endeavor.*

Furthermore, reactions are performed in disposable glass vials, thus minimising the chance of obtaining anomalous results due to contaminated equipment, and automated purging cycles ensure adequate inerting to avoid air-induced degradation of the catalyst.

In order to overcome the issue of losses due to evaporation of the relatively volatile benzyl alcohol (**1.53**), the decision was made to perform screening experiments on methyl 2-naphthoate (**2.18**). In addition to the simplified handling by virtue of being a solid, the high absorbance in the UV region of both methyl 2-naphthoate (**2.18**) and the corresponding alcohol, naphthalen-2-yl methanol (**2.19**), at 220 nm would allow for the reaction mixtures to be conveniently analysed by HPLC.

The reduction of methyl 2-naphthoate (**2.18**) was performed in a Biotage Endeavor (**Scheme 45**).

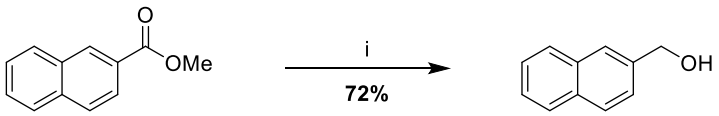

2.18 **2.19**

Reagents and conditions; (i) 2 mol% Ru(PNP)Cl_2(NHC) **(1.51)**, 20 mol% KO*t*-Bu, 2 bar H_2, THF, 40 °C, 3 h.

Scheme 45 *Reduction of methyl 2-naphthoate (**2.18**) performed in a Biotage Endeavor.*

The reaction proceeded smoothly, and following flash column chromatography, naphthalen-2-yl methanol (**2.19**) was obtained in good yield (72%). The reaction mixtures themselves were beige coloured suspensions, which immediately darkened upon being removed from Endeavor and being exposed to air, suggesting degradation of the ruthenium complex was taking place, consistent with previous observations. Running the reaction using ammonium formate in the place of hydrogen resulted in no conversion. While transfer hydrogenations have previously been explored, typically using an alcohol such as ethanol as the reducing agent, these will not be considered here, due to the known issue of forming mixtures and difficulty driving reactions to completion.[149]

Following this, the same reaction was performed at 30 °C and 50 °C, and the gas uptake data measured by the instrument over the course of the three experiments were overlaid (**Figure 24**). It should be noted that the data obtained has been normalised, such that all curves plateau at 100% of the measured gas uptake. The quantity of hydrogen uptake measured varied by ~±40% between the various trials, despite having employed the same quantity of methyl 2-naphthoate (**2.18**) in each case. This deviation from the actual amount of gas consumed is likely to be a machine artefact arising from the way the gas uptake is measured by the instrument. As such the data obtained is qualitative, rather than quantitative in nature at this scale, however, it can be used to facilitate comparison between individual runs.

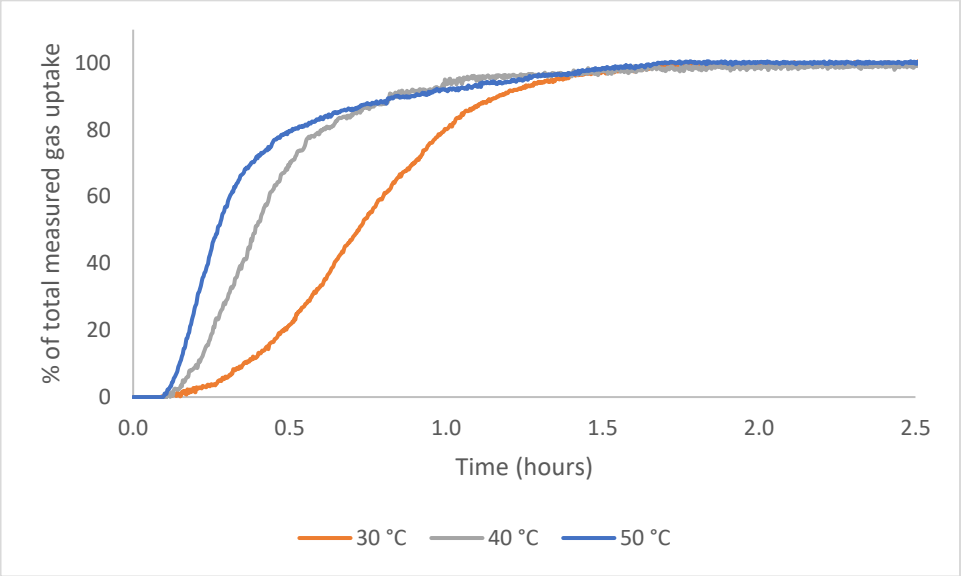

Figure 24 *Gas uptake data from Biotage Endeavor for reduction of methyl 2-naphthoate (**2.18**) at different temperatures.*

Despite these caveats, the plots observed for the reactions run at 40 °C and 50 °C are similar in nature, with a sudden onset immediately after hydrogen gas is applied to the reaction mixture. This initial steep slope is likely to be an indication that the reaction is in a mass transfer limited regime, implying that factors such as the rate of dissolution of hydrogen and stirring are slower than the kinetics of the reaction.[150] There is a distinct change in gradient after 20 mins for the reaction run at 50 °C, and 35 mins for the reaction run at 40 °C. This relatively abrupt change in rate implies that the mass transfer is no longer rate limiting, but rather the reactions have entered a kinetic regime, whereby the lower concentration of substrate and possibly deactivation of the catalyst over time results in the kinetics of the reaction being the rate limiting factor.

Intriguingly, all gas uptake curves had plateaued after 1.5 h. The work previously reported stated that all reactions were run for 5 h, regardless of the temperatures and pressures applied, though no explanation was given for this.[104] Future reductions would thus be run for shorter periods of time in light of this observation.

Interestingly, the reaction conducted at 30 °C displays a profile resembling that of a sigmoidal curve suggesting there is an initial induction period, wherein other processes are taking place

prior to the ester reduction itself. This interesting phenomenon will be explored in more detail in subsequent sections.

1.3.8 Catalyst Screen

Having identified the Biotage Endeavour as an appropriate piece of apparatus for screening purposes, and methyl 2-naphthoate (**2.18**) as a readily reducible and commercially available ester, the four catalysts (**1.51, 2.1, 2.2** and **2.16**) were compared by subjecting these to identical conditions (**Table 13**).

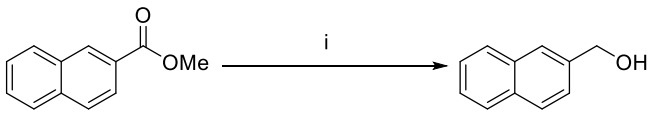

2.18 **2.19**

Reagents and conditions; (i) 1 mol% Ru(PNP)Cl_2(NHC) **(1.51)**, 20 mol% KO*t*-Bu, 5 bar H_2, 2-MeTHF, 45 °C.

Catalyst	% product[a]
Ru(PNP)Cl_2(NHC) (**1.51**)	96%
Ru(diEtSNS)Cl_2(NHC) (**2.1**)	93%
Ru(di*n*-BuSNS)Cl_2(NHC) (**2.16**)	95%
Ru(diPhSNS)Cl_2(NHC) (**2.2**)	72%
[a]Reaction conversion assessed by HPLC at 220 nm.	

Table 13 *Comparison of the catalytic activity with respect to reduction of methyl 2-naphthoate (**2.18**).*

The model substrate, methyl 2-naphthoate (**2.18**) was seen to reduce most cleanly with Ru(PNP)Cl_2(NHC) (**1.51**). Furthermore, examination of the gas-uptake curves revealed Ru(PNP)Cl_2(NHC) (**1.51**) to reduce the ester at the fastest rate (**Figure 25**), despite the computational study having suggested otherwise. This may be in part due to the calculations employing the continuum methanol reaction field DFT analysis, as was performed by Dub, Ikariya and co-workers[100] as opposed to 2-MeTHF, the reaction solvent in this instance.

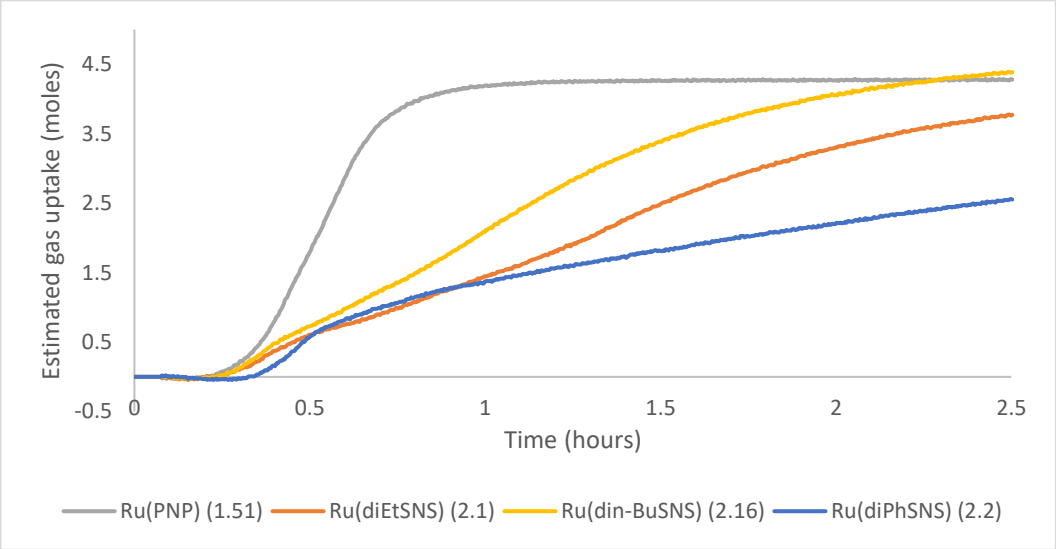

Figure 25 *Overlay of gas-uptake curves from catalyst screen.*

The Ru(SNS) complexes also displayed significantly longer induction periods for reasons which are unclear. Accordingly, Ru(PNP)Cl_2(NHC) (**1.51**) was used for the remainder of this study.

1.3.9 Solvent Screen

The choice of solvent in any process in of great importance. Many factors, including ability to facilitate the desired reaction, minimise formation of side-products, safety, environmental impact, amongst others are considered during solvent selection.[151] Indeed, typically between 80 and 90% of the total mass used in the production of an active pharmaceutical ingredient (API) may be attributed to solvent use.[152, 153] Consequently, industrial scale processes are typically run at high concentrations whenever this is feasible to reduce the cost associated with both purchase of the solvent and subsequent post treatment of the resulting waste streams. Several solvent selection guides have been reported by large pharmaceutical companies, including GSK[154] and Pfizer[155] which consider factors including environmental impact, recyclability and regulatory restrictions, amongst others to produce an overall

assessment of solvents commonly employed within the pharmaceutical industry. This allows classes of solvent to be ranked on a scale of "most preferred" to "least preferred".

The GSK solvent sustainability guide ranks THF as being a solvent with major issues, and is thus not a preferred solvent for large scale preparation. The low boiling and flash points of THF, along with its propensity to form explosive peroxides make its use undesirable.[156]

In order to identify a more suitable solvent for Chemical Development applications, a solvent screen was performed using a variety of alcohols, dipolar aprotic and non-polar solvents, all which were classified as having fewer issues on the GSK solvent sustainability guide (**Table 14**).

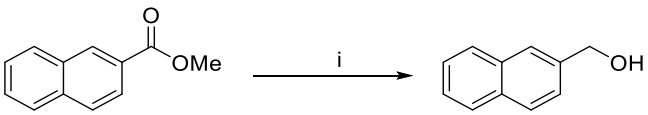

2.18 **2.19**

Reagents and conditions; (i) 2 mol% Ru(PNP)Cl_2(NHC) (**1.51**), 20 mol% KO*t*-Bu, 2 bar H_2, 40 °C, 3 h.

Entry	Solvent	% product (2.19)[a]
1	THF	92
2	2-MeTHF	91
3	Toluene	76
4	Methanol	3
5	Ethanol	3
6	Isopropanol	20
7	Acetonitrile	6

[a]Assessed by HPLC at 220 nm.

Table 14 *Results from solvent screen.*

Surprisingly, none of the alcoholic solvents allowed the reaction to run to completion. Particularly for methanol, this result was unexpected given that methanol is the solvent used when performing reductions with the closely related Ru-MACHO (**1.44**).[97] The reactions run in ethanol and isopropanol resulted primarily in transesterification (**Scheme 46**).

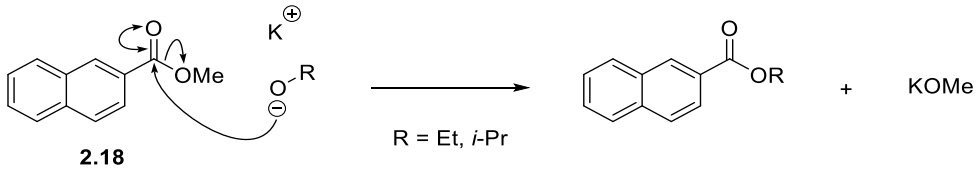

Scheme 46 *Formation of side-product following base mediated transesterification reaction.*

The dipolar aprotic solvent, acetonitrile, also provided unsatisfactory results with near complete recovery of starting material. This may be in part due to the active catalyst reducing the nitrile group present in the solvent, rather than the substrate. While previous work by Beller and co-workers[157] suggests this to be possible, this was difficult to monitor, as neither acetonitrile nor ethylamine are detectable by HPLC. Acetonitrile is also known to coordinate to $Ru(PNP)Cl_2(NHC)$ (**1.51**), which may also lead to deactivating pathways.[104] Toluene appeared to be more promising and gave the desired alcohol as the major product, and no unreacted starting material was observed by HPLC. Compared to THF, however, significantly more side-products were observed by ^1H NMR. The solubility of hydrogen has been measured to be slightly higher in toluene than in THF, so it is unlikely that this increased formation of side products is as a result of hydrogen starvation.[158]

After THF, 2-MeTHF gave the most promising results. The reaction proceeded cleanly and afforded the desired product (**2.19**) in good yield. 2-MeTHF is considered a greener and more process-friendly alternative to THF due to it being bioderived and having a higher boiling point.[156] Additionally, 2-MeTHF has the additional characteristic of being water immiscible, hence potentially allowing for more convenient work-up of reaction mixtures by means of an aqueous extraction. Thus 2-MeTHF has been identified as a suitable alternative to THF and will be used as the solvent in subsequent reactions.

1.3.10 Base Screen

All the reactions run thus far have used potassium *tert*-butoxide as the base in the form of a 1 M solution in THF, as previously described by Ogata and co-workers.[104] Accordingly, it was

of interest to determine if other bases were able to effectively promote the reaction. Based on this, a screen was performed with the aim of establishing how the identity of the base affects the reaction outcome (**Table 15**). A broad range of organic and inorganic bases were examined encompassing a wide range of pK_a values, physical form factors and cations where applicable.

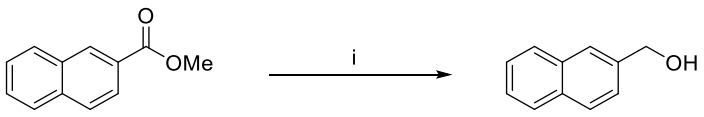

2.18 **2.19**

Reagents and conditions; 1 mol% $Ru(PNP)Cl_2(NHC)$ (**1.51**), 20 mol% base, 5 bar H_2, 2-MeTHF.

Base	Conversion (%area by HPLC)
Sodium ethoxide	0
Lithium isopropoxide	0
KHMDS	31
LDA	0
Triethylamine	3
Sodium methoxide	12
Potassium *tert*-butoxide	86
Potassium phosphate	0
Potassium carbonate	0
Potassium hydroxide	0
Lithium *tert*-butoxide	0
tert-Butylimino-tri(pyrrolidino)phosphorane	0
Potassium methoxide	92

Table 15 *Screen of different bases.*

Perhaps unexpectedly, only bases with a potassium cation appeared to be competent in promoting the reaction to any great extent, with potassium *tert*-butoxide and potassium methoxide both leading to high conversions. Notably, solid potassium *tert*-butoxide promoted the reaction efficiently as opposed to using potassium *tert*-butoxide as a solution

in THF, despite apparently reduced solubility in the reaction solvent. Bases with sodium or lithium cations either promoted the reaction poorly or did not promote the reaction at all. In those instances starting material was recovered, and in some cases along with side-products arising from the bases undergoing transesterification reactions. It was postulated that potassium salts would have the highest solubilities in the reaction solvent and could thereby promote the reaction most effectively. The neutral bases triethylamine and *tert*-butylimino-tri(pyrrolidino)phosphorene, however, both failed to promote the reaction, despite both being miscible in 2-MeTHF. Furthermore, the strong base, KHMDS was also employed, and this only promoted the reaction to a limited extent.

Based on these results, it appears that the solubility and strength of the bases alone do not fully explain which base is most suitable. Alkoxide bases bearing a potassium cation appear to be uniquely ideal in promoting the desired ester reduction. As such, potassium methoxide and potassium *tert*-butoxide are to be used as the preferred bases for future reductions. Potassium *tert*-butoxide in particular is more suitable for most applications as this is commercially available as a solution in THF, better facilitating handling. A similar conclusion with regard to the privileged nature of potassium alkoxides has been noted by Dub and co-workers during the study of a related Ru(SNP) catalytic system.[159] Interestingly, Saudan and co-workers observed a curious trend with their catalytic system whereby KOMe efficiently promotes the reaction, and addition of 18-crown-6 severely impeded the reaction.[68] The exact reason for this has yet to be elucidated, though direct involvement of the K^+ ion has been suggested by Dub and co-workers. [159] This involves replacing the N-H bond for a N^-K^+ ion pair which can partake in non-covalent interactions and form a low energy catalyst–substrate complex and could explain the apparent lack of correlation between pK_a and activity.

At this stage a suitable catalytic system employing Ru(PNP)Cl_2(NHC) (**1.51**) had been identified which was capable of reducing model substrates under mild conditions readily attainable within general purpose hydrogenation vessels typically encountered within the pharmaceutical industry. The switch from THF to 2-MeTHF was made as the latter is preferred from both environmental and safety standpoints. While gas-uptake data had also made apparent that altering the temperature significantly alters the rate of reaction, no significant understanding of the effect of altering other continuous variables had been

obtained. This is to be examined in more detail using a statistical experimental design (DoE) approach which is outlined in the following section.

1.3.11 Experimental Design

1.3.11.1 Introduction to Experimental Design

Moving forward, the aim was to optimise the reaction parameters and to gain a better understanding of how these affect the reaction. As there were several continuous variables affecting the reaction outcome, it was decided to employ a statistical design of experiments (DoE) approach to facilitate this process.

The advantage of experimental design as a tool is that it allows several factors to be varied simultaneously, thereby allowing a greater amount of chemical space to be explored compared to traditional a one variable at a time (OVAT) approach (**Figure 26**).[160]

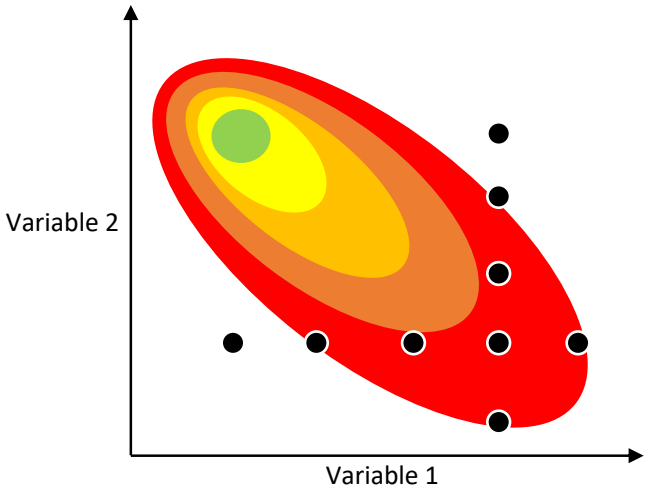

Figure 26 *Example plot of yield as a function of 2 different variables; highest obtainable yield represented by green area; black points represent iterative optimisation perform by varying one variable at a time.*

The black points represent experiments performed with the OVAT approach, with the green area representing the optimum set of conditions. In this case, the OVAT approach fails to identify the optimum conditions, despite numerous experiments being performed. However, by varying both variables simultaneously using an experimental design approach, the same number of experiments yield a better overall understanding of the reaction, and where to operate in order to obtain the best results, in this example, yield (**Figure 27**).

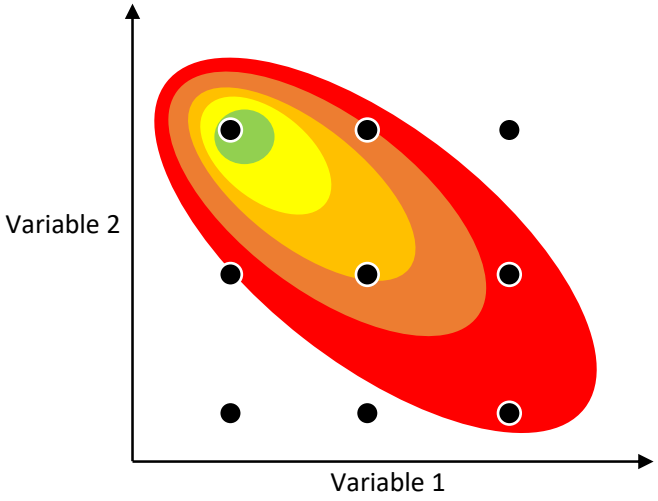

Figure 27 *Example plot of yield as a function of 2 different variables; highest obtainable yield represented by green area; black points represent optimisation performed using experimental design.*

The OVAT approach also works under the assumption that each variable is independent from all other variables. In reality, however, variable interactions need to be taken into account when optimising a reaction. Furthermore, OVAT does not take into account experimental noise, the variability between experimental runs.[161]

Indeed, the use of experimental design has become increasingly common, particularly within the pharmaceutical industry,[161] where it serves two purposes. The first of these is to find ideal conditions under which to run a process (ie. yield and quality). The second is to gain an understanding of the robustness of a process. This means understanding how a process responds to small but deliberate changes from an ideal set of conditions in order to establish acceptable operating ranges, an important consideration in a manufacturing environment.

Advancement in both parallel reactors and analytical assays have also facilitated the practical aspects of carrying these experiments out.

From a regulatory perspective, there has also been a definitive move towards quality by design (QbD) in favour of the traditional quality by testing. As such, significant process understanding has to be demonstrated, and regulatory authorities including the FDA and EMA have an expectation for design space to be included as part of NDA submissions.[162]

For the purposes of the current study, the aim was to use experimental design to evaluate the reaction parameters and to determine if any of them have a statistically significant effect on the outcome of the reduction of methyl 2-naphthoate (**2.18**). In doing so, improved reaction conditions and an increased understanding of the reaction may be obtained. The results are to be deconvoluted and interpreted using Stat Ease's Design Expert (DX-10) software.[163]

1.3.11.2 Experimental Design Plan for Scoping

In this investigation, the parameters to be explored were base quantity (A), hydrogen pressure (B), concentration (C) and reaction temperature (D) which were assessed as being the most likely to affect the reaction outcome. In this case, a two level design was selected, meaning that a pre-determined minimum and maximum value was selected for each of the variables (**Table 16**). In this instance a wide range was selected for each of the parameters to stretch the previously used conditions. The catalyst loading was not explored in this instance, due to this being more closely related to substrate purity. The reaction time was also kept constant at 2.5 h as previous experiments had suggested gas-uptake to cease within this timeframe. Consequently, 16 (2^4) factorial runs were added to the design, in addition to 4 centre points were incorporated in order to determine the variability present within the experimental set-up, giving a total of 20 individual experiments.

Factor	Parameter	Investigation Range
A	Base Quantity	5 – 35 mol%
B	Hydrogen Pressure	1 – 9 bar
C	Concentration	0.25 – 1.00 mol/L
D	Reaction Temperature	25 – 65 °C

Table 16 *Summary of parameters to be investigated and associated study ranges for scoping experimental design.*

The responses to be investigated were the relative amounts of starting material, methyl 2-naphthoate (**2.18**), product, naphthalen-2-yl methanol (**2.19**), and hydrolysis side-product, 2-naphthoic acid (**2.21**). These quantities were to be represented as area percentages on the HPLC traces. A summary of the key parameter settings and responses are summarised below (**Table 17**).

	Reaction conditions				Measured Responses		
Entry	**Base Quantity (A) (mol%)**	**Hydrogen Pressure (B) (bar)**	**Concentration (C) (mol/L)**	**Reaction Temperature (D) (°C)**	**SM[a] (2.18) (%area)**	**Product[a] (2.19) (%area)**	**Hydrolysis Product[a] (2.21) (%area)**
1	5	1	0.25	25	85	5	6
2	35	1	0.25	25	4	70	12
3	5	9	0.25	25	66	7	4
4	35	9	0.25	25	0	90	9
5	5	1	1	25	81	2	4
6	35	1	1	25	12	66	6
7	5	9	1	25	35	48	3
8	35	9	1	25	1	93	3
9	5	1	0.25	65	82	8	4
10	35	1	0.25	65	1	89	9
11	5	9	0.25	65	38	43	7
12	35	9	0.25	65	1	88	9
13	5	1	1	65	52	27	3
14	35	1	1	65	16	67	6
15	5	9	1	65	19	68	2
16	35	9	1	65	0	97	2
17	20	5	0.625	45	0	95	4
18	20	5	0.625	45	0	90	4
19	20	5	0.625	45	0	95	3
20	20	5	0.625	45	1	92	5

[a]Relative quantities assessed by HPLC with UV detection at 220 nm.

Table 17 Conditions and responses from scoping experimental design.

1.3.11.3 Factors Affecting Product Formation

The effect of base quantity (A) appears to be, by some considerable distance, the most influential parameter in this experimental design, with more base being favourable for formation of product (**2.19**) as can be seen in the half-normal plot (**Figure 28**).

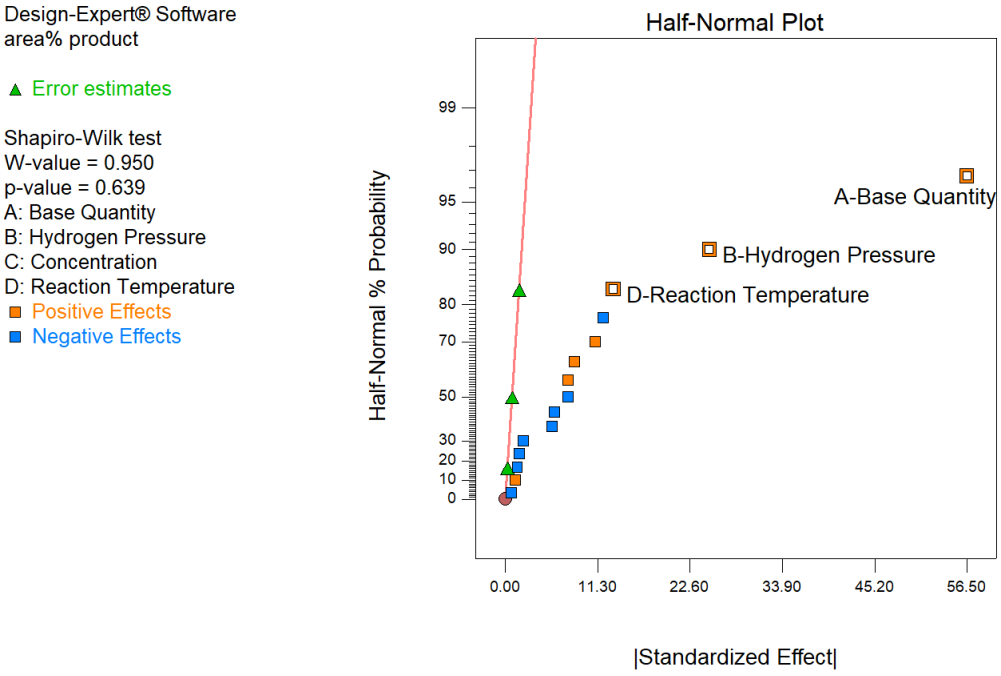

***Figure 28** Half-normal plot for formation of product (**2.19**) (scoping experimental design).*

The half-normal plots generated by the software are a statistical interpretation of the data, with the statistically most significant effects appearing on the right of the plot, and those which are least significant (within the range of experimental error as inferred from centre-point analysis) appearing on the left. For more details of the statistical model, including the ANOVA tables (test of overall statistical significant of variable on responses) see the appendix. The effects plot for the influence of the base quantity (A) on the formation of product is shown below (**Figure 29**).

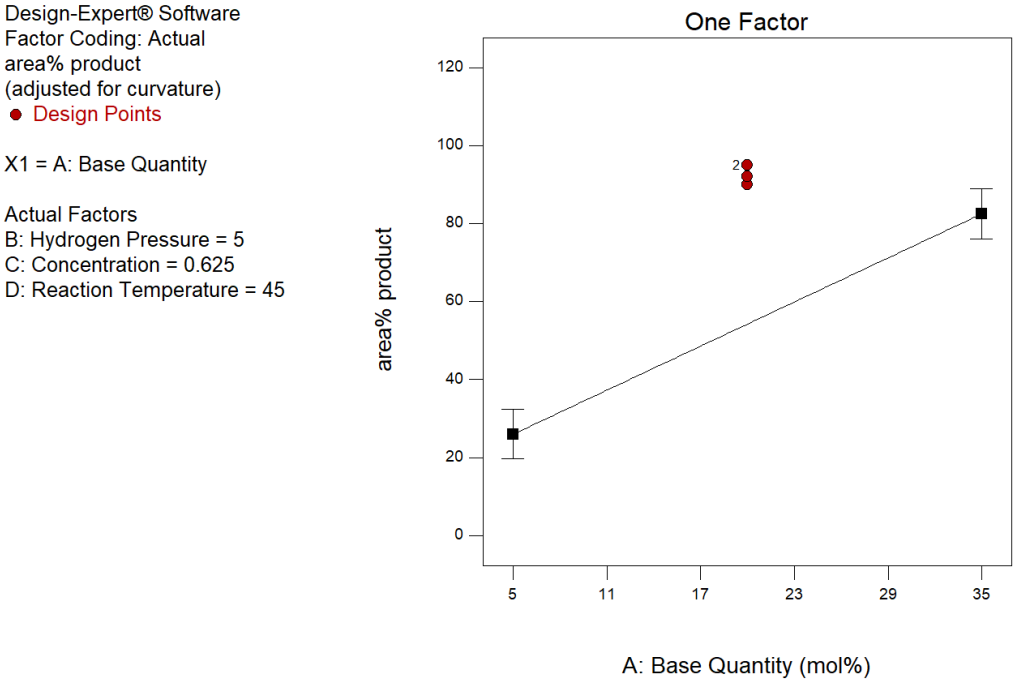

Figure 29 *Effects plot for influence of base quantity (A) on product (**2.19**).*

While the model built shows significant curvature, that is a non-linear change in response as a function of the continuous variable being altered, this would appear to be an artefact due to the wide range investigated for the base quantity (A). This caused several reactions to stall at the low value (5 mol%), thus leading to significant recovery of starting material (**2.18**). It could nonetheless be concluded that this variable does have a high significance on the outcome of the reaction, even if this model is not predictive at values between the extremes.

Hydrogen Pressure (B) is also shown to have a beneficial effect with respect to product formation (**Figure 30**).

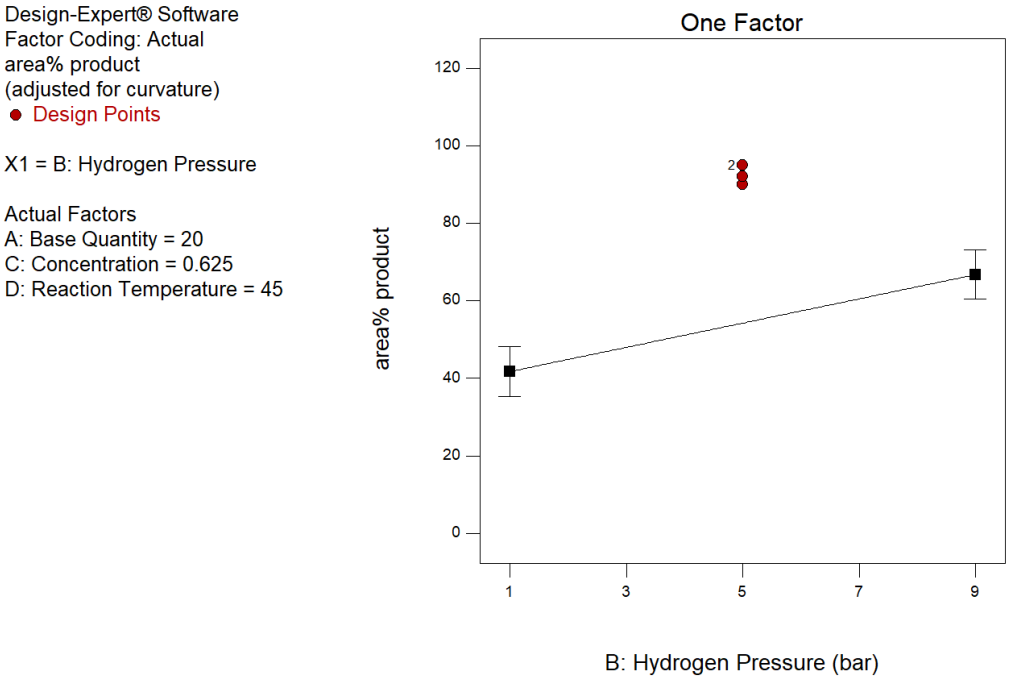

Figure 30 *Effects plot for influence of hydrogen pressure (B) on product (**2.19**).*

This result is consistent with what would be expected from a reversible reaction. By increasing the hydrogen pressure (B), and thereby increasing the quantity of hydrogen present in solution, the equilibrium is driven towards product formation as would be predicted by Le Chatelier's principle.[164]

Lastly, reaction temperature (D) is shown to have a slight positive effect on product formation (**Figure 31**).

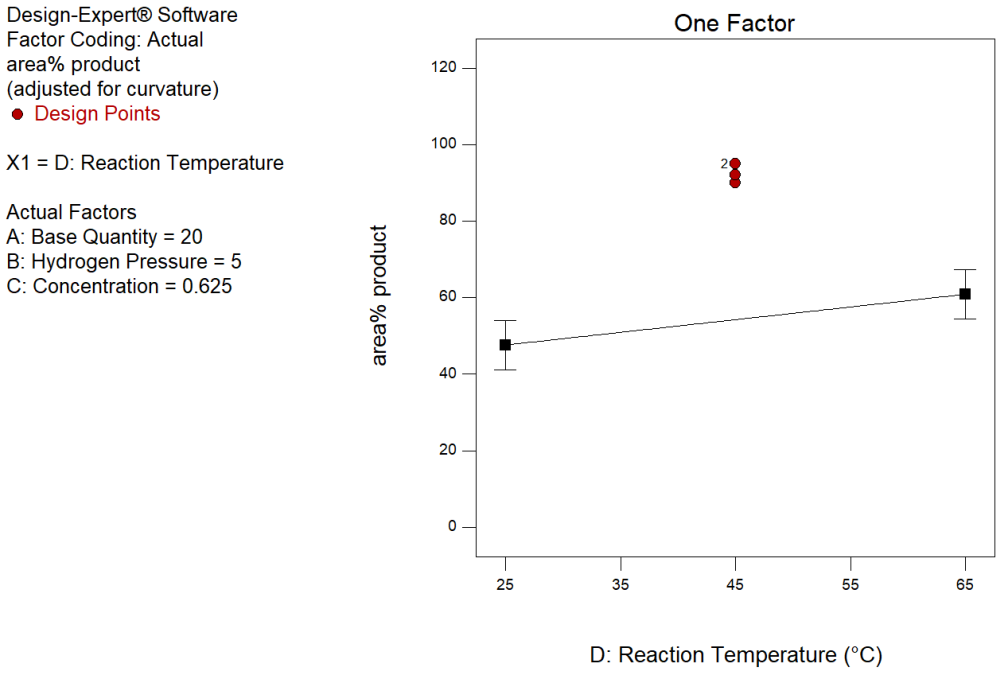

Figure 31 *Effects plot for influence of reaction temperature (D) on product (**2.19**).*

This is likely as reactions run at low temperatures (25 °C) were generally slower when compared with those run at higher temperatures.

1.3.11.4 Factors Affecting Formation of Hydrolysis Side-Product

The two parameters which were shown to have a statistically significant effect on formation of hydrolysis side product (**2.21**) were the base quantity (A) and the concentration (C) (**Figure 32**).

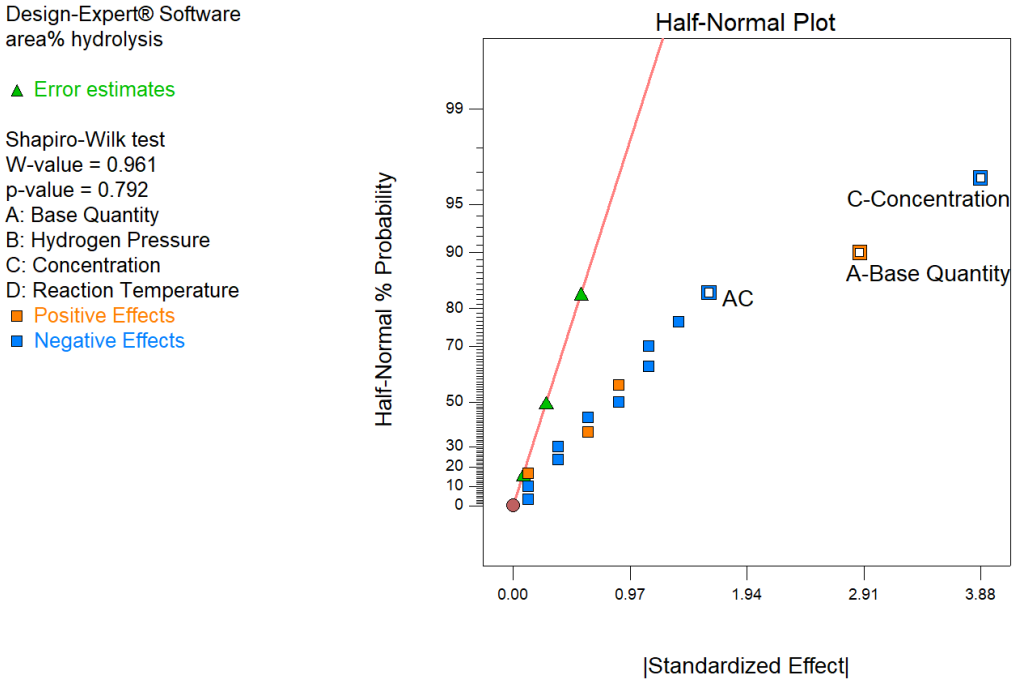

Figure 32 *Half-normal plot for formation of hydrolysis side-product (**2.21**) (scoping experimental design).*

In this case a response surface provided the best representation of the data. This illustrates the relationship between the two parameters as shown below (**Figure 33**).

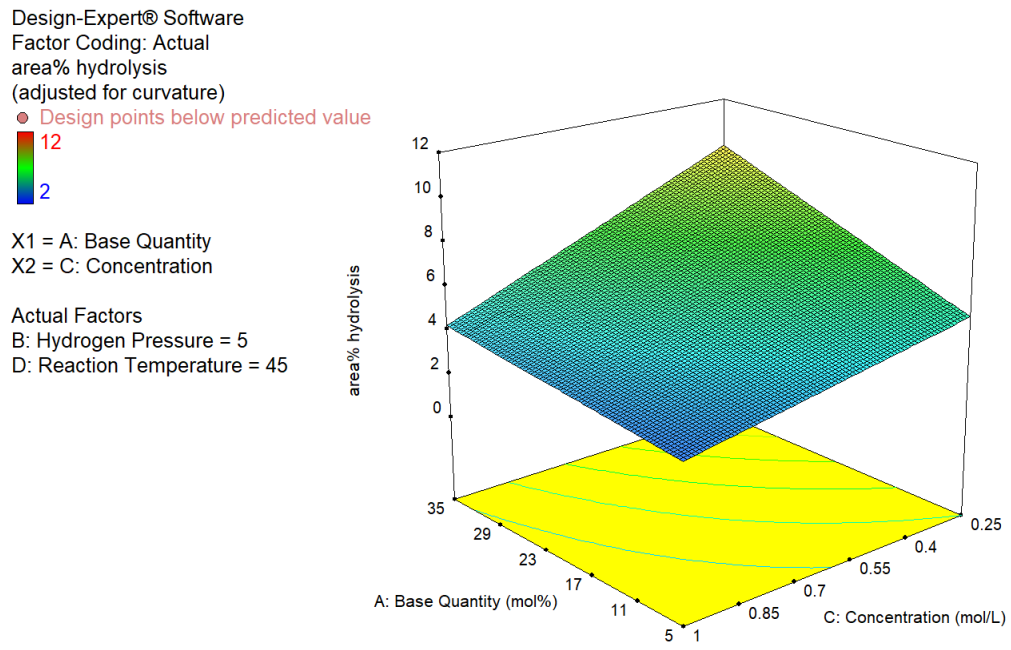

Figure 33 *Response surface for formation of hydrolysis side-product (**2.21**).*

Interestingly, increasing the concentration (C) is shown to reduce to amount of hydrolysis side-product (**2.21**) observed while increasing the base quantity (A) increases this response. The fact that hydrolysis takes place under what are highly basic conditions is understandable, though what is unclear is what the source of water is in this instance, which is required for hydrolysis to take place. Dry 2-MeTHF was employed for all reactions, and the base was drawn using a syringe from a sealed bottle as a solution in THF. Nonetheless, Karl Fischer (KF) analysis indicated approximately 0.0015% of water present in the 2-MeTHF accounting for approximately 3% the hydrolysis taking place at 0.625 mol/L with the remaining water/hydroxide content likely being present in the KO*t*-Bu solution. Therefore decreasing the concentration (C) by reducing the quantity of substrate in effect results in a greater proportion of the substrate being hydrolysed by the presence of hydroxide ions. The fact that low levels of this hydrolysis side-product (**2.21**) are present in every case would also suggest that this hydrolysis side-product (**2.21**) is not readily reducible under the conditions examined. This too is unsurprising, given the comparatively low electrophilicity of carboxylate anions.

1.3.11.5 Summary of Conclusion of Scoping Experimental Design results

Though a significant proportion of the reactions examined had stalled as a consequence of insufficient base being added on the low boundary of the design space, a more complete understanding of the importance of each of the parameters was obtained. In particular, base quantity (A) was found to be critical for the catalytic performance, and reactivity was generally more capricious at 5 mol%.

Increasing the hydrogen pressure (B) was generally found to be beneficial for the reaction. This resulted partly in an increased rate, but also resulted in generally higher conversions to product.

The concentration (C) and base quantity (A) were both found to affect the extent to which hydrolysis would take place in these reactions. Interestingly, running reactions at high concentration reduces the quantity of this impurity. This has the additional benefit of reducing solvent usage and is advantageous within the context of process design.

Reaction temperature (D) appeared also to have a positive effect of the yield of product, albeit a more modest one. These finding are summarised below (**Table 18**).

Factor		**Product (2.19) (%area)**	**Hydrolysis Side-Product (2.21) (%area)**
Optimisation goal		Maximise	Minimise
Range observed	**Max**	97	12
	Min	2	2
Curvature		Significant	Significant
Adjusted R^2		0.8562	0.7290
(A) Base Quantity		↑	↑
(B) Hydrogen Pressure		↑	-
(C) Concentration		-	↓
(D) Reaction Temperature		↑	-

Table 18 *Summary of data from scoping experimental design.*

With this this knowledge in hand, it was established that the reaction is tolerant to a range of reaction temperatures (D) and concentrations (C). Meanwhile, changes in the base quantity (A) and hydrogen pressure (B) were found to be particularly detrimental to the reaction at the lower end of the ranges investigated in this study.

There were also a number of unanswered questions which arose during analysis of the results. There was interest in determining which factors affected the time taken for reactions to go to completion based on the gas uptake curves. Building such a model was, however not possible in this instance as a result of several reactions stalling and thereby never reaching full conversion. Furthermore, aside from the hydrolysis side-product (**2.21**), the presence of other side-products was noted in the HPLC chromatograms, and so there was interest in characterising these and understanding which factors affect their formation. The plan therefore was to use a statistical experimental design approach once more, while looking at a narrower range of parameters in order to gain insight into these finer details.

1.3.11.6 Experimental Design Plan for Robustness

It was reasoned that the other impurities observed may be formed as a result of transesterification, similar to what was previously observed during the solvent screen. In this instance transesterification could also occur with the base, potassium *tert*-butoxide, or the product alcohol (**2.19**). Homocoupled ester side-products have indeed previously been noted by Kayaki and co-workers while studying this transformation.[104]

By way of preparatory work, authentic samples of the transesterification product were prepared by orthogonal methods which could then be used as HPLC standards.

The synthesis of the homocoupled ester (**2.22**) was achieved by conversion of 2-naphthoic acid (**2.21**) to the corresponding alkanoyl chloride, followed by condensation with naphthalen-2-yl methanol (**2.19**) (**Scheme 47**).

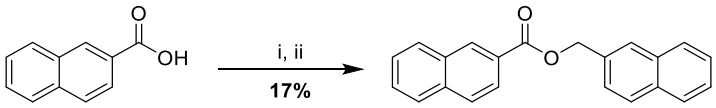

2.21 **2.22**

Reagents and conditions; (i) $SOCl_2$, toluene, 92 °C; (ii) naphthalen-2-yl methanol (**2.19**), triethylamine, DCM, rt.

Scheme 47 *Synthesis of homocoupled side product (**2.22**).*

Likewise, synthesis of an authentic sample of the *tert*-butyl ester (**2.23**) was achieved *via* a similar method (**Scheme 48**).

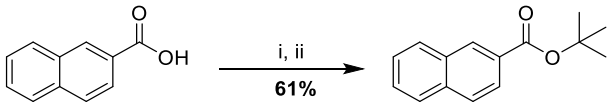

2.21 **2.23**

Reagents and conditions; (i) $(COCl)_2$, DMF, DCM; (ii) $HNEt_2$, HO*t*-Bu, KO*t*-Bu, DCM/THF.

Scheme 48 *Synthesis of side product arising from transesterification with base (**2.23**).*

The retention time of these compounds was identical to that of the impurities previously observed, confirming that these compounds can indeed be formed in low levels. It was also postulated that 2-naphthaldehyde could form under these conditions, though this was not observed by HPLC.

In order to get a more accurate assessment of the relative quantities of each component, triphenylphosphine oxide was added as an external standard to the analytical samples after reaction.

A narrower range of parameters was investigated in this design. Reactions were left to run for 16 h, in order to allow each reaction to reach its thermodynamic equilibrium, even at lower reaction temperatures (**Table 19**). Furthermore, the catalyst loading was reduced to 0.5 mol% as this was found to be sufficient for the purposes of reducing this relatively pure substrate.

Factor	Parameter	Investigation Range
A	Base Quantity	10 – 20 mol%
B	Hydrogen Pressure	2 – 8 bar
C	Concentration	0.25 – 1.00 mol/L
D	Reaction Temperature	30 – 60 °C

Table 19 *Summary of parameters to be investigated and associated study ranges for robustness experimental design.*

The reaction behaved more predictably under these conditions, and as such an improved models could be built. The mass balances in each case were typically around ~95%, and thus there was a high level of understanding of the fate of the ester under the reaction conditions. A summary of the key parameter settings and responses are depicted below (**Table 20**).

	Reaction conditions				Measured responses					
Entry	**Base Quantity (A) (mol%)**	**Hydrogen Pressure (B) (bar)**	**Concentration (C) (mol/L)**	**Reaction Temperature (D) (°C)**	**% SM[a] (2.18)**	**% Product[a] (2.19)**	**% Hydrolysis[a] (2.21)**	**% Homocoupled[a] (2.22)**	**% *tert*-Butyl[a] (2.23)**	**Time to completion[b] (h)**
1	20	2	0.25	30	0.0	82.1	13.3	0.0	0.0	5
2	10	8	0.25	30	1.1	78.4	9.4	0.0	6.9	6
3	10	2	0.25	30	8.0	76.8	9.4	1.0	2.3	4
4	10	8	1	30	0.6	87.2	5.1	0.0	0.0	5
5	10	2	1	30	6.4	75.9	6.9	0.6	0.3	5
6	20	8	0.25	30	0.0	77.7	14.6	0.0	0.0	3
7	20	8	1	30	0.0	88.7	5.9	0.0	0.0	4
8	20	2	1	30	0.0	86.7	10.6	0.0	0.0	8
9	15	5	0.625	45	0.0	88.2	8.6	0.0	0.0	2
10	15	5	0.625	45	0.0	88.2	8.1	0.0	0.0	2
11	15	5	0.625	45	0.0	88.4	8.5	0.0	0.0	2
12	15	5	0.625	45	0.0	85.4	9.9	0.0	0.0	2
13	20	8	0.25	60	0.0	79.7	15.0	0.0	0.0	0.5
14	20	2	1	60	0.0	87.5	9.6	0.0	0.0	3
15	10	8	1	60	0.0	90.2	4.7	0.0	0.0	2
16	20	8	1	60	0.0	91.7	5.7	0.0	0.0	0.8
17	10	2	0.25	60	17.9	60.7	8.7	2.5	6.5	1
18	10	8	0.25	60	1.3	80.6	8.4	0.0	6.3	1
19	20	2	0.25	60	0.0	84.2	11.8	0.0	0.0	0.5
20	10	2	1	60	0.0	87.5	7.4	0.0	0.0	5

[a]Relative amounts of each component assessed by HPLC at 225 nm with triphenylphosphine oxide as an external standard. [b]Time to completion estimated from gas uptake curves.

Table 20 Conditions and responses from robustness experimental design.

1.3.11.7 Factors Affecting Product formation

Unlike the model built during the scoping experimental design, concentration was now identified as the most statistically significant factor in this instance. This will in part be due to the revised ranges that were used for this second study. Base quantity (A) the hydrogen pressure (B) were also included in this model (**Figure 34**).

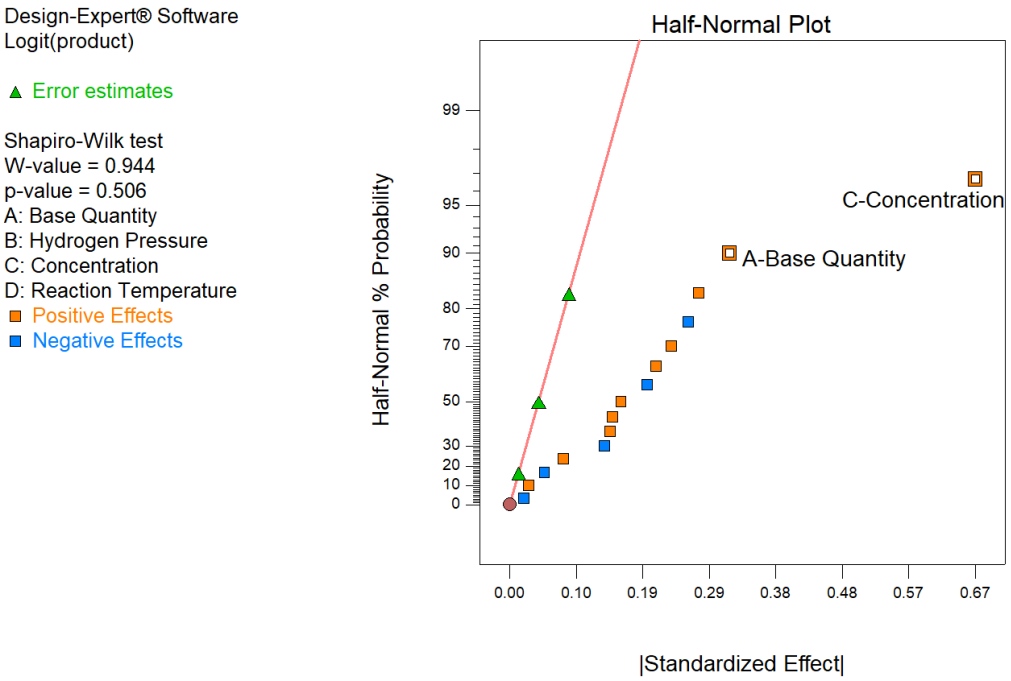

Figure 34 *Half-normal plot for formation of product (**2.19**) (robustness experimental design).*

As the solution yields of product were generally high within the ranges examined, concentration (C) likely has increased significance as the hydrolysis side-product (**2.21**) was the most prominent side-product observed. Consequently, running reactions more concentrated is advantageous (**Figure 35**).

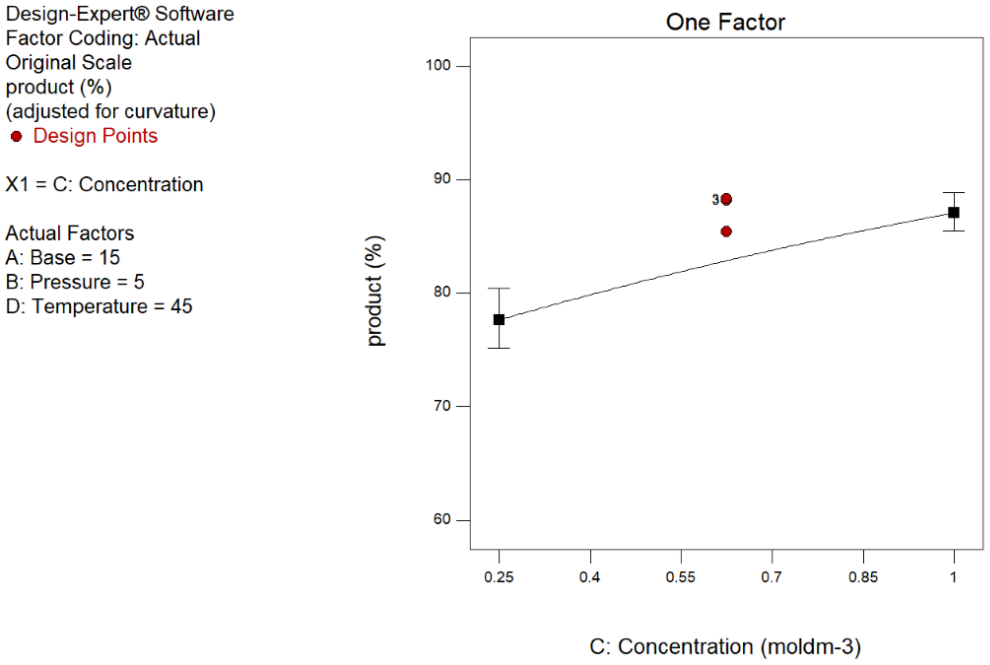

Figure 35 *Effects plot for influence of concentration (C) on formation of product.*

The positive effects of base quantity (A) added is also consistent with previous observations, albeit with reduced significance under the ranges examined (**Figure 36**).

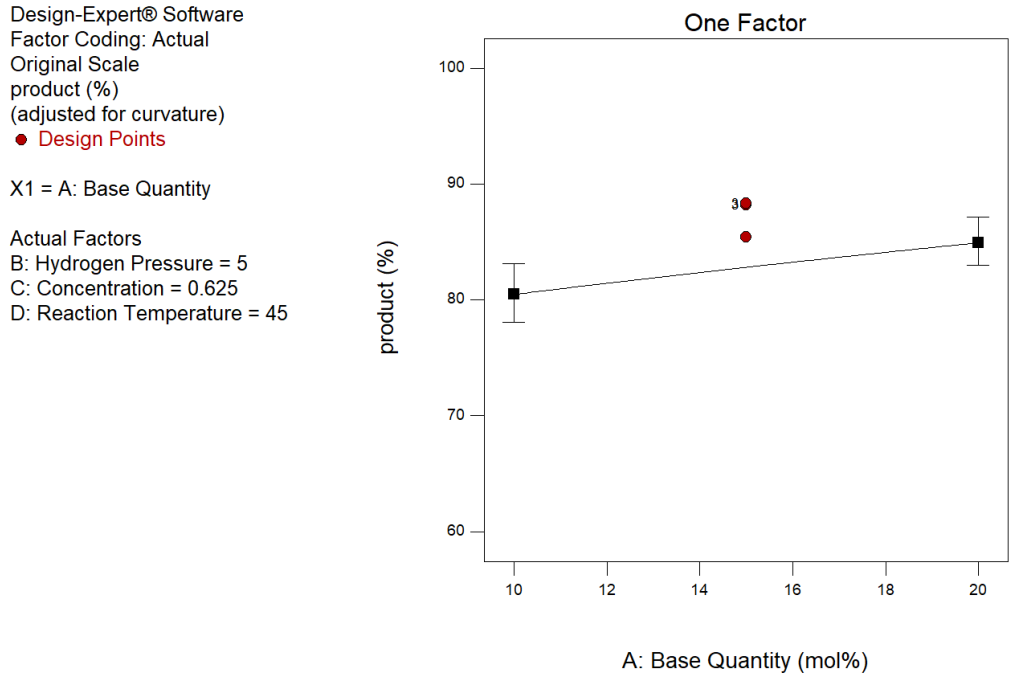

Figure 36 *Effects plot for influence of base quantity (A) on formation of product (**2.19**).*

1.3.11.8 Factors Affecting Formation of Hydrolysis Side-Product (2.21)

As before, the base and concentration were the main factors affecting this response (**Figure 37**).

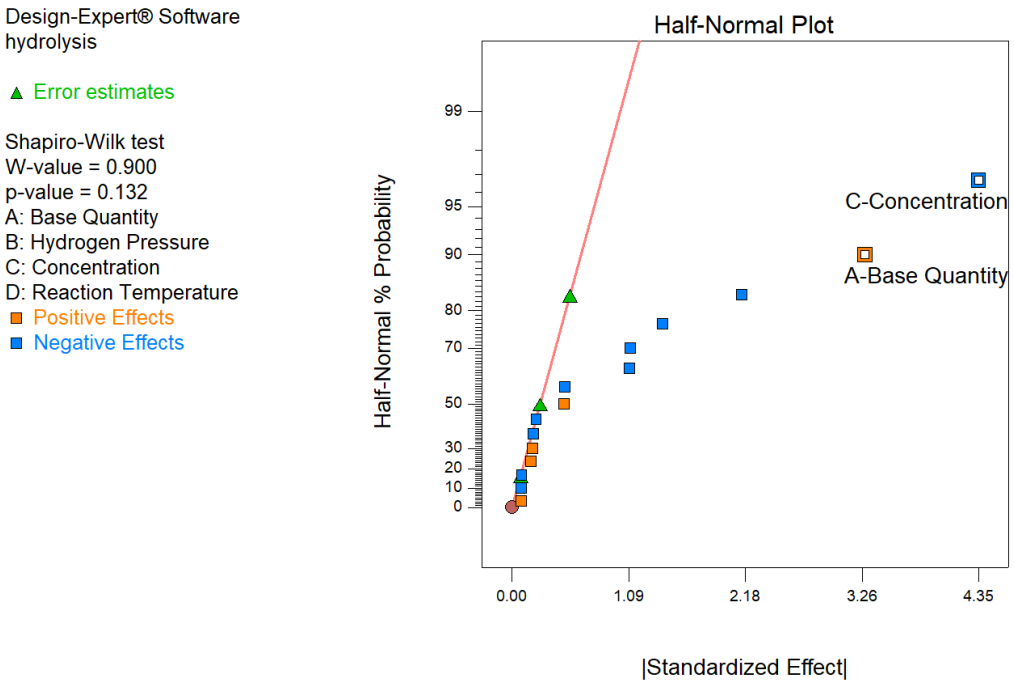

Figure 37 *Half-normal plot for formation of hydrolysis side-product (**2.21**) corrected for curvature (robustness experimental design).*

The response surface again illustrates the relationship between the two parameters as shown below (**Figure 38**).

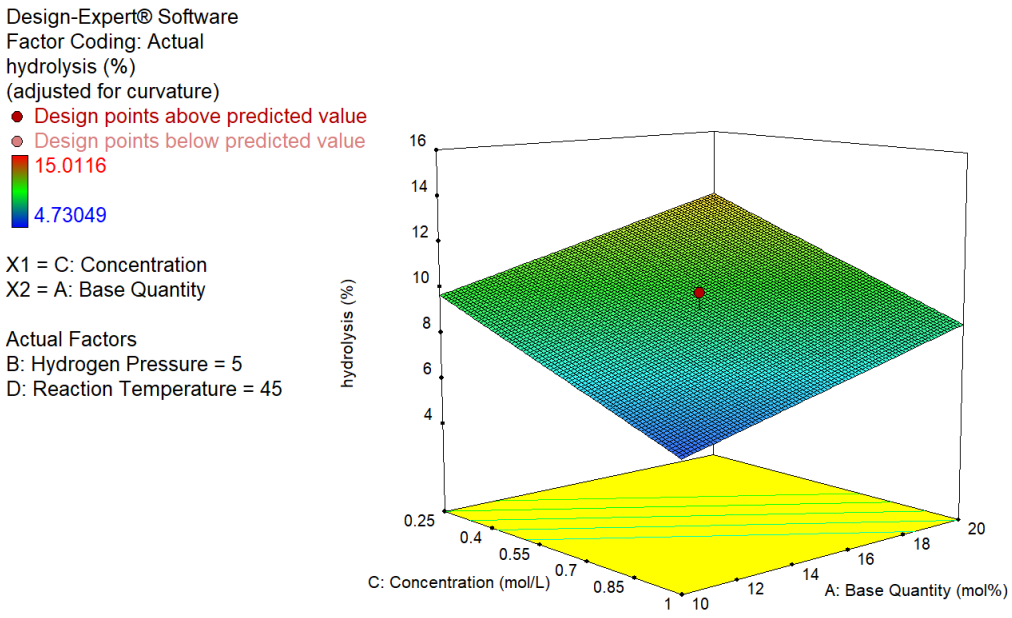

Figure 38 *Response surface for formation of hydrolysis side-product (**2.21**).*

Since an HPLC assay was developed for quantification, a more accurate understanding of the relative quantity of the hydrolysis side-product (**2.21**) was obtained. Surprisingly, as much as 15% could be lost to hydrolysis alone. While this could be partially suppressed by reducing the amount of base and solvent added, this discovery also prompted further investigation into other means of reducing the quantity of this side-product (**Table 21**).

Entry	Comment	%product (2.19)	%hydrolysis (2.21)	%transesterification + %SM (2.18)	Mass balance accounted for (%)
1	Centre-point conditions from robustness DoE	85	11	0	96
2	As entry 1 + molecular sieves	82	9	1	92
3	As entry 1 + 10% triethyl orthoacetate	83	11	0	94
4	As entry 1 + 110% triethyl orthoacetate	83	12	0	95
5	Premix solvent and base with sacrificial ester (methyl benzoate); then add substrate, catalyst and hydrogen	90	5	4	99
6	Repeat of entry 5 with hydrogenation run at 7 bar	91	5	0	96

Table 21 *Investigation into suppressing formation of the hydrolysis side-product (**2.21**).*

Addition of molecular sieves (**entry 2**) only made a marginal difference, and were used only for the purposes of this experiment. For larger scale applications these would not routinely be considered due to abrasion and vessel contamination which may arise. For these reasons chemical drying by means of adding triethyl orthoacetate (**entries 3 & 4**) was attempted but did not result in any benefit whether 10 mol% or 110 mol% was added. This is likely due to the absence of acidic conditions required by triethyl orthoacetate to react with water.

Premixing the base and solvent with a sacrificial ester (**entries 5 & 6**) did, however, result in a noticeable decrease in the hydrolysis or the substrate observed. This methodology has the added benefit of being less susceptible to varying levels of residual water present in the solvent and base.

1.3.11.9 Factors Affecting Formation of Transesterification Side-Products

The models built for formation of both the homocoupled ester side-product (**2.22**) and the *tert*-butyl ester side-product (**2.23**) were deemed as being statistically insignificant. In the majority of instances, the quantity of these compounds were below the limits of detection within the ranges studied. These impurities would typically be present when generally less forcing sets of conditions were used, as would perhaps be expected. This is advantageous from a processing standpoint as these data suggest these impurities not to be present over a wide range of conditions.

1.3.11.10 Factors Affecting Time to Completion

At low reaction temperature (D) a clear induction period is observed, as well as a transition from mass transfer limited to a kinetically limited regime. At high reaction temperature (D) neither the induction period, nor the transition to the kinetically controlled regime are observed, and reactions go to completion in as little as half an hour. While the time taken for the reactions to go to completion could only be estimated by the gas-uptake curves, these data could nonetheless be used to build a model (**Figure 39**).

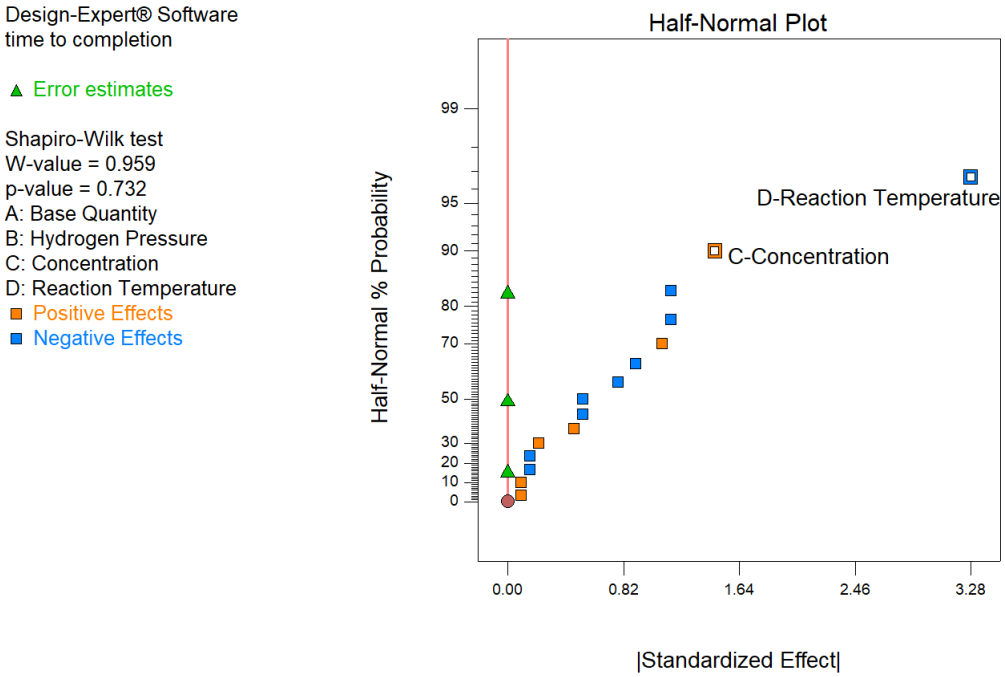

Figure 39 *Half-normal plot for time taken for reaction to go to completion (robustness experimental design).*

Reaction temperature (D) was found to be the most statistically significant factor in this instance, in line with what would be expected (**Figure 40**).

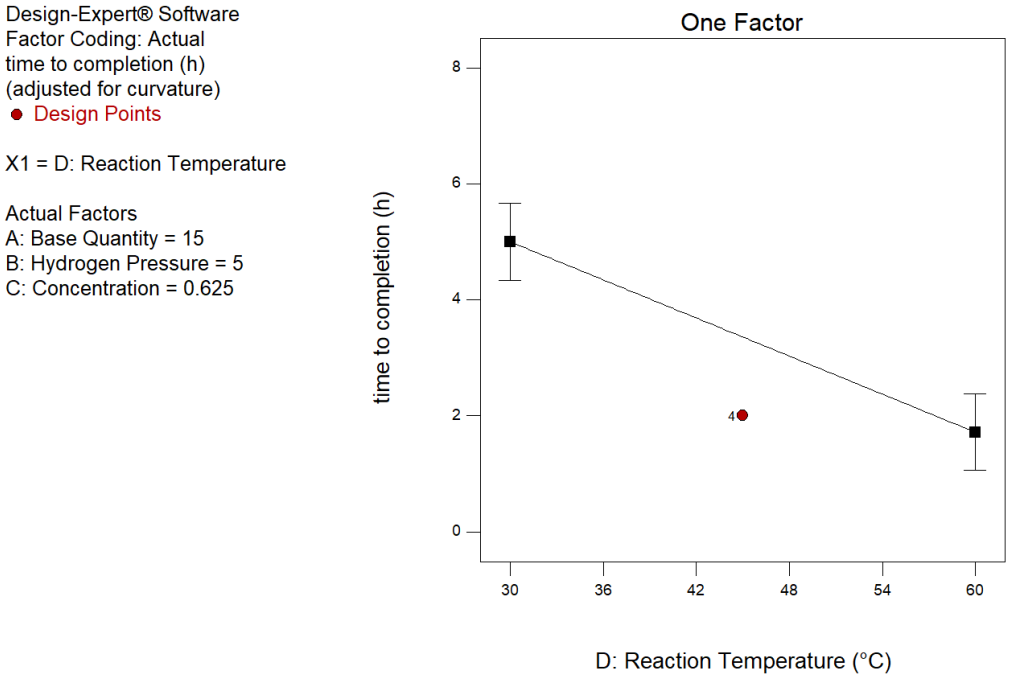

Figure 40 *Effects plot for influence of reaction temperature (D) on time taken for reaction to go to completion.*

Concentration was also included in this model, though with a p-value prob > F of 0.0431, is on the border of what would be considered statistically significant. Counterintuitively, this model suggests high concentration lengthens the reaction time. This observation may be an artefact in the data, possibly due to difficulty in assessing precisely when the reaction has gone to completion. In the case that this is a real phenomenon, this could be as a result of reduced solubility of the reaction components including hydrogen gas at increased concentration (C). Given that the end-of-reaction mixtures were white suspensions, with large amounts of solids being seen particularly at high concentration (C), this is indeed feasible. This is, however, a relatively small effect and can be more effectively modulated by altering the reaction temperature (**Figure 41**).

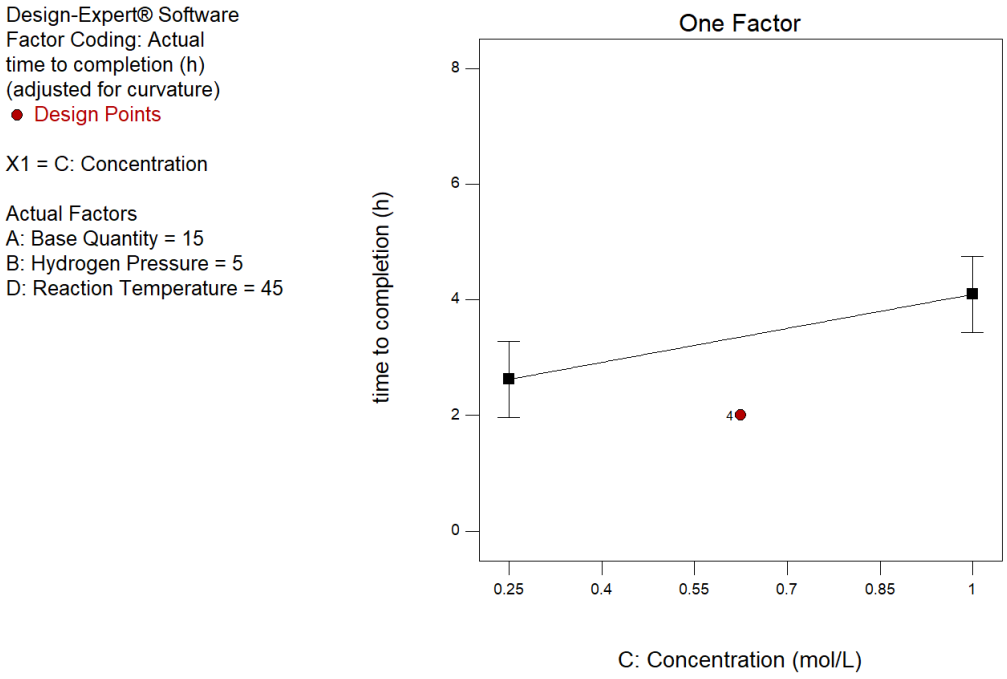

Figure 41 *Effects plot for influence of concentration (C) on time taken for reaction to go to completion.*

1.3.11.11 Summary of Robustness Experimental Design

In summary, an increased understanding has been obtained on how the continuous variables can be altered in order to maximise the positive responses (e.g. conversion to product) and minimise the undesirable responses (e.g. generation of side-products) (**Table 22**).

Factor		Product (%)	Hydrolysis Side-Product (2.21) (%)	Time to completion (h)
Optimisation goal		Maximise	Minimise	Minimise
Range observed	**Max**	91.7	15.0	8
	Min	60.7	4.7	0.5
Curvature		Not significant	Not significant	Not significant
Adjusted R^2		0.5351	0.7146	0.6353
(A) Base Quantity		↑	↑	-
(B) Hydrogen Pressure		-	-	-
(C) Concentration		↑	↓	↑
(D) Reaction Temperature		-	-	↓

Table 22 *Summary of data from robustness experimental design.*

The centre point conditions were highly reproducible, with the hydrolysis side-product (**2.21**) being the biggest single factor affecting the yield. It was established, however, that by pre-mixing the base, solvent, and a sacrificial ester prior to adding the catalyst and substrate ester, the extent to which hydrolysis takes place could be reduced. Unreacted starting material and impurities arising from transesterification were also observed when less forcing conditions were in operation. This has demonstrated the robustness of this methodology towards the reduction of the model substrate, methyl 2-naphthoate (**2.18**), and the much flatter responses in this experimental design demonstrate this process to be operable over a wide range of pressures and temperatures. Accordingly, the optimised conditions for this transformation are shown below (**Scheme 49**). It should be noted, however that these conditions may not necessarily be transferable when examining other substrates but would be expected to represent a reasonable starting point.

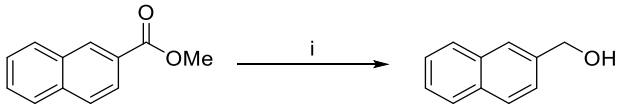

2.18 **2.19**

Reagents and conditions; (i) 0.5 mol% Ru(PNP)Cl_2(NHC) (**1.51**), 15-20 mol% KO*t*-Bu, 5-9 bar H_2, 2-MeTHF (1 mol/L), 45-60 °C.

Scheme 49 *Optimised conditions for reduction of the model substrate, methyl 2-naphthoate (**2.18**).*

1.3.12 Substrate Scope

Based on the DoE analysis outlined above, a favourable set of operating conditions for the Ru-mediated hydrogenation of esters has been identified. Following on from this, additional substrates were examined to gain further understanding of how Ru(PNP)Cl_2(NHC) (**1.51**) responds to various functional groups. This is pertinent given the additional degree of functionality encountered in the context of pharmaceutical research. The successfully reduced esters are shown below (**Table 23**).

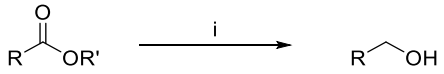

Reagents and conditions; (i) 1.5 mol% Ru(PNP)Cl_2(NHC) (**1.51**), 20 mol% KO*t*-Bu, 5 bar H_2, 2-MeTHF,45 °C.

Entry	Ester	Product	Yield/%[c] (Conversion/%[d])
1	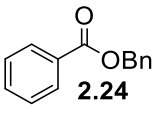 **2.24**	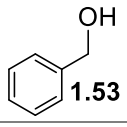 **1.53**	67 (>95)
2	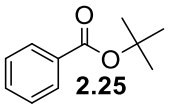 **2.25**	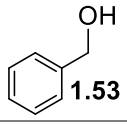 **1.53**	58 (>90)
3	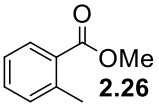 **2.26**	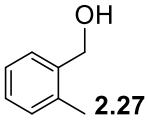 **2.27**	17 (>50)

4	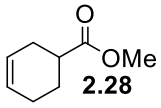 **2.28**	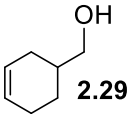 **2.29**	39
5	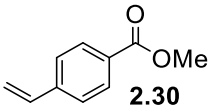 **2.30**	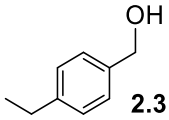 **2.31**	23 (>80)
6	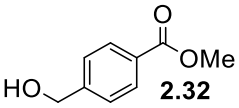 **2.32**	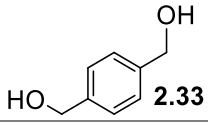 **2.33**	63 (>95)
7	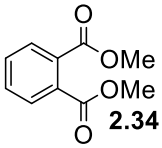 **2.34**	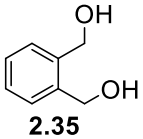 **2.35**	10 (>50)
8	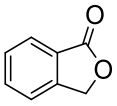 **2.36**	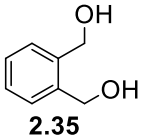 **2.35**	36 (>50)
9	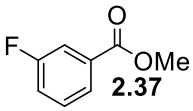 **2.37**	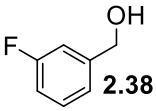 **2.38**	75 (>90)
10	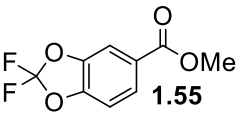 **1.55**	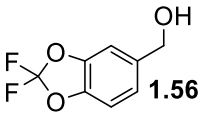 **1.56**	75 (>95)
11	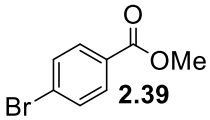 **2.39**	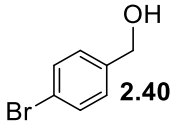 **2.40**	68 (>95)
12[a]	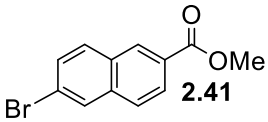 **2.41**	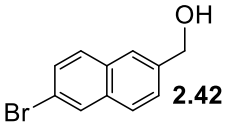 **2.42**	37 (>95)
13	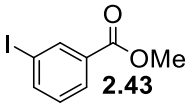 **2.43**	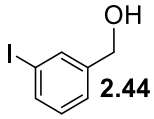 **2.44**	66 (>95)
14[b]	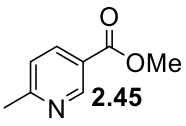 **2.45**	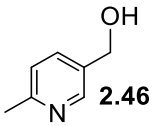 **2.46**	79 (>95)
15	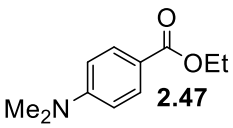 **2.47**	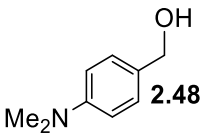 **2.48**	46 (>70)
16	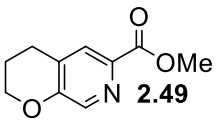 **2.49**	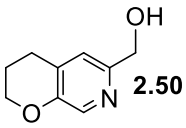 **2.50**	62 (>95)

17	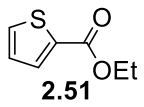 **2.51**	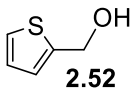 **2.52**	52 (>95)

[a]Isolated by vacuum distillation. [b]Isolated by aqueous extraction. [c]Yields of isolated product following purification by flash column chromatography except where otherwise noted. [d]Quantified by HPLC with UV detection at 220 nm.

Table 23 *Successfully reduced esters and resultant products*

Of the substrates examined, several of the corresponding product alcohols have been reported in medicinal chemistry patents and process development[119, 165-168] For example, derivatives of pyrano-pyridyl alcohol (**2.50**) in particular have shown promise for treating bacterial infections.[169] Difluoroalcohol (**1.56**) is an intermediate en route to a compound being investigated for treatment of cystic fibrosis.[119] Pyridyl alcohol (**2.46**) is an intermediate en route to a series of HDAC inhibitors.[168] Naphthyl bromide alcohol (**2.42**) is further functionalised using palladium mediated cross-coupling chemistry en route to an H_3 antagonist.

Though predominately methyl esters were examined, ethyl (**2.51**), benzyl (**2.24**), *tert*-butyl (**2.25**) esters as well as lactone (**2.36**) were also readily reduced within this substrate scope. Furthermore, various functionality groups were tolerated including thiophene (**2.51**), nucleophilic alcohols (**2.32**) and pyridines (**2.46** and **2.49**), and potentially labile C-F (**2.38**), C-Br (**2.39** and **2.41**) and C-I bonds (**2.43**). The *tert*-butyl ester (**entry 2**) reduced particularly smoothly, without a significant drop in reaction rate compared to typical methyl esters. Methyl 2-methylbenzoate (**entry 3**) and phthalide (**entry 8**) in contrast were both significantly hampered by the presence of *ortho*-methyl and *ortho*-methylene groups respectively as evident by the gas uptake curve. This indicates that the reaction is sensitive to steric hindrance, though only in certain positions relative to the reactive site.

The sensitivity of the reaction to steric hindrance was also apparent in **entry 7**, whereby dimethyl phthalate (**2.34**) was reduced, but was further complicated by the presence of a second ester group. The HPLC chromatogram indicated more than 20 components, with the majority of this (30 %area) being unreacted starting material (**2.34**). The desired product diol (**2.35**) was isolated in poor yield (10%), along with a complex mixture of numerous side-products, which likely formed as a result of oligomerisation promoted by the presence of butoxide (**Figure 42**).

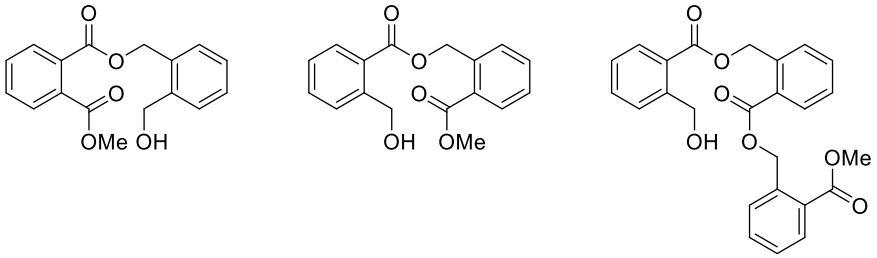

Figure 42 *Possible side-products formed during reduction of dimethyl phthalate (**2.34**).*

This could likely be overcome by prolonging reaction times and possibly increasing the temperature, as all the species formed should ultimately be reduced to the desired diol (**2.35**).

Entry 5 utilised styrene ester (**2.30**) and underwent almost complete conversion as determined by HPLC analysis. The reaction mixture, however, had significantly increased in viscosity over the course of the reaction and formed an insoluble black material. Analysis of the crude reaction mixture by ^{1}H NMR suggested that the double bond had been fully reduced, and indeed, only saturated alcohol (**2.31**) was isolated from the reaction mixture in poor yield (23%). The remainder of the material was attributed to have been lost due to polymerisation,[170] which may possibly have been facilitated by the reaction conditions. Internal alkene containing ester in contrast (**2.28**) in **entry 4** exhibited selectivity towards reducing the ester, while leaving the alkene intact.

Ethyl 4-(dimethylamino)benzoate (**2.47**) also underwent particularly slow reduction, though this was attributed to be an electronic, rather than a steric phenomenon. The electron rich aromatic ring presumably attenuated the electrophilicity of the ester (**Figure 43**).

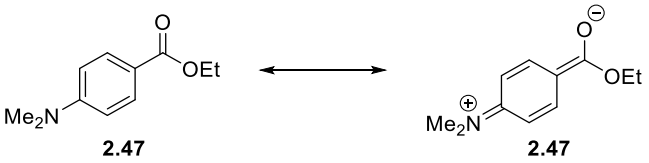

Figure 43 *Contributing resonance form of ester (**2.47**) resulting in reduced electrophilicity.*

In this particular example, in addition to isolating the desired product alcohol (**2.48**), a number of other side products were also isolated and characterised (**Figure 44**).

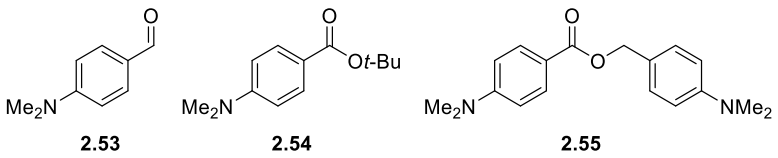

Figure 44 *Isolated side-products.*

The aldehyde side product (**2.53**) is formed as a result of partial reduction of the ester. Aldehyde intermediates are of particular interest as these, along with a hemiacetal intermediates have previously been mechanistically invoked by Gusev[112] and Milstein[79] while catalytically reducing methyl benzoate (**1.52**), though neither of these intermediates were directly observed. Gusev and co-workers suggested that while such intermediates may transiently be formed, they remain bound to the ruthenium centre, and as such do not accumulate in solution. While it is possible that electron-rich ethyl 4-(dimethylamino)benzoate (**2.47**) may be reduced to the alcohol *via* a different mechanism compared to electron-neutral substrates such as methyl benzoate (**1.52**), this result nevertheless demonstrates that under certain conditions and for certain substrates, free aldehyde intermediates may be formed in sufficient quantities to be isolable.

The *tert*-butyl ester (**2.54**) and homocoupled ester (**2.55**) side-products are both a result of transesterification of the potassium *tert*-butoxide additive and the product alcohol with the starting material, respectively. Indeed, transesterification side-products have also been observed during the reduction of methyl 2-naphthoate (**2.18**), though usually as low-level impurities as these too, eventually reduce to the desired product alcohol. The hydrolysis side-product was also likely to have formed under these conditions, though was not observable by LCMS or isolated by chromatography, likely due to its zwitterionic nature, and therefore high polarity.

From consideration of these isolated intermediates, the following general pathway is proposed for the reduction of esters under the conditions may be proposed (**Figure 45**).

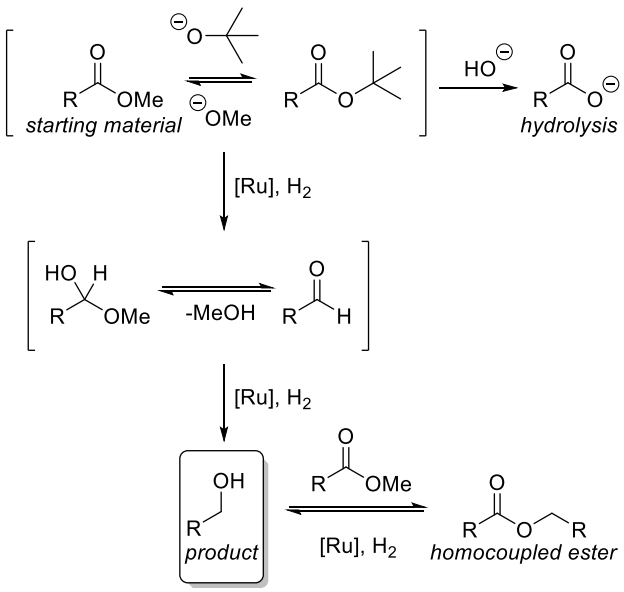

Figure 45 *Proposed fate of ester based on isolated intermediates.*

The starting material ester undergoes transesterification with the base during the induction period, resulting in a mixture of both the methyl and *tert*-butyl esters. The initial reduction then takes place to reduce the ester to the aldehyde oxidation level, presumably *via* a hemiacetal intermediate. This then further reduces to give the desired product alcohol. The product alcohol itself may undergo base-mediated transesterification to give a homocoupled ester. Sufficiently forcing conditions, however, may also reduce this to give the desired product. It is important to note that all intermediates, with the exception of the hydrolysis side-product, eventually led to the product alcohol. As such, minimising the quantity of water present is advantageous as a means of maximising the yield of product alcohol obtained as was also evidenced during the experimental design work.

Several substrate esters were found not to reduce to afford the corresponding alcohol and are listed below (**Figure 46**). In general these contain a greater degree of complexity and are discussed further below.

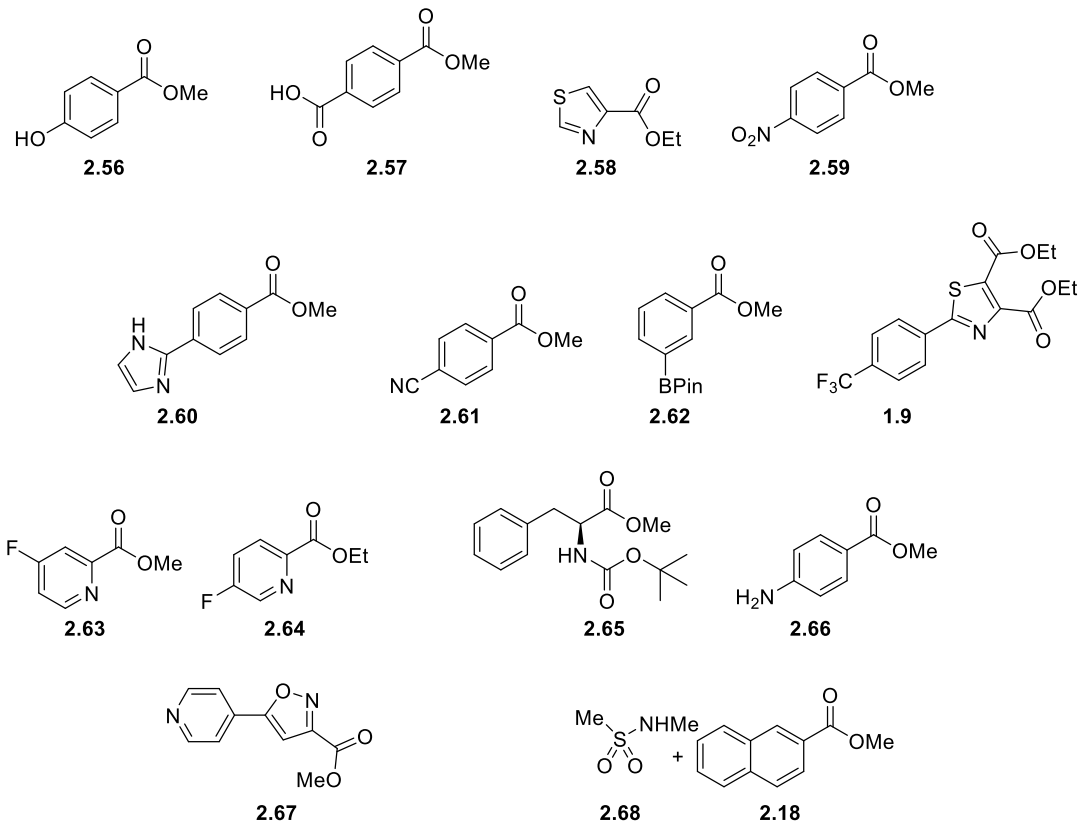

Figure 46 *List of substrates which did not undergo catalytic reduction to afford the corresponding alcohol.*

All substrates examined in **Figure 42** were obtained commercially, with the exception of thiazole diester (**1.9**) which was prepared by following a condensation procedure previously described by Guo and co-workers (**Scheme 50**).[30]

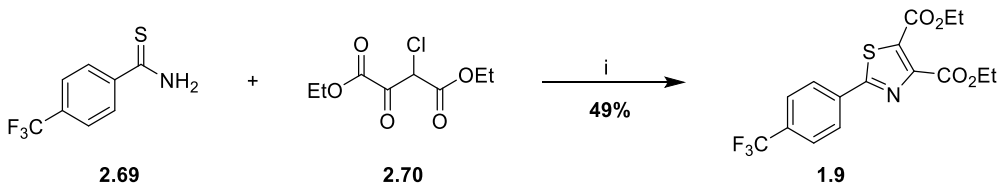

Reagents and conditions; (i) ethanol, 71 °C.

Scheme 50 *Formation of thiazole diester (3).*

It is clear from this list of substrates that this methodology is more appropriate for earlier stage intermediates where it is perhaps likely that less functionality is present. In particular, acidic functional groups, such as phenols, carboxylic acids or imidazoles, and indeed Lewis acidic groups such as boronic esters are not tolerated. It was thought that the reason for this was consumption of the base, potassium *tert*-butoxide, by the substrate thereby preventing the active form of the catalyst being formed. In an attempt to overcome this, methyl 4-hydroxy benzoate (**2.56**) and acid ester (**2.57**) were subjected to reduction conditions, but using an additional equivalent of sacrificial base, such that the remaining quantity may react with the pre-catalyst. Unfortunately, this also resulted in complete recovery of starting material. It is unclear whether this is due to the reduced solubility of the resulting alkoxide anion in the reaction solvent, 2-MeTHF, or whether the anionic nature of the intermediates formed are inherently more resistant to reduction.

A variety of other functional groups were also shown to inhibit the reaction, such as nitriles, primary amines, thiazoles, isoxazoles as well as nitro groups. Substrate scopes reported in the literature often do not to include unreactive substrates and consequently, this makes direct comparison to other catalytic systems non-trivial for certain substrates. That said, Beller and co-workers have previously demonstrated reduction of nitriles to primary amines using iron catalyst (**1.61**) in high yields using 30 bar of hydrogen pressure, which could account for the incompatibility observed in the current study.[157] Schörgenhumer and co-workers reported the inhibitory effect of nitro groups, as well as the impeding effect of substituents *ortho* with respect to the ester group, again potentially explaining the issues with nitro ester (**2.59**) and dimethyl phthalate (**2.34**).[106]

To understand whether the lack of reactivity was due to low-level impurities present, the reduction of thiazole diester (**1.9**), nitro ester (**2.59**), isoxazole ester (**2.67**) and nitrile ester (**2.61**) were re-subjected to the reaction conditions using both 10% and 100 mol% catalyst. This, however, also failed to furnish the desired product alcohol and formation of intractable mixtures was noted. This suggests the reaction is being inhibited by the substrate rather than a low level impurity. Thus, increased catalyst loading, aside from making processes economically less viable, also appears not to aid with unreactive substrates.

In the case of thiazoles, there was interest in understanding whether these substrates are inherently unreactive, or whether they have an inhibitory effect on the catalyst. As such a

reaction was carried out containing 50% thiazole ester (**2.58**), and 50% ethyl 2-thiophenecarboxylate (**2.51**), a substrate previously shown to reduce smoothly (**Scheme 51**).

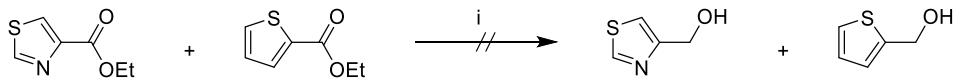

2.58 **2.51** **2.52**

Reagents and conditions; (i) 1.5 mol% Ru(PNP)Cl_2(NHC) (**1.51**), 20 mol% KO*t*-Bu, 5 bar H_2, 2-MeTHF,45 °C.

Scheme 51 *Experiment demonstrating the inhibitory effect of thiazole ester (**2.58**).*

The outcome was quantitative recovery of both starting materials. This suggests that thiazoles do indeed interfere with the catalyst, most likely through coordination.

The extent to which sulfonamides, an important moiety within medicinal chemistry[171] are tolerated was assessed by adding 1 eq. of sulfonamide (**2.68**) during the reduction of methyl 2-naphthoate (**2.18**) in a manner not dissimilar to the robustness screening methodology developed by Glorius and co-workers (**Scheme 52**).[172]

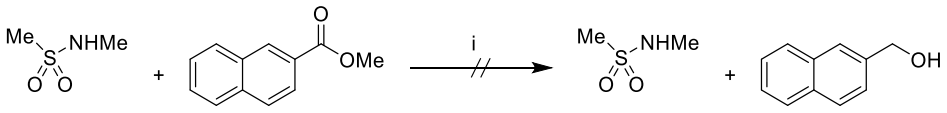

2.68 **2.18** **2.68** **2.19**

Reagents and conditions; (i) 1.5 mol% Ru(PNP)Cl_2(NHC) (**1.51**), 20 mol% KO*t*-Bu, 5 bar H_2, 2-MeTHF,45 °C.

Scheme 52 *Experiment demonstrating the inhibitory effect of sulfonamide (**2.68**).*

As can be inferred from **Scheme 52**, no conversion or gas uptake was observed as would be expected from this highly coordinating functional group.

The methyl ester of phenylalanine (**2.65**) was another substrate which was not successfully reduced under these conditions and formation of a complex mixture was noted. This outcome was of interest given that Kuriyama and co-workers had previously demonstrated reduction of related methyl esters derived from amino-acids in good yield with minimal loss of optical purity.[93] Aside from the different catalyst used, 50 bar of hydrogen was applied,

which may have benefited the reaction. While it is anticipated that re-running the reaction at this higher hydrogen pressure may lead to superior results, doing so would require specialised high-pressure hydrogenation equipment, which is again less favoured in a pharmaceutical development setting.

Interestingly, pyridyl ester (**2.45**) and aryl fluoride ester (**2.38**) were both shown to reduce smoothly, whereas the presence of both functional groups in the case of fluoro-pyridyl esters (**2.63** and **2.64**) resulted in no observable reduction to the primary alcohol, possible due to increased propensity of the Ar-F bond to react *via* nucleophilic aromatic substitution (**Scheme 53**).

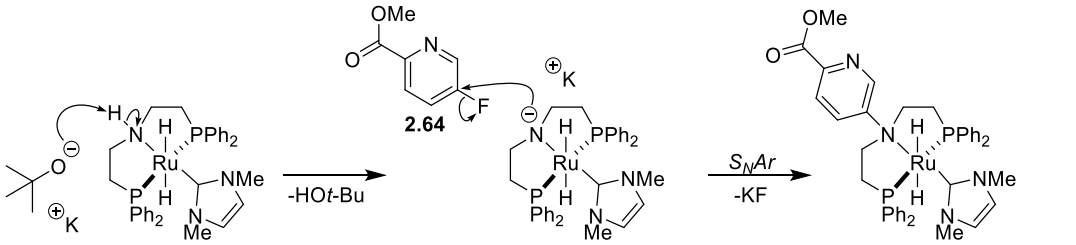

Scheme 53 *Proposed mechanism for reaction of catalyst (**2.20**) with substrate to generate a catalytically inactive complex (**2.71**).*

Substitution of the NH is known to give complexes incapable of performing catalytic ester reductions.[112] While this deactivating pathway was proposed based on mechanistic considerations, no evidence for the formation of the catalytically inactive complex (**2.71**) was acquired, likely due to the relative instability of such a complex.

In summary, a better understanding of the functional group tolerance and limitations of Ru(PNP)Cl_2(NHC) (**1.51**) catalyst system has been obtained. While a number of interesting substrates are well tolerated, many of the functional groups commonly encountered in pharmaceutical research and development have been demonstrated to be incompatible with this catalytic system. Furthermore, combinations of functional groups can unexpectedly result in a loss of activity, even when each functional group is well tolerated on an individual basis. Consequently, while this substrate scope may be used to give a preliminary indication

whether or not a new substrate is compatible, the definitive answer has to be established empirically on a case-by-basis, with simpler substrates generally being more amenable to undergoing the required transformation.

1.3.13 Time-Course Experiments using Process Analytical Technology

With a set of optimised operating conditions identified, and an elevated understanding of the scope of the reaction obtained, there was interest in getting a better understanding of the kinetics of the reaction, and at which stage different intermediates evolve, and in particular around the induction period which had been noted in the earlier part of our study. *In situ* monitoring for this specific transformation was a challenge given that the reactor is sealed and pressurised. While depressurising and venting the reactor is an option, it could only give information on the state of a reaction at a given time point. Importantly, during this process, exposure to air would likely terminate the reaction, rendering a time-course of the reaction unfeasible without recourse to running multiple experiments. As such, other means of *in situ* monitoring were examined, and ReactIR was deemed the most suitable. In addition to being operable under pressure and not interfering with the reaction, ReactIR has the additional advantage of being able to monitor the C=O stretch as a convenient handle to assess consumption of starting material.

Methyl benzoate (**1.52**) was selected as the substrate to be investigated in this instance, as both the starting material and product are liquids. Having this homogeneity is essential to ensure the solution analysed by the probe is an accurate representation of the bulk. Running the reduction of methyl benzoate (**1.52**) showed a clear decay of the starting material and formation of product, benzyl alcohol (**1.53**). Formation of the hydrolysis side-product , potassium benzoate (**2.72**) was also observed at 1552 cm^{-1} (**Figure 49**), consistent with what has been previously reported.[173] In order to make an assessment of whether the true kinetics of the reaction were being measured, reactions were also run at different impeller speeds.

Initial experiments showed that varying the impeller speed also affected the rate of reaction which implied the reaction was limited by mass transfer of hydrogen gas. Furthermore, transesterification with the base was seen to take place to afford *tert*-butyl benzoate (**2.25**) during the earliest stages of the reaction (**Figure 47**). Benzyl benzoate (**2.24**), while known to

form under these conditions as a result of the product undergoing a transesterification reaction with the starting material, could not be differentiated from the starting material by ReactIR.

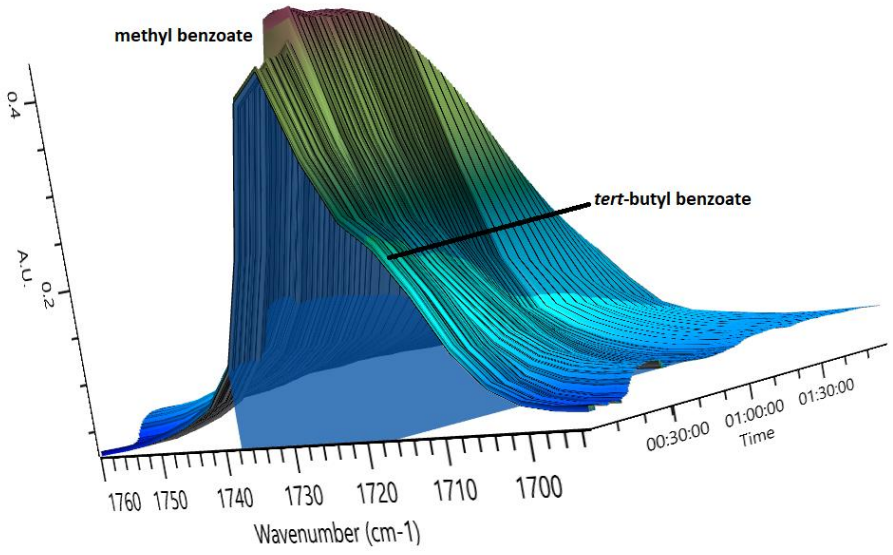

Figure 47 *Formation of tert-butyl benzoate (**2.25**) observed by IR.*

As such, the reaction temperature and catalyst loadings were lowered and the reactions were run at higher dilution (**Figure 48**). The added complexity caused by formation of *tert*-butyl benzoate was eliminated by replacing potassium *tert*-butoxide with potassium methoxide.

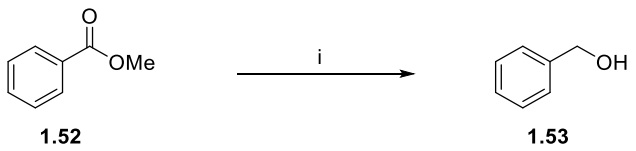

1.52 **1.53**

Reagents and conditions; 0.1 mol% Ru(PNP)Cl_2(NHC) (**1.51**), 20 mol% KOMe, 5 bar H_2, 30 °C, 2-MeTHF.

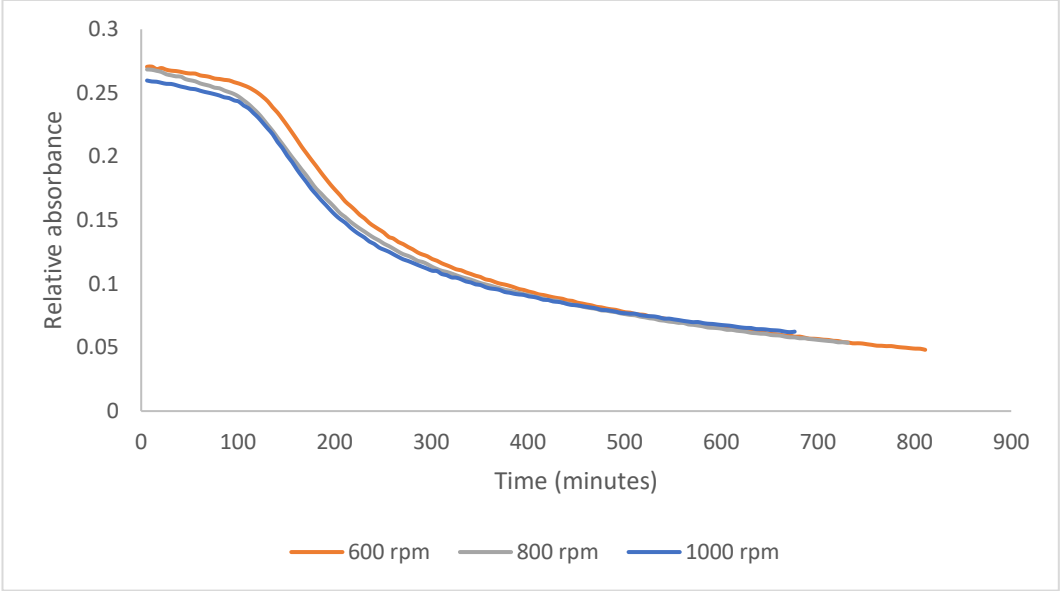

Figure 48 *Consumption of ester over time at higher dilution and lower temperature as a function of impeller speed.*

This resulted in identical rates of reaction, regardless of the impeller speed, suggesting that the true kinetics of the reaction were being observed. This lower temperature also prolonged the induction period in each instance to approximately 2 h.

During the preparation of the vessel, before any hydrogen pressure was applied, formation of the hydrolysis side-product, potassium benzoate (**2.72**) was observed (**Figure 49**). Interestingly, however, no benzaldehyde (**2.73**) was detected in any of the experiments. In contrast to the reduction of ethyl *para*-dimethylaminobenzoate (**2.47**), where the intermediate aldehyde (**2.53**) could be isolated, benzaldehyde (**2.73**) does not appear to accumulate sufficiently to be detectable, either due to rapid reduction to benzyl alcohol (**1.53**), or due to being masked as a hemiacetal.

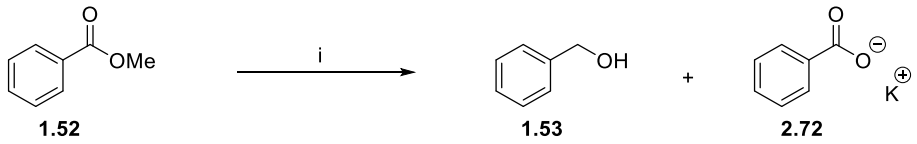

Reagents and conditions; 0.1 mol% $Ru(PNP)Cl_2(NHC)$ (**1.51**), 20 mol% KOMe, 5 bar H_2, 30 °C, 2-MeTHF.

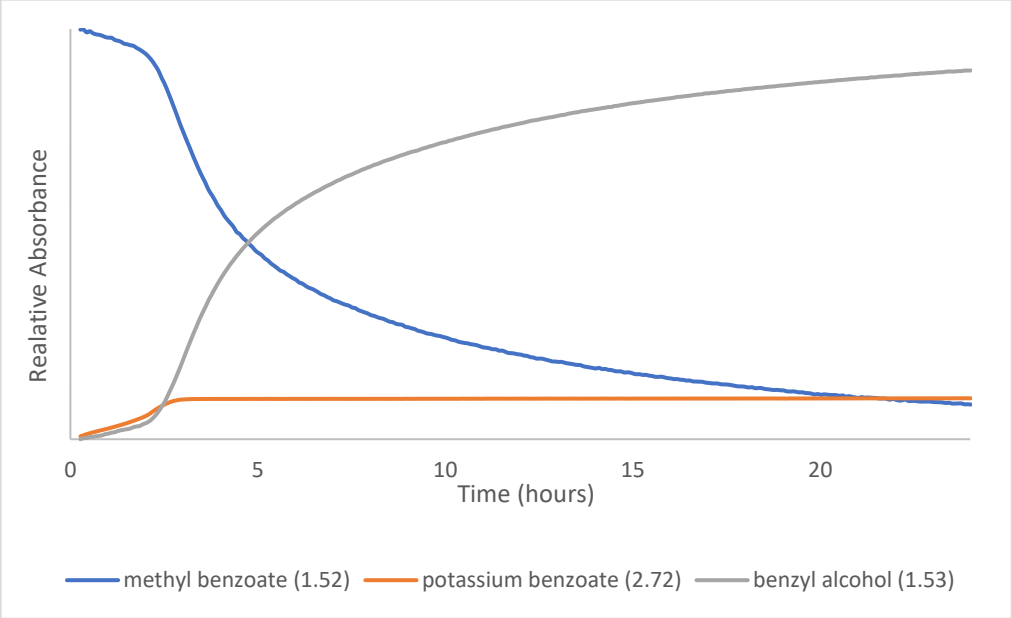

Figure 49 *Time course of reduction of methyl benzoate (**1.52**).*

These time-course reactions would reproducibly show formation of the hydrolysis side-product (**2.72**) plateauing to coincide with the induction period ending, and the rate of the productive reaction to increase significantly. The two plausible explanations for this phenomenon were the following: (i) either formation of potassium benzoate (**2.72**) has an autocatalytic effect which is beneficial to the rate of the catalytic reaction, or (ii) the presence of residual water has an inhibitory effect on the catalyst. To assess validity of the first hypothesis, a repeat reaction was run under otherwise identical conditions, but with the addition of 20 mol% exogenous potassium benzoate (**2.72**). Should this hypothesis be true, then this would result in a significantly reduced or complete removal of this induction period. It transpired that there was identical behaviour to other reactions, with the added potassium benzoate (**2.72**) seemingly having neither a beneficial nor detrimental effect on the reaction profile. As such, the conclusion drawn with regards to the origin behind the induction period is that this is essentially due to the presence of adventitious water inhibiting the catalyst (**1.51**). Though no water was deliberately added into the reaction, and dry solvents were used

in all cases, the deliquescent nature of potassium alkoxide bases, such as potassium methoxide and the notorious difficulty involved in drying hydrogenation vessels render the presence of low levels of water inevitable. Indeed, the work reported by Nguyen and co-workers on a related catalyst also reached the conclusion of water having an inhibitory effect on ruthenium complexes.[148] The understanding gained from this suggests a fraction of the substrate to be acting as a drying agent – that is to react with water (or more likely potassium hydroxide under these conditions) to form potassium benzoate (**2.72**), an organic compound which has been demonstrated to be a spectator with respect to the catalyst, rather than an inhibitor as water and the hydroxide ion are.

In addition to inhibition by the presence of residual moisture, there was also interest in determining whether product inhibition or catalyst deactivation is in operation. The products, benzyl alcohol (**1.53**) and methanol are both nucleophilic and could plausibly co-ordinate to the catalyst. Furthermore, results from the solvent screen indicated alcohols to be inappropriate solvents when utilising this particular catalyst (**1.51**). A reliable method for assessing the extent of product inhibition named the "same excess " experiment was pioneered by Blackmond and co-workers.[174] This technique allows one to artificially enter the reaction at any point, and by overlaying and comparing the time-course data of the same excess experiment with that of the original reaction, an assessment can me made about whether or not catalyst deactivation is taking place. In this instance the reaction was simulated at 50% conversion.

The reaction was prepared containing equimolar quantities of methyl benzoate (**1.52**), benzyl alcohol (**1.53**) and methanol, in addition to the typical catalyst and base loading. Inert and reactive purges were performed in a manner identical to previous runs and the result of this was complete inhibition of the reaction, and no consumption of the methyl benzoate (**1.52**) was observed. This rather puzzling result does indeed suggest product inhibition to be an issue. The key differences, however, between artificially entering the reaction at 50% conversion using this methodology and achieving this point of the reaction by allowing 50% conversion to take place are (i), the ruthenium complex being introduced as the pre-catalyst (**1.51**), as opposed to converting to the active catalyst (**2.20**) and (ii), the residual water being removed by virtue of hydrolysing the starting material (**1.52**). It would appear that either of these factors, or possibly a combination of the two renders the catalyst more resilient to the presence of alcohols such as methanol or benzyl alcohol (**1.53**), thereby allowing reactions

to run their course to completion. The “same excess” experiment starting with 50% starting material (**1.52**) and deliberate omission of the product alcohol (**1.53**) was also set-up. In this case the reaction did indeed proceed as expected to form benzyl alcohol (**1.53**). Overlaying these plots with time-course data from the original reduction performed did not allow for meaningful conclusions to be drawn, due to the key points of comparison being obscured by the relatively long induction period.

Lastly, the reduction of benzaldehyde (**2.73**) was investigated in order to gain an appreciation for how such an intermediate may behave under the reaction conditions, particularly given that this assumed intermediate has remained elusive thus far. The same conditions were used as in the previous reactions, but starting with benzaldehyde (**2.73**) rather than methyl benzoate (**1.52**). The ReactIR showed a very rapid decay of the signal corresponding to benzaldehyde (**2.73**) (**Figure 50**), and while rapid growth of the signal corresponding to benzyl alcohol (**1.53**) was also observed, formation and consumption of an intermediate species was also noted. This intermediate signal was observed at 1726 cm^{-1}, consistent with being an ester, though the exact identity of this intermediate ester could not be confirmed.

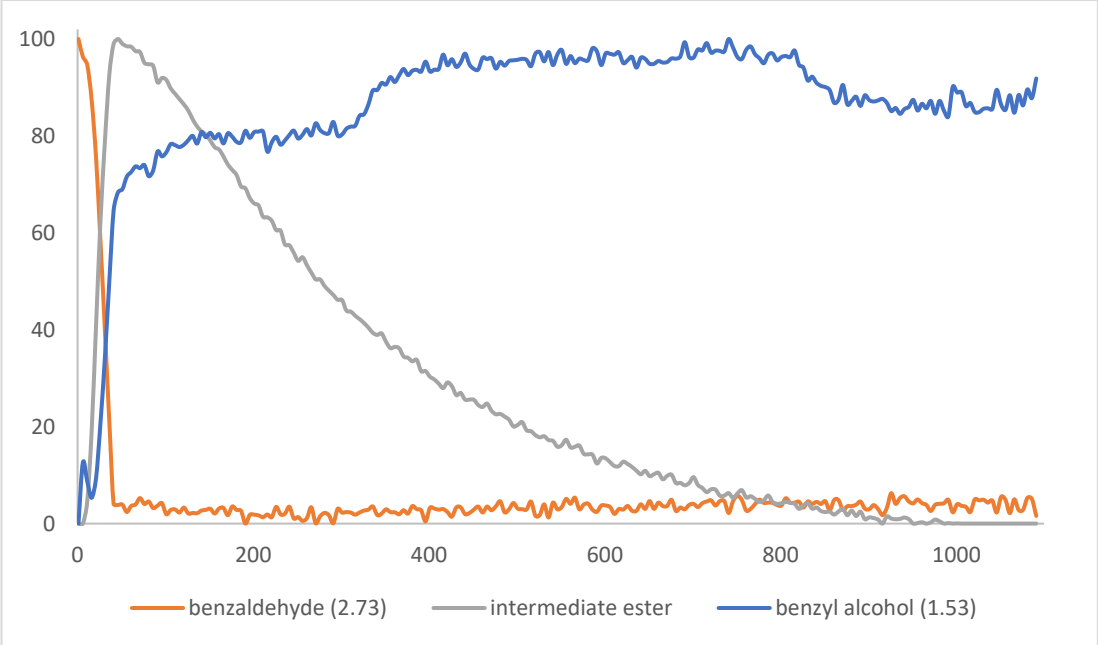

Figure 50 *Time-course reduction of benzaldehyde (**2.72**). All curves normalised for clarity.*

This result also seemed counterintuitive and appears to suggest benzaldehyde (**2.73**), in addition to being reduced to the alcohol, (**1.53**) is also undergoing an oxidative process to generate an ester containing intermediate. The best possible explanation in this instance is a base mediated Tishchenko type disproportionation resulting in conversion of the aldehyde to form an ester containing substrate, most likely benzyl benzoate (**2.24**) (**Scheme 54**).[175] This would explain why formation of the alcohol continues long after full consumption of the aldehyde has apparently taken place as the catalyst (**1.51**) has previously been demonstrated to efficiently reduce benzyl benzoate (**2.24**). A Tishchenko mechanism has previously been invoked in the context of acceptorless dehydrogenative ruthenium catalysed ester synthesis from alcohols by Ngyuen and co-workers, the microscopic reverse process of ester reductions is plausible given the strongly basic nature of the reaction mixture.[148]

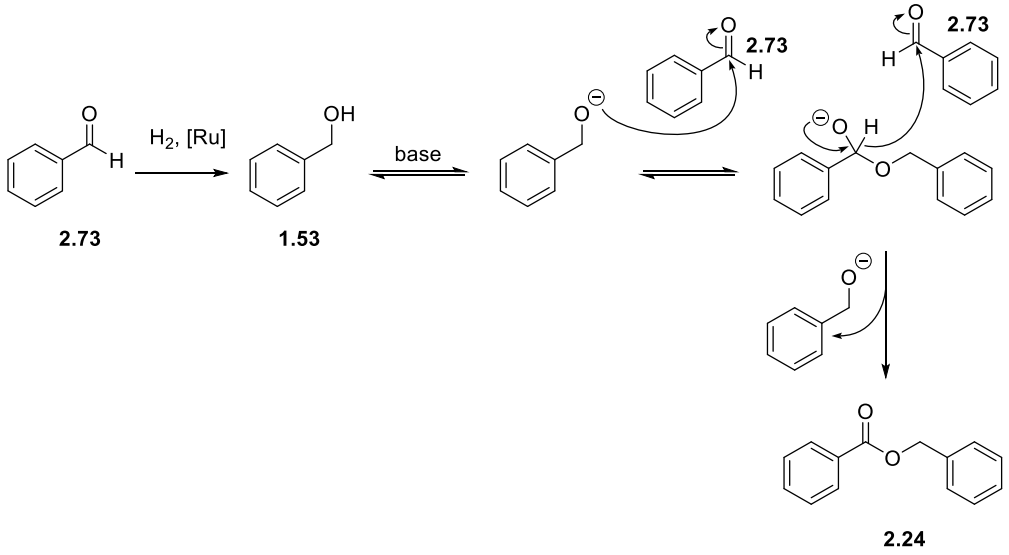

Scheme 54 *Possible mechanism for conversion of aldehyde (**2.73**) to ester (**2.24**) via Tishchenko reaction.*

To what extent this Tishchenko reaction takes place within a typical ester reduction process is unclear, particularly given that the concentration of free aldehyde is known to remain below the limits of detection in this case of the reduction of methyl benzoate (**1.52**). Nevertheless, this does provide another example of the possible base-mediated background processes which may take place.

In summary it has been established that transesterification with the base, potassium *tert*-butoxide to give *tert*-butyl esters takes place before hydrogen pressure is applied. Since the *tert*-butyl ester itself is reducible, this does not appear to have any negative implications on the reaction. The induction period appears to be linked to the presence of water, a known inhibitor to this class of catalysts. Formation of the hydrolysis side-product appears to take place during this induction period, and once its formation plateaus, the desired ester reduction pathway picks-up significantly in rate. Reduction of aldehydes to alcohols using this methodology unexpectedly appears to proceed *via* an intermediate ester. Formation of such an ester would likely be due to Tishchenko type reactions taking place which offers an additional reason why aldehydes are not routinely observed.

1.3.14 Reduction Methyl 6-Bromo-2-Naphthoate (2.41)

Having obtained a greater understanding of the process of interest using *in situ* monitoring techniques, attention then turned to examining the applicability of the ester hydrogenation at larger preparative scales. In order to obtain a primary indication of the scalability of such a process, a large-scale reduction was performed in a Buchi Ecoclave, a jacketed glass vessel equipped with a gas-entrainment impeller capable of performing hydrogenations. This setup more closely mimics the mass and heat-transfer characteristics of a large-scale reaction vessel than conventional glassware or the Biotage Endeavor previously used in the study (**Figure 51**).

Figure 51 *Ecoclave hydrogenation vessel equipped with gas-entrainment impeller.*

Methyl 6-bromo-2-naphthoate (**2.41**) was chosen as a pharmaceutically relevant intermediate, which has previously been used *en-route* to a H_3 antagonist.[167] The reaction was performed starting with 10 g of the ester substrate with 1 mol% of Ru(PNP)Cl_2(NHC) (**1.51**) (**Scheme 55**).

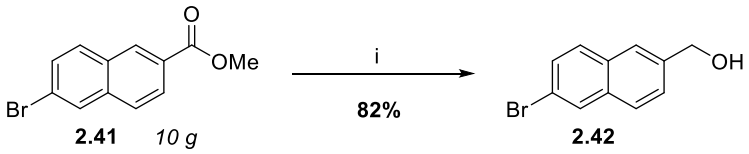

2.41 *10 g* **2.42**

Reagents and conditions; 1 mol% Ru(PNP)Cl_2(NHC) (**1.51**), 20 mol% base, 4 bar H_2, 2-MeTHF.

Scheme 55 *Large scale catalytic reduction of methyl 6-bromo-2-naphthoate (**2.41**) in batch.*

Due to the nature of the setup, no samples could be taken while the vessel was pressurised to monitor the progress of the reaction. As such the rate at which the hydrogen generator was producing hydrogen was used to assess the reaction progress. Towards the start of the reaction, this was generating significant quantities of hydrogen gas, such that the reaction vessel was maintained at 4 bar. The reduced hydrogen formation over time suggested consumption of the starting material (**2.41**) had taken place, and after 4 hours, the reaction was deemed to have gone to completion. At this point, the vessel could be vented and directly sampled, and indeed, a reaction profile concordant with that seen on a smaller scale run was observed, with full consumption of the starting material (**2.41**) (**Table 23**). Additionally, the transparent nature of the vessel gave further information on the properties of the reaction mixture over time. Solids were seen to precipitate which eventually formed a crust around the sides of the vessel, presumably the product (**2.42**) itself possibly also containing the potassium salt of the conjugate base (**Figure 52**).

Figure 52 *Precipitate formed over the course of the reaction.*

For the purpose of demonstrating facile scalability, flash-chromatography was avoided in the isolation process of the product alcohol (**2.42**). Instead, the workup was performed within the Ecoclave by slow addition of aqueous hydrochloric acid, which caused all solids to go into solution. After removal of the aqueous material, the organic phase was transferred into a separate vessel in which the solvent was distilled off with concurrent addition of isooctane. This induced precipitation of the product alcohol (**2.42**) out of solution which was then isolated by filtration and dried. Compared to the existing process in which the reduction was performed with DIBAL, the isolation procedure was significantly simplified and a more favourable waste stream composition was achieved. No issues with exotherms or formation of emulsions took place during the work-up. A PMI of 38 was obtained for this process. While the PMI value of a previous process could not be quantified due to insufficient data being reported,[167] it is expected to be substantially higher due to (i) employing DIBAL, a stoichiometric reducing agent as opposed to hydrogen and 1 mol% $Ru(PNP)Cl_2(NHC)$ (**1.51**) and (ii) the inefficient solvent swap from toluene to heptane by means of a constant volume distillation which would likely require a significant quantity of heptane in order to achieve the desired end point. Examination of the washings revealed that these were enriched with two impurities. Isolation the of first one of these of these revealed them to be the hydrolysis side-product, 6-bromo-2-naphthoic acid (**2.74**) (2 %area present in the reaction mixture after the reaction was terminated) and the desbromo side-product, 2-naphthalene methanol (**2.19**) (4 %area present in the reaction mixture after the reaction was terminated) (**Figure 53**). The former was consistent with what has been seen in previous experiments, whereas the latter was attributed to residual palladium present in the reaction vessel, as homogeneous ruthenium complexes of this nature have not previously been reported to

cleave aryl-bromide bonds.[104] A third low level impurity was present in 1 %area and was not isolated. This was suspected to be 2-naphthoic acid (**2.21**).

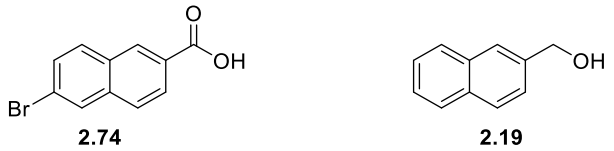

2.74 **2.19**

Figure 53 *Isolated side-products from large-scale reduction.*

While the hydrolysis side-product (**2.74**) could easily be purged by extraction into aqueous base, the desbromo compound (**2.19**) tracked through as its solubility and acid-base properties were similar to that of the desired product (**2.42**). Since the product alcohol (**2.42**) is later elaborated by means of palladium mediated cross-coupling chemistry, this would likely provide an alternative means of purging the desbromo compound (**2.19**) which is unlikely to partake in such a reaction.[167]

ICP analysis was performed and revealed 511 ppm of ruthenium within the product. While this is substantially above the limit of 10 ppm typically placed on precious metals within an API, this is a reasonable starting point.[127] This could be further reduced by recrystallisation, or by washing with coordinating ligands such as cysteine or 2-mercaptonicotinic acid.[176]

In summary, a scaled-up reduction has been demonstrated and the desired product (**2.42**) has been obtained in satisfactory yield without the need for flash-chromatography to isolate the product alcohol (**2.42**). Two side-products have been identified, one of which was effectively purged, the other which tracked through into the product, but would likely be easily purged in downstream chemistry.

1.3.15 Extension to CSTR Flow Reactor

The area of flow chemistry has gained significant attention recently, including the possibility of running gas-liquid reactions. A continuous setup offers a number of advantages over running reactions in conventional batch reactors such as higher throughput and increased

safety as a result of lower reactive inventory.[138-140] The main challenge with flow systems is the propensity for reactors to become blocked over time, particularly when attempting to flow solids. For the purposes of the current study, this was identified as a challenge, as previous reactions have shown to precipitate over time as a result of the product alcohol being inherently less soluble in the solvent compared to the starting material. Based on these reasons, the idea of employing a segmented flow reactor similar to that used by Kappe and co-workers[141] (**Scheme 27**) for this purpose was avoided.

This led to the consideration of a bespoke CSTR (continuous stirred tank reactor) setup (**Figure 54**). Flow setups typically comprise of tubing which optionally also contain static mixers within. Over time, deposited solids may accumulate and eventually lead to restricted flow or indeed complete blockage. The CSTR setup in contrast has a significantly wider diameter, and has running through it, a magnetically driven horizontal agitator, thus ensuring solids are constantly being suspended, and larger deposits are ground up. The key advantage of this setup is that plug-flow behaviour is retained, while also ensuring efficient gas-liquid contact and mixing characteristics which do not solely rely on turbulence. As such this system benefits from tolerating inclusion of solids while still offering reduced reactive inventory. In this particular case, due to the rating of certain external components coupled to the system, the reactor was limited to 5 bar of hydrogen pressure.

Figure 54 *A CSTR flow reactor.*

A more detailed schematic of the complete set-up including feed and product line and temperature control is given below (**Figure 55**).

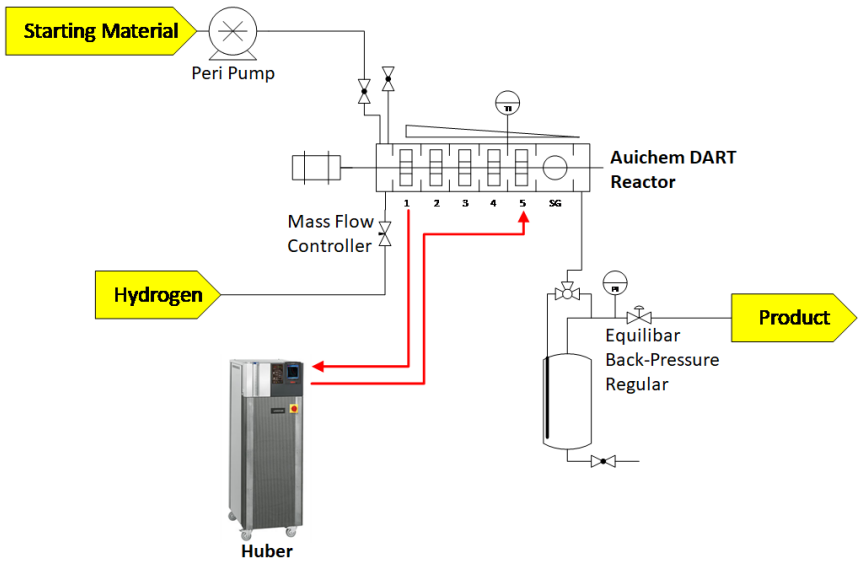

Figure 55 *Schematic of CSTR flow rig.*

The gas-feed inlet is placed below the liquid-feed such that the gas phase is forced to pass through the liquid phase. This along with the movement from the agitator encourages efficient gas-liquid contact. The reactor itself is jacketed which allows for accurate temperature control through an external thermostat. Once the reaction mixture has passed through the reactor, it is then transferred to a collection vessel using pressurised nitrogen gas. This may then be sampled and analysed.

For this setup, methyl 6-bromonaphthoate (**2.41**) was selected again as the pharmaceutically relevant intermediate to be reduced (**Scheme 56**). This substrate was also chosen on the basis that solids are known to precipitate over the course of the reaction, and close attention was to be given to how well these would be suspended and passed through the reactor.

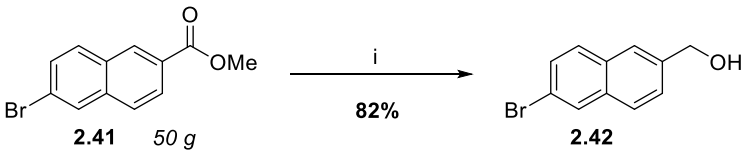

2.41 *50 g* **2.42**

Reagents and conditions; 1 mol% $Ru(PNP)Cl_2(NHC)$ (**1.51**), 20 mol% base, 5 bar H_2, 2-MeTHF, 65 °C.

Scheme 56 *Large scale catalytic reduction of methyl 6-bromo-2-naphthoate (**2.41**) in flow.*

The ester (**2.41**), solvent, catalyst (**1.51**) and base were all charged into the liquid feed tank. This was pumped into the reactor, at which point hydrogen gas was mixed into the liquid phase. It was found that solid potassium *tert*-butoxide was an unsuitable choice of base for this setup. While the reactor itself is designed to pass solids through, the tank containing the starting material and the tubing leading up to the reactor were not. The liquid feed tank in particular was equipped with an overhead stirrer which was unsuitable for suspending the solid potassium *tert*-butoxide. Furthermore, the base was also found to deposit in the tubing leading up to the reactor, such that the mixture entering the reactor contained insufficient base and hence resulted in no conversion of the starting material. To overcome this, a solution of potassium *tert*-butoxide in THF was used instead of solid potassium *tert*-butoxide. This entered the reactor without the issue of solids settling in the feed lines and becoming immobilised. Particularly low flow rates of both the liquid and gas feeds were required to achieve the long residence times required for the reaction. Setting the hydrogen flow rate too high also resulted in rapid expulsion of the reaction mixture from the reactor, preventing it from having the necessary residence time to react. Once the reactor had reached a steady state, reaction mixtures were sampled and analysed by HPLC (**Table 24**).

Residence time (mins)	**% product (2.42)[a]**
54	90
23	65
12	38

[a]Reaction conversion assessed by HPLC at 220 nm.

Table 24 *Results from reduction of methyl 6-bromonaphthoate (**2.41**) in continuous flow.*

Varying the residence time revealed that the longest residence time led to the highest conversions and would allow the 50 g of input ester (**2.41**) to be processed in approximately 17 hours. This is simply a result of allowing the reaction enough time to reach completion.

In summary, catalytic ester reduction has been demonstrated in flow as a means of increasing the scale of such reactions and potentially making them amenable to more forcing conditions. No blocking caused by precipitates was observed during the trial even with the relatively low flow rates required. Furthermore, the throughput could in principle be increased by applying higher temperatures and pressures, particularly as larger variants of these reactors are commercially available.

1.3.16 Reduction of Pyrano-Pyridyl Ester (2.49)

The reduction of pyrano-pyridyl ester (**2.49**) to pyridyl alcohol (**2.50**) was previously demonstrated in the early part of the current study. For the purpose of further elaborating product alcohol (**2.50**), the reaction was scaled up in a HEL AutoMATE, starting with 10 g of ester input (**Scheme 57**).

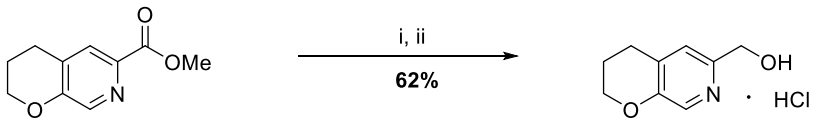

2.49 **2.50•HCl**

Reagents and conditions; (i) 1 mol% $Ru(PNP)Cl_2(NHC)$ (**1.51**), 20 mol% KO*t*-Bu, 5 bar H_2, 2-MeTHF; (ii) HCl, dioxane.

Scheme 57 *Large-scale reduction of pyranopyridyl ester (**2.49**).*

The reaction outcome on this scale was in good accordance with that seen on smaller scale. The reaction mixture was passed through a pad of silica to aid with removal of coloured impurities stemming from the ruthenium complex and its degradants. Additionally, the product (**2.50**) was converted to the corresponding hydrochloride salt (**2.50·HCl**), which upon addition of TBME precipitated out of solution as a free flowing yellow powder.

With a substantial quantity of alcohol (**2.50·HCl**) to hand, the following aim was to convert this through to a known API, Gepotidacin, which belongs to a new class of antibiotics, currently in phase III clinical trials with the primary indications being uncomplicated urinary tract infection and gonorrhoea.[177] Achieving this would require oxidation of the alcohol (**2.50·HCl**) to the aldehyde oxidation level, followed by a reductive amination with amine (**2.77**).

The oxidation of the alcohol (**2.50·HCl**) to the aldehyde oxidation level (**2.75**) was effected using sulfur trioxide, DMSO and triethylamine, otherwise referred to as the Parikh-Doering oxidation (**Scheme 58**).[178] The key advantage of this approach over the classic Swern conditions[11] are operability without the requirement for cryogenic conditions.

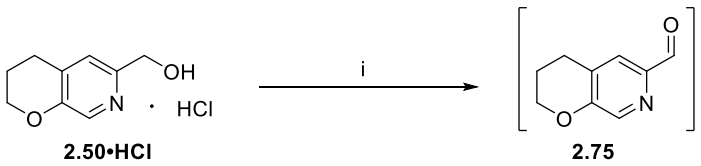

2.50•HCl **2.75**

Reagents and conditions; (i) SO_3·pyridine, Et_3N, DMSO, DCM.

Scheme 58 *Synthesis of aldehyde (**2.75**).*

After multiple attempts, it was concluded that the reaction temperature had to be maintained at 5 °C in order for the reaction to proceed to completion. Allowing the reaction mixture to warm to room temperature would result in the reaction stalling, even after additional oxidant had been introduced. Once < 2 %area of the starting material (**2.50**) was observed by HPLC, the reaction was worked up and telescoped into the next stage as a solution in DCM.

The requisite amine (**2.76**) which was available elsewhere in our laboratories and aldehyde (**2.75**) were left to stir in solvent for 1 h to allow for partial conversion to the imine. To this mixture was added a small excess of sodium triacetoxyborohydride (**Scheme 59**).

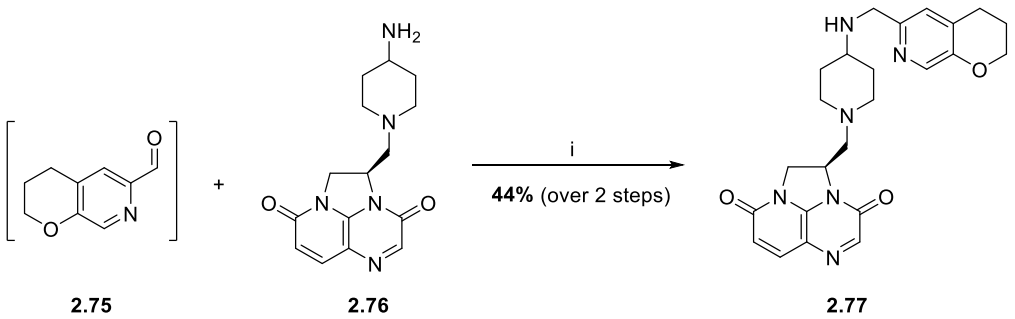

2.75 **2.76** **2.77**

Reagents and conditions; (i) sodium triacetoxyborohydride, solvent.

Scheme 59 *Reductive amination to afford Gepotidacin (**2.77**).*

After being left to stir overnight, the product (**2.77**) was present in 88 %area by HPLC, with 3 %area starting amine (**2.75**) and 2 %area of low-level side-products, likely the side-product arising from two successive reductive aminations. No additional sodium triacetoxyborohydride was added at this stage, as the excess aldehyde (**2.75**) had apparently been reduced to the corresponding alcohol (**2.50**) and increasing the equivalents of aldehyde (**2.75**) was avoided to prevent further impurities being formed. Following the isolation procedure the product was isolated in very good purity (98 %area by HPLC), and dark impurities which arose were also effectively removed.

1.3.17 Reduction of Methyl 6-Methyl Nicotinate (2.45)

Further demonstration of amenability to scale-up was performed by reducing 200 g of methyl 6-methylnicotinate (**2.45**) in a single reaction using just 0.1 mol% $Ru(PNP)Cl_2(NHC)$ (**1.51**). The reaction was run in a 5 L hastelloy pressure vessel equipped with a gas-entrainment impeller (**Scheme 60**).

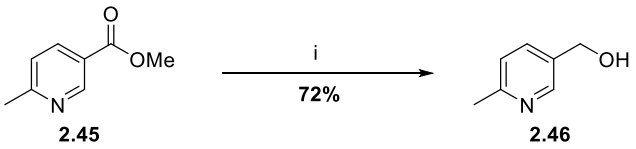

2.45 **2.46**

Reagents and conditions; (i) 0.1 mol% $Ru(PNP)Cl_2(NHC)$ (**1.51**), 20 mol% KO*t*-Bu, 5 bar H_2, 2-MeTHF, 50 °C.

Scheme 60 *Large-scale reduction of methyl 6-methyl nicotinate (**2.45**).*

The reagents were charged to the reactor and the vessel was inerted by performing three nitrogen pressurisation cycles and then charged with hydrogen. After an initial induction period of about 15 minutes, hydrogen consumption was observed to increase very rapidly, and of the 50 L of hydrogen gas uptake measured in total, 47 L were consumed within the first 1.5 hours. During this time, the highest recorded temperature was 53 °C, which was only 3 °C above the jacket temperature. This reflected insignificant exothermic activity, and consequently no additional restrictions on the feed-rate of hydrogen gas were deemed necessary at this scale. More typical heterogeneous hydrogenation reactions would be expected to produce a significant exotherm with consumption at this rate.[150, 179] Once the reaction had reached completion, the solvent was distilled off and the product was isolated from the crude residue by vacuum distillation using a wiped film evaporator. In addition to effectively purging the less volatile hydrolysis side-product, 6-methylnicotinic acid, this also reduced the level of residual ruthenium to 10 ppm. Compared to an existing LAH mediated process which has been previously reported,[168] a significantly improved PMI was achieved (20 vs. 190), and may be further improved by reducing the mechanical losses which occurred during the isolation process. This improved PMI is both a reflection of employing a catalytic rather than a stoichiometric method, as well as less solvent being required for the quench and work-up of the reaction. Further to this, the waste stream consisted of residues enriched in ruthenium which could be sent directly for metal recovery.

The product alcohol (**2.46**) was then further elaborated to generate an intermediate *en route* to a HDAC inhibitor (**2.80**) (**Scheme 61**).[168] The reaction was performed in a 1 L controlled laboratory reaction with jacketed temperature control and overhead stirring starting with 50 g of pyridyl alcohol (**2.46**).

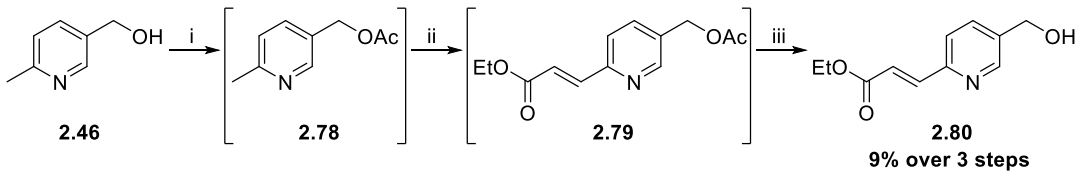

Reagents and conditions; (i) Ac_2O, toluene; (ii) ethyl glyoxylate, $ZnCl_2$, toluene; (iii) HCl, ethanol.

Scheme 61 *Large scale synthesis of ethyl (E)-3-(5-(hydroxymethyl)pyridin-2-yl)acrylate (**2.80**).*

The initial acetylation proceeded in near quantitative yield as evident by HPLC, and this product (**2.78**) was telescoped into the following stage. The second stage also underwent good conversion by HPLC, though it became apparent that a significant proportion of the ethyl glyoxylate, in addition to undergoing the desired condensation to afford the carbon-carbon double bond (**2.79**), had polymerised to give an opaque, black tar. This brought about noticeable complications during the work-up of this stage as these coloured impurities obscured the interface during aqueous extraction. Significant loss of material during the phase separations took place, as the location of the interface had to be estimated based in the quantities of input materials. Dilution with solvent, passing the reaction mixture through a pad of silica, use of increased illumination around the area of the interface were all performed but did not offer any palpable improvements. Lastly, the HCl/ethanol mediated deprotection afforded the product acrylate (**2.80**) in good purity following recrystallisation from TBME, albeit in low overall yield.

Nonetheless, this is further exemplification of value-added products accessible from primary alcohols furnished through catalytic homogeneous ester reductions under mild conditions and it is anticipated that yield could be increased through further optimisation if required.

1.4 CONCLUSIONS

The applicability of ruthenium catalysed ester reductions under conditions achievable in a multi-purpose pressure-reactor for pharmaceutical purposes has been demonstrated. Following selection of an optimal catalyst for such processes, reaction conditions have been optimised following extensive screening to identify 2-MeTHF as a more environmentally sustainable solvent for this transformation, as well as understanding the functional group limitations of the catalyst established.

Additional process understanding was generated using both statistical and kinetic analysis of reactions. In particular, it was found that the reaction performed well under a wide range of parameter setting and were highly reproducible. A better understanding of the side-products which may arise and methods were outlined on how to either suppress their formation or remove these during the work-up procedure. Kinetically, reactions exhibit an induction period, which depending on the temperature, lasts anywhere from minutes to hours. This phenomenon has been attributed to the presence of traces of water in the solvent and reaction vessel. These observations demonstrate a higher than expected level of complexity for what initially appears to be a deceptively simple transformation. The low exothermicity of the reaction, however does not pose any thermal hazard.

Selected substrates were also scaled-up both in batch and in a CSTR flow reactor. Compared to process descriptions which employed LAH and related metal hydride reducing agents, superior PMI values, greater ease of work-up, and reduced waste streams were noted. The product primary alcohols were amenable to further functionalisation to generate value-added intermediates and this approach has also been incorporated in the synthesis of the API Gepotidacin (**2.77**).

1.5 FUTURE WORK

There still remains an interest in synthesising Ru(NNN) (**2.3**), which was predicted to further lower the energetic barrier with respect to ester reductions (**Scheme 62**).

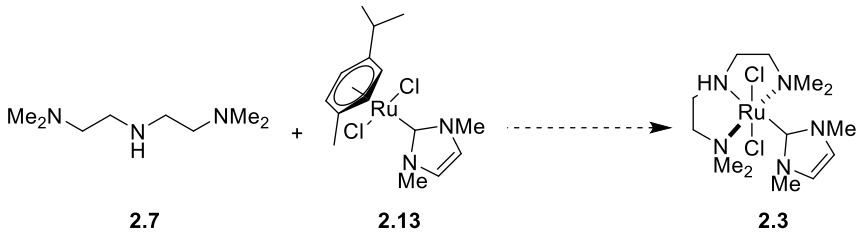

Scheme 62 *Proposed synthesis of Ru(NNN) catalyst (**2.3**).*

Experimentation showed an apparent reluctance of the NNN ligand (**2.7**) to bind to ruthenium complex (**2.13**). Repeating this reaction with higher boiling solvents, such as 1-butanol or toluene may provide an avenue to enable this.

Further testing of the CSTR flow equipment at high pressures (> 50 bar of hydrogen) and temperatures (> 60 °C) is also of interest in order to minimise the necessary residence time and maximise potential throughput. These optimisations would be performed on bromonaphthyl ester (**2.41**) in the first instance, and would be followed up with an extended run (> 24 hour run time). Close attention would be paid to the composition of the output as well as how well the precipitated solids are suspended over this extended duration.

The reduction of amides catalysed by Ru(PNP)Cl_2(NHC) (**2.51**) has also been reported under high pressure (50 bar of hydrogen). Interestingly, this proceeds *via* N-C bond cleavage, giving complementary selectivity to that typically observed for LAH mediated amide reductions (**Scheme 63**).

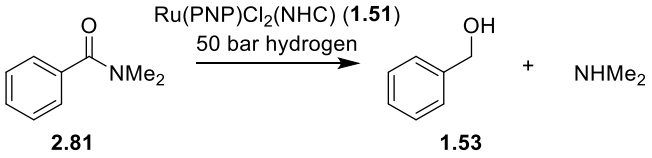

Scheme 63 *Reduction of amines proceeding with N-C bond cleaving reported by Ogata and co-workers.*[180]

While such conditions would not be readily be attainable in batch on scale, the CSTR flow platform could present itself as an enabling technology. This would be trialled on the reduction of Weinreb amide (**2.82**)[181] with the aim of generating an aldehyde as a value added product (**Scheme 64**).

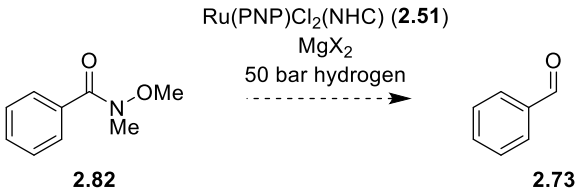

Scheme 64 *Proposed selective reduction of Weinreb amide (**2.82**) to benzaldehyde (**2.73**).*

A metal salt would likely be necessary to chelate and stabilise the presumed tetrahedral intermediates which would form.

2 PHOTOCHEMICAL BROMINATION IN PRODUCTION OF PHARMACEUTICAL INGREDIENTS

2.1 INTRODUCTION

Photochemistry has become an increasingly useful synthetic tool for improving reaction efficiency and for accessing novel chemical space.[182] Numerous reviews on this topic have been published.[183-185] For these reasons, significant efforts into broadening the understanding and applicability towards the synthesis of drug-like molecules have been made.[186] A number of key challenges exist within this field however, including understanding of irradiation requirements and reaction scale-up.[187] As a means of gaining insight into these factors Bonfield, Edwards and co-workers in our laboratories have developed and evaluated the PHIL Pacer as a photochemical screening platform (**Figure 56**).[188]

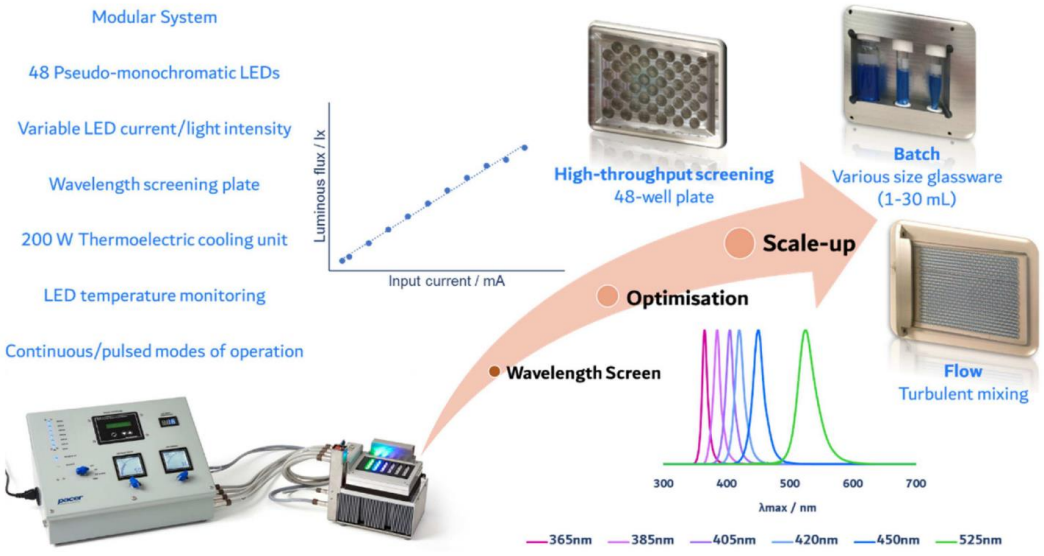

Figure 56 *PHIL Pacer developed and evaluated by Bonfield, Edwards and co-workers.*[189]

The irradiation is performed using powerful pseudomonochromatic LEDs with tuneable wavelength and intensity.[189] This approach addresses issues which have arisen, such as literature procedures exhibiting poor reproducibility due to insufficient understanding of irradiation requirements and indeed the light source itself.[188] The modularity of the PHIL Pacer also allows initial screening to be performed in high-throughput using 48-well plates. Optimised conditions may then be scaled-up either in batch using large test tubes or in flow using the same LED configuration to give hundreds of grams of material.[189] Scaling-up further however, to pilot scale and beyond still remains a gap within the capability of process chemistry in our laboratories, and the pharmaceutical industry in general. According to the Beer-Lambert law, light intensity decreases exponentially as a function of the path length travelled and thus provides a fundamental restriction when attempting to scale this class of reaction in standard batch reactors.[187] Doing so would result in the reaction mixture being subjected to considerably higher light exposure near the light source (i.e. the sides of the vessel) compared to where the reaction mixture is more distant from the light source (i.e. the middle of the vessel). Based on this consideration, the majority of scaling efforts have focussed on leveraging continuous processing as a tool to provide more uniform irradiation by virtue of the decreased path length and increased control over the irradiation time.[186]

One such example reported by Harper and co-workers at AbbVie employed a continuous stirred tank reactor (CSTR) equipped with a high-intensity laser to promote photochemical transformations (**Scheme 65**).[190]

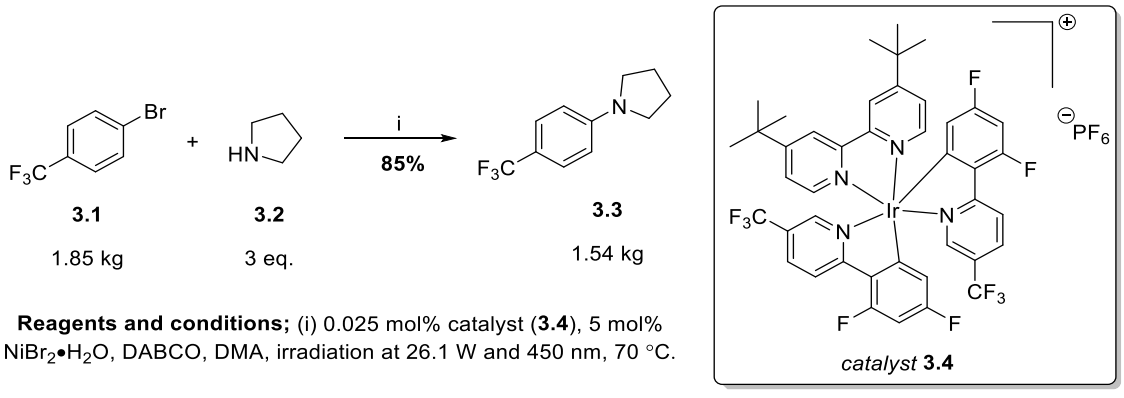

Scheme 65 *Scale-up of photochemical C-N coupling using a CSTR reactor equipped with a laser reported by Harper and co-workers.*[190]

It should be noted that while catalyst (**3.4**) above is depicted as an iridium(III) complex bearing PF_6^- as weakly coordinating anion,[191] the authors refer to a neutral iridium(II) complex bearing no counterion. Such an iridium(II) complex is neither known nor commercially available, and is likely an erroneous depiction. The reactor size and concentration of reagents were optimised according to the Beer-Lambert law to maximise throughput during the development of the photochemical C-N coupling reaction. This approach remarkably furnished 1.54 kg of product (**3.3**) in just 32 h using a 100 mL reactor. The potential issue with such a set-up, however compared to a plug flow reactor are less well-defined residence times, an important consideration for certain photochemical transformations.[192]

In another example reported by Sezen-Edmonds, Tabora and co-workers at Bristol Myers Squibb, a plug flow reactor consisting of FEP tubing combined with an array of high-intensity LEDs was demonstrated to furnish multiple kilograms of product per day.[193] This approach benefits from the short path length and turbulent mixing associated with plug flow reactors, but is less well set-up to tolerate the presence of solids. Fouling on the side of the tubing would result in reduced exposure of the reaction mixture to the light source as well as restricted flow.

Based on the considerations listed above, there still remains the need to develop a platform capable of scaling this challenging class of reactions. This led to the recent development of a photochemical DART (Directly Agitated Reaction Tube) reactor prototype as an alternative approach towards addressing this issue (**Figure 57**).

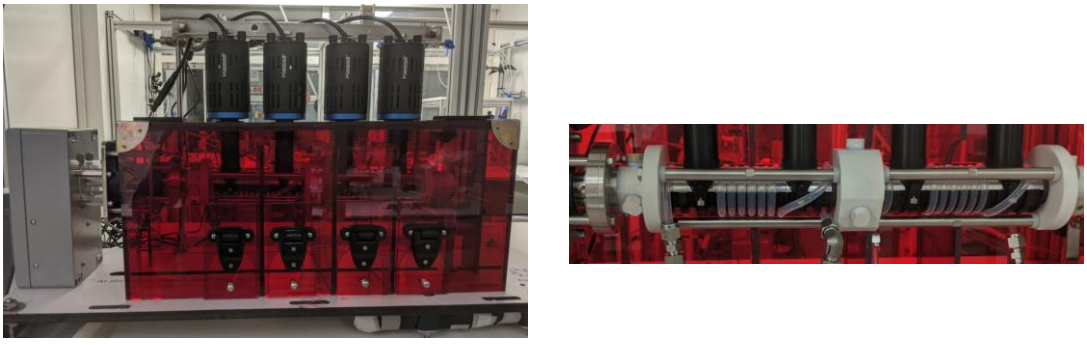

Figure 57 *Photo DART Reactor with 4 Kessil lamps (400 nm) mounted on top.*

The reactor design, not dissimilar from that previously used for continuous hydrogenation reactions (**Figure 54**), incorporates transparent construction materials to allow for light to be introduced *via* 4 Kessil lamps. As with the previous set-up, this offers control over residence time in line with that provided by plug flow reactors while also being capable of tolerating the presence of solids. It is believed that this design will provide the flexibility required for even more challenging photochemical transformations, including heterogeneous photoredox catalysis.[194]

Radical brominations and more specifically benzylic brominations are of particular interest as the resulting benzyl bromide derivates are amenable to further functionalisation through alkylation reactions with a wide range of nucleophiles.[195] Some examples of interest to the pharmaceutical industry are shown below (**Scheme 66**).

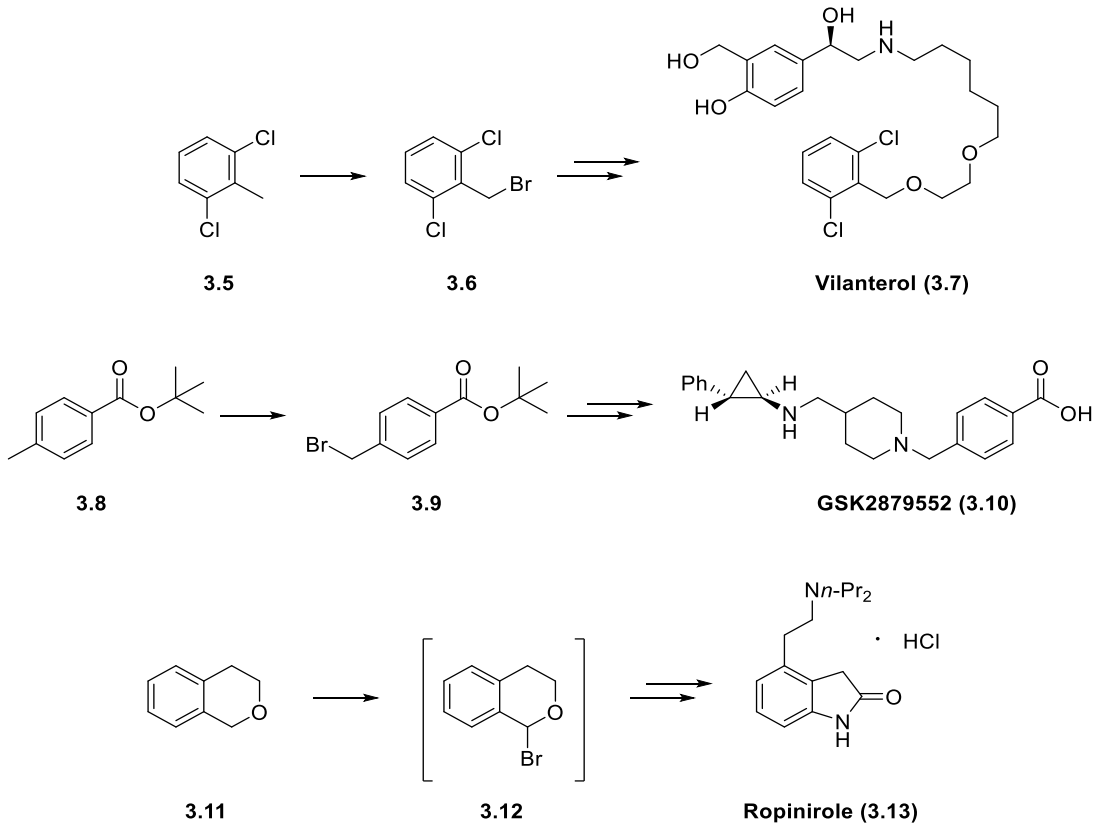

Scheme 66 *Examples of radical brominations used en route to APIs.*[196-198]

Reaction of 2,5-dichloro benzyl bromide (**3.6**) with the oxygen nucleophile, ethylene glycol, is used *en route* to Vilanterol (**3.7**), an ultra-long acting β_2 adrenoreceptor agonist used for treatment of chronic obstructive pulmonary disorder.[196] In another example, *tert*-butyl benzyl bromide (**3.9**) undergoes nucleophilic displacement with a nitrogen-based nucleophile *en route* to GSK2879552 (**3.10**), a lysine-specific histone demethylase 1 inhibitor targeted to treat acute myelogenous leukemia.[197] The last example depicts the benzylic bromination of isochroman (**3.11**) to give an intermediate en route to Ropinirole (**3.13**), a potent non-ergot dopamine receptor agonist used in treatment for Parkinson's disease.[199] Hayler and co-workers noted that scale-up of this process, in batch, resulted in a significant reduction of the yield to 46% compared with 85% yield on laboratory scale. This issue rendered this route commercially unviable, and consequently a new route free of photochemical transformations was developed.[198]

Based on all of the above, gaining access to a range of bromide derivatives using contemporary photochemical methods on scale would be of considerable interest to the preparation of a range of API molecules. Accordingly, this section of the thesis will focus on the application of emerging photochemical platforms to realise this goal.

2.2 AIMS AND OBJECTIVES

The photochemical bromination of benzodiazepine (**4.1**), a compound of interest to an on-going development campaign in our laboratories will be examined in the first instance (**Scheme 67**).

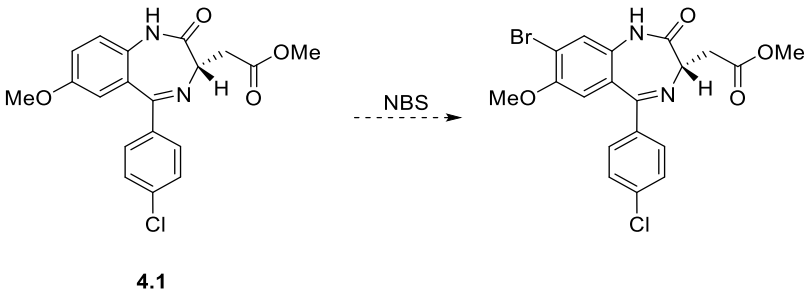

4.1

Scheme 67 *Benzodiazepine (**4.1**) to be examined and possible site of bromination.*

This substrate has not previously been subjected to radical bromination conditions. In addition to gaining increased understanding and optimising the reaction conditions themselves, work will also be conducted to streamline the work-up and isolation procedure (ie. process design). The optimised conditions are to be run in continuous flow in the PHIL Pacer in the first instance and thereafter in the photochemical DART reactor. This will give an indication of how reactions behave in the two set-ups with the longer-term goal of developing a standardised workflow from HPLC vials through to pilot plant scale reactions.

2.3 Results and Discussion

2.3.1 Bromination of Benzodiazepine (4.1)

Benzodiazepine (**4.1**) is an intermediate *en route* to a potent epigenetic regulator of current interest to our laboratories and contains several elements of structural complexity.[200] As such it was pertinent to subject this substrate to photochemical bromination conditions to demonstrate this as a means of late-stage functionalisation. The longer-term aim of this project would be to further elaborate the resulting aryl bromides using photoredox catalysis methodologies previously reported by Buchwald, MacMillan and co-workers to form C-N bonds.[192, 201] Interestingly, as soon as a solution of benzodiazepine (**4.1**) in MeCN came into contact with AcOH, the solution turned from clear and colourless to bright yellow, and a distinct peak was noted in the UV-visible spectrum (**Figure 58**).

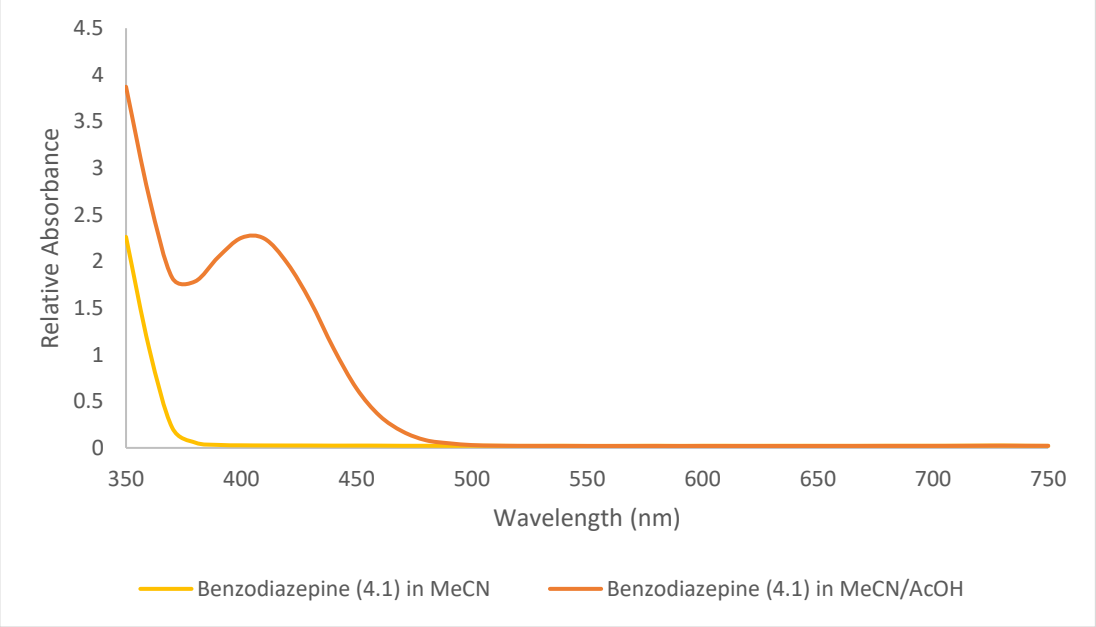

Figure 58 *UV-visible spectra of benzodiazepine (**4.1**) with and without AcOH*

Benzodiazepine (**4.1**) was subjected to bromination conditions similar to those previously employed by Bonfield, Edwards and co-workers.[188] The key difference between this work and

the previous findings is that the reaction was run at much higher dilution due to poor solubility of benzodiazepine (**4.1**) in MeCN/AcOH (**Table 25**). It was expected that the relatively electron rich methoxy bearing benzoid ring would be the site of reactivity in this instance. It should be noted that while the input material was of high enantiomeric excess, no chiral HPLC analysis was performed on any of the products obtained, and as such the stereochemical information on these is deliberately omitted.

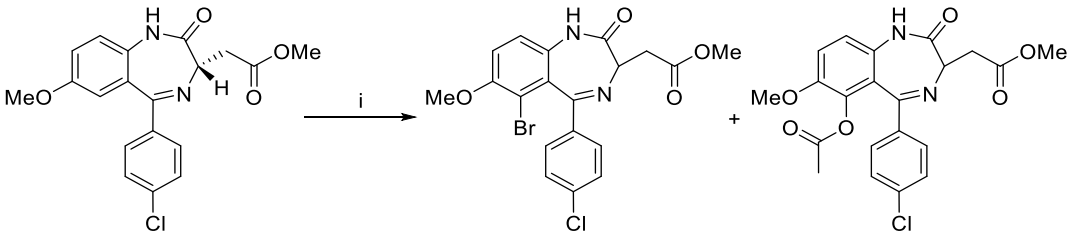

4.1 **4.2** **4.3**

Reagents and conditions; (i) NBS, MeCN/AcOH, irradiation at 250 mA, 35 mins.

Wavelength (nm)	%Area composition[a] (4.1/4.2/4.3)
365	43/15/36
385	38/17/39
405	36/17/41
420	30/18/45
450	27/19/48
525	29/18/53

[a]Assessed by HPLC with UV-detection at 220 nm

Table 25 *Wavelength screen for bromination of Benzodiazepine (**4.1**).*

Unexpectedly, after 35 minutes of irradiation, HPLC analysis revealed that the reaction mixture contained 29 – 43 %area unreacted starting material, and formation of two new products was observed across all wavelengths (365, 385, 405, 420, 450, 525 nm). Interestingly, however, reactions subjected to longer wavelengths (420, 450 and 525 nm) contained slightly less unreacted starting material (**4.1**) compared to reactions subjected to shorter wavelengths (365, 385 and 405 nm). This may be due to the stronger absorption, and

therefore inferior penetration of the light at these lower wavelengths, consistent with the absorbances noted in the UV-visible spectrum (**Figure 58**). Characterisation of the first product (**4.2**) revealed, somewhat surprisingly, that bromination had taken place at the seemingly most hindered site as became apparent based on the disappearance of the characteristic doublet at δ = 6.75 ppm. Of the two *ortho* positions with respect to the methoxy group, the position closer to the neighbouring phenyl group appeared to be favoured. Examination of the ^{1}H NMR spectrum of the starting material (**4.1**) revealed that this aromatic proton is, by far the furthest upfield, with a chemical shift of δ = 6.75 ppm being 0.5 ppm away for the next aromatic signal. Presumably the high electron density around this proton provides an explanation for the observed selectivity.

In addition to bromination, an *O*-acylated phenol product (**4.3**) was also observed. Both of products (**4.2** and **4.3**) isolated may have formed as a result of a radical cationic intermediate being trapped by nucleophilic attack of either bromide or acetate (**Scheme 68**). Such a radical cation would be formed by initial single electron oxidation of benzodiazepine (**4.1**). Though further experimentation would be necessary to determine the exact nature of oxidant A, bromine radicals or acetyl hypobromite could possibly serve this purpose. Subsequent trapping of the radical intermediate by molecular oxygen and elimination of a hydroperoxide radical to rearomatise would then serve to afford the products. This pathway involving triplet oxygen has previously been proposed in studies carried out by Nicewicz and co-workers.[202]

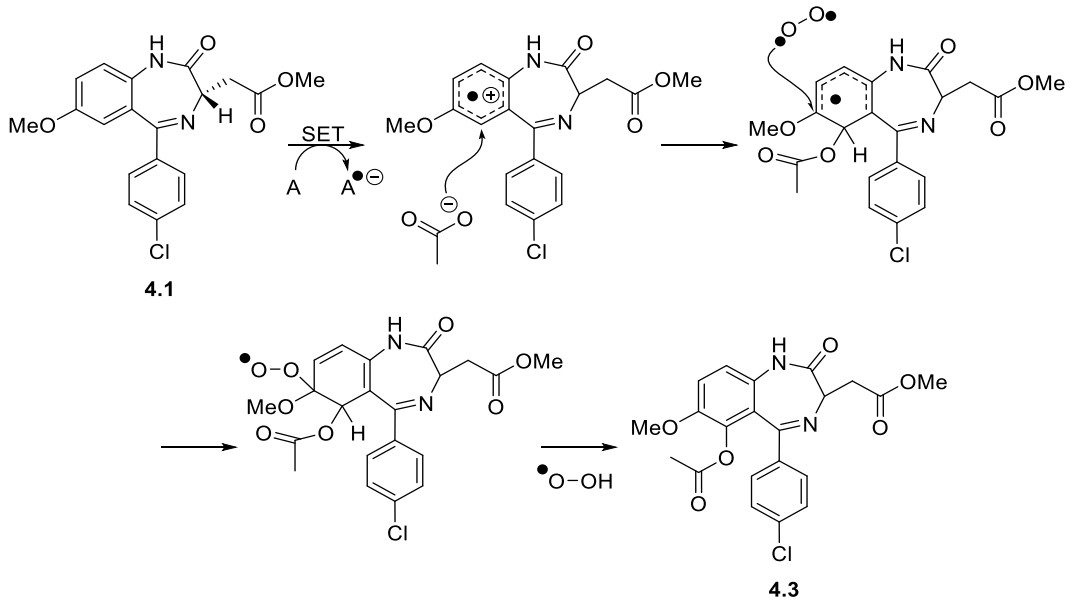

Scheme 68 *Proposed mechanism for formation of O-acylated phenol (**4.3**).*

Such radical cations formed by single electron oxidation of anisole derivatives have been frequently involved in numerous methodologies utilising various nucleophiles including bromide[202-204] and nitrogen-based nucleophiles.[202] These methodologies typically rely on the presence of an organic photocatalyst to induce the initial single electron transfer. While no such photocatalyst was added in the current study, bromine radicals, or indeed acetyl hypobromite may serve this purpose, either directly, or *via* formation of an electron donor-acceptor complex with benzodiazepine (**4.1**) and induced by the availability of high-energy photons.[205] Alternatively, the substrate itself may be acting as a photosensitiser, a hypothesis made more credible by the fact that benzodiazepine (**4.1**) absorbs strongly above 400 nm when in the presence of acetic acid.

Conversion of the brominated product (**4.2**) to the *O*-acylated phenol (**4.3**) *via* a nucleophilic substitution process was also considered a possibility, though this was deemed less likely as (i) no displacement of the chloride on the second aromatic ring was observed, which would presumably be more susceptible to an S_NAr process; and, (ii) stirring the brominated product (**4.2**) in a MeCN/AcOH mixture did not result in any formation of the *O*-acylated phenol product (**4.3**) (**Scheme 69**).

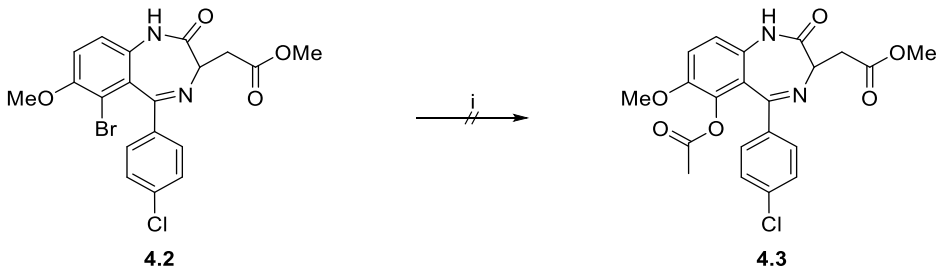

4.2 **4.3**

Reagents and conditions; (i) 1:1 MeCN/AcOH, 1 week.

Scheme 69 *Control experiment suggesting O-acylated phenol (**4.3**) is likely not formed via a nucleophilic aromatic substitution process.*

Intrigued by these unexpected outcomes, control experiments were performed to gain additional insight into the nature of how these products are formed. Repeating the reaction with the addition of an equivalent of TEMPO (acting as a radical trap) resulted in no consumption of the starting material, consistent with a radical mechanism being in operation (**Scheme 70**). No inhibition, by contrast, would be more indicative of a cationic mechanism.

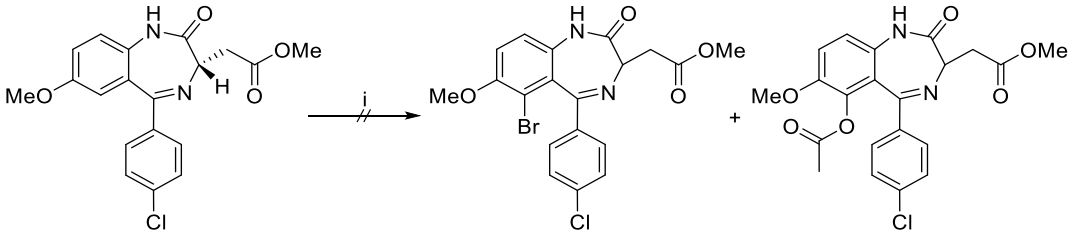

4.1 **4.2** **4.3**

Reagents and conditions; (i) NBS, TEMPO, 1:1 MeCN/AcOH.

Scheme 70 *Control experiment underwent no conversion due to presence of the radical trap, TEMPO.*

Leaving the unirradiated reaction in the dark at rt did result in formation of the brominated product (**4.2**) and the *O*-acylated phenol (**4.3**), albeit at a significantly reduced rate compared to when the reaction mixture was irradiated. Given the presence of oxygen and the lack of any radical initiator, this finding would, paradoxically, be more consistent with an electrophilic aromatic substitution process being in operation. Omission of NBS resulted in complete recovery of the starting material, indicating that NBS is the key oxidant in the

formation of both products. The exact nature of the mechanism based on these finding is not clear, and the reaction appears to exhibit characteristics typical for both radical and cationic pathways. Further experimentation using radical initiators such as benzoyl peroxide or Lewis acids to encourage formation of cationic intermediates could be used to provide further insight into this unsolved question.

As this stage, there was a relatively high degree of confidence that formation of the *O*-acylated phenol (**4.3**) was a consequence of employing AcOH as part of the solvent system. The obvious way to suppress its formation and thereby increase selectivity towards formation of the brominated product (**4.2**) was to omit AcOH completely. It was realised, however, that the presence of acetic acid serves to increase rate of reactivity by weakening the N-Br bond, and in removing this, the need for longer reaction times was anticipated. This time running the reaction in MeCN unexpectedly resulted in the formation of two new isomeric vinyl bromides (**4.4 & 4.5**) being formed as was evident by appearance of two new olefinic resonances in the ^{13}C NMR spectrum, with no evidence of the aryl bromide (**4.2**) or indeed *O*-acylated phenol (**4.3**) being formed (**Scheme 71**).

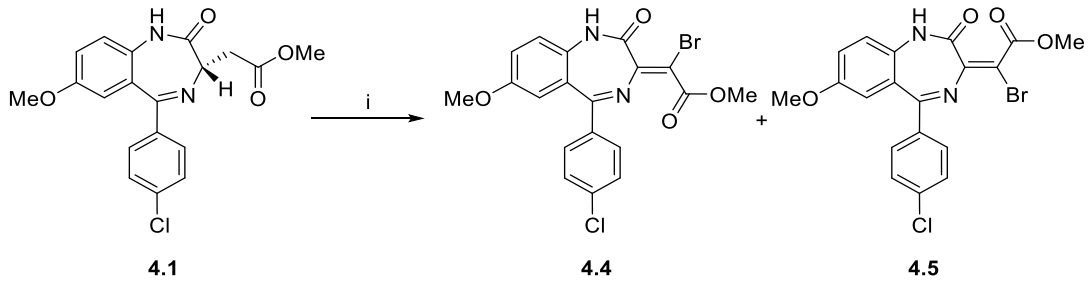

Reagents and conditions; (i) NBS, MeCN, irradiation at 385 nm, 300 mA, 2 h.

Scheme 71 *Subjection of benzodiazepine (**4.1**) to radical bromination conditions in absence of AcOH to generate vinyl bromide products (**4.4 & 4.5**).*

These isomeric products were likely formed as a result of two consecutive bromination reactions taking place, followed by elimination of HBr to form a more highly conjugated system (**Scheme 72**).

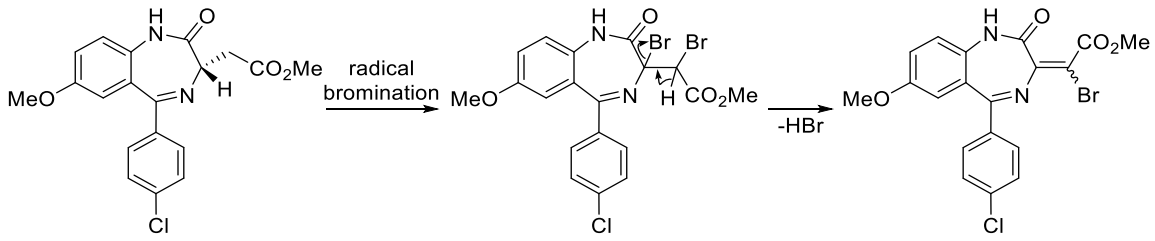

Scheme 72 *Proposed mechanism for formation of vinyl bromides (**4.4 & 4.5**).*

Similar reactivity in such 1,4 dicarbonyl systems has previously been reported under thermal conditions using molecular bromine (**Scheme 73**).[206]

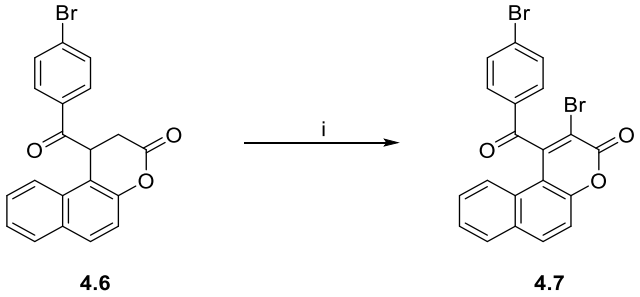

Reagents and conditions; (i) Br_2, AcOH, reflux, 4 h.

Scheme 73 *Formation of vinyl bromide (**4.7**) from 1,4-dicarbonyl (**4.6**) under thermal conditions reported by El-Kady and co-workers.*[206]

It appears therefore, that in addition to the colour change caused by addition of AcOH, the change to the electronics of the system also causes aryl bromination to be favoured over alkyl bromination. Whether the presence of AcOH results in electrophilic aromatic susbtitution being favoured, or whether AcOH facilitates certain mechanistic pathways through hydrogen bonding interactions is unclear and requires further experimentation to be fully understood.

At this stage, the decision was made, due to the difficulty in working with benzodiazepine (**4.1**) as a result of unselective processes and relative insolubility, to deprioritise investigating this molecule and instead switch to a simplified model substrate.

For future investigations there is interest, however, in examining a broader range of solvents in order to run processes at more acceptable concentrations. Furthermore, an acid screen, including various organic acids such as *p*-toluenesulfonic acid and acidic solvents such as HFIP would also be of interest, as the presence of AcOH has been shown to fundamentally change the reactive nature of this molecule. Addition of Lewis acids, such as $AlBr_3$ or $FeBr_3$ could also be investigated, and may provide further insight into the nature of the mechanism in operation. NMR analysis of benzodiazepine (**4.1**) in the presence of acetic acid may also provide insight on the nature of the electronic changes in the molecule, including the preferred site of protonation.

2.3.2 Optimisation of Benzylic Bromination

Moving forwards, it was decided to investigate ethyl 4-methylbenzoate (**4.8**) as a model substrate for bromination. In addition to being cheap and readily available, a detailed study on the photochemical bromination of this substrate has previously been described.[188] This included scale-up to 47 g input using continuous processing (**Scheme 74**). Further characterisation of this reaction on a range of photochemical platforms and scales could offer further insight into the preparation of APIs of the type previously discussed (**Scheme 66**).

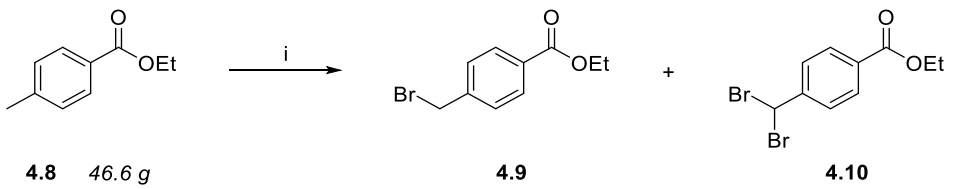

4.8 *46.6 g* **4.9** **4.10**

Reagents and conditions; (i) NBS, MeCN/AcOH, irradiation at 385 nm, 200 mA, 1.36 min residence time.

Scheme 74 *Benzylic bromination described by Bonfield, Edwards and co-workers.*[188]

These conditions provided a good starting point, however, did require further optimisation for further scale-up. The use of AcOH as a co-solvent is sub-optimal due to both its corrosive nature and difficulties to remove. This results in an arduous work-up procedure, which both requires large volumes of water and multiple extractions to be performed. In light of these

issues, the goal was to identify an optimised procedure, including work-up and isolation of the product prior to further scale-up.

In the first part of the study, a wavelength screen was carried out on a 1 mL scale in a high-throughput manner to determine how this affects reactivity (**Table 26**). It should also be noted that ~ 80 %area product corresponds to the maximum attainable product yield by virtue of full consumption of the brominating reagent, NBS. Though a small excess of NBS is present, approximately 8 %area of unreacted starting material (**4.8**) and up to 10 %area of dibrominated product (**4.10**) are routinely observed due to the selectivity of the reaction. The presence of 1.05 equivalents of NBS has previously been shown to maximise the yield of the mono-brominated product (**4.9**) and, will be used throughout this investigation. Addition of a greater excess of NBS results in marginal reduction of the residual starting material (**4.8**), while substantially increasing the quantity of the dibrominated side-product (**4.10**).[188]

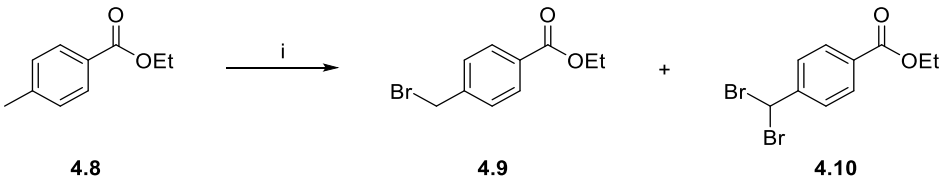

4.8 **4.9** **4.10**

Reagents and conditions; (i) NBS, MeCN/AcOH, wavelength, 200 mA.

Wavelength (nm)	%Area composition after 5 mins[a] (4.8/4.9/4.10)	%Area composition after 10 mins[a] (%) (4.8/4.9/4.10)
365	8/83/5	7/83/6
385	96/4/0	6/83/6
405	8/83/5	7/83/6
420	8/83/5	7/83/6
450	8/83/5	8/82/5
525	100/0/0	9/82/5

[a]Assessed by HPLC with UV-detection at 220 nm

Table 26 *Wavelength screen for benzylic bromination of ethyl 4-methylbenzoate (**4.8**).*

Comparable performance was seen across the wavelengths examined, and within 10 mins all reactions had reached the maximum conversion attainable based on the quantities of input material. The longer wavelength of 525 nm was noted to be significantly slower to react compared with the other wavelengths used, but did also reach the same endpoint after 10 mins. The relatively low yield seen for 385 nm at 5 mins is likely an anomaly for reasons not fully understood, though is suspected to be caused by an extended induction period. In this instance, a wavelength close to 400 nm will be favoured, as the DART reactor available in our laboratories is equipped with 400 nm Kessil lamps.

A solvent screen was then performed utilising an array of commonly employed laboratory solvents (**Table 27**), with the aim of finding a solvent system, which could either reduce or eliminate the use of AcOH.

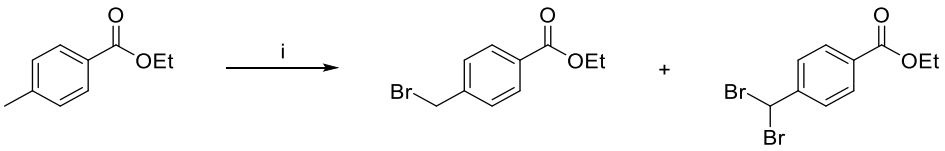

4.8 **4.9** **4.10**

Reagents and conditions; (i) NBS, solvent, irradiation at 385 nm, 300 mA.

Solvent	**Yield[a]/ %** **(4.8/4.9/4.10)**
THF	100/0/0
2-MeTHF	100/0/0
EtOAc	17/73/3
Acetone	10/81/5
MeCN	6/85/6

[a]Assessed by HPLC with UV-detection at 220 nm.

Table 27 *Solvent screen for benzylic bromination of ethyl 4-methylbenzoate (**4.8**).*

Puzzlingly, reactions in THF and 2-MeTHF underwent no conversion, despite readily solubilising all the reagents and being solvents known to allow photochemical processes to take place.[207, 208] It was later established that the most probable reason for this is the

presence of the radical inhibitor, butylated hydroxytoluene. While inhibitor-free THF and 2-MeTHF are commercially available, employing these is non-preferred due to increased risk of forming unstable peroxides, particularly as these reactions were not inerted with nitrogen. EtOAc efficiently promoted the reaction under photochemical conditions. Heating the reagents dissolved in EtOAc to reflux for 2 h resulted in formation of approximately 12 %area of monobrominated product (**4.9**). This indicates that while thermal background reactivity is possible, it is most likely negligibly low on the time scale examined here. The use of EtOAc was, however, ultimately abandoned due to the need to run reactions at unfavourably high dilutions due to the low solubility of NBS in this solvent. Acetone also efficiently promoted the reaction, while additionally allowing for reactions to be run more concentrated compared to EtOAc. This solvent, too, was abandoned due to the risk of forming toxic and volatile bromoacetone.[209] Lastly, it was found that use of neat acetonitrile provided a satisfactory rate of reaction without the need for high dilution or the risk of forming toxic and volatile side-product. In this instance it appears that ethyl 4-methylbenzoate (**4.8**) is sufficiently amenable to bromination without the need for an acidic promotor to be present. Consequently, MeCN will be employed as the solvent of choice moving forwards.

Solubility data was also gathered, and it was established that NBS has a higher solubility in neat MeCN than it does in MeCN/AcOH (1:1). Thus, the concentration of the reaction was varied to identify whether further intensification was feasible (**Table 28**).

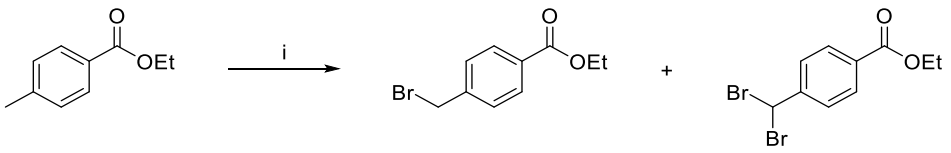

4.8 **4.9** **4.10**

Reagents and conditions; (i) NBS, MeCN, irradiation at 405 nm, 300 mA, 5 mins.

Concentration (mol/L)	Yield[a]/ % (4.8/4.9/4.10)
0.10	6/85/5
0.30	5/86/6
0.50	5/86/7
0.68	5/86/7

[a]Assessed by HPLC with UV-detection at 220 nm.

Table 28 *Variation of concentration during bromination of ethyl 4-methylbenzoate.*

Although there were concerns that increasing the concentration could impede light penetration, this did not appear to be an issue within the study range. Increasing the concentration still allowed reactions to go to reach high conversions within a relatively short timeframe. No precipitation was observed during any of the reactions, suggesting that these new conditions are suitable for scale-up under flow conditions. Assuming that reactions run at this higher concentration can be processed at the same rate reported by Bonfield, Edwards and co-workers,[188] then this should theoretically more than double the throughput compared to what was previously achieved. One key difference which was noted, however, at the highest concentration examined (0.68 mol/L) was the increased exothermicity of the reaction. Vials became warm to the touch and this observation prompted further quantitative investigation to assess whether thermal output from the reaction is of concern with regards to reaction scale-up.

Time-course reactions were set up to assess, as a function of time, both the temperature (**Figure 60**) and %area product present in solution (**Figure 59**). Due to the fast reaction kinetics, samples were taken as frequently as every 10 s in order to capture the most information-rich stages of the reactions.

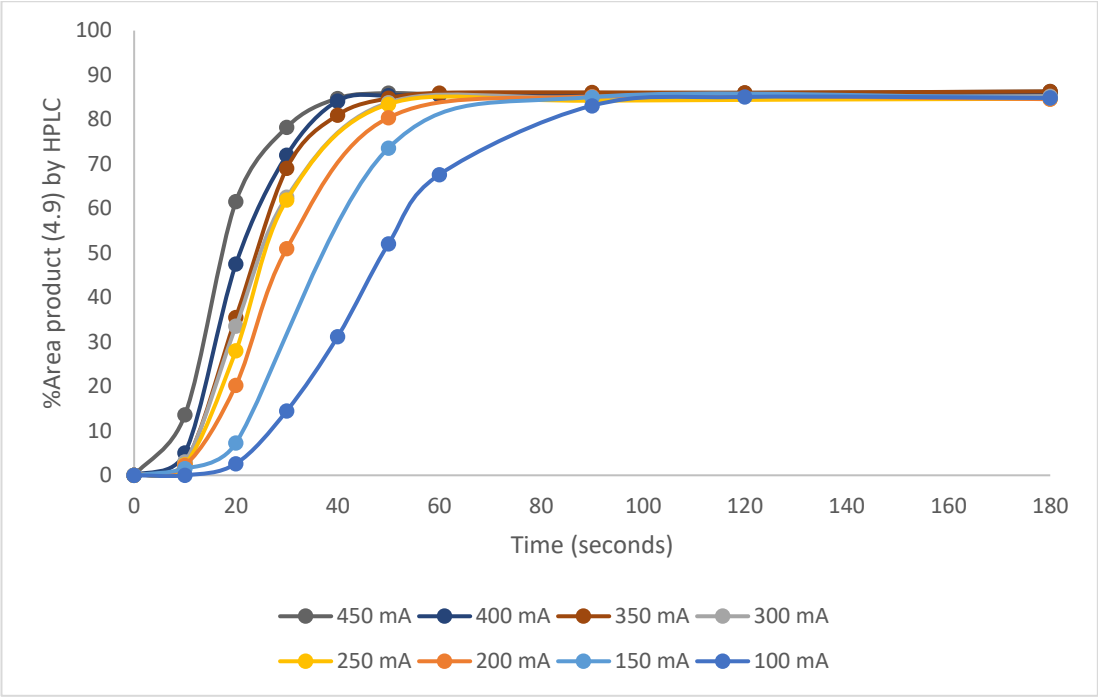

Figure 59 *HPLC data for benzylic bromination of ethyl 4-methylbenzoate (**4.8**) promoted by irradiation using PHIL Pacer collected as a function of time.*

A short induction period was observed in each case, during which time presumably low levels of residual bromine in NBS are homolysed to generate bromine radicals.[188] With the exception of reactions run at lower light intensities (< 150 mA), product formation typically plateaued within 1 min of irradiation. Furthermore, light intensities above 300 mA appear to provide diminishing returns in terms of benefiting the reaction, suggesting the reaction mixture is adequately irradiated, and photons are no longer the limiting reaction component. The very marginal improvements still observed at light intensities above 300 mA are likely due to the increased temperature at these higher intensities leading to faster diffusion, particularly since only passive mixing was in operation. Based on this, 300 mA will be chosen as the appropriate light intensity for scale-up in flow, as this strikes a balance between reaction rate, energy consumption and cooling requirements.

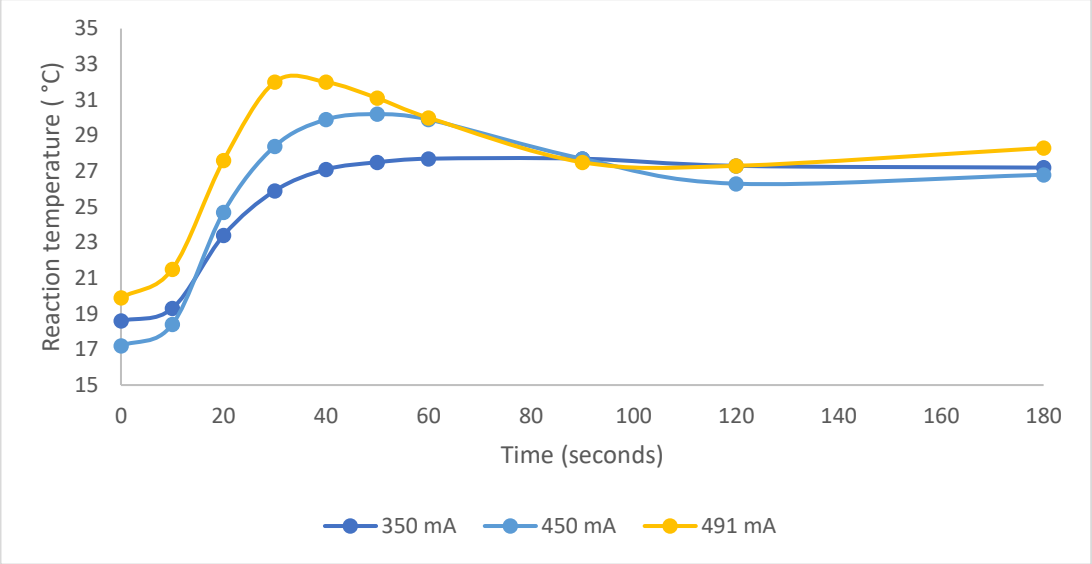

Figure 60 *Temperature data for benzylic bromination of ethyl 4-methylbenzoate (**4.8**) promoted by irradiation using PHIL Pacer collected as a function of time.*

Visible exotherms were also observed by inserting a thermocouple into the HPLC vials containing the reaction mixture. These would, however, quickly dissipate thereafter as a result of the efficient heat transfer characteristics on this small scale. Nonetheless, it became apparent that the majority of the heat output from the reaction would take place during the first 40 seconds of the reaction (**Figure 60**). Higher light intensities resulted in this exotherm taking place more quickly and peaking at a higher temperature, the highest recorded temperature being 32 °C in the case where the light intensity was set to 491 mA. Interestingly, even after full consumption of the NBS had taken place, vials would cool down to 28 °C, noticeably above ambient temperature, either due to conversion of the incident light into heat energy, or due to direct heating from the LEDs themselves.

With better understanding of the kinetics and exothermic activity of the reaction in HPLC vials, a similar experimental plan was set up using a Kessil lamp identical to that used in the Photo DART reactor and a larger 4 mL vial (**Figure 61**). This was for the purpose of gaining a better understanding of how the reaction may behave in the Photochemical DART reactor, particularly due to the increased path length of the light and slower mass and energy transfer which would take place on this larger scale. This would also allow for the performance of the Kessil lamp to be compared to that of the LEDs present in the PHIL Pacer. It should be noted

that the light well attached to the Kessil lamp serves to focus the light emitted, thereby increasing the intensity by a factor of 7 at 400 nm.

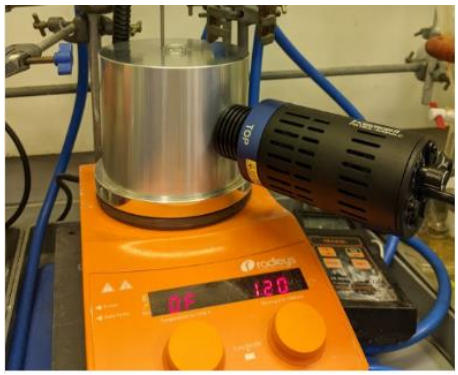

Figure 61 *Irradiation of vial containing reaction mixture with 45 W Kessil lamp (reaction is in the centre of the aluminium black).*

Longer reaction times were noted, in line with what would be expected from larger scale reactions, though reactions at the highest intensity setting (100%) were nonetheless complete after 90 seconds (**Figure 62**). Slower performance was noted at 75% and 50% intensity, while still following a similar kinetic profile. A reaction run at 25% intensity in contrast underwent significantly slower conversion, with an apparently linear kinetic profile showing the effects of inadequate irradiation. Presumably the reaction rate is limited, in this case, by supply of photons rather than the kinetics of the reaction or mass transfer.

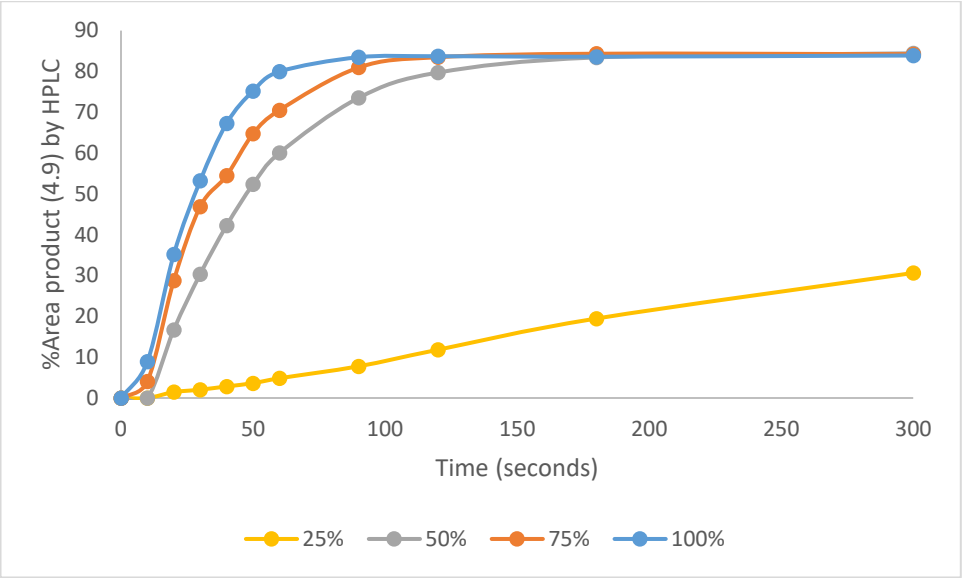

Figure 62 *HPLC data for benzylic bromination of ethyl 4-methylbenzoate (**4.8**) promoted by irradiation with Kessil lamp collected as a function of time.*

The temperature data also reflects the slower mass and heat transfer characteristics. In particular, higher temperatures were noted compared with reactions run in the PHIL Pacer, with a highest recorded temperature of 46 °C at 100% intensity (**Figure 63**). Furthermore, irradiating blank MeCN to demonstrate the background heating capacity increased to just 30 °C, a difference of 6 °C above ambient.

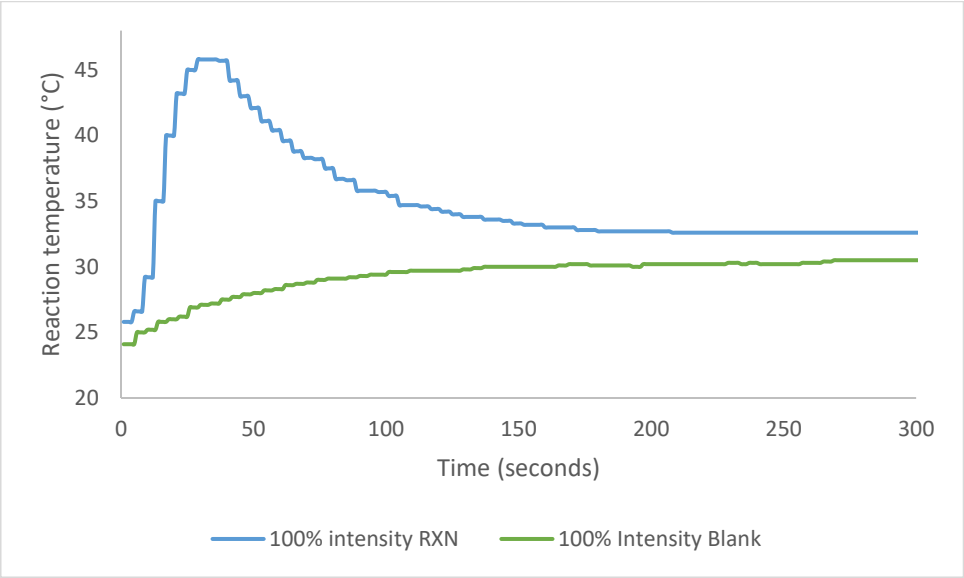

Figure 63 *Temperature data for benzylic bromination of ethyl 4-methylbenzoate (**4.8**) promoted by irradiation with Kessil lamp at 100% intensity collected as a function of time.*

The temperature data at 75% and 50% intensity showed a similar exothermic activity profile, with the exotherm being prolonged in duration and peaking at a lower maximum temperature (**Figure 64**).

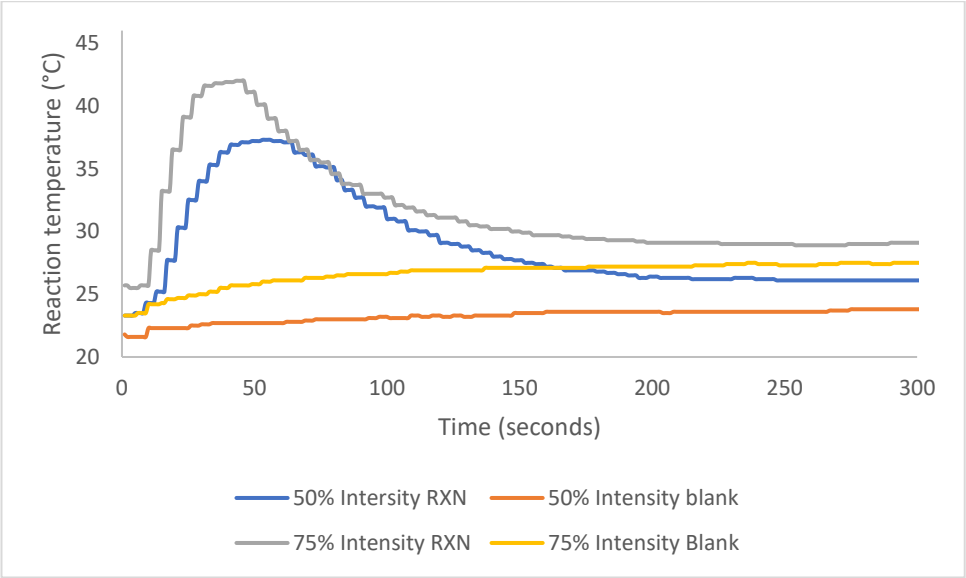

Figure 64 *Temperature data for benzylic bromination promoted by irradiation with Kessil lamp at 75% and 50% intensity collected as a function of time versus control.*

Consequently, 100% intensity is the most appropriate light intensity to start off with when transferring reactions to the Photo DART reactor in order the maximise potential throughput. The end of the exotherm has also been shown to coincide with reactions reaching maximum conversion and therefore temperature may be used as a means of monitoring reaction progress. Finally, the highest recorded temperature, 46 °C is well below the boiling point of acetonitrile (82 °C). Since no other thermal events or decomposition were noted under typical reaction conditions, the reaction was deemed safe to scale-up further in flow. It should be noted that it has been demonstrated that reactions could be aborted instantly by removing the light source should this be necessary. The oxygen present then presumably terminates all radical chains.

The last aspect to address prior to examining a scaled-up run was work-up and isolation of the product benzyl bromide (**4.9**). The previous procedure required a large excess of water to remove the acetic acid. Aqueous base and aqueous thiosulfate washes were also performed to remove succinimide and residual bromine or NBS, respectively. Following this a solvent exchange into heptane was performed, from which the product was crystallised. Examination of this suggested that direct extraction into heptane would be advantageous and would reduce the solvent usage drastically. Investigating this on a small scale, however, revealed that the product was significantly more soluble in the reaction solvent, MeCN than

in heptane. This was addressed by addition of water, which displaced the product from the MeCN layer into the heptane layer. In principle, this heptane layer could then be concentrated as necessary and cooled to induce product crystallisation. This would be favourable as both solvent usage and the number of unit operations compared to the previous process would be significantly reduced.

Based on the optimisation work carried out, the next step was to demonstrate this process on a ~60 g scale to understand how the process would perform.

2.3.3 Scale-up in Flow using PHIL Pacer

Scale-up in the PHIL Pacer system was performed with 65 g in ethyl 4-methylbenzoate (**4.8**) in solution with 1.05 eq. NBS to give a total volume of ~0.6 L. The flow plate depicted below has previously been employed by Bonfield, Edwards and co-workers in effecting this transformation and has been noted to induce highly turbulent mixing by virtue of the meandering nature of the channel (**Figure 65**).

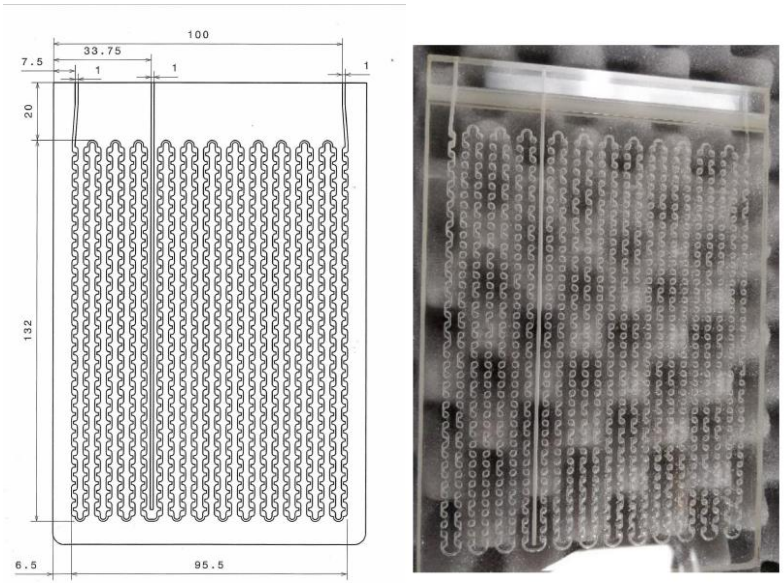

Figure 65 *Diagram and picture of glass plate used for flow experimentation in PHIL Pacer.*

The flow rate was gradually ramped up until a high flow rate of 8 mL/min corresponding to a residence time of 30 s was achieved. Intriguingly, 82 area% product was achieved at this relatively short residence time and consistent product output was noted (**Table 29**). This is in spite of prior experiments in HPLC vials suggesting incomplete conversion after this duration of time (**Figure 59**). These favourable kinetics in the flow set-up were attributed to (i) reduced path length required for the light to travel through, presumably leading to more uniform and intense exposure of the solution to light, and (ii) the highly turbulent mixing which would arise when pumping the solution at this fast rate.

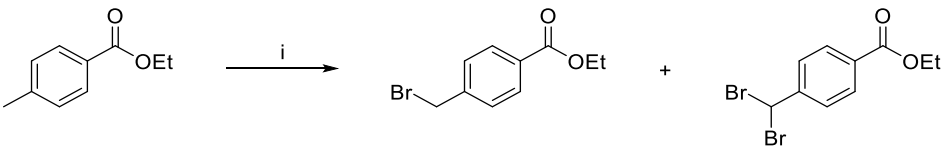

4.8 **4.9** **4.10**

Reagents and conditions; (i) NBS, MeCN, irradiation at 405 nm, 300 mA, 30 s residence time.

Analysis performed	**%Area composition[a] (4.8/4.9/4.10)**
output sampled after 20 mins at steady-state	6/82/11
output sampled after 60 mins at steady-state	6/82/11
output sampled after 75 mins at steady-state	6/82/11
combined end-of-reaction mixture	6/82/11
[a]Assessed by HPLC with UV-detection at 220 nm.	

Table 29 *Analysis of samples collected from flow run in PHIL Pacer.*

All the reaction components remained in solution and no formation of precipitates or unusual exothermic activity were noted during the ~1.5 hour run time. The pressure remained steadily around 2.2 bar, significantly below the 20 bar rating of the glass flow plate. It is also worth noting that running this intensified process continuously could theoretically process ethyl 4-methylbenzoate (**4.8**) at a rate of 1 kg/day. This represents an almost 5-fold increase in throughput compared to previous efforts to scale-up this reaction using the same experimental set-up.

Following successful processing of the input material, the modified work-up procedure was then investigated. It transpired that addition of an insufficient quantity heptane would result in an unfavourable outcome whereby three layers would form (**Figure 66**).

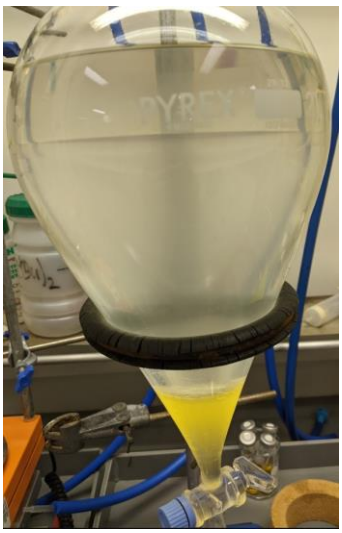

Figure 66 *Formation of triphasic system; top layer: heptane, middle layer: aqueous acetonitrile, bottom layer: organic acetonitrile.*

Analysis of each layer by ^{1}H NMR and HPLC revealed the top layer to contain the majority of the product (**4.9**), along with unreacted starting material (**4.8**) and the dibromo side-product (**4.10**) dissolved in heptane and the middle layer to consist of an aqueous acetonitrile mixture containing very little product (**4.9**) in line with what was expected. The bottom layer, which was also the smallest, consisted of a highly concentrated solution of product (**4.9**), unreacted starting material (**4.8**) and dibromo side-product (**4.10**) in acetonitrile. Evidently this mixture was immiscible with both heptane and aqueous acetonitrile and thus separated to form its own layer. Owing to the high density of this composition, it resided at the bottom of the vessel. This issue was ultimately overcome by addition of a further quantity of heptane. Doing so resulted in all the organic compounds moving into the heptane layer, which in turn led to disappearance of the lower acetonitrile layer, and restoration of a biphasic system (**Figure 67**). Further NMR analysis confirmed that the succinimide by-product resided exclusively in the aqueous acetonitrile phase, obviating the need for further washes with aqueous base.

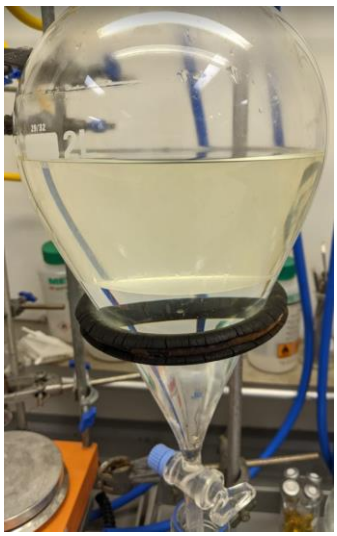

Figure 67 *Restoration of a biphasic system by increasing amount of heptane added; a significant portion of aqueous layer has been drained off for clarity.*

It is also expected that the quantity of heptane necessary to effect formation of two distinct phases could also be reduced if partial removal of acetonitrile by means of a put-and-take distillation employing heptane is performed prior to commencing the extraction process. Given the lower boiling point of acetonitrile compared to heptane and good solubility of succinimide in water, it is anticipated this would be a relatively facile operation and would ultimately result in clear phases free from precipitates.

Following on from this, the goal was to isolate the product from the heptane solution. Concentration to dryness is non-preferred on this scale due to the high energy consumption, poor control over particle morphology and concentration of potentially unstable impurities. For these reasons, recrystallisation is the preferred means of isolating solid compounds.

The heptane layer was distilled down to a reduced volume (~300 mL, approximately 5 volumes) and cooled to 20 °C, at which point seed crystals were added and persisted (**Figure 68**). This volume was chosen on the basis of prior experimentation which demonstrated a balance between lower concentrations reducing the yield of product obtained, and higher concentrations resulting in the solution solidifying and becoming unmixable.[188]

Figure 68 *Seeded cooling crystallisation process of benzyl bromide ester (**4.9**).*

Thereafter, the solution was left to cool on a ramp to induce further precipitation, with particular care taken to do so at a slow rate to promote crystal growth. Overhead stirring was chosen to minimise attrition of the crystals formed, as is characteristically the case when magnetic stirring is in operation.

The rapid filtration process which followed confirmed that either significant growth or agglomeration had taken place, and washing the wet cake with cold heptane removed the remaining unreacted ethyl 4-methylbenzoate (**4.8**) starting material to below the limits of detection by HPLC. The dibromo side-product (**4.10**), in contrast did not purge well under these conditions, with 9 %area being observed by HPLC (level at end of reaction was 11 %area). However, this compares unfavourably to the previous report, which had noted 95 %area purity of the product (**4.9**). Though no further information was given on which compounds gave rise to the remaining 5 %area in the chromatogram, it could indeed also be due to the presence of dibromo side-product (**4.10**). Alternatively, this may have been purged more effectively due to the different temperature gradient used, or possibly may have partially hydrolysed to more water soluble compounds, including diols or hydrates, during the aqueous caustic washes, designed to remove succinimide.

Drying was performed under reduced pressure at ambient temperature to afford the product (**4.9**) as a free flowing, white powder (**Figure 69**). Elevated temperatures could not be used due to the low melting point of the product (35 – 36 °C),[210] and indeed, melting of this compound would likely result in it being reformed into an intractable, hard, glassy substance.

Figure 69 *Isolated and dried product bromo benzyl bromide (**4.9**).*

In summary, ethyl 4-bromomethylbenzoate (**4.9**) was successfully furnished through an improved process with a markedly improved PMI compared to the previous process[188] (53 vs. 239), due in part to the increased concentration at which the reaction was run, and in part due to the simplified work-up procedure. This PMI could likely be further improved by further optimisation of the extraction process as outlined earlier. The dibromo side-product (**4.10**) tracked through the crystallisation and further work would be needed to assess the most effective method of removing this. This could be achieved by vacuum distillation using a wiped-film evaporator by leveraging the lower boiling point of the product (**4.9**) compared to the dibromo side-product (**4.10**). Alternatively, differences in rates of reactivity with nucleophiles in subsequent chemical transformations could be exploited in order to achieve separation. This approach has previously been demonstrated by Kappe and co-workers, whereby morpholine selectively reacted with a range of benzyl bromide derivatives in the presence of corresponding dibrominated side-products.[211] The feasibility of this approach could be assessed by monitoring reactivity of these benzyl bromide derivatives with nucleophiles (such as water or benzyl amine) as a function of time using process analytical technology or regular analytical sampling.

While these optimisations have provided tangible benefits with respect to brominating this particular substrate, it is anticipated the findings of the study may also be applicable to other substrates[188] amenable to benzylic bromination *via* this methodology.

2.3.4 Scale-up in Flow using Photochemical DART Reactor

While this prototype Photo DART reactor is designed specifically to process multiple kilograms of input per day and tolerate the presence of solid material, homogeneous chemistry was to be examined in the first instance. Having already successfully performed the benzylic bromination of ethyl 4-methylbenzoate (**4.8**) in flow using the PHIL Pacer, the aim was to run this same transformation in the Photo DART reactor to serve as a direct comparator. An engineering line diagram of the setup is shown below (**Figure 70**).

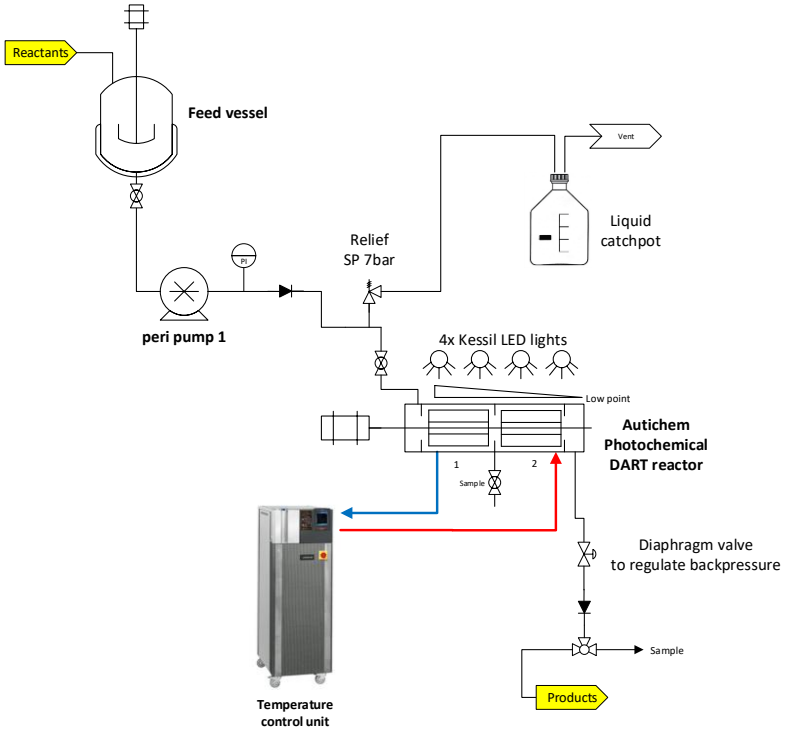

Figure 70 *Engineering line diagram of Photochemical DART reactor flow set-up.*

All four Kessil lamps were set to 100% intensity in the first instance. Assuming the light is well dispersed throughout the Photochemical DART reactor, a minimum residence time of approximately 1 minute was thought to be appropriate. During the start of the process, however, it became apparent that significant oscillations in the flow rate were occurring as a result of the pulsing nature of the feed pump. This complicated residence time calculations which depend on well-defined flow rates of the reaction mixture. These oscillations diminished by addition of check valves in the tubing directly before and after the reactor, as well as applying 0.1 bar of backpressure. It was believed that these oscillations in the flow-rate would average out over the course of the reaction to give a relatively constant residence time and average flow rates were used to estimate this. Results from HPLC analysis of the product stream at regular intervals are shown below (**Table 30**).

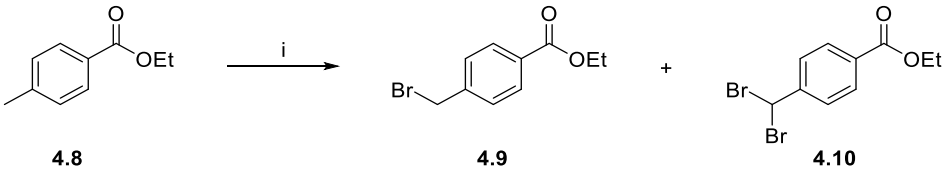

4.8 **4.9** **4.10**

Reagents and conditions; (i) NBS, MeCN, irradiation at 400 nm, 100% intensity, ~1 min residence time.

Time point at which output was analysed (mins)	%Area composition[a] (4.8/4.9/4.10)
2	53/46/1
5	51/48/1
10	41/57/1
15	34/63/2
21	26/70/3

[a]Assessed by HPLC with UV-detection at 220 nm.

Table 30 *Analysis of output with ~1 min residence time (18 mL/min).*

The reaction mixture was smoothly transferred through the reactor, and no issues with corrosion, precipitation or build-up of backpressure were noted. Furthermore, the exotherm produced by the reaction was dispersed passively to a sufficient extent such that the active cooling capabilities were not required. Unexpectedly, however, high variability was seen in

the composition of the output material as indicated by the fluctuation in conversion observed as a function of sampling time. While it was expected that the reaction would reach a steady state within a few minutes at this flow rate, these data suggest otherwise. Furthermore, none of the samples taken indicated full conversion, despite what previous experimentation may have suggested. These data prompted extending the residence time to approximately 2 minutes (**Table 31**).

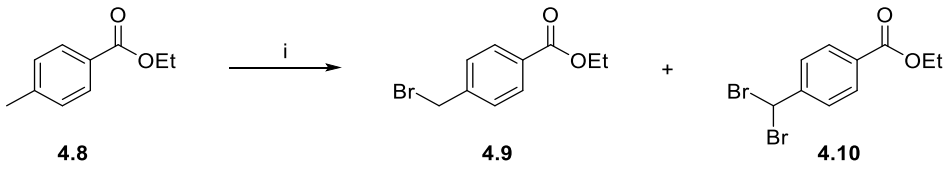

4.8 **4.9** **4.10**

Reagents and conditions; (i) NBS, MeCN, irradiation at 400 nm, 100% intensity, ~2 min residence time.

Time point at which output was analysed (mins)	%Area composition[a] (4.8/4.9/4.10)
5	9/84/7
10	14/79/6
25	32/64/3
30	14/79/6

[a]Assessed by HPLC with UV-detection at 220 nm.

Table 31 *Analysis of output with ~2 min residence time (10 mL/min).*

Increasing the residence time led to a corresponding increase in conversion, and analysis of a sample taken after 5 minutes of continuous running showed essentially full conversion. Nonetheless, the output composition was still observed to fluctuate over time and incomplete conversions were noted at the other time-points examined. These results suggest a lack of homogeneity in the reaction mixture flowing out of the Photochemical DART reactor, most probably due to insufficient exposure to light. While the fluorinated ethylene propylene (FEP) stirrer was measured to transmit ~80% of incident light at 400 nm, it is possible that this attenuation is sufficient in preventing the solution furthest away from the Kessil lamps from receiving the necessary irradiation, even with reflectors present on the inside of the aluminium jacket. Having the lamps radially arranged around the reactor would likely solve

the issue of lacking homogeneity by ensuring all of the solution is irradiated directly, without loss in intensity during transmission through other components.

The use of IR thermal imaging was also used to gain an understanding of how the exotherm produced during the process was distributed around the apparatus (**Figure 71**).

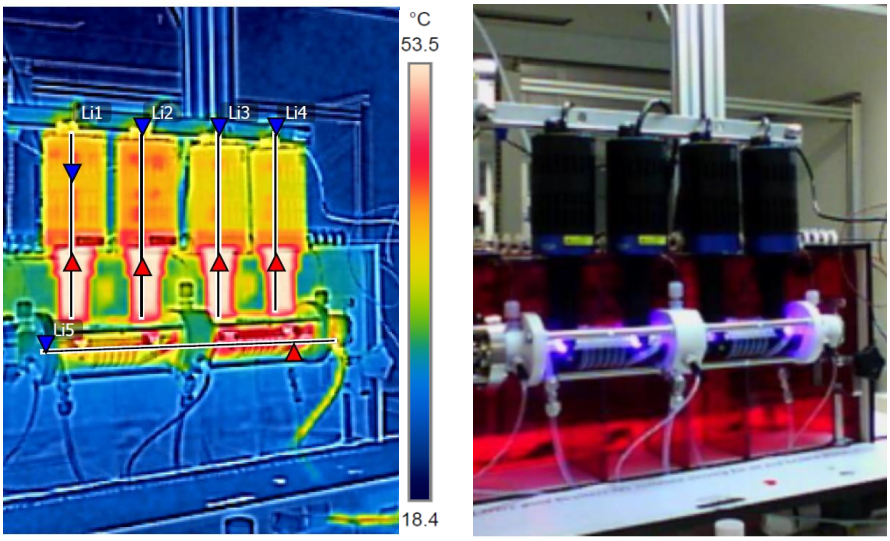

Figure 71 *IR thermal imaging (left) and photograph (right) of Photo DART reactor after running continuously for 15 mins at 2 min residence time; the direction of flow is from left to right.*

It had been established previously that following a short induction period, typically less than 10 seconds provided there is adequate irradiadiation, a sharp exotherm would follow. Therefore following this exotherm may be used to assess which stage of the reactor the formation of product was most prevalent in. The first half of the reactor, which was irradiated by two of the four Kessil lamps appeared at approximately 35 °C, suggesting little reactivity to be taking place. The second half of the reactor by contrast appeared much warmer at approximately 45 °C, suggesting that this is the stage where the majority of the conversion is taking place. This protracted induction period also suggests the rate of reactivity to be limited by the supply of photons rather than mixing or the kinetics of the reaction.

While it was anticipated that conversion could be increased further by lengthening the residence time, it became clear at this point the Photochemical DART reactor in its current form would not provide increased throughput compared to the PHIL Pacer, and would be

more suited to lab-scale, rather than pilot-scale appliations. Nonetheless, the Photochemical DART reactor provides complimentary capabilities to the PHIL Pacer, including good toleration of solids as well as the capability of running very long residence times.

The learnings from this scoping experiment have been applied in the design of the next iteration of this class of reactor, which is currently in development. A computationally generated model is depicted below (**Figure 72**).

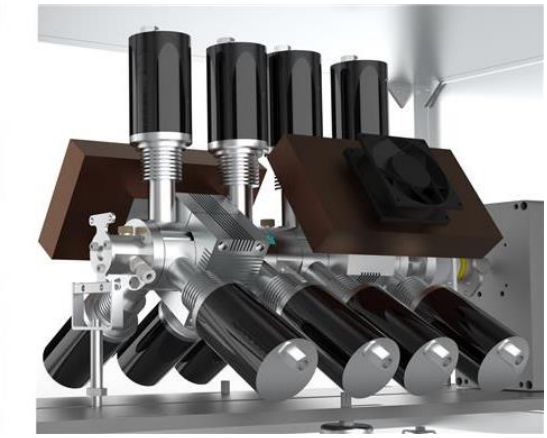

Figure 72 *Computationally generated 3D model of next iteration of Photo DART Reactor design.*

In order to address the requirement for more irradiation, the next prototype Photochemical DART reactor is to incorporate (i) custom made 160 W Kessil lamps in place of the 45 W Kessil lamps used in the current reactor and (ii) 12 Kessil lamps in total distributed radially with respect to the reactor to provide both increased and more even irradiation. It is hoped that these modifications will help realise the longer-term goal of achieving pilot-scale photochemical reactions in flow. It is also realised, however, that this may be subject to additional challenges. While the active cooling capability on the Photochemical DART Reactor was ultimately not used, having twelve 160 W Kessil lamps running at full intensity would consume a total of almost 2 kW and passive cooling alone may not keep the reactor sufficiently cool. Success of this ongoing endeavour will ultimately be achieved only if both chemical and engineering considerations are accounted for, and as such it is believed that the flexibility provided by this design will facilitate making any future adaptations which may be deemed necessary.

2.4 CONCLUSIONS

In summary, the photochemical bromination of two substrates has been examined with the longer-term goal of developing a scalable process. Benzodiazepine (**4.1**) was brominated at what appeared to be the regiochemically less favourable site to give aryl bromide (**4.2**). Control experiments were performed to understand the origin behind formation of *O*-acylated phenol (**4.3**), though ultimately a more selective process was not found. This, along with the high dilutions required resulted in the decision to pause further examination of this substrate.

Increased process understanding for the benzylic bromination of ethyl 4-methylbenzoate (**4.8**) has been obtained. By selecting MeCN as the solvent, reactions could be run at higher concentration without sacrificing conversion or selectivity. This, along with time course experimentation allowed for a 5-fold increase in throughput compared to a previous process. Temperature data showed a measurable exotherm which was ultimately deemed safe due to the low reactive inventory in the flow set-up and good heat dissipation characteristics. The work-up procedure was also improved by directly extracting the product into heptane before crystallisation and isolation. The dibromo side-product (**4.10**) did not purge well during the isolation procedure and possible methods for addressing this issue have been outlined. Aside from the reduction in the number of unit operations, the PMI of this process was reduced by almost a factor of 4, making this new process the preferred option for further scale-up activities.

This same benzylic bromination process was also examined in the prototype Photochemical DART reactor. Though high conversions could be obtained at longer residence times, it became apparent that more intense illumination would be required in order for this reactor to deliver multiple kg/day of throughput. These findings have been used to inform the design of the next iteration of this class of reactors and is to be trialled in due course.

2.5 FUTURE WORK

Further optimisation of the bromination of benzodiazepine (**4.1**) is to be performed (**Scheme 75**). Specifically, identification of a solvent which would enable reactions to be run at higher concentrations than the reactions run in MeCN and MeCN/AcOH would be favourable (DMSO, NMP and chlorobenzene to be tested). This would likely be accompanied by a screen of acidic additives, given that the presence of acetic acid has been shown to alter the reactive behaviour of benzodiazepine (**4.1**). Further mechanistic studies are to be performed to establish whether photochemical or thermal conditions are more favourable towards the reaction outcome.

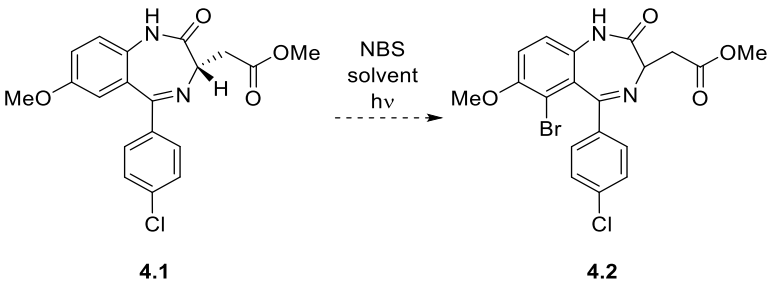

Scheme 75 *Bromination of benzodiapepine (**4.1**).*

A set of conditions is to be developed to allow for a more selective bromination process and then to be demonstrated on multiple kilogram scale, either using the PHIL Pacer or the next-generation photochemical DART reactor.

The benzylic bromination of isochroman (**3.11**) is another target compound of interest, particularly given the reported issues with scaling this process.[198] Leveraging the recent advancements in understanding and operation of photochemical transformations, it is hoped that these issues may be addressed and thereby enable a previously unfeasible process.

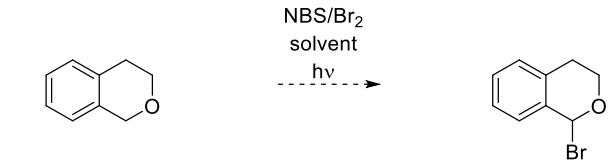

isochroman (3.11) **3.12**

Scheme 76 *Photochemical bromination of isochroman (**3.11**).*[199]

A set of optimised conditions are to be developed using the PHIL Pacer. Scale-up runs may again then be run in flow both in the PHIL Pacer and the next-generation photochemical DART reactor.

3 EXPERIMENTAL

3.1 GENERAL

Anhydrous Solvents: CH_2Cl_2, THF, 2-MeTHF, EtOH and toluene were obtained from commercial sources and used without further purification.

Reagents: were purchased from commercial sources and used without further purification and handled in accordance with COSHH and local regulations.

Infra red spectra: were recorded on a PerkinElmer Spectrum One FT-IR Spectrometer equipped with a Universal ATR Sampling Accessory. Only selected absorbances (ν_{max}) are reported.

ReactIR: was conducted using a Mettler Toledo ReactIR iC10 system with a AgX/DiComp fibre conduit probe which was attached to a HEL AutoMATE pressure reactor. The scan range was from 650 – 2200 cm^{-1}. IR data was visualised and interpreted using Mettler Toledo iC IR software v7.0.

NMR spectra: were recorded at 400 MHz (^1H), 101 MHz (^{13}C), 162 MHz (^{31}P) and 376 MHz (^{19}F) on a Bruker AMX-400 or at 500 MHz (^1H), 126 MHz (^{13}C) and 202 MHz (^{31}P) on a Bruker AMX-500 instrument. Chemical shifts are quoted in parts per million (ppm) and referenced to the appropriate residual solvent peak for ^1H and ^{13}C: DMSO-*d6* (δ_H =2.50, δ_C = 39.5), $CDCl_3$ (δ_H =7.26, δ_C = 77.2), CD_2Cl_2 (δ_H = 5.32, δ_C = 54.0). ^{31}P is referenced externally to 85% phosphoric acid (δ_P = 0). ^{19}F is referenced externally to $CFCl_3$ (δ_F = 0). Coupling constants are given to the nearest 0.5 Hz.

Melting points: were recorded using Buchi Melting point M-565 apparatus.

TLC: was performed using polyester sheets pre-coated with 0.20 mm of silica gel 60 with fluorescent indicator purchased from Macherey-Nagel.

Flash Column Chromatography: was performed on a Biotage Isolera Four using cartridges prepacked with normal phase silica (unless otherwise stated). Elution gradients were

determined based on retention times observed by TLC. UV response was monitored as an average of wavelengths between 200 and 400 nm.

HPLC: was performed on an Agilent instrument equipped with a Waters CSH column (30 mm length, 2.10 internal diameter, 2.5 µm packing diameter). The method was run for 5 mins with a gradient of 97% of 0.05% v/v of trifluoroacetic acid in water / 3% of 0.05% v/v of trifluoroacetic acid in acetonitrile to 3% of 0.05% v/v trifluoroacetic acid in water / 97% of 0.05% v/v of trifluoroacetic acid in acetonitrile. UV detection was performed at 220 nm except where otherwise noted.

LCMS (low resolution): was performed on a Waters instrument. The HPLC analysis was conducted on an Acquity Xselect C18 column (30 mm length, 2.1 mm internal diameter, 2.5 µm packing diameter). The method was run for 5 mins with a gradient of 97% of 0.1% v/v of trifluoroacetic acid in water / 3% of 0.1% v/v of trifluoroacetic acid in acetonitrile to 3% of 0.1% v/v trifluoroacetic acid in water / 97% of 0.1% v/v of trifluoroacetic acid in acetonitrile. The UV detection was a summed signal from wavelength of 210 nm to 350 nm. The mass spectrometry was performed on a Waters QDA using positive electrospray ionisation.

LCMS (high resolution): was recorded using an LTQ Orbitrap equipped with a Phenomenex Luna C18 column (50 mm length, 2.1 mm internal diameter, 3.0 µm packing diameter). The chromatography was run for 10 mins with a gradient of 99% of 0.05% v/v of trifluoroacetic acid in water / 1% of 0.05% v/v of trifluoroacetic acid in acetonitrile to 1% of 0.05% v/v trifluoroacetic acid in water / 99% of 0.05% v/v of trifluoroacetic acid in acetonitrile.

CSTR flow reactor: supplied on loan by Autichem Ltd. (number of stages: 7, internal volume: 27 mL).

Prototype Photochemical DART reactor: supplied on loan by Autichem Ltd. (internal volume: 20 mL).

High Resolution Atmospheric Surface Analysis Probe Mass Spectrometry: was performed with a Thermo Orbitrap Velos Pro.

Mass Directed Automated Preparative HPLC (MDAP): were conducted on a Waters FractionLynx system comprising of a Waters 600 pump with extended pump heads, Waters 2700 autosampler, Waters 996 diode array, and Gilson 202 fraction collector. The high performance liquid chromatography (HPLC) separation was conducted on an X-select C18

column (150 mm × 30 mm internal diameter, 5 µm packing diameter) at ambient temperature, utilising acetonitrile and water modified with ammonium bicarbonate as the solvent system. The elution gradient was set as appropriate based on the retention times observed by analytical LCMS. Mass spectra were recorded on a Waters ZQ mass spectrometer using alternate-scan positive and negative electrospray ionisation (ES+ and ES–) with a scan range of 100 to 1500 atomic mass units, scan time of 0.50 s, and an inter-scan delay of 0.25 s.

PHIL Pacer: was obtained from Pacer Components Ltd. Irradiation was performed using the contiuous wave setting with the specified wavelength and intensity. Screening experiments were performed using HPLC vials and 48-well plates. Batch scale-up was performed in 50 mL test tubes. Scale-up using continuous processing was perfomed by passing the reaction mixture through a glass plate (internal volume: 4.1 mL) using a HPLC pump. Extensive characterisation information on this equipment has previously been carried out and documented by Bonfield, Edwards and co-workers.[188, 189]

All pressures are given in bar gauge.

Novel compounds have been characterised as a minimum by IR, ^{1}H and ^{13}C NMR and HRMS with additional tests being run as appropriate for the compound.

Literature compounds have been characterised by comparison of ^{1}H and ^{13}C NMR as a minimum against the specified literature reference.

3.2 Computational Analysis of Transition State

The M06-L functional was used with a 6-31G**[LANL2DZ for Ru] for geometry optimisations in Gaussian 16.[212] Stationary points were verified as either minima or transition-state structures by calculation and visualisation of vibrational frequencies. Intrinsic reaction coordinate (IRC) calculations verified connection between transition states and intermediates. Reported free energies at 1 atm and room temperature with an ultrafine integration correspond to M06-L/def2-TZVP//M06-L/6-31G**[LANL2DZ for Ru]. Continuum methanol reaction field DFT analysis with the solvation model based on density of the hydrogenation of methyl trifluoroacetate was performed.[213] Calculations for the transitions states were run Doo-Hyun Kwon (GSK).

3.3 General Procedures for Ester Reductions in Biotage Endeavor

General Procedure I: Variation of Temperature

To a glass vial was added Ru(PNP)Cl_2(NHC) (**1.51**) (14 mg, 0.020 mmol, 0.02 eq.), methyl 2-naphthoate (**2.18**) (186 mg, 1.0 mmol, 1.0 eq.), potassium *tert*-butoxide (0.2 mL, 0.2 mmol, 0.2 eq., 1 M in THF) and THF (2 mL). The vial was placed in a Biotage Endeavor reaction system, then pressurised with nitrogen (5 bar) and vented (x3), then pressurised with hydrogen (2 bar) and vented (x3), then pressurised with hydrogen (2 bar) and left to stir at 800 rpm at the specified temperature for 5 h. After being cooled to rt, the vial was purged with nitrogen. The normalised hydrogen gas uptake curves are shown in **Figure 24**.

General Procedure II: Catalyst Screen

To a glass vial was added ruthenium catalyst (masses given in **Table 32**, 0.025 mmol, 0.01 eq.), methyl 2-naphthoate (**2.18**) (470 mg, 2.5 mmol, 1.0 eq.), potassium *tert*-butoxide (0.5 mL, 0.5 mmol, 0.2 eq., 1 M in THF) and 2-MeTHF (3.5 mL). The vial was placed in a Biotage

Endeavor reaction system, then pressurised with nitrogen (5 bar) and vented (x3), then pressurised with hydrogen (5 bar) and vented (x3), then pressurised with hydrogen (5 bar) and left to stir at 700 rpm at 45 °C for 2.5 h. After being left to cool to rt, the vial was purged with nitrogen. The conversion was assessed using HPLC (**Table 13**). The hydrogen gas uptake curves are shown in **Figure 25**.

Catalyst	Mass (mg)
Ru(PNP)Cl_2(NHC) (**1.51**)	18
Ru(diEtSNS)Cl_2(NHC) (**2.1**)	12
Ru(di*n*-BuSNS)Cl_2(NHC) (**2.16**)	13
Ru(diPhSNS)Cl_2(NHC) (**2.2**)	14

Table 32 *Masses of ruthenium catalysts employed.*

General Procedure III: Solvent Screen

To a glass vial was added Ru(PNP)Cl_2(NHC) (**1.51**) (28 mg, 0.039 mmol, 0.02 eq.), methyl 2-naphthoate (**2.18**) (370 mg, 2.0 mmol, 1.0 eq.), potassium *tert*-butoxide (0.40 mL, 0.40 mmol, 0.20 eq., 1 M in THF) and solvent (4 mL). The vial was placed in a Biotage Endeavor, then pressurised with nitrogen (4 bar) and vented (x3), then pressurised with hydrogen (4 bar) and vented (x3), then pressurised with hydrogen (2 bar) and left to stir at 700 rpm at 40 °C for 3 h. After being left to cool to rt, the vial was purged with nitrogen and the mixture was passed through a short silica pad and flushed with EtOAc. The conversion was then assessed using HPLC (**Table 14**). This process was performed with THF, 2-MeTHF, toluene, methanol, ethanol, isopropanol and MeCN.

General Procedure IV: for Base Screen

To a glass vial was added Ru(PNP)Cl_2(NHC) (**1.51**) (18 mg, 0.025 mmol, 0.01 eq.), methyl 2-naphthoate (**2.18**) (470 mg, 2.5 mmol, 1 eq.), base (0.5 mmol, 0.2 eq.) and 2-MeTHF (4 mL). The vial was placed in a Biotage Endeavor, then pressurised with nitrogen (5 bar) and vented (x3), then pressurised with hydrogen (5 bar) and vented (x3), then pressurised with hydrogen (5 bar) and left to stir at 700 rpm at 45 °C for 2.5 hr. After being left to cool to rt, the vial was purged with nitrogen. The conversion was assessed using HPLC (**Table 15**).

General Procedure V: Scoping Experimental Design

To a glass vial was added Ru(PNP)Cl_2(NHC) (**1.51**) (0.015 eq.), methyl 2-naphthoate (**2.18**) (1.0 eq.), potassium *tert*-butoxide and solvent (made up to 4 mL total volume). Reactions were run at constant volume to minimise physical differences such as surface area to volume ratio, mass transfer characteristics, and in order to obtain more consistent gas uptake data. The vessel was placed in a Biotage Endeavor, then pressurised with nitrogen (4 bar) and vented (x3), pressurised with hydrogen and vented (x3), heated to the specified temperature and pressurised with hydrogen and left to stir at 700 rpm for 2.5 h. After being left to cool to rt, the vessel was purged with nitrogen. This process was repeated with varying quantity of base, pressure, concentration and temperature. Quantities of reagents and setpoints of parameters are given in the table below (**Table 33**).

	Reaction conditions								Measured Responses		
Entry	**Base Quantity (A) (mol%)**	**Hydrogen Pressure (B)(bar)**	**Concentration (C) (mol/L)**	**Reaction Temp. (D) (°C)**	**Mass of ester (2.18) (mg)**	**Mass of catalyst (1.51) (mg)**	**Volume of KO*t*-Bu[a] (mL)**	**Volume of 2-MeTHF (mL)**	**SM[b] (2.18) (%area)**	**Product[b] (2.19) (%area)**	**Hydrolysis Product[b] (2.21) (%area)**
1	5	1	0.25	25	185	11.5	0.05	3.95	85	5	6
2	35	1	0.25	25	188	11.4	0.35	3.65	4	70	12
3	5	9	0.25	25	186	11.4	0.05	3.95	66	7	4
4	35	9	0.25	25	185	11.3	0.35	3.65	0	90	9
5	5	1	1	25	752	45.7	0.2	3.8	81	2	4
6	35	1	1	25	747	46.2	1.4	2.6	12	66	6
7	5	9	1	25	751	46.2	0.2	3.8	35	48	3
8	35	9	1	25	753	45.9	1.4	2.6	1	93	3
9	5	1	0.25	65	186	11.5	0.05	3.95	82	8	4
10	35	1	0.25	65	185	11.6	0.35	3.65	1	89	9
11	5	9	0.25	65	186	11.5	0.05	3.95	38	43	7
12	35	9	0.25	65	188	11.7	0.35	3.65	1	88	9
13	5	1	1	65	742	46.0	0.2	3.8	52	27	3
14	35	1	1	65	751	45.7	1.4	2.6	16	67	6
15	5	9	1	65	751	46.0	0.2	3.8	19	68	2
16	35	9	1	65	750	45.7	1.4	2.6	0	97	2
17	20	5	0.625	45	463	28.7	0.5	3.5	0	95	4
18	20	5	0.625	45	464	28.8	0.5	3.5	0	90	4
19	20	5	0.625	45	466	28.9	0.5	3.5	0	95	3
20	20	5	0.625	45	466	28.7	0.5	3.5	1	92	5

[a]1 M solution in THF used. [b]Relative quantities assessed by HPLC with UV detection at 220 nm.

Table 33 Conditions and responses from scoping experimental design.

General Procedure VI: Robustness Experimental Design

To a glass vial was added Ru(PNP)Cl_2(NHC) (**1.51**) (0.005 eq.), methyl 2-naphthoate (**2.18**) (1.0 eq.), potassium *tert*-butoxide and 2-MeTHF (4 mL). Reactions were run at constant volume to minimise physical differences such as surface area to volume ratio, mass transfer characteristics, and in order to obtain more consistent gas uptake data. The vial was placed in a Biotage Endeavor, then pressurised with nitrogen (4 bar) and vented (x3), pressurised with hydrogen and vented (x3), heated to the specified temperature then pressurised with hydrogen and left to stir at 700 rpm for 16 h. After being left to cool to rt, the vial was purged with nitrogen. To the reaction mixtures was added triphenylphosphine oxide as an external standard and the mixture was made up to 100 mL total volume by addition of 10% water in methanol to give a homogeneous solution. Assay yields of each component were obtained by HPLC analysis with UV detection at 225 nm. This process was repeated with varying quantities of base, pressure, concentration and temperature. Quantities of reagents and setpoints of parameters are given in the table below (**Table 34**).

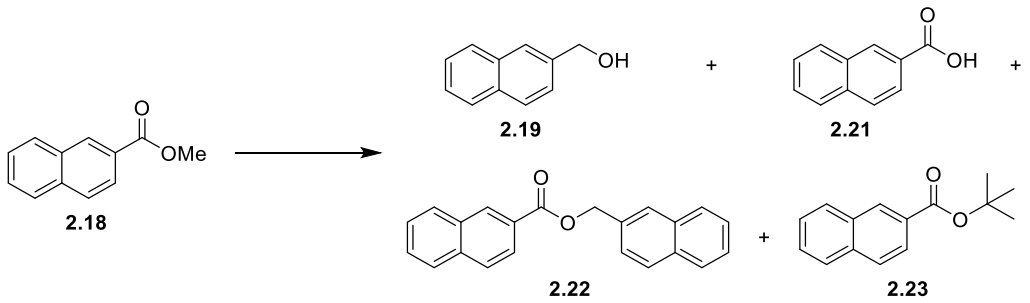

Figure 73 *Components analysed after subjecting methyl 2-naphthoate (**2.18**) to hydrogenation conditions; relative quantities of each shown in **Table 34**.*

	Reaction conditions							Measured responses					
Entry	**Base Quantity (A) (mol%)**	**Hydrogen Pressure (B) (bar)**	**Concentration (C) (mol/L)**	**Reaction Temperature (D) (°C)**	**Mass of ester (2.18) (mg)**	**Mass of catalyst (1.51) (mg)**	**Mass of KO*t*-Bu[a] (mg)**	**% SM[b] (2.18)**	**% product[b] (2.19)**	**% hydrolysis[b] (2.21)**	**% homocoupled[b] (2.22)**	**% tert-butyl[b] (2.23)**	**Time to completion[c] (h)**
1	20	2	0.25	30	186	4	22	0.0	82.1	13.3	0.0	0.0	5
2	10	8	0.25	30	186	4	11	1.1	78.4	9.4	0.0	6.9	6
3	10	2	0.25	30	186	4	11	8.0	76.8	9.4	1.0	2.3	4
4	10	8	1	30	744	14	45	0.6	87.2	5.1	0.0	0.0	5
5	10	2	1	30	744	14	45	6.4	75.9	6.9	0.6	0.3	5
6	20	8	0.25	30	186	4	22	0.0	77.7	14.6	0.0	0.0	3
7	20	8	1	30	744	14	90	0.0	88.7	5.9	0.0	0.0	4
8	20	2	1	30	744	14	90	0.0	86.7	10.6	0.0	0.0	8
9	15	5	0.625	45	465	9	42	0.0	88.2	8.6	0.0	0.0	2
10	15	5	0.625	45	465	9	42	0.0	88.2	8.1	0.0	0.0	2
11	15	5	0.625	45	465	9	42	0.0	88.4	8.5	0.0	0.0	2
12	15	5	0.625	45	465	9	42	0.0	85.4	9.9	0.0	0.0	2
13	20	8	0.25	60	186	4	22	0.0	79.7	15.0	0.0	0.0	0.5
14	20	2	1	60	744	14	90	0.0	87.5	9.6	0.0	0.0	3
15	10	8	1	60	744	14	45	0.0	90.2	4.7	0.0	0.0	2
16	20	8	1	60	744	14	90	0.0	91.7	5.7	0.0	0.0	0.8
17	10	2	0.25	60	186	4	11	17.9	60.7	8.7	2.5	6.5	1
18	10	8	0.25	60	186	4	11	1.3	80.6	8.4	0.0	6.3	1
19	20	2	0.25	60	186	4	22	0.0	84.2	11.8	0.0	0.0	0.5
20	10	2	1	60	744	14	45	0.0	87.5	7.4	0.0	0.0	5

[a]Solid KOtBu used. [b]Relative amounts of each component assessed by HPLC at 225 nm with triphenylphosphine oxide as an external standard. [c]Time to completion estimated from gas uptake curves.

Table 34 Conditions and responses from robustness experimental design.

Calculation of HPLC Assay Yields

The following equation was used to calculate k_x values for each reaction component:

$$k_x = \frac{\%_{PPh_3O}}{\%_x} \div \frac{m_{PPh_3O}}{m_x}$$

Where:

k_x is the absorbance ratio of the reaction component

$\%_{PPh_3O}$ is the %area of triphenylphosphine oxide by HPLC

$\%_x$is the %area of the reaction component by HPLC

m_{PPh_3O} is the mass of the triphenylphosphine oxide

m_x is the mass of the reaction component

The following k_x values were determined as an average of at least four samples (**Table 35**). Triphenyl phosphine oxide was used as the external standard and UV detection was performed at 225 nm:

Compound	k_x Value
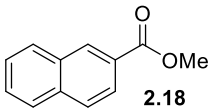 **2.18**	0.4813
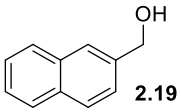 **2.19**	0.1849
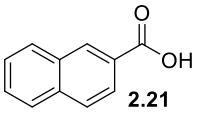 **2.21**	0.4271
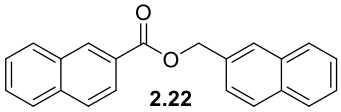 **2.22**	0.3382
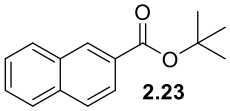 **2.23**	0.5543

Table 35 *Caclulated absorbance ratios for components investigated in robustness experimental design.*

The following equation was used to determine the mass of each component present in solution:

$$m_x = k_x \times m_{PPh_3O} \times \frac{\%_x}{\%_{PPh_3O}}$$

Where:

m_x is the mass of the reaction component

k_x is the absorbance ratio of the reaction component

m_{PPh_3O} is the mass of triphenylphosphine oxide

$\%_{PPh_3O}$ is the %area of triphenylphosphine oxide by HPLC

$\%_x$is the %area of the reaction component by HPLC

A representative chromatogram is depicted below illustrating the retention times of the various reaction components (**Figure 74**).

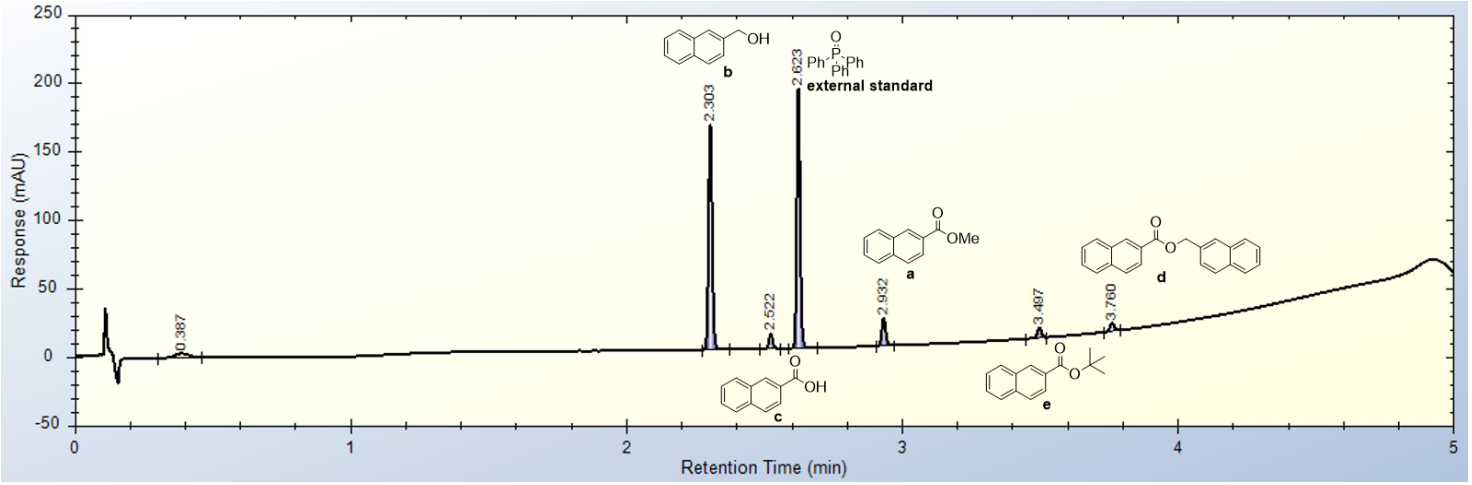

Signal 1: DAD1 A, Sig=225,4 Ref=off

Peak #	RT (min)	Width (min)	Height	Area	Area %
1	0.39	0.051	3.114	11.245	3.028
2	2.30	0.014	163.603	153.678	41.381
3	2.52	0.015	10.872	10.264	2.764
4	2.62	0.013	188.856	161.052	43.366
5	2.93	0.016	20.260	20.525	5.527
6	3.50	0.017	7.383	7.919	2.132
7	3.76	0.018	5.630	6.692	1.802

Figure 74 Example chromatogram from Experimental Design (10 mol% base, 2 bar, 0.25 mol/L, 60 °C); N.B. the peak at 0.387 mins is either a carry-over peak or contamination in the diluent and was thus excluded during analysis.

General Procedure VII: Pre-mix with Sacrificial Ester Followed by Ester Reduction

To a glass vial was added methyl benzoate (**1.52**) (34 mg, 0.25 mmol, 0.1 eq.), potassium *tert*-butoxide (42 mg, 0.38, 0.15 eq.) and 2-MeTHF (4 mL). The vial was placed in a Biotage Endeavor and stirred under a sealed nitrogen atmosphere at 50 °C for 2 h. After cooling to rt, the system was depressurised and charged with Ru(PNP)Cl_2(NHC) (**1.51**) (9 mg, 0.013 mmol, 0.005 eq.) and methyl 2-naphthoate (**2.18**) (465 mg, 2.5 mmol, 1.0 eq.). The Biotage Endeavor was sealed, then pressurised with nitrogen (4 bar) and vented (x3), then pressurised with hydrogen and vented (x3), then heated to 45 °C and pressurised to the specified hydrogen pressure and left to stir at 700 rpm for 16 h. After being left to cool to rt, the vial was purged with nitrogen. To the reaction mixture was then added triphenylphosphine oxide as an external standard and the mixture was made up to 100 mL total volume by addition of 10% water in methanol to give a homogeneous solution which was analysed by HPLC (**Table 36**). This procedure was repeated at different hydrogen pressures.

Entry	Hydrogen Pressure (bar)	%product	%hydrolysis	%transesterification + %SM	Mass balance accounted for (%)
1	5	90	5	4	99
2	7	91	5	0	96

Table 36 *Assay yields from pre-mix experiments.*

General Procedure VIII: Ester Reductions Performed in Substrate Scope

To a glass vial was added Ru(PNP)Cl_2(NHC) (**1.51**), ester, potassium *tert*-butoxide and 2-MeTHF. The vial was placed in a Biotage Endeavor, then pressurised with nitrogen (5 bar) and vented (x3), then pressurised with hydrogen (5 bar) and vented (x3), then pressurised with hydrogen (5 bar) and left to stir at 700 rpm at 45 °C for 2.5 h except where otherwise noted. After being left to cool to rt, the vial was purged with nitrogen. The product alcohol was then purified by chromatography except where otherwise noted (**Table 23**).

General Procedure IX: Time-Course Ester Reductions using ReactIR

Methyl benzoate (**1.52**) (4.0 mL, 32 mmol, 1.0 eq.), base (6.4 mmol, 0.2 eq.), $Ru(PNP)Cl_2(NHC)$ (**1.51**) (23 mg, 0.033 mmol, 0.001 eq.) and 2-MeTHF (96 mL) were charged into a Hastelloy pressure vessel. The vessel was sealed and IR scans were performed every 5 minutes. The vessel was pressurised with nitrogen (5 bar) and vented (x3), then pressurised with hydrogen (5 bar), and vented (x3), then pressurised and maintained with hydrogen (5 bar). The mixture was heated to 30 °C and the reaction was left to stir overnight before being cooled to rt.

This procedure was repeated varying impeller speed (600, 800 or 1000 rpm) and with the presence of potassium benzoate (**2.72**) (1.0 g, 6.4 mmol, 0.2 eq.) as an additive and using benzaldehyde (3.2 mL, 32 mmol, 1.0 eq.) instead of methyl benzoate.

3.4 General Procedures for Photochemical Brominations

General Procedure X: Wavelength Screen for Bromination of Benzodiazepine (4.1)

A stock solution was prepared containing benzodiazepine (**4.1**) (1.11 g, 2.97 mmol, 1.0 eq.) and *N*-bromo succinimide (663 mg, 3.72 mmol, 1.3 eq.) in acetonitrile (45 mL) and acetic acid (15 mL). 1 mL of this stock solution was dispensed into 6 HPLC vials which were then placed inside the PHIL Pacer. Irradiation was performed at all wavelengths (365, 385, 405, 420, 450, 525 nm) at 250 mA for 35 mins. Analysis of the reaction mixtures was performed by HPLC (**Table 25**). Compounds **4.2** and **4.3** are characterised on page 233.

General Procedure XI: Wavelength Screen for Benzylic Bromination

A stock solution was prepared containing ethyl 4-methylbenzoate (**4.8**) (504 mg, 3.07 mmol, 1 eq.) and *N*-bromo succinimide (562 mg, 3.16 mmol, 1.03 eq.) in acetonitrile (15 mL) and acetic acid (15 mL). 1 mL of this stock solution was dispensed into 12 HPLC vials which were then placed inside the PHIL Pacer. Irradiation was performed at all wavelengths (365, 385,

405, 420, 450, 525 nm) at 200 mA. The first and second rows of vials were removed after 5 mins and 10 min of irradiation, respectively. Analysis of the reaction mixtures was performed by HPLC (**Table 26**).

General Procedure XII: Solvent Screen for Benzylic Bromination

The following stock solutions were prepared:

THF: contained ethyl 4-methylbenzoate (**4.8**) (186 mg, 1.13 mmol, 1 eq.) and *N*-bromo succinimide (203 mg, 1.14 mmol, 1.01 eq.) in THF (10 mL).

2-MeTHF: contained ethyl 4-methylbenzoate (**4.8**) (163 mg, 0.99 mmol, 1 eq.) and *N*-bromo succinimide (192 mg, 1.07 mmol, 1.08 eq.) in 2-MeTHF (10 mL).

EtOAc: contained ethyl 4-methylbenzoate (**4.8**) (180 mg, 1.10 mmol, 1 eq.) and *N*-bromo succinimide (205 mg, 1.15 mmol, 1.05 eq.) in EtOAc (10 mL).

Acetone: contained ethyl 4-methylbenzoate (**4.8**) (165 mg, 1.01 mmol, 1 eq.) and *N*-bromo succinimide (188 mg, 1.05 mmol, 1.05 eq.) in acetone (10 mL).

MeCN: contained ethyl 4-methylbenzoate (**4.8**) (162 mg, 0.98 mmol, 1 eq.) and *N*-bromo succinimide (190 mg, 1.07 mmol, 1.09 eq.) in MeCN (10 mL).

1 mL of each stock solution was dispensed into separate HPLC vials which were then placed inside the PHIL Pacer. Irradiation was performed at 385 nm and 200 mA for 5 mins. Analysis of the reaction mixtures was performed by HPLC (**Table 27**).

General Procedure XIII: Variation of Concentration for Benzylic Bromination

The following stock solutions were prepared:

0.10 mol/L: contained ethyl 4-methylbenzoate (**4.8**) (0.82 g, 5.0 mmol, 1 eq.) and *N*-bromo succinimide (0.93 g, 5.2 mmol, 1.04 eq.) in THF (50 mL).

0.30 mol/L: contained ethyl 4-methylbenzoate (**4.8**) (2.46 g, 15 mmol, 1 eq.) and *N*-bromo succinimide (2.80 g, 15.7 mmol, 1.05 eq.) in THF (50 mL).

0.50 mol/L: contained ethyl 4-methylbenzoate (**4.8**) (4.11 g, 25.1 mmol, 1 eq.) and *N*-bromo succinimide (4.67 g, 26.2 mmol, 1.04 eq.) in THF (50 mL).

0.68 mol/L: contained ethyl 4-methylbenzoate (**4.8**) (4.11 g, 25.1 mmol, 1 eq.) and *N*-bromo succinimide (4.67 g, 26.2 mmol, 1.04 eq.) in THF (37 mL).

1 mL of each stock solution was dispensed into separate HPLC vials which were then placed inside the PHIL Pacer. Irradiation was performed at 405 nm and 300 mA for 5 mins. Analysis of the reaction mixtures was performed by HPLC (**Table 28**).

General Procedure XIV: Time-Course Benzylic Brominations in PHIL Pacer

A stock solution was prepared containing ethyl 4-methylbenzoate (**4.8**) (8.23 g, 50.1 mmol, 1 eq.) and *N*-bromo succinimide (9.36 g, 52.6 mmol, 1.05 eq.) in acetonitrile (74 mL). 1 mL of this stock solution was dispensed into sets of 9 HPLC vials which were then placed inside the PHIL Pacer. Irradiation was performed at 405 nm and the given intensity. Vials were sequentially removed at the following intervals: 10, 20, 30, 40, 50, 60, 90, 120, 180 s, then analysed by HPLC (**Figure 59**). Some vials were equipped with a thermocouple which was used to log temperature data (**Figure 60**).

General Procedure XV: Time-Course Benzylic Brominations using Kessil Lamp

A stock solution was prepared containing ethyl 4-methylbenzoate (**4.8**) (8.23 g, 50.1 mmol, 1 eq.) and *N*-bromo succinimide (9.36 g, 52.6 mmol, 1.05 eq.) in acetonitrile (74 mL). 4 mL of this stock solution were dispensed into 4 separate vials equipped with a magnetic stirrer and thermocouple. The vials were sealed and in turn placed inside an aluminium block, stirred at 1200 rpm and irradiation was performed at 400 nm across all the intensity settings (25%, 50%, 75%, 100%). Samples were taken at the following intervals using a syringe: 10, 20, 30, 40, 50, 60, 90, 120, 180, 300 s, then analysed by HPLC (**Figure 62**). The thermocouple was

used to log temperature data (**Figure 75**). This procedure was repeated using neat acetonitrile (4 mL) during which time only data from the thermocouple were collected.

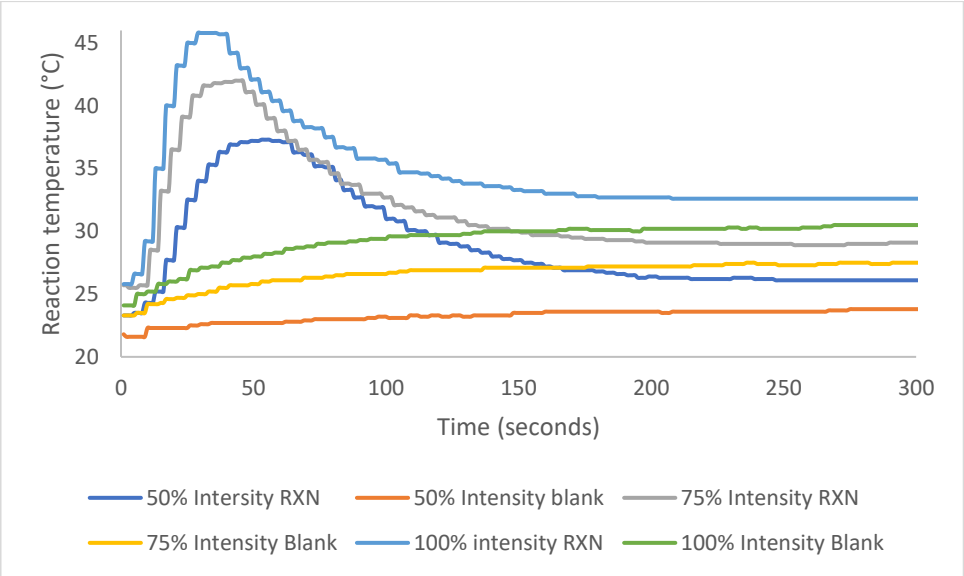

Figure 75 *Temperature data for benzylic bromination promoted by irradiation with Kessil lamp at varying intensities collected as a function of time.*

General Procedure XVI: Benzylic Brominations in Photochemical DART Reactor

A stock solution was made up containing ethyl 4-methylbenzoate (**4.8**) (64.7 g, 394 mmol, 1 eq.) and *N*-bromo succinimide (74.1 g, 416 mmol, 1.05 eq.) in acetonitrile (576 mL). The reaction mixture was pumped through the reactor at the appropriate flow-rate (18 mL/min for residence time of approximately 1 minute; 10 mL/min for residence time of approximately 2 minutes), the agitator speed was set to 360 rpm and the four 400 nm Kessil lamps were each set to 100% intensity. Samples collected were analysed by HPLC (**Table 30**, **Table 31**).

3.5 INDIVIDUAL PROCEDURES

Diethyl 2-(4-(trifluoromethyl)phenyl)thiazole-4,5-dicarboxylate (1.9)

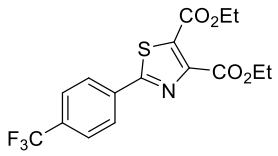

To a solution of 4-(trifluoromethyl)benzothioamide (**2.69**) (4.97 g, 24.2 mmol, 1.0 eq.) in ethanol (8 mL) under an atmosphere of nitrogen was added dropwise diethyl 2-chloro-3-oxosuccinate (**2.70**) (5.94 g, 26.7 mmol, 1.1 eq.) in ethanol (5 mL). The mixture was stirred and heated to 71 °C for 6 h before cooling to rt, and being stirred at this temperature overnight. 50% aqueous ethanol (10 mL) was added and the resulting precipitate was collected by filtration. The crude residue was then purified by flash column chromatography (eluent: 5 to 20% EtOAc/heptane gradient) to afford the product as a white powder (4.41 g, 11.8 mmol, 49%).

^{1}H NMR (400 MHz, $CDCl_3$): δ 8.11 (d, 2H, *J* = 8.5 Hz, 2 x CF_3CCHCH), 7.73 (d, 2H, *J* = 8.5 Hz, 2 x CF_3CCH), 4.99 (q, 2H, *J* = 7.0 Hz, OCH_2CH_3), 4.40 (q, 2H, *J* = 7.0 Hz, OCH_2CH_3), 1.44 (t, 3H, *J* = 7.0 Hz, OCH_2CH_3), 1.39 (t, 3H, *J* = 7.0 Hz, OCH_2CH_3);

^{13}C NMR (101 MHz, $CDCl_3$): δ 169.3, 163.0, 161.1, 151.2, 135.4, 133.2 (q, $^{2}J_{C\text{-}F}$ = 33.0 Hz), 129.5, 127.5, 126.3 (q, $^{3}J_{C\text{-}F}$ = 4.0 Hz), 123.8 (Q, $^{1}J_{C\text{-}F}$ = 272.0 Hz), 62.7, 62.6, 14.3, 14.2;

^{19}F NMR (376 MHz, $CDCl_3$): δ –63.0.

Analytical data obtained consistent with that previously reported.[30]

Ru(PNP)Cl_2(NHC) (1.51)

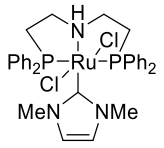

To a solution of $RuCl_2$(*p*-cymene)Cl_2(NHC) (**1.51**) (3.49 g, 8.67 mmol, 1.0 eq.) in dry, deoxygenated ethanol (18 mL) under nitrogen was added bis(2-(diphenylphosphino)ethyl)amine (**2.4**) (4.08 g, 9.24 mmol, 1.1 eq.) and the mixture was heated to 80 °C for 30 mins before being left to stir overnight at rt. The reaction mixture was concentrated under reduced pressure and the residue was suspended in ethanol (10 mL) and heptane (30 mL). The resulting precipitate was collected by filtration under an inert atmosphere, washed with heptane (30 mL) and ethyl acetate (30 mL), then died under reduced pressure at 40 °C overnight to afford the product as a free-flowing yellow powder (3.42 g, 4.82 mmol, 56%).

$\boldsymbol{\nu_{max}}$ (neat): 1432, 822, 695, 663 cm^{-1};

^{1}H NMR (500 MHz, CD_2Cl_2): δ 7.41 – 7.21 (m, 20H, Ph-H), 6.82 – 6.79 (m, 2H, HC=CH), 4.35 – 4.25 (m, 1H, NH), 3.47 – 3.21 (m, 4H, CH_2NCH_2), 3.20 (s, 3H, NCH_3), 3.12 – 3.01 (m, 2H, PCH_2), 3.06 (s, 3H, NCH_3), 2.73 – 2.61 (m, 2H, PCH_2);

^{13}C NMR (126 MHz, CD_2Cl_2): δ 183.7 (t, $^2J_{C\text{-}P}$ = 11.5 Hz), 138.7 (T, $^1J_{C\text{-}P}$ = 18.4 Hz), 137.7 (T, $^1J_{C\text{-}P}$ = 17.2 Hz), 134.2 (t, $J_{C\text{-}P}$ = 5.3 Hz), 129.3, 129.2, 128.1 (t, $J_{C\text{-}P}$ = 4.3 Hz), 128.0 (t, $J_{C\text{-}P}$ = 4.3 Hz), 123.2, 123.1, 50.5 (t, $J_{C\text{-}P}$ = 2.6 Hz), 40.4, 39.7, 34.5 (t, $J_{C\text{-}P}$ = 10.3 Hz);

^{31}P{^{1}H} NMR (202 MHz, CD_2Cl_2): δ 42.9.

Analytical data consistent with that previously reported.[104]

Benzyl alcohol (1.53)

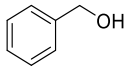

Procedure A

To a suspension of Ru(PNP)Cl_2(NHC) (**1.51**) (18 mg, 0.026 mmol, 0.026 eq.) in dry, deoxygenated THF (2 mL) under nitrogen was added methyl benzoate (0.13 mL, 1.0 mmol, 1.0 eq.), and potassium *tert*-butoxide (0.20 mL, 0.20 mmol, 0.2 eq., 1 M in THF). The flask was evacuated and then back filled with hydrogen (4 x 1 atmosphere). The reaction mixture was heated to 50 °C and stirred for 16 h, then left to cool to rt. The reaction mixture was concentrated and the crude residue was purified by flash column chromatography (eluent: 0 to 30% EtOAc/heptane gradient) to afford the product as a clear, colourless liquid (35 mg, 0.32 mmol, 31%).

^{1}H NMR (400 MHz, $CDCl_3$): δ 7.40 – 7.27 (m, 5H, 5 x ArH), 4.70 (d, 2H, *J* = 5.5 Hz, CH_2), 1.69 (br. s, 1H, OH);

^{13}C NMR (101 MHz, $CDCl_3$): δ 141.0, 128.7, 127.8, 127.1, 65.5.

Analytical data consistent with that previously reported.[104]

Procedure B

This was carried out according to General Procedure VIII starting with Ru(PNP)Cl_2(NHC) (**1.51**) (28 mg, 0.039 mmol, 0.016 eq.), *tert*-butyl benzoate (**2.25**) (442 mg, 2.48 mmol, 1.0 eq.), potassium *tert*-butoxide (0.50 mL, 0.50 mmol, 0.20 eq., 1 M in THF) and 2-MeTHF (3.5 mL). The crude conversion was assessed to be > 90% by HPLC. The crude residue was purified by flash column chromatography (eluent: 10 to 80% EtOAc/heptane gradient) to afford the product as a clear, colourless oil (155 mg, 1.43 mmol, 58%).

Analytical data consistent with that described in Procedure A.

Procedure C

This was carried out according to General Procedure VIII starting with Ru(PNP)Cl_2(NHC) (**1.51**) (3.3 mg, 0.0047 mmol, 0.0022 eq.), benzyl benzoate (**2.24**) (445 mg, 2.10 mmol, 1.0 eq.), potassium *tert*-butoxide (0.50 mL, 0.50 mmol, 0.20 eq., 1 M in THF) and 2-MeTHF (3.5 mL). The crude conversion was assessed to be > 95% by HPLC. The crude residue was purified by

flash column chromatography (eluent: 10 to 80% EtOAc/heptane gradient) to afford the product as a clear, colourless oil (303 mg, 2.80 mmol, 67%).

Analytical data consistent with that described in Procedure A.

(2,2-Difluorobenzo[*d*][1,3]dioxol-5-yl)methanol (1.56)

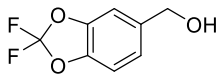

This was carried out according to General Procedure VIII starting with Ru(PNP)Cl_2(NHC) (**1.51**) (18 mg, 0.025 mmol, 0.010 eq.), methyl 2,2-difluorobenzo[d][1,3]dioxole-5-carboxylate (**1.55**) (550 mg, 2.54 mmol, 1.0 eq.), potassium *tert*-butoxide (0.50 mL, 0.50 mmol, 0.20 eq., 1 M in THF) and 2-MeTHF (3.5 mL). The reduction was performed at 50 °C. The crude conversion was assessed to be > 90% by HPLC. The crude residue was purified by flash column chromatography (eluent: 10 to 80% EtOAc/heptane gradient) to afford the product as a pale yellow oil (357 mg, 1.90 mmol, 75%).

^{1}H NMR (400 MHz, $CDCl_3$): δ 7.12 (s, 1H, ArH), 7.07 – 7.00 (m, 2H, 2 x ArH), 4.67 (d, 2H, *J* = 4.5 Hz, CH_2), 1.79 (t, 1H, *J* = 4.5 Hz, OH);

^{13}C NMR (101 MHz, $CDCl_3$): δ 144.2, 143.3, 137.2, 131.8 (T, $^1J_{C\text{-}F}$ = 256 Hz), 122.1, 109.4, 108.6, 64.9;

^{19}F{^{1}H} NMR (376 MHz, $CDCl_3$): δ –50.1.

Analytical data consistent with that previously reported.[214]

Ru(diEtSNS)Cl_2(NHC) (2.1)

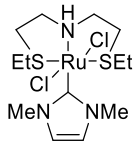

To a suspension of bis(2-(ethylthio)ethyl)amine hydrochloride (**2.5·HCl**) (311 mg, 1.35 mmol) in DCM (5 mL) was added aqueous sodium hydroxide (5 mL, 4 M) and the mixture was stirred at rt for 30 mins. The organic layer was separated and concentrated to dryness to afford the free-base.

The free-base, bis(2-(ethylthio)ethyl)amine (**2.5**) (177 mg, 0.915 mmol, 1.1 eq.) was dissolved in dry, deoxygenated ethanol (3 mL) under nitrogen and to this was added Ru(*p*-cymene)Cl_2(NHC) (**2.13**) (351 mg, 0.872 mmol, 1.0 eq.) and the mixture was stirred and heated to 70 °C overnight before being left to cool to rt. Dry, degassed heptane (2 mL) was added to the mixture and was stirred for 5 mins before decanting the liquid phase using a filtered cannula. Additional heptane (5 mL) was added and stirred followed by decanting the liquid phase using a filtered cannula. The residue was dried under reduced pressure to afford the product as an orange powder (308 mg, 0.667 mmol, 77%).

M.pt.: decomposes >147 °C;

ν_{max} (neat): 3179, 2920, 1624, 1223, 1080, 966 cm^{-1};

^{1}H NMR (500 MHz, $CDCl_3$): δ 6.86 (s, 2H, HC=CH), 4.25 – 4.13 (m, 1H, NH), 4.08 (s, 6H, 2 x NCH_3), 3.45 – 2.42 (m, 12H, 6 x CH_2), 1.11 (t, 3H, *J* = 7.5 Hz, SCH_2CH_3), 0.96 (t, 3H, *J* = 7.5 Hz, SCH_2CH_3);

^{13}C NMR (126 MHz, $CDCl_3$): δ 186.3, 122.9, 48.4, 47.5, 40.5, 39.6 (br.), 38.8, 29.3, 27.0, 12.2, 11.7;

HRMS: ($C_{13}H_{27}N_3{}^{35}Cl_2{}^{96}RuS_2$) [$M^+$] requires 455.0094, found [M^+] 455.0106.

Ru(diPhSNS)Cl_2(NHC) (2.2)

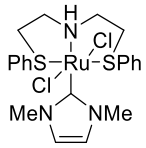

To a suspension of bis(2-(phenylthio)ethyl)amine hydrochloride (**2.6·HCl**) (516 mg, 1.58 mmol) in DCM (7 mL) was added aqueous sodium hydroxide (5 mL, 4 M) and the mixture was stirred at rt for 30 mins. The organic layer was separated and concentrated to dryness to afford the free-base.

The free-base, bis(2-(phenylthio)ethyl)amine (**2.6**) (312 mg, 1.08 mmol, 4.0 eq.) was dissolved in dry, deoxygenated ethanol (3 mL) under nitrogen and to this was added Ru(*p*-cymene)Cl_2(NHC) (**2.13**) (428 mg, 1.06 mmol, 1.0 eq.) and the mixture was stirred and heated to 75 °C for three days before being left to cool to rt. Dry, degassed heptane (10 mL) was added to the mixture and was stirred for 5 mins before decanting the liquid phase using a filtered cannula. Additional heptane (2 x 5 mL) was added and stirred followed by decanting the liquid phase using a filtered cannula. The residue was dried under reduced pressure to afford the product as an orange powder (62 mg, 0.11 mmol, 41%).

M.pt.: decomposes >150 °C;

$\boldsymbol{\nu}_{\mathbf{max}}$ (neat): 3163, 2945, 1580, 1449, 1227, 1078, 991, 741, 685 cm^{-1};

^{1}H NMR (500 MHz, $CDCl_3$): δ 7.52 – 7.35 (m, 4H, 4 x ArH), 7.25 – 7.15 (m, 6H, 6 x ArH), 6.92 (s, 2H, HC=CH), 4.66 – 4.49 (m, 1H, NH), 4.04 (br. s, 6H, 2 x NCH_3), 3.74 – 3.15 (m, 8H, 4 x CH_2);

^{13}C NMR (126 MHz, $CDCl_3$): δ 185.4, 135.3, 130.4 (br. s), 128.8, 128.0, 123.3, 48.6, 39.3;

HRMS: ($C_{21}H_{27}N_3{}^{35}Cl_2{}^{96}RuS_2$) [$M^+$] requires 551.0094, found [M^+] 551.0105.

Bis(2-(diphenylphosphino)ethyl)amine (2.4)

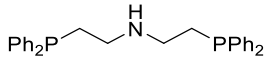

To a suspenson of bis(2-(diphenylphosphino)ethyl)amine hydrochloride (**2.4·HCl**) (701 mg, 1.47 mmol) in DCM (10 mL) was added aqueous sodium hydroxide (10 mL, 2.5 M) and the resulting solution was stirred for 30 mins. The organic layer was separated and the aqueous layer was extracted with DCM (2 x 5 mL). The combined organic phases were washed with saturated brine, dried over sodium sulfate, filtered and concentrated under reduced pressure to afford the product as a clear, thick oil (504 mg, 1.14 mmol, 78%).

^{1}H NMR (400 MHz, $CDCl_3$): δ 7.45 – 7.28 (m, 20H, 20 x ArH), 2.71 (q, 4H, *J* = 8.0 Hz, C*H*$_2$NC*H*$_2$), 2.25 – 2.19 (m, 4H, C*H*$_2$CH$_2$NCH$_2$C*H*$_2$), 1.34 (br. s, 1H, NH);

^{13}C NMR (101 MHz, $CDCl_3$): δ 138.5 (D, $^{1}J_{C\text{-}P}$ = 12.5 Hz), 132.8 (d, $^{2}J_{C\text{-}P}$ = 19.0 Hz), 128.7 (d, $^{3}J_{C\text{-}P}$ = 20.0 Hz), 126, 46.5 (D, $^{1}J_{C\text{-}P}$ = 21.0 Hz), 29.1. (d, $^{2}J_{C\text{-}P}$ = 12.0 Hz).

Analytical data consistent with that previously reported.[215]

Bis(2-(diphenylphosphino)ethyl)amine hydrochloride (2.4·HCl)

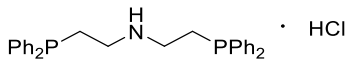

To a suspension of KO*t*-Bu (9.1 g, 81 mmol, 3.1 eq.) in dry, deoxygenated THF (162 mL) under nitrogen was added dropwise diphenylphosphine (9.1 mL, 52 mmol, 2.0 eq.). The reaction mixture was left to stir at rt for 5 mins before portionwise addition of bis(2-chloroethyl)amine hydrochloride (**2.8·HCl**) (4.6 g, 26 mmol, 1.0 eq.). The reaction was heated to reflux for 22 h, then cooled to rt, the reaction mixture was added to heptane (250 mL). This was washed with aqueous sodium hydroxide (300 mL, 2.5 M) and saturated brine (230 mL). The organic layer was separated and to this was added aqueous hydrochloric acid (250 mL, 3 M). This caused formation of a white precipitate which was isolated by filtration. The resulting solids were recrystallised from acetonitrile (190 mL) under nitrogen, and dried at 40 °C under reduced pressure to afford the product as white crystals (6.3 g, 13 mmol, 51%).

M. pt. (acetonitrile): 170.8 – 174.0 °C [lit.[143]: 174.5 – 175.5 °C (acetonitrile)];

$\boldsymbol{\nu}_{\mathbf{max}}$ (neat): 2714, 1456, 1432, 1044, 695 cm^{-1};

^{1}H NMR (400 MHz, $CDCl_3$): δ 9.92 (s, 2H, NH_2), 7.36 – 7.30 (m, 20H, 20 x ArH), 2.99 – 2.86 (m, 4H, C*H*$_2$NC*H*$_2$), 2.56 – 2.48 (m, 4H, C*H*$_2$CH$_2$NCH$_2$C*H*$_2$);

^{13}C NMR (101 MHz, $CDCl_3$): δ 136.2 (D, $^{1}J_{C\text{-}P}$ = 12.0 Hz), 132.8 (d, $^{2}J_{C\text{-}P}$ = 19.0 Hz), 129.4, 129.0 (d, $^{3}J_{C\text{-}P}$ = 7.0 Hz), 44.4 (d, $^{2}J_{C\text{-}P}$ = 27.0 Hz), 24.0 (D, $^{1}J_{C\text{-}P}$ = 16.0 Hz);

^{31}P{^{1}H} (161 MHz, $CDCl_3$): δ –21.07.

Analytical data consistent with that previously reported.[143]

Bis(2-(ethylthio)ethyl)amine hydrochloride (2.5·HCl)

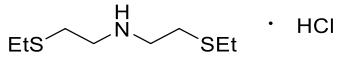

To a solution of sodium hydroxide (11.1 g, 278 mmol, 4.9 eq.) in deoxygenated methanol (50 mL) under nitrogen was added ethanethiol (11 mL, 149 mmol, 2.7 eq.) and the mixture was left to stir for 30 mins. To this was added a solution of bis(2-chloroethyl)amine hydrochloride (**2.8·HCl**)(10 g, 56 mmol, 1.0 eq.) in methanol (40 mL) over 5 mins and the reaction was left to stir at 35 °C for three days. The reaction mixture was concentrated and the residue was suspended in pentane (200 mL) and passed through a plug of basic alumina. To the resulting clear solution was added aqueous hydrochloric acid (100 mL, 3 M). The resulting precipitate was recrystallised from toluene (60 mL), collected by filtration, washed with pentane (200 mL) and dried under reduced pressure to afford the product as an off-white solid (7.55 g, 33 mmol, 58%).

^{1}H NMR (500 MHz, $CDCl_3$): δ 9.72 (br. s, 2H, NH_2), 3.27 – 3.16 (m, 4H, C*H*$_2$NC*H*$_2$), 3.03 (t, 4H, *J* = 7.5 Hz, C*H*$_2$CH$_2$NCH$_2$C*H*$_2$), 2.61 (q, 4H, *J* = 7.5 Hz, 2 x SC*H*$_2$CH$_3$), 1.28 (t, 6H, *J* = 7.5 Hz, 2 x SCH$_2$C*H*$_3$);

^{13}C NMR (126 MHz, $CDCl_3$): δ 47.2, 27.2, 26.2, 14.8.

Analytical data consistent with that previously reported.[106]

Bis(2-(phenylthio)ethyl)amine hydrochloride (2.6·HCl)

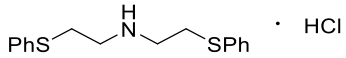

To a solution of sodium hydroxide (11.0 g, 275 mmol, 4.9 eq.) in deoxygenated methanol (50 mL) under nitrogen was added thiophenol (16 mL, 156 mmol, 2.8 eq.) and the mixture was left to stir for 30 mins. To this was added a solution of bis(2-chloroethyl)amine hydrochloride (**2.8·HCl**)(10 g, 56 mmol, 1.0 eq.) in methanol (40 mL) over 5 mins and the reaction was left to stir at 35 °C for three days. The reaction mixture was concentrated and the residue was suspended in pentane (200 mL) and passed through a plug of basic alumina. To the clear solution was added aqueous hydrochloric acid (100 mL, 3 M) and the resulting precipitate was recrystallised from toluene (60 mL), collected by filtration, washed with pentane (200 mL) and dried under reduced pressure to afford the product as a white solid (7.3 g, 25 mmol, 45%).

^{1}H NMR (500 MHz, $CDCl_3$): δ 9.90 (br. s, 2H, NH_2), 7.37 – 7.34 (m, 4H, 4 x SCCH), 7.30 (t, 4H, *J* = 8.0 Hz, 4 x SCCHC*H*), 7.24 (tt, 4H, 2H, *J* = 7.5, 2.0 Hz, 2 x SCCHCHC*H*), 3.39 (t, 4H, *J* = 7.5 Hz, CH_2CH$_2$NCH$_2$CH_2), 3.17 – 3.06 (m, 4H, CH_2NCH_2);

^{13}C NMR (126 MHz, $CDCl_3$): δ 133.0, 130.8, 129.6, 127.6, 46.9, 29.7.

Analytical data consistent with that previously reported.[106]

Bis(2-(*n*-butylthio)ethyl)amine hydrochloride (2.10·HCl)

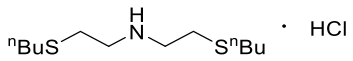

To a solution of sodium hydroxide (8.20 g, 205 mmol, 3.3 eq.) in deoxygenated methanol (50 mL) under nitrogen was added 1-butanethiol (14.5 mL, 135 mmol, 2.2 eq.) and the mixture was left to stir for 30 mins. To this was added a solution of bis(2-chloroethyl)amine hydrochloride (**2.8·HCl**) (11 g, 62 mmol, 1.0 eq.) in methanol (50 mL) over 15 mins and the reaction was left to stir at rt for three days. The reaction mixture was concentrated and the residue was suspended in hexane (200 mL) and passed through a plug of basic alumina. To the clear solution was added aqueous hydrochloric acid (100 mL, 2 M) and the resulting precipitate was recrystallised from toluene (50 mL), collected by filtration, washed with hexane (150 mL) and dried under reduced pressure to afford the product as a white solid (10.2 g, 35.7 mmol, 58%).

^{1}H NMR (500 MHz, $CDCl_3$): δ 9.76 (br. s, 2H, NH_2), 3.23 – 3.14 (m, 4H, CH_2NH_2), 3.02 (t, 4H, *J* = 7.5 Hz, $CH_2CH_2NCH_2CH_2$), 2.58 (t, 4H, *J* = 7.5 Hz, 2 x $NCH_2CH_2SCH_2$), 1.58 (apparent quint., 4H, *J* = 7.5 Hz, 2 x $SCH_2CH_2CH_2CH_3$), 1.41 (apparent sextet, 4H, *J* = 7.5 Hz, 2 x $SCH_2CH_2CH_2CH_3$), 0.92 (t, 6H, *J* = 7.5 Hz, 2 x $SCH_2CH_2CH_2CH_3$);

^{13}C NMR (126 MHz, $CDCl_3$): δ 47.1, 32.1, 31.7, 27.8, 22.0, 13.8.

Analytical data consistent with that previously reported.[216]

$RuCl_2$(*p*-cymene)Cl_2(NHC) (2.13)

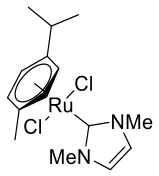

To a solution of dichloro(*p*-cymene)ruthenium(II) dimer (**2.11**) (5.14 g, 8.39 mmol, 1.0 eq.) in dry, deoxygenated DCM (80 mL) under nitrogen was added 1,3-dimethylimidazol-2-ylidene silver iodide (**2.15**) (5.80 g, 17.5 mmol, 2.1 eq.) and left to stir for 6 h at rt. The reaction mixture was then passed through a pad of diatomite rinsing with additional DCM (7 mL) to remove the precipitated AgI. The resulting dark solution was concentrated under reduced pressure to afford the product as an orange powder (6.54 g, 16.3 mmol, 97%).

$\boldsymbol{\nu}_{\mathbf{max}}$ (neat): 3095, 1457, 1229, 762, 685 cm^{-1};

^{1}H NMR (400 MHz, CD_2Cl_2): δ 7.03 (s, 2H, HC=CH), 5.39 (d, 2H, *J* = 5.7 Hz, 2 x $(CH_3)_2CHCCH$), 5.06 (d, 2H, *J* = 5.7 Hz, 2 x CH_3CCH), 3.96 (s, 6H, 2 x NCH_3), 2.92 (sept., 1H, *J* = 6.9 Hz, $(CH_3)_2CH$), 1.98 (s, 3H, $ArCH_3$), 1.25 (d, 6H, *J* = 6.9 Hz, $(CH_3)_2CH$);

^{13}C NMR (101 MHz, CD_2Cl_2): δ 174.6, 124.3, 110.0, 99.4, 86.3, 82.5, 40.0, 31.4, 22.7, 19.0.

Analytical data consistent with that previously reported.[104]

1,3-Dimethylimidazol-2-ylidene silver iodide (2.15)

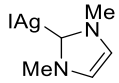

Silver oxide (7.86 g, 33.9 mmol, 1.00 eq.), 1,3-dimethylimidazolium iodide (**2.14**) (15.0 g, 67.0 mmol, 2.0 eq.) and DCM (60 mL) were added to a miniclave pressure vessel. The miniclave was pressurised with nitrogen (3 bar) and vented (x3), then pressurised with nitrogen (1 bar) and heated to 55 °C and left to stir overnight. After leaving the reaction mixture to cool to rt, the cream coloured suspension was filtered. The resulting solids were suspended in DMSO (85 mL) and heated to 125 °C. A hot filtration was performed, and the liquors were left to cool to rt. The precipitated solids were collected by filtration, washed with DCM (45 mL) and dried under reduced pressure at 45 °C to afford the product as a white powder (17.0 g, 51.3 mmol, 77%).

$\boldsymbol{\nu}_{\mathbf{max}}$ (neat): 2934, 1463, 1225, 741 cm^{-1};

^{1}H NMR (400 MHz, DMSO-d_6): δ 7.42 (s, 2H, HC=CH), 3.81 (s, 6H, 2 x NCH_3);

^{13}C NMR (101 MHz, DMSO-d_6): δ 181.3, 122.9, 37.9.

Analytical data consistent with that previously reported.[145]

Ru(di*n*-BuSNS)Cl_2(NHC) (2.16)

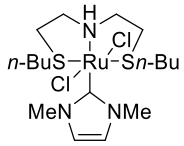

To a suspension of bis(2-(n-butylthio)ethyl)amine hydrochloride (**2.10·HCl**) (393 mg, 1.37 mmol) in DCM (6 mL) was added aqueous sodium hydroxide (5 mL, 4 M) and the mixture was stirred at rt for 30 mins. The organic layer was separated and concentrated to dryness to afford the free-base.

The free-base, bis(2-(n-butylthio)ethyl)amine (**2.10**) (281 mg, 1.13 mmol, 1.1 eq.) was dissolved in dry, deoxygenated ethanol (3 mL) under nitrogen and to this was added Ru(*p*-cymene)Cl_2(NHC) (**2.13**) (428 mg, 1.06 mmol, 1.0 eq.) and the mixture was stirred and heated to 70 °C overnight before being left to cool to rt. Dry, degassed heptane (9 mL) was added to the mixture and was stirred for 5 mins before decanting the liquid phase using a filtered cannula. Additional heptane (5 mL) was added and stirred followed by decanting the liquid phase using a filtered cannula. The residue was dried under reduced pressure to afford the product as an orange powder (329 mg, 0.636 mmol, 60%).

M.pt.: decomposes >130 °C;

$\boldsymbol{\nu}_{\mathbf{max}}$ (neat): 3184, 2928, 1726, 1520, 1450, 1144, 993, 729 cm^{-1};

^{1}H NMR (500 MHz, $CDCl_3$): δ 6.86 (s, 2H, HC=CH), 4.24 – 4.13 (m, 1H, NH), 4.07 (s, 6H, 2 x NCH_3), 3.42 – 2.40 (m, 12H, 6 x CH_2), 1.57 – 1.25 (m, 8H, 4 x CH_2), 0.90 – 0.76 (m, 6H, 2 x CH_2CH_3);

^{13}C NMR (126 MHz, $CDCl_3$): δ 186.5, 122.9, 48.4, 47.4, 40.5, 39.4 (br.), 38.5, 35.5, 33.1, 29.8, 29.4, 22.3, 22.2, 14.0;

HRMS: ($C_{17}H_{35}N_3{}^{35}Cl_2{}^{96}RuS_2$) [$M^+$] requires 511.0720, found [M^+] 511.0715.

Ru(PNP)(NHC)BH (2.17)

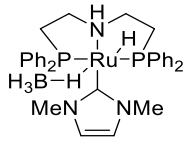

To a Schlenk flask was added Ru(PNP)Cl_2(NHC) (**1.51**) (149 mg, 0.210 mmol, 1.0 eq.) and THF (3 mL) under nitrogen. Lithium borohydride (26.1 mg, 1.20 mmol, 5.7 eq.) was added portion wise and the mixture was left to stir overnight at rt. ^{31}P NMR indicated complete consumption of starting material and formation of a single product. The product was characterised as a brown solution in THF.

^{1}H NMR (400 MHz, THF-d_8): δ 7.54 – 7.14 (m, 20H, Ph-H), 6.70 (d, 1H, *J* = 2.0 Hz, C=C-H), 6.65 (d, 1H, *J* = 2.0 Hz, C=C-H), 4.65 (m, 1H, NH), 3.47 – 3.30 (m, 2H, CH_2), 3.28 (s, 3H, NCH_3), 2.92 (s, 3H, NCH_3), 2.72 – 2.32 (m, 6H, 3 x CH_2), –1.65 – –2.73 (m, 4H, BH_4), –16.06 (t, 1H, $^{2}J_{H\text{-}P}$ = 21.5 Hz, Ru-H);

^{13}C NMR (101 MHz, THF-d_8): δ 144.6 (t, $J_{C\text{-}P}$ = 18.0 Hz), 140.6 (t, $J_{C\text{-}P}$ = 15.5 Hz), 134.1 (t, $J_{C\text{-}P}$ = 6.5 Hz), 132.9 (t, $J_{C\text{-}P}$ = 6.0 Hz), 129.1, 129.0, 1 (t, $J_{C\text{-}P}$ = 4.0 Hz), 128.5 (t, $J_{C\text{-}P}$ = 4.0 Hz), 128.3 (t, $J_{C\text{-}P}$ = 4.0 Hz), 54.2 (t, $J_{C\text{-}P}$ = 5.0 Hz), 40.3, 39.1, 34.9 (t, $J_{C\text{-}P}$ = 10.0 Hz);

^{31}P{^{1}H} NMR (162 MHz, THF-d_8): δ 58.0.

N.B. Further characterisation data could not be obtained due to the instability of the complex.

Naphthalen-2-ylmethanol (2.19)

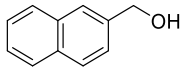

To a glass vial was added Ru(PNP)Cl_2(NHC) (**1.51**) (22.8 mg, 0.032 mmol, 0.016 eq.), methyl 2-naphthoate (**2.18**) (371 mg, 1.99 mmol, 1.0 eq.), potassium *tert*-butoxide (0.4 mL, 0.4 mmol, 0.20 eq., 1 M in THF) and THF (4 mL). The vial was placed in a Biotage Endeavor, then pressurised with nitrogen (5 bar) and vented (x3), then pressurised with hydrogen (2 bar) and vented (x3), then pressurised with hydrogen (2 bar) and left to stir at 700 rpm at 40 °C for 3 h. The reaction mixture was cooled to rt, and the vial was purged with nitrogen (3 x 5 bar). The reaction mixture was concentrated and purified by flash column chromatography (eluent: 5 to 20% EtOAc/heptane gradient) to afford the product as a white solid (227 mg, 1.43 mmol, 72%).

^{1}H NMR (400 MHz, $CDCl_3$): δ 7.88 – 7.78 (m, 4H, 4 x ArH), 7.52 – 7.44 (m, 3H, 3 x ArH), 4.86 (d, 2H, *J* = 6.0 Hz, CH_2), 1.80 (t, 1H, *J* = 6.0 Hz, OH);

^{13}C NMR (101 MHz, $CDCl_3$): δ 138.5, 133.5, 133.1, 128.5, 128.0, 127.9, 126.4, 126.1, 125.6, 125.3, 65.7.

Analytical data consistent with that previously reported.[217]

Formation of ruthenium hydride species (2.20)

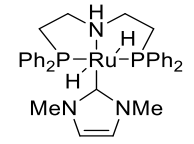

tentative structure

To a NMR tube was added Ru(PNP)Cl_2(NHC) (**1.51**) (2.6 mg, 3.7 µmol, 1.0 eq.), potassium *tert*-butoxide (4.1 mg, 37 µmol, 10 eq.) and THF-d_8 (0.25 mL) under nitrogen. The mixture was sonicated before being evacuated and backfilled with hydrogen gas. After 1 h complete consumption of the starting material and formation of a single new product was observed by ^{31}P NMR. The product was characterised as a pale yellow solution in THF-d_8.

^{1}H NMR (400 MHz, THF-d_8): *discernible data* δ 7.71 – 7.11 (m, Ph-H), 6.89 – 6.86 (m, HC=CH), 4.40 – 4.27 (m, NH), 3.40 (s, NCH_3), 3.23 (s, NCH_3), 3.21 – 2.05 (m, 4 x CH_2), –7.33 (td, J = 21.0, 9.5 Hz, Ru-H) , –7.75 (td, $^2J_{H\text{-}P}$ = 21.0, 9.5 Hz, Ru-H).

^{31}P{^{1}H} NMR (162 MHz, THF-d_8): δ 68.6.

N.B. Although clean conversion to a new signal by ^{31}P NMR indicated complete conversion, satisfactory integrations could not be obtained for the ^{1}H NMR spectrum due to the high dilution of the reaction and complexity of the data.

Naphthalen-2-ylmethyl 2-naphthoate (2.22)

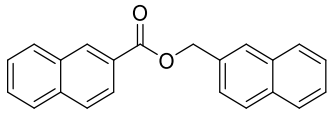

To a suspension of 2-naphthoic acid (**2.21**) (3.00 g, 17.4 mmol, 1.0 eq.) in anhydrous toluene (10 mL) was added dropwise thionyl chloride (2.54 mL, 34.8 mmol, 2 eq.). The mixture was heated to 92 °C for 3 h, during which time a clear solution formed, before being left to cool to rt. The solvent was removed under reduced pressure and then DCM (10mL) was added. To this was added dropwise naphthalen-2-yl methanol (**2.19**) (1.70 g, 11 mmol, 0.61 eq.) in a mixture of DCM (5 mL) and triethylamine (4.8 mL) at 0 °C and left to stir overnight while slowly warming to rt. DCM (20 mL) and water (20 mL) were added. The organic layer was separated and washed with aqueous hydrochloric acid (20 mL, 1 M) and saturated brine (20 mL), dried over sodium sulfate, filtered and concentrated under reduced pressure. The residue was purified by flash column chromatography (eluent: 10 to 40% EtOAc/heptane gradient) to afford the product as a white crystalline solid (0.92 g, 3.0 mmol, 17%).

^{1}H NMR (400 MHz, $CDCl_3$): δ 8.68 (s, 1H, ArH), 8.13 (dd, 1H, *J* = 8.5, 1.5 Hz, ArH), 7.99 – 7.84 (m, 7H, 7 x ArH), 7.65 – 7.48 (m, 5H, 5 x ArH), 5.61 (s, 2H, CH_2);

^{13}C NMR (101 MHz, $CDCl_3$): δ 166.8, 135.7, 133.7, 133.4, 133.3, 132.6, 131.4, 129.5, 128.6, 128.4, 128.3, 128.2, 127.91, 127.88, 127.6, 127.5, 126.8, 126.5, 126.4, 126.1, 125.5, 67.2.

Analytical data obtained consistent with that previously reported.[218]

***tert*-Butyl 2-naphthoate (2.23)**

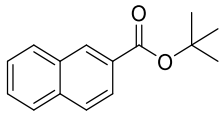

To a suspension of 2-naphthoic acid (**2.21**) (2.01 g, 11.7 mmol, 1.0 eq.) and DMF (1 drop) in DCM (10 mL) was added dropwise oxalyl chloride (1.2 mL, 13.7 mmol, 1.2 eq.). Once effervescence had ceased, the reaction mixture was concentrated and DCM (5 mL) was added followed by diisopropyl ethylamine (2.3 mL, 13.2 mmol, 1.1 eq.) and *tert*-butanol (1.2 mL, 12.7 mmol, 1.1 eq.) and the mixture was left to stir at rt overnight. Potassium *tert*-butoxide (10 mL, 10 mmol, 1 M in THF) was added dropwise and the mixture was left to stir for 1 h at rt. Water (20 mL) and DCM (30 mL) were then added and the organic layer was separated and concentrated. The crude residue was then purified by flash column chromatography (eluent: 10 to 80% EtOAc/heptane gradient) to afford the product as a cream coloured solid (1.63 g, 7.14 mmol, 61%).

^{1}H NMR (400 MHz, $CDCl_3$): δ 8.54 (s, 1H, ArH), 8.02 (dd, 1H, *J* = 8.5, 1.5 Hz, ArH), 7.95 (d, 1H, *J* = 8.0 Hz, ArH), 7.89 – 7.84 (m, 2H, 2 x ArH), 7.60 – 7.50 (m, 2H, 2 x ArH), 1.65 (s, 9H, 3 x CH_3);

^{13}C NMR (101 MHz, $CDCl_3$): δ 166.1, 135.4, 132.7, 130.8, 129.4, 129.4, 128.1, 128.0, 127.8, 127.6, 125.5, 81.3, 28.4.

Analytical data obtained consistent with that previously reported.[219]

_o_-Tolylmethanol (2.27)

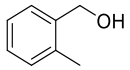

This was carried out according to General Procedure VIII starting with Ru(PNP)Cl_2(NHC) (**1.51**) (29 mg, 0.040 mmol, 0.016 eq.), methyl 2-methylbenzoate (**2.26**) (0.35 mL, 2.5 mmol, 1.0 eq.), potassium *tert*-butoxide (0.50 mL, 0.50 mmol, 0.20 eq., 1 M in THF) and 2-MeTHF (3.5 mL). The crude conversion was assessed to be > 50% by HPLC. The crude residue was purified by flash column chromatography (eluent: 10 to 80% EtOAc/heptane gradient) to afford the product as a colourless oil (51 mg, 0.42 mmol, 17%).

^{1}H NMR (400 MHz, $CDCl_3$): δ 7.40 – 7.32 (m, 1H, ArH), 7.25 – 7.14 (m, 3H, 3 x ArH), 4.71 (s, 2H, CH_2), 2.37 (s, 3H, CH_3);

^{13}C NMR (101 MHz, $CDCl_3$): δ 138.8, 136.3, 130.5, 128.0, 127.7, 126.2, 63.7, 18.8.

Analytical data consistent with that previously reported.[220]

Cyclohex-3-en-1-ylmethanol (2.29)

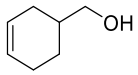

This was carried out according to General Procedure VIII starting with Ru(PNP)Cl_2(NHC) (**1.51**) (28 mg, 0.039 mmol, 0.015 eq.), methyl cyclohex-3-ene-1-carboxylate (**2.28**) (361 mg, 2.58 mmol, 1.0 eq.), potassium *tert*-butoxide (0.50 mL, 0.50 mmol, 0.20 eq., 1 M in THF) and 2-MeTHF (3.5 mL). The crude residue was purified by flash column chromatography (eluent: 10 to 80% EtOAc/heptane gradient) to afford the product as a colourless oil (112 mg, 0.994 mmol, 39%).

^{1}H NMR (400 MHz, $CDCl_3$): δ 5.72 – 5.63 (m, 2H, 2x C=CH), 3.49 – 3.58 (m, 2H, C*H*$_2$OH), 2.71 – 1.68 (m, 6H, 3 x CH_2), 1.44 (br. s, 1H, OH), 1.34 – 1.22 (m, 1H, C*H*CH_2OH);

^{13}C NMR (101 MHz, $CDCl_3$): δ 127.3, 126.0, 68.0, 36.5, 28.2, 25.3, 24.8.

Analytical data consistent with that previously reported.[221]

(4-Ethylphenyl)methanol (2.31)

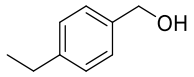

This was carried out according to General Procedure VIII starting with Ru(PNP)Cl_2(NHC) (**1.51**) (30 mg, 0.042 mmol, 0.016 eq.), methyl 4-vinylbenzoate (**2.30**) (415 mg, 2.56 mmol, 1.0 eq.), potassium *tert*-butoxide (0.50 mL, 0.50 mmol, 0.20 eq., 1 M in THF) and 2-MeTHF (3.5 mL). The crude conversion was assessed to be > 80% by HPLC. The crude residue was purified by flash column chromatography (eluent: 10 to 80% EtOAc/heptane gradient) to afford the product as a colourless oil (80 mg, 0.58 mmol, 23%).

^{1}H NMR (400 MHz, $CDCl_3$): δ 7.29 (d, 2H, *J* = 8.0 Hz, 2 x $HOCH_2CC\mathit{H}$), 7.20 (d, 2H, *J* = 8.0 Hz, 2 x $H_3CCH_2CC\mathit{H}$), 4.66 (s, 2H, CH_2), 2.66 (q, 2H, *J* = 7.5 Hz, $H_3CC\mathit{H}_2$), 1.64 (br. s, 1H, OH), 1.24 (t, 3H, *J* = 7.5 Hz, CH_3);

^{13}C NMR (101 MHz, $CDCl_3$): δ 144.0, 138.3, 128.2, 127.3, 65.5, 28.7, 15.8.

Analytical data consistent with that previously reported.[222]

1,4-Phenylenedimethanol (2.33)

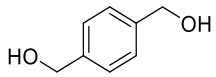

This was carried out according to General Procedure VIII starting with Ru(PNP)Cl_2(NHC) (**1.51**) (29 mg, 0.040 mmol, 0.016 eq.), methyl 4-(hydroxymethyl)benzoate (**2.32**) (430 mg, 2.50 mmol, 1.0 eq.), potassium *tert*-butoxide (0.50 mL, 0.50 mmol, 0.20 eq., 1 M in THF) and 2-MeTHF (3.5 mL). The crude conversion was assessed to be > 95% by HPLC. The crude residue was purified by flash column chromatography (eluent: 10 to 80% EtOAc/heptane gradient) to afford the product as a white powder (226 mg, 1.63 mmol, 63%).

^{1}H NMR (400 MHz, $CDCl_3$): δ 7.37 (s, 4H, 4 x ArH), 4.70 (s, 4H, 2 x CH_2), 1.63 (br. s, 2H, 2 x OH);

^{13}C NMR (101 MHz, $CDCl_3$): δ 140.5, 127.4, 65.3.

Analytical data consistent with that previously reported.[223]

1,2-Phenylenedimethanol (2.35)

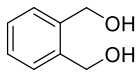

Procedure A

This was carried out according to General Procedure VIII starting with Ru(PNP)Cl_2(NHC) (**1.51**) (29 mg, 0.040 mmol, 0.016 eq.), dimethyl phthalate (**2.34**) (488 mg, 2.51 mmol, 1.0 eq.), potassium *tert*-butoxide (0.50 mL, 0.50 mmol, 0.20 eq., 1 M in THF) and 2-MeTHF (3.5 mL). The crude conversion was assessed to be > 50% by HPLC. The crude residue was purified by flash column chromatography (eluent: 10 to 80% EtOAc/heptane gradient) to afford the product as a white solid (33 mg, 0.24 mmol, 10%).

^{1}H NMR (400 MHz, DMSO-d_6): δ 7.41 – 7.35 (m, 2H, 2 x ArH), 7.25 – 7.20 (m, 2H, 2 x ArH), 5.05 (t, 2H, *J* = 5.5 Hz, 2 x OH), 4.53 (d, 4H, *J* = 5.5 Hz, 2 x CH_2);

^{13}C NMR (101 MHz, DMSO-d_6): δ 139.4, 126.7, 126.5, 60.4.

Analytical data consistent with that previously reported.[129]

Procedure B

This was carried out according to General Procedure VIII starting with Ru(PNP)Cl_2(NHC) (**1.51**) (28 mg, 0.039 mmol, 0.015 eq.), phthalide (**2.36**) (351 mg, 2.62 mmol, 1.0 eq.), potassium *tert*-butoxide (0.50 mL, 0.50 mmol, 0.19 eq., 1 M in THF) and 2-MeTHF (3.5 mL). The crude conversion was assessed to be > 50% by HPLC. The crude residue was purified by flash column chromatography (eluent: 10 to 80% EtOAc/heptane gradient) to afford the product as a yellow solid (129 mg, 0.934 mmol, 36%).

Analytical data consistent with that described in Procedure A.

(3-Fluorophenyl)methanol (2.38)

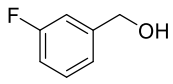

This was carried out according to General Procedure VIII starting with Ru(PNP)Cl_2(NHC) (**1.51**) (26 mg, 0.037 mmol, 0.014 eq.), methyl 3-fluorobenzoate (**2.37**) (390 mg, 2.53 mmol, 1.0 eq.), potassium *tert*-butoxide (0.50 mL, 0.50 mmol, 0.20 eq., 1 M in THF) and 2-MeTHF (3.5 mL). The reaction was left for 12 h. The crude conversion was assessed to be > 90% by HPLC. The crude residue was purified by flash column chromatography (eluent: 10 to 80% EtOAc/heptane gradient) to afford the product as a colourless oil (239 mg, 1.90 mmol, 75%).

^{1}H NMR (400 MHz, $CDCl_3$): δ 7.35 – 7.28 (m, 1H, ArH), 7.15 – 7.06 (m, 2H, 2 x ArH) 6.98 (td, 1H, *J* = 8.5, 2.5 Hz, ArH); 4.70 (d, 2H, *J* = 5.5 Hz, CH_2), 1.81 – 1.72 (m, 1H, OH);

^{13}C NMR (101 MHz, $CDCl_3$): δ 163.1 (D, $^1J_{C\text{-}F}$ = 245.0 Hz), 143.6 (d, $^3J_{C\text{-}F}$ = 7.0 Hz), 130.1 (d, $^3J_{C\text{-}F}$ = 8.5 Hz), 122.3 (d, $^4J_{C\text{-}F}$ = 3.0 Hz), 114.4 (d, $^2J_{C\text{-}F}$ = 21.5 Hz), 113.7 (d, $^2J_{C\text{-}F}$ = 22.0 Hz), 64.5 (d, $^4J_{C\text{-}F}$ = 1.5 Hz);

^{19}F{^{1}H} NMR (376 MHz, $CDCl_3$): δ –113.1.

Analytical data consistent with that previously reported.[224]

(4-bromophenyl)methanol (2.40)

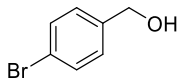

This was carried out according to General Procedure VIII starting with Ru(PNP)Cl_2(NHC) (**1.51**) (29 mg, 0.041 mmol, 0.016 eq.), methyl 4-bromobenzoate (**2.39**) (538 mg, 2.50 mmol, 1.0 eq.), potassium *tert*-butoxide (0.50 mL, 0.50 mmol, 0.20 eq., 1 M in THF) and 2-MeTHF (3.5 mL). The crude conversion was assessed to be > 95% by HPLC. The crude residue was purified by flash column chromatography (eluent: 10 to 80% EtOAc/heptane gradient) to afford the product as a white crystalline solid (316 mg, 1.69 mmol, 68%).

^{1}H NMR (400 MHz, $CDCl_3$): δ 7.51 – 7.46 (m, 2H, 2 x BrCC*H*), 7.26 – 7.21 (m, 2H, 2 x BrCCHC*H*), 4.66 (s, 2H, CH_2), 1.69 (br. s, 1H, OH);

^{13}C NMR (101 MHz, $CDCl_3$): δ 139.9, 131.8, 128.7, 121.6, 64.8.

Analytical data consistent with that previously reported.[225]

(6-Bromonaphthalen-2-yl)methanol (2.42)

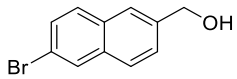

Procedure A

This was carried out according to General Procedure VIII starting with Ru(PNP)Cl_2(NHC) (**1.51**) (19 mg, 0.027 mmol, 0.010 eq.), methyl 6-bromo-2-naphthaote (**2.41**) (686 mg, 2.59 mmol, 1.0 eq.), potassium *tert*-butoxide (0.50 mL, 0.50 mmol, 0.20 eq., 1 M in THF) and 2-MeTHF (2 mL). The crude conversion was assessed to be > 95% by HPLC. To the reaction mixture was added saturated aqueous ammonium chloride solution (2 mL), water (5 mL) and 2-MeTHF (5 mL). The organic layer was separated, washed with aqueous hydrochloric acid (5 mL, 1 M), and passed through a short silica pad. Isooctane (45 mL) was added and approximately half the solvent volume was removed by distillation. The precipitate was collected by filtration and dried to afford product as a pale brown solid (218 mg, 0.919 mmol, 37%).

^{1}H NMR (400 MHz, $CDCl_3$): δ 8.00 (d, 1H, *J* = 1.5 Hz, ArH), 7.79 (s, 1H, ArH), 7.75 (d, 1H, *J* = 8.5 Hz), 7.71 (d, 1H, *J* = 8.5 Hz), 7.56 (dd, 1H, *J* = 8.5, 2.0 Hz, ArH), 7.51 (dd, 1H, *J* = 8.5, 1.5 Hz, ArH), 4.86 (s, 2H, CH_2O), 1.80 (br. s, 1H, OH);

^{13}C NMR (101 MHz, $CDCl_3$): δ 139.0, 134.1, 132.0, 129.9, 129.74, 129.68, 127.6, 126.3, 125.4, 120.0, 65.4.

Procedure B

To a 500 mL pressure vessel equipped with a gas-entrainment impeller was added methyl 6-bromo-2-naphthoate (**2.41**) (10 g, 38 mmol, 1.0 eq.) and Ru(PNP)Cl_2(NHC) (**1.51**) (268 mg, 0.377 mmol, 0.01 eq.). The vessel was left to purge with nitrogen for 5 mins before adding 2-MeTHF (100 mL) and potassium *tert*-butoxide (847 mg, 7.54 mmol, 0.20 eq.). The vessel was sealed and the impeller was set to stir at 300 rpm. The vessel was pressurised with nitrogen (3.5 bar) then vented (x3), then pressurised with hydrogen (3.5 bar) then vented (x3). The vessel was then pressurised and maintained with hydrogen (4.0 bar). The reaction was heated to 45 °C, the impeller was adjusted to 700 rpm and the mixture was left in this state for 4 h. Analysis by HPLC indicated > 99% conversion. Aqueous hydrochloric acid (100 mL, 1 M) was added and the mixture was stirred for 10 mins. The organic phase was separated and passed through a silica pad (16 g, 2.5 cm depth). The mixture was distilled down to ~30 mL, isooctane was added (90 mL), and the resulting mixture was concentrated to ~70 mL then

placed in an ice bath. The precipitated solids were collected by filtration and dried under reduced pressure to afford the product as a pale yellow powder (7.3 g, 31 mmol, 82%).

Analytical data consistent with that described in Procedure A.

In addition to the product alcohol (**2.42**), the following side products were also isolated and identified:

6-Bromo-2-naphthoic acid (2.74)

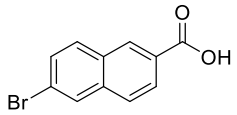

^{1}H NMR (400 MHz, DMSO-d_6): δ 8.51 (s, 1H, ArH), 8.24 (d, 1H, *J* = 1.5 Hz, ArH), 8.06 – 8.00 (m, 2H, 2 x ArH), 7.89 (d, 1H, *J* = 8.5 Hz, ArH), 7.66 (dd, 1H, *J* = 9.0, 2.0 Hz, ArH);

^{13}C NMR (101 MHz, DMSO-d_6): δ 167.3, 136.1, 131.6, 130.8, 130.6, 130.0, 129.8, 128.8, 127.6, 126.4, 121.9.

Analytical data consistent with that previously reported.[226]

Naphthalen-2-ylmethanol (2.19)

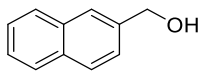

Previously characterised on page 211.

Procedure C

A stirred charge vessel was charged under a flow of nitrogen with Ru(PNP)Cl_2(NHC) (**1.51**) (668 mg, 0.941 mmol, 0.0050 eq.), methyl 6-bromo-2-naphthoate (**2.41**) (50 g, 189 mmol, 1.0 eq.), potassium *tert*-butoxide (38 mL, 38 mmol, 1 M in THF) and 2-MeTHF (500 mL).

Through a CSTR flow reactor was pumped the reaction mixture while also being supplied with hydrogen gas (5 bar). The jacket of the reactor was set to 65 °C and the agitator was set to 219 rpm. The residence time of the reaction mixture was varied by altering the rate at which the mixture was pumped (54, 23 and 12 mins). The reaction was left to reach a steady state before directly sampling the resulting reaction mixture and assessing conversion by HPLC (**Table 24**).

(3-Iodophenyl)methanol (2.44)

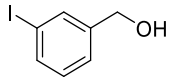

This was carried out according to General Procedure VIII starting with Ru(PNP)Cl_2(NHC) (**1.51**) (29 mg, 0.041 mmol, 0.016 eq.), methyl 3-iodobenzoate (**2.43**) (655 mg, 2.50 mmol, 1.0 eq.), potassium *tert*-butoxide (0.50 mL, 0.50 mmol, 0.20 eq., 1 M in THF) and 2-MeTHF (3.5 mL). The crude conversion was assessed to be > 95% by HPLC. The crude residue was purified by flash column chromatography (eluent: 10 to 80% EtOAc/heptane gradient) to afford the product as a yellow oil (384 mg, 1.64 mmol, 66%).

^{1}H NMR (400 MHz, $CDCl_3$): δ 7.74 (s, 1H, ICC*H*CCH_2), 7.63 (d, 1H, *J* = 8.0 Hz, ICCH), 7.32 (d, 1H, *J* = 8.0 Hz, ICCHCHC*H*), 7.09 (t, 1H, *J* = 8.0 Hz, ICCHC*H*), 4.65 (d, 2H, *J* = 5.5 Hz, CH_2), 1.74 (t, 1H, *J* = 5.5 Hz, OH);

^{13}C NMR (101 MHz, $CDCl_3$): δ 143.3, 136.8, 136.0, 130.4, 126.2, 94.6, 64.6.

Analytical data consistent with that previously reported.[227]

(6-Methylpyridin-3-yl)methanol (2.46)

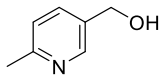

Procedure A

This was carried out according to General Procedure VIII starting with Ru(PNP)Cl_2(NHC) (**1.51**) (51 mg, 0.072 mmol, 0.0079 eq.), methyl 6-methylnicotinate (**2.45**) (1.37 g, 9.06 mmol, 1.0 eq.), potassium methoxide (120 mg, 1.71 mmol, 0.19 eq.) and 2-MeTHF (4 mL). The crude conversion was assessed to be > 95% by HPLC. Saturated aqueous ammonium chloride solution (0.5 mL) was added, and the mixture was concentrated to dryness. The crude residue was purified by vacuum distillation to afford the product as a white solid (878 mg, 7.13 mmol, 79%).

^{1}H NMR (400 MHz, $CDCl_3$): δ 8.34 (s, 1H, NCH), 7.59 (dd, 1H, *J* = 8.0, 2.0 Hz, NCCHC*H*), 7.12 (d, 1H, *J* = 8.0 Hz, NCCH). 4.64 (s, 2H, CH_2), 3.77 (br. s, 1H, OH), 2.50 (s, 3H, CH_3);

^{13}C NMR (101 MHz, $CDCl_3$): δ 157.5, 147.8, 136.7, 133.8, 123.3, 62.4, 24.0.

Analytical data consistent with that previously reported.[168]

Procedure B

To a 5 L Büchi Kiloclave equipped with a gas-entrainment impeller was added methyl 6-methylnicotinate (**2.45**) (200 g, 1.32 mol, 1.0 eq.), Ru(PNP)Cl_2(NHC) (**1.51**) (937 mg, 1.32 mmol, 0.0010 eq.), potassium *tert*-butoxide (29.7 g, 265 mmol, 0.20 eq.) and 2-MeTHF (2.5 L). The vessel was sealed and purged with nitrogen (3 x 3 bar), then hydrogen (3 x 2.5 bar) before being filled and maintained with hydrogen (2.8 bar). The reaction was heated to 50 °C and the impeller was adjusted to 750 rpm. After 1.5 h, the hydrogen pressure was increased (5 bar) and the reaction was left to stir overnight. The reaction was cooled to 20 °C, the hydrogen was released and the vessel was purged with nitrogen (3 x 5 bar). HPLC analysis indicated > 98% conversion. Saturated aqueous ammonium chloride solution (30 mL) was added, and the solvent was distilled off under reduced pressure. The crude residue was purified by vacuum distillation (100 °C, 0.7 mbar) to afford the product as a yellow solid (118 g, 955 mmol, 72%).

Analytical data consistent with that described in Procedure A.

4-(Dimethylamino)phenyl)methanol (2.48)

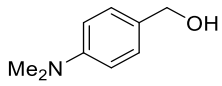

This was carried out according to General Procedure VIII starting with Ru(PNP)Cl_2(NHC) (**1.51**) (28 mg, 0.039 mmol, 0.016 eq.), ethyl 4-(dimethylamino)benzoate (**2.47**) (489 mg, 2.53 mmol, 1.0 eq.), potassium *tert*-butoxide (0.50 mL, 0.50 mmol, 0.20 eq., 1 M in THF) and 2-MeTHF (3.5 mL). The crude conversion was assessed to be > 70% by HPLC. The crude residue was purified by flash column chromatography (eluent: 10 to 80% EtOAc/heptane gradient) to afford the product as a colourless oil (175 mg, 1.16 mmol, 46%).

^{1}H NMR (400 MHz, $CDCl_3$): δ 7.27 (d, 2H, *J* = 8.5 Hz, 2 x NCCH), 6.76 (d, 2H, *J* = 8.5 Hz, 2 x $CH_2CC\mathit{H}$), 4.59 (s, 2H, CH_2), 2.98 (s, 6H, $N(CH_3)_2$);

^{13}C NMR (101 MHz, $CDCl_3$): δ 150.5, 129.1, 128.8, 112.8, 65.5, 40.8.

Analytical data consistent with that previously reported.[228]

In addition to the product alcohol, the following side products were also isolated and identified:

4-(Dimethylamino)benzaldehyde (2.53)

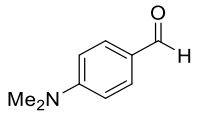

^{1}H NMR (400 MHz, $CDCl_3$): δ 9.75 (s, 1H, C(O)H), 7.77 – 7.72 (m, 2H, 2 x C(O)CCH), 6.73 – 6.68 (m, 2H, 2 x NCCH), 3.09 (s, 6H, 2 x NCH_3)

LCMS: t_R: 1.08 min, $[MH]^+$ 150.0.

Analytical data consistent with that previously reported.[229]

***tert*-Butyl 4-(dimethylamino)benzoate (2.54)**

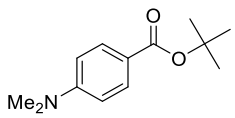

Product characterised on page 228.

4-(Dimethylamino)benzyl 4-(dimethylamino)benzoate (2.55)

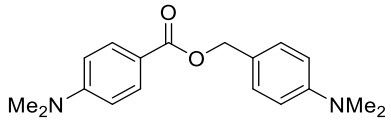

^{1}H NMR (400 MHz, $CDCl_3$): δ 7.95 – 7.89 (m, 2H, 2 x C(O)CCH), 7.36 – 7.31 (m, 2H, 2 x CH_2CCH), 6.75 – 6.71 (m, 2H, 2 x C(O)CCHCH), 6.64 – 6.59 (m, 2H, 2 x OCH_2CCHCH), 5.22 (s, 2H, OCH_2), 3.02 (s, 6H, 2 x NCH_3), 2.95 (s, 6H, 2 x NCH_3);

LCMS: t_R: 1.19 min, $[MH]^+$ 299.2.

Analytical data consistent with that previously reported.[230]

(3,4-Dihydro-2*H*-pyrano[2,3-*c*]pyridin-6-yl)methanol (2.50)

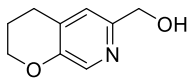

This was carried out according to General Procedure VIII except starting with $Ru(PNP)Cl_2(NHC)$ (**1.51**) (23 mg, 0.033 mmol, 0.017 eq.), methyl 3,4-dihydro-2*H*-pyrano[2,3-*c*]pyridine-6-carboxylate (**2.49**) (0.398 g, 2.06 mmol, 1.0 eq.), potassium *tert*-butoxide (0.40 mL, 0.40 mmol, 0.20 eq., 1 M in THF) and 2-MeTHF (3.6 mL). The reaction mixture was heated to 65 °C. The crude conversion was assessed to be > 95% by HPLC. The crude residue was purified by flash column chromatography (eluent: 15 to 100% EtOAc/heptane gradient) to afford the product as a yellow crystalline solid (212 mg, 1.28 mmol, 62%).

^{1}H NMR (400 MHz, $CDCl_3$): δ 8.08 (s, 1H, NCH), 6.93 (s, 1H, NCCHC), 4.63 (s, 2H, CH_2OH), 4.23 – 4.19 (m, 2H, OCH_2), 3.45 (s, 1H, OH), 2.77 (t, 2H, *J* = 6.5 Hz, $OCH_2CH_2CH_2$), 2.07 – 1.99 (m, 2H, OCH_2CH_2);

^{13}C NMR (101 MHz, $CDCl_3$): δ 151.3, 150.4, 138.1, 131.5, 121.1, 66.7, 64.3, 24.4, 21.8.

Analytical data consistent with that previously reported.[169]

(3,4-Dihydro-2*H*-pyrano[2,3-*c*]pyridin-6-yl)methanol hydrochloride (2.50·HCl)

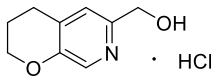

Reduction

Methyl 3,4-dihydro-2*H*-pyrano[2,3-*c*]pyridine-6-carboxylate (**2.49**) (9.8 g, 51 mmol, 1.0 eq.), potassium *tert*-butoxide (1.1 g, 9.7 mmol, 0.2 eq.), Ru(PNP)Cl_2(NHC) (**1.51**) (0.35 g, 0.5 mmol, 0.01 eq.) and 2-MeTHF (110 mL) were charged into a Hastelloy pressure vessel. The vessel was pressurised with nitrogen (5 bar) and vented (x3), then pressurised with hydrogen (5 bar), and vented (x3), then pressurised and maintained with hydrogen (6.5 bar). The mixture was heated to 45 °C and the reaction was left to stir at 800 rpm for 12 h before being cooled to rt. The vessel was then purged with nitrogen (3 x 5 bar). The reaction mixture was concentrated and the residue was partitioned between DCM (150 mL) and aqueous saturated sodium bicarbonate solution (150 mL). The organic layer was separated and passed through a plug of silica, flushed with ethyl acetate (150 mL) and concentrated under reduced pressure.

Salt formation

The residue was suspended in 1-propanol (20 mL) and hydrochloric acid (15 mL, 4 M in dioxane) was added which induced precipitation. TBME (50 mL) was added, and the solids were collected by filtration, and washed with further TBME (50 mL). The collected solids were left to dry overnight at 40 °C under reduced pressure to afford the product as a free-flowing yellow powder (6.3 g, 31 mmol, 62%).

^{1}H NMR (400 MHz, DMSO-d_6): δ 8.30 (s, 1H, NCH), 7.65 (s, 1H, NCCHC), 4.67 (s, 2H, CH_2OH), 4.35 – 4.28 (m, 2H, OCH_2), 2.97 (t, 2H, *J* = 6.5 Hz, OCH_2CH_2CH_2), 2.04 – 1.96 (m, 2H, OCH_2CH_2);

^{13}C NMR (101 MHz, $CDCl_3$): δ 152.4, 147.3, 142.1, 129.6, 124.5, 67.0, 59.3, 24.4, 20.0.

Analytical data consistent with that previously reported.[169]

Thiophen-2-ylmethanol (2.52)

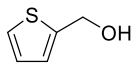

This was carried out according to General Procedure VIII starting with Ru(PNP)Cl_2(NHC) (**1.51**) (23 mg, 0.0033 mmol, 0.016 eq.), ethyl thiophene-2-carboxylate (**2.51**) (312 mg, 2.00 mmol, 1.0 eq.), potassium *tert*-butoxide (0.50 mL, 0.50 mmol, 0.20 eq., 1 M in THF) and 2-MeTHF (3.5 mL). The crude conversion was assessed to be > 95% by HPLC. The crude residue was purified by flash column chromatography (eluent: 10 to 80% EtOAc/heptane gradient) to afford the product as a yellow oil (118 mg, 1.03 mmol, 52%).

^{1}H NMR (400 MHz, $CDCl_3$): δ 7.28 (dd, 1H, *J* = 5.0 Hz, 1.0 Hz, Ar-H), 7.03 – 6.95 (m, 2H, 2 x Ar-H), 4.82 (d, 2H, *J* = 5.5 Hz, CH_2), 1.97 – 1.88 (m, 1H, OH);

^{13}C NMR (101 MHz, $CDCl_3$): δ 144.1, 127.0, 125.7, 125.6, 60.1.

Analytical data consistent with that previously reported.[231]

***tert*-Butyl 4-(dimethylamino)benzoate (2.54)**

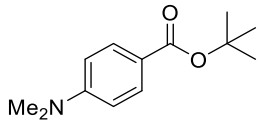

To a suspension of 4-(dimethylamino)benzoic acid (1.04 g, 6.27 mmol) and DMF (1 drop) in DCM (10 mL) was added dropwise oxalyl chloride (0.64 mL, 7.3 mmol, 1.2 eq.) and the mixture was left to stir at rt for 2 h. The reaction mixture was then concentrated and DCM (5 mL) was added, followed by dropwise addition of potassium *tert*-butoxide (10 mL, 10 mmol, 1.6 eq., 1 M in THF). The mixture was left to stir for 2 h at rt before addition of water (50 mL), aqueous sodium hydroxide (2 mL, 5 M) and DCM (50 mL). The organic layer was separated and passed through a plug of silica, which was then flushed with ethyl acetate (50 mL). The combined organic layers were concentrated to afford the product as a pale orange solid (1.34 g, 6.04 mmol, 96%).

M. pt.: 56.1 – 59.0 °C;

ν_{max} (neat): 2977, 1687, 1600, 1386, 1290, 771 cm^{-1};

^{1}H NMR (400 MHz, DMSO-d_6): δ 7.86 (d, 2H, *J* = 9.0 Hz, 2 x C(O)CCH), 6.64 (d, 2H, *J* = 9.0 Hz, 2 x NCCH), 3.02 (s, 6H, $N(CH_3)_2$), 1.57 (s, 9H, $OC(CH_3)_3$);

^{13}C NMR (400 MHz, DMSO-d_6): δ 166.5, 153.2, 131.1, 119.2, 110.8, 79.8, 40.2, 28.5;

LCMS: t_R: 1.31 min, $[MH]^+$ 222.1;

HRMS: ($C_{13}H_{19}NO_2$) $[MH]^+$ requires 222.1494, found $[MH]^+$ 222.1495.

(*R*)-2-((4-(((3,4-dihydro-2*H*-pyrano[2,3-*c*]pyridin-6-yl)methyl)amino)piperidin-1-yl)methyl)-1,2-dihydro-3*H*,8*H*-2*a*,5,8*a*-triazaacenaphthylene-3,8-dione (2.77)

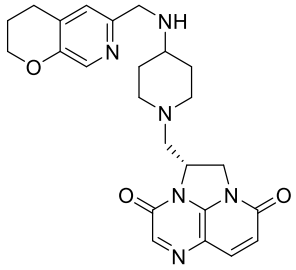

Oxidation

(3,4-dihydro-2*H*-pyrano[2,3-*c*]pyridin-6-yl)methanol hydrochloride (**2.50·HCl**) (1.00 g, 4.96 mmol, 1.0 eq.) was suspended in DCM (1.5 mL) and cooled to 0 °C. DMSO (0.74 mL, 10.4 mmol, 2.1 eq.) was added in a dropwise manner, followed by dropwise addition of triethylamine (2.9 mL, 20.8 mmol, 4.2 eq.). Sulfur trioxide pyridine complex (1.67 g, 10.5 mmol, 2.1 eq.) was added portionwise. The reaction mixture was warmed to 5 °C and left to stir at this temperature overnight. Additional sulfur trioxide pyridine complex was added (0.53 g, 3.3 mmol, 0.7 eq.) and the mixture was left to stir at 5 °C for an additional 4 days. The reaction mixture was warmed to rt and was quenched by addition of saturated aqueous sodium bicarbonate solution (20 mL). The organic layer was separated and the aqueous layer was further extracted with DCM (2 x 20 mL). The combined organic layers were washed with a solution of 5% aqueous citric acid solution (20 mL) to afford the crude aldehyde as a solution in DCM which was telescoped onto the subsequent stage without further purification.

Reductive amination

This transformation was performed according to a detailed process description developed at GSK. The aldehyde (**2.75**) was mixed with (*R*)-2-((4-aminopiperidin-1-yl)methyl)-1,2-dihydro-3*H*,8*H*-2*a*,5,8*a*-triazaacenaphthylene-3,8-dione bis-hydrochloride monohydrate (**2.76·2HCl·H_2O**) (1.43 g, 3.62 mmol, 0.73 eq. 76.3% active) in solvent and treated with sodium triacetoxyborohydride (1.30 g, 6.13 mmol, 1.2 eq.). Following the work-up and isolation procedure, the product was isolated as a pale yellow powder (987 mg, 2.20 mmol, 44%).

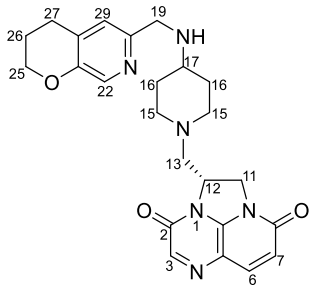

^{1}H NMR (400 MHz, $CDCl_3$): δ 8.08 (s, 1H, H22), 7.82 (s, 1H, H3), 7.76 (d, 1H, *J* = 9.5 Hz, H6), 6.95 (s, 1H, H29), 6.38 (d, 1H, *J* = 9.5 Hz, H7), 5.07 – 4.98 (m, 1H, H12), 4.55 (dd, 1H, *J* = 12.5, 5.5 Hz, H11), 4.37 (dd, 1H, *J* = 12.5, 9.5 Hz, H11), 4.22 – 4.18 (m, 2H, H25), 3.77 (s, 2H, H19), 3.12 (dd, 1H, *J* = 13.0, 3.5 Hz, H13), 2.96 – 289 (m, 1H, H15), 2.75 (t, 2H, *J* = 6.5 Hz, H27), 2.72 (dd, 1H, *J* = 13.0, 4.5 Hz, H13), 2.69 – 2.62 (m, 1H, H15), 2.55 – 2.46 (m, 1H, H17), 2.33 (td, 1H, *J* = 11.5, 2.5 Hz, H15), 2.25 (td, 1H, *J* = 11.5, 2.5 Hz, H15), 2.05 – 1.97 (m, 2H, H26), 1.91 – 1.77 (m, 2H, H16), 1.42 – 1.28 (m, 2H, H16)

^{13}C NMR (101 MHz, $CDCl_3$): δ 159.8, 153.9, 150.9, 143.0, 139.5, 139.1, 138.8, 131.1, 122.8, 116.4, 114.5, 66.7, 57.4, 54.4, 54.3, 52.8, 51.9, 48.4, 32.9, 32.8, 24.4, 21.8.

Analytical data consistent with that previously reported.[177]

Ethyl (*E*)-3-(5-(hydroxymethyl)pyridin-2-yl)acrylate (2.80)

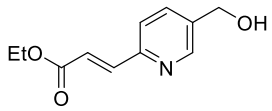

***O*-Acylation**

(6-Methylpyridin-3-yl)methanol (**2.46**) (50 g, 0.41 mol, 1.0 eq.) and toluene (300 mL) were added to a 1 L laboratory reactor equipped with an overhead stirrer under an atmosphere of nitrogen until a yellow solution was obtained. To this solution was added acetic anhydride (54 mL, 0.57 mol, 1.4 eq.), and the reaction mixture was heated to 80 °C. The reaction was left to stir at this temperature for 7 h, before being left to cool slowly to rt. HPLC analysis indicated full consumption of the starting material. The reaction was quenched by addition of water (400 mL), followed by slow addition of solid sodium bicarbonate (70 g), until the pH of the aqueous layer was ~7. Toluene (150 mL) was added, and the organic layer was separated. The aqueous layer was then extracted with toluene (2 x 150 mL) and the combined organic layers were concentrated under reduced pressure to a total volume of 100 mL (2 vols) to afford the crude *O*-acyl product as a solution in toluene which was telescoped to the next stage.

Condensation

Acetic anhydride (164 mL, 1.74 mol, 4.2 eq.) and anhydrous zinc chloride (5.4 g, 39 mmol, 0.1 eq.) were added to the toluene solution, and the temperature was adjusted to 105 °C. Ethyl glyoxylate (240 mL, 1.16 mol, 2.8 eq., 50% solution in toluene) was added dropwise over 6 h and left to stir overnight before being cooled to rt. HPLC analysis indicated 5 %area remaining starting material. Water (300 mL) was added, and the pH was adjusted to ~8 by addition of aqueous sodium hydroxide (5 M) and sodium bicarbonate. Ethyl acetate (150 mL) was added and the organic layer was separated. The aqueous layer was extracted with ethyl acetate (2 x 150 mL) and the combined organic layers were passed through a pad of silica, then concentrated under reduced pressure. KF analysis indicated 0.14 %w/w water. The crude *α*,*β*-unsaturated ester residue was telescoped through to the next stage.

Deprotection

To the crude *α*,*β*-unsaturated ester (**2.79**) was added hydrochloric acid (250 mL, 1.25 M in ethanol) and the temperature adjusted to 50-55 °C and left to stir overnight before being

cooled to rt. HPLC analysis indicated ~1 %area residual starting material. Aqueous hydrochloric acid (100 mL, 1 M) and DCM (300 mL) were added. The organic layer was separated, and the aqueous layer was further extracted with DCM (2 x 300 mL). The combined organic layers were discarded. The pH of the aqueous layer was adjusted to ~9 by addition of aqueous sodium hydroxide (5 M). TBME (300 mL) was added and the organic layer was separated. The aqueous layer was further extracted with TBME (2 x 150 mL), and the combined organic layers were filtered and concentrated. Toluene (50 mL) was added, and the solvent was removed under reduced pressure. The crude product residue was telescoped through to the next stage.

Recrystallisation

Toluene (150 mL) was added and the temperature was adjusted to 55 °C and stirred until all solids dissolved. The solution was cooled at a rate of 10 °C/h until the temperature reached 2 °C. The precipitate was collected by filtration, and the cake was washed with cold toluene (200 mL) and dried in a vacuum oven overnight at 50 °C to afford the product as a beige powder (7.5 g, 36 mmol, 9%).

^{1}H NMR (400 MHz, $CDCl_3$): δ 8.62 (d, 1H, *J* = 2.0 Hz, NCH), 7.74 (dd, 1H, *J* = 8.0, 2.0 Hz, NCHCC*H*), 7.68 (d, 1H, *J* = 16.0 Hz, C(O)CHC*H*), 7.43 (d, 1H, *J* = 8.0 Hz, NCCH), 6.90 (d, 1H, *J* = 16.0 Hz, C(O)CH), 4.77 (d, 2H, *J* = 5.0 Hz, CH_2OH), 4.27 (q, 2H, *J* = 7.0 Hz, CH_2CH$_3$), 1.93 (t, 1H, *J* = 5.0 Hz, OH), 1.34 (t, 3H, *J* = 7.0 Hz, CH_3);

^{13}C NMR (101 MHz, $CDCl_3$): δ 166.9, 152.6, 149.1, 143.1, 136.9, 135.5, 124.0, 122.6, 62.7, 60.8, 14.4.

Analytical data consistent with that previously reported.[168]

Methyl (*S*)-2-(6-bromo-5-(4-chlorophenyl)-7-methoxy-2-oxo-2,3-dihydro-1*H*-benzo[*e*][1,4]diazepin-3-yl)acetate (4.2) and **Methyl (*S*)-2-(6-acetoxy-5-(4-chlorophenyl)-7-methoxy-2-oxo-2,3-dihydro-1*H*-benzo[*e*][1,4]diazepin-3-yl)acetate (4.3)**

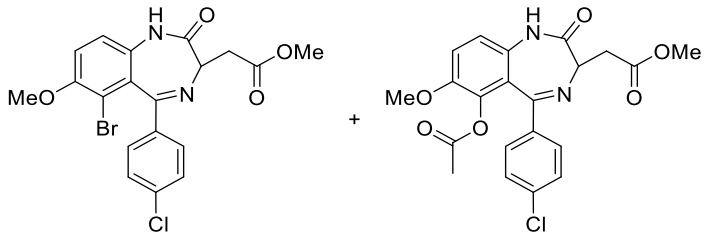

Methyl (*S*)-2-(5-(4-chlorophenyl)-7-methoxy-2-oxo-2,3-dihydro-1*H*-benzo[*e*][1,4]diazepin-3-yl)acetate (**4.1**) (299 mg, 0.802 mmol, 1.0 eq.) and *N*-bromo succinimide (157 mg, 0.882 mmol, 1.1 eq.) were stirred in acetonitrile (25 mL) and acetic acid (25 mL) at rt in the dark for 10 days. The mixture was then diluted with water (50 mL) and extracted with DCM (50 mL). The organic layer was concentrated under reduced pressure and the residue was purified by MDAP.

Methyl (*S*)-2-(6-bromo-5-(4-chlorophenyl)-7-methoxy-2-oxo-2,3-dihydro-1*H*-benzo[*e*][1,4]diazepin-3-yl)acetate (**4.2**) was obtained as a brown solid (17 mg, 0.038 mmol, 4%).

M. pt.: decomposes >102 °C;

$\boldsymbol{\nu}_{\mathbf{max}}$ (neat): 2950, 1682, 1475, 1277, 812 cm^{-1};

^{1}H NMR (400 MHz, DMSO-d_6): δ 10.57 (s, 1H, NH), 7.46 – 7.42 (m, 3H, 3 x ArH) 7.36 – 7.31 (m, 3H, 3 x ArH), 4.08 – 4.01 (m, 1H, NCH), 3.89 (s, 3H, CH_3), 3.60 (s, 3H, CH_3), 3.19 (dd, 1H, *J* = 16.5, 7.5 Hz, NCHCH_2), 3.05 (dd, 1H, *J* = 16.5, 6.5 Hz, NCHCH_2);

^{13}C NMR (400 MHz, DMSO-d_6): δ 171.3, 170.5, 165.5, 152.2, 137.2, 134.7, 133.7, 129.5, 128.5, 127.5, 121.7, 115.9, 110.3, 60.6, 56.8, 51.3, 35.4;

HRMS: ($C_{19}H_{17}{}^{79}Br^{35}ClN_2O_4$) $[MH]^+$ requires 451.0055, found $[MH]^+$ 451.0057.

Methyl (*S*)-2-(6-acetoxy-5-(4-chlorophenyl)-7-methoxy-2-oxo-2,3-dihydro-1*H*-benzo[*e*][1,4]diazepin-3-yl)acetate (**4.3**) was obtained as a brown solid (10 mg, 0.023 mmol, 3%).

M. pt.: decomposes > 70 °C;

ν_{max} (neat): 2951, 1769, 1732, 1682, 1486, 1168, 1052, 733 cm^{-1};

^{1}H NMR (400 MHz, DMSO-d_6): δ 10.56 (s, 1H, NH), 7.49 (d, 1H, *J* = 9.0 Hz, ArH) 7.45 (d, 2H, *J* = 8.5 Hz, 2 x ArH), 7.32 (d, 2H, *J* = 8.5 Hz, 2 x ArH), 7.20 (d, 1H, *J* = 9.0 Hz, ArH) 3.97 (dd, 1H, *J* = 8.0, 6.0 Hz, NCH), 3.80 (s, 3H, CH_3), 3.60 (s, 3H, CH_3) 3.20 (dd, 1H, *J* = 16.5, 8.0 Hz, NCHCH_2), 2.99 (dd, 1H, *J* = 16.5, 8.0 Hz, NCHCH_2), 1.62 (s, 3H, $CH_3C(O)$);

^{13}C NMR (101 MHz, DMSO-d_6): δ 171.3, 170.1, 166.7, 163.7, 147.2, 137.4, 135.9, 134.7, 132.4, 129.4, 128.2, 121.1, 119.4, 116.9, 60.4, 56.3, 51.3, 35.7, 19.5;

HRMS: ($C_{21}H_{20}{}^{35}ClN_2O_6$) $[MH]^+$ requires 431.1004, found $[MH]^+$ 431.1005.

Methyl (*E*)-2-bromo-2-(5-(4-chlorophenyl)-7-methoxy-2-oxo-1,2-dihydro-3*H*-benzo[*e*][1,4]diazepin-3-ylidene)acetate and **methyl (*Z*)-2-bromo-2-(5-(4-chlorophenyl)-7-methoxy-2-oxo-1,2-dihydro-3*H*-benzo[*e*][1,4]diazepin-3-ylidene)acetate (4.4 & 4.5)**

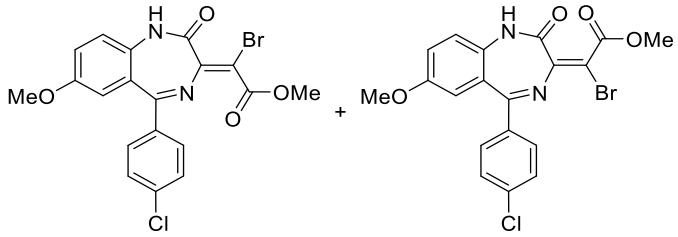

Methyl (*S*)-2-(5-(4-chlorophenyl)-7-methoxy-2-oxo-2,3-dihydro-1*H*-benzo[*e*][1,4]diazepin-3-yl)acetate (**4.1**) (311 mg, 0.834 mmol, 1.0 eq.) and N-bromosuccinimide (159 mg, 0.893 mmol, 1.1 eq.) were taken up into acetonitrile (400 mL). 150 mL of the resulting clear solution was placed in a PHIL Pacer and was irradiated at 385 nm, 300 mA for 2 h. The resulting solution was concentrated under reduced pressure to give an orange foam which was purified by MDAP to afford the title compounds.

Isomer 1 was isolated as a yellow solid (10 mg, 0.022 mmol, 3%).

M. pt.: decomposes >108 °C;

ν_{max} (neat): 1678, 1589, 1258, 837, 730 cm^{-1};

^{1}H NMR (400 MHz, DMSO-d_6): δ 11.17 (s, 1H, NH), 7.73 (d, 2H, *J* = 8.5 Hz, 2 x ArH), 7.61 (d, 2H, *J* = 8.5 Hz, 2 x ArH), 7.31 – 7.23 (m, 2H, 2 x ArH), 6.73 (d, 1H, *J* = 2.5 Hz, ArH), 3.73 (s, 3H, CH_3), 3.70 (s, 3H, CH_3);

^{13}C NMR (400 MHz, DMSO-d_6): δ 164.0, 163.3, 161.9, 154.7, 152.5, 136.7, 135.5, 131.9, 131.0, 128.8, 127.1, 123.6, 119.4, 114.0, 93.1, 55.6, 53.3;

HRMS: ($C_{19}H_{15}{}^{79}Br^{35}ClN_2O_4$) $[MH]^+$ requires 448.9898, found $[MH]^+$ 448.9896.

Isomer 2 was isolated as a yellow solid (39 mg, 0.087 mmol, 10%).

M. pt.: decomposes >230 °C;

ν_{max} (neat): 1714, 1667, 1266, 1045, 832, 552 cm^{-1};

^{1}H NMR (400 MHz, DMSO-d_6): δ 11.10 (s, 1H, NH), 7.75 (d, 2H, *J* = 8.5 Hz, 2 x ArH), 7.63 (d, 2H, *J* = 8.5 Hz, 2 x ArH), 7.29 – 7.21 (m, 2H, 2 x ArH), 6.78 – 6.74 (m, 1H, ArH), 3.70 (s, 3H, CH_3), 3.69 (s, 3H, CH_3);

^{13}C NMR (400 MHz, DMSO-d_6): δ 165.5, 163.4, 162.2, 154.5, 153.4, 136.9, 135.3, 132.0, 131.8, 128.8, 126.5, 123.8, 119.7, 113.9, 99.5, 55.6, 53.2;

HRMS: ($C_{19}H_{15}{}^{79}Br^{35}ClN_2O_4$) $[MH]^+$ requires 448.9898, found $[MH]^+$ 448.9900.

N.B. Attempts to assign the alkene geometry using nOe experiments were inconclusive.

Ethyl 4-(bromomethyl)benzoate (4.9)

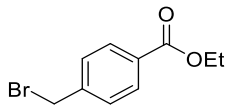

A homogeneous, clear feed solution was prepared by stirring ethyl 4-methylbenzoate (**4.8**) (64.6 g, 393 mmol, 1.0 eq.), *N*-bromo succinimide (73.9 g, 415 mmol, 1.05 eq.) and acetonitrile (576 mL). The solution was pumped at a rate of 8.0 mL/min (residence time: 0.5 min) through a glass plate flow reactor (internal volume: 4.1 mL) whilst being irradiated with an array of 48 LEDs (405 nm, 300 mA). The resulting yellow solution was diluted with water (1100 mL) and extracted with heptane (1000 mL, then 500 mL). The combined organic layers were then concentrated to ~300 mL (5 vols) under reduced pressure. The solution was cooled to 20 °C, then seeded and cooled to 0 °C on a linear gradient over 3 h. The resulting solids were collected by filtration and washed with additional cold heptane (200 mL) before being dried under reduced pressure at rt overnight to afford the product as a white crystalline powder (60.3 g). The collected solid contained 91 %area product (54 g, 223 mmol, 57%) by HPLC and 9 %area of the dibrominated side-product.

^{1}H NMR (400 MHz, $CDCl_3$): δ 8.02 (d, 2H, *J* = 8.5, 2 x ArH), 7.46 (d, 2H, *J* = 8.5 Hz, 2 x ArH), 4.50 (s, 2H, CH_2Br), 4.38 (q, 2H, *J* = 7.0 Hz, OCH_2), 1.39 (t, 3H, *J* = 7.0 Hz, OCH_2CH_3);

^{13}C NMR (101 MHz, $CDCl_3$): δ 166.1, 142.6, 130.6, 130.1, 129.1, 61.2, 32.4, 14.4.

Analytical data consistent with that previously reported.[210]

Ethyl 4-(dibromomethyl)benzoate (4.10)

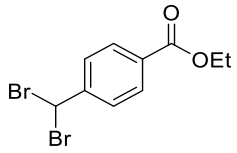

^{1}H NMR (400 MHz, $CDCl_3$): δ 8.05 (d, 2H, *J* = 8.5 Hz, 2 x ArH), 7.63 (d, 2H, *J* = 8.5 Hz, 2 x ArH), 6.66 (s, 1H, CH), 4.39 (q, 2H, *J* = 7.0 Hz, CH_2);

^{13}C NMR (101 MHz, DMSO-d_6): δ 165.6, 146.0, 131.8, 130.0, 126.7, 61.3, 39.9.

Analytical data consistent with that previously reported.[232]

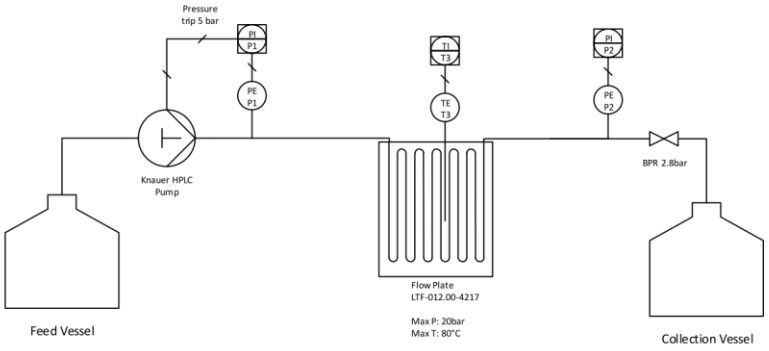

Figure 76 *Engineering line diagram of flow system used. The flow plate is located above the LED array and photoreactor housing.*

REFERENCES

1. Magano, J.; Dunetz, J. R., Large-Scale Carbonyl Reductions in the Pharmaceutical Industry, *Org. Process Res. Dev.* **2012,** *16*, 1156-1184.
2. Nicolaou, K. C.; Yang, Z.; Liu, J. J.; Ueno, H.; Nantermet, P. G.; Guy, R. K.; Claiborne, C. F.; Renaud, J.; Couladouros, E. A.; Paulvannan, K.; Sorensen, E. J., Total synthesis of taxol, *Nature* **1994,** *367*, 630-634.
3. Lennon, I., *presentation at the 6th Winter Process Chemistry Conference* **2019**.
4. Hughes, D. L., Review of Synthetic Routes and Final Forms of Integrase Inhibitors Dolutegravir, Cabotegravir, and Bictegravir, *Org. Process Res. Dev.* **2019,** *23*, 716-729.
5. Gaich, T.; Baran, P. S., Aiming for the ideal synthesis, *J. Org. Chem.* **2010,** *75*, 4657-4673.
6. Richter, J. M.; Ishihara, Y.; Masuda, T.; Whitefield, B. W.; Llamas, T.; Pohjakallio, A.; Baran, P. S., Enantiospecific total synthesis of the hapalindoles, fischerindoles, and welwitindolinones via a redox economic approach, *J. Am. Chem. Soc.* **2008,** *130*, 17938-17954.
7. Saudan, L. A., Hydrogenation processes in the synthesis of perfumery ingredients, *Acc. Chem. Res.* **2007,** *40*, 1309-1319.
8. Fairweather, N. T.; Gibson, M. S.; Guan, H., Homogeneous Hydrogenation of Fatty Acid Methyl Esters and Natural Oils under Neat Conditions, *Organometallics* **2015,** *34*, 335-339.
9. Lipton, M. F.; Barrett, A. G. M., Introduction: Process Chemistry, *Chem. Rev.* **2006,** *106*, 2581-2582.
10. Caron, S.; Dugger, R. W.; Ruggeri, S. G.; Ragan, J. A.; Ripin, D. H., Large-scale oxidations in the pharmaceutical industry, *Chem. Rev.* **2006,** *106*, 2943-2989.
11. Omura, K.; Swern, D., Oxidation of alcohols by “activated” dimethyl sulfoxide. a preparative, steric and mechanistic study, *Tetrahedron* **1978,** *34*, 1651-1660.
12. Hartmann, C.; Meyer, V., Ueber Jodobenzoësäure, *Ber. Dtsch. Chem. Ges.* **1893,** *26*, 1727-1732.
13. Dess, D. B.; Martin, J. C., Readily accessible 12-I-5 oxidant for the conversion of primary and secondary alcohols to aldehydes and ketones, *J. Org. Chem.* **1983,** *48*, 4155-4156.
14. Anelli, P. L.; Montanari, F.; Quici, S., A General Synthetic Method for the Oxidation of Primary Alcohols to Aldehydes:(S) - (+) - 2 - Methylbutanal, *Org. Synth.* **1990,** *69*, 212-212.

15. Bouveault, L.; Blanc, G., Transforming saturated monobasic acids into the corresponding primary alcohols, *Bull. Soc. Chim. Fr.* **1904,** *31*, 666-672.
16. Bouveault, L.; Blanc, G., Preparation of primary alcohols by means of the corresponding acids, *Compt. Rend.* **1903,** *137*, 60-62.
17. Bouveault, L.; Blanc, G., Hydrogenation of the ether of the acids furthermore possessing the ether-oxide or acetal functions, *Bull. Soc. Chim. Fr.* **1904,** *31*, 1210-1213.
18. Bouveault, L.; Blanc, G., More Dissolving metal reductions, *Compt. Rend.* **1903,** *136*, 1676-1678.
19. Wang, Z., Bouveault-Blanc Reduction. In *Comprehensive Organic Name Reactions and Reagents*, **2010**; pp 493-496.
20. Niemann, C.; Redemann, C. T., The Reduction of Ethyl a-Benzylamino-β-methoxy-n-caproate with Sodium and Butyl Alcohol, *J. Am. Chem. Soc.* **1946,** *68*, 1932-1934.
21. Cossy, J.; Gille, B.; Bellosta, V., Facile Synthesis of Spirocyclic Systems through the Intramolecular Addition of Ketyl Radicals via the Sodium/Ammonia Reduction of δ,ε-Unsaturated Carboxylic Esters, *J. Org. Chem.* **1998,** *63*, 3141-3146.
22. Bodnar, B. S.; Vogt, P. F., An Improved Bouveault−Blanc Ester Reduction with Stabilized Alkali Metals, *J. Org. Chem.* **2009,** *74*, 2598-2600.
23. An, J.; Work, D. N.; Kenyon, C.; Procter, D. J., Evaluating a sodium dispersion reagent for the Bouveault-Blanc reduction of esters, *J. Org. Chem.* **2014,** *79*, 6743-6747.
24. Glattfeld, J. W. E.; Mochel, W. E., The Preparation of dl-α,β-Diacetoxyisobutyric Aldehyde1, *J. Am. Chem. Soc.* **1938,** *60*, 1011-1014.
25. Kaiser, E. M.; Benkeser, R. A., Δ9,10-Octalin, *Org. Synth.* **1970,** *50*, 88.
26. Birch, A. J., The Birch reduction in organic synthesis, *Pure Appl. Chem.* **1996,** *68*, 553-556.
27. Clayden, J.; Greeves, N.; Warren, S., *Organic Chemistry*. Oxford University Press: **2012**.
28. Walker, E. R. H., The functional group selectivity of complex hydride reducing agents, *Chem. Soc. Rev.* **1976,** *5*, 23-50.
29. Winterfeldt, E., Applications of Diisobutylaluminium Hydride (DIBAH) and Triisobutylaluminium (TIBA) as Reducing Agents in Organic Synthesis, *Synth.* **1975,** *1975*, 617-630.
30. Guo, J.; Erickson, G. A.; Fitzgerald, R. N.; Matsuoka, R. T.; Rafferty, S. W.; Sharp, M. J.; Sickles, B. R.; Wisowaty, J. C., An efficient synthesis of a potent PPARpan agonist, *J. Org. Chem.* **2006,** *71*, 8302-8305.

31. Rozema, M. J.; Kruger, A. W.; Rohde, B. D.; Shelat, B.; Bhagavatula, L.; Tien, J. J.; Zhang, W.; Henry, R. F., Synthesis of a novel farnesyl transferase inhibitor, ABT-100; selective preparation of a stereogenic tertiary carbinol, *Tetrahedron* **2005,** *61*, 4419-4425.
32. Fujino, K.; Takami, H.; Atsumi, T.; Ogasa, T.; Mohri, S.-i.; Kasai, M., Development of a Practical Synthetic Route of a PDE V Inhibitor KF31327, *Org. Process Res. Dev.* **2001,** *5*, 426-433.
33. Abe, T.; Haga, T.; Negi, S.; Morita, Y.; Takayanagi, K.; Hamamura, K., Large scale synthesis of N-benzyl-4-formylpiperidine through partial reduction of esters using aluminum hydride reagents modified with pyrrolidine, *Tetrahedron* **2001,** *57*, 2701-2710.
34. Trost, B. M., Atom Economy—A Challenge for Organic Synthesis: Homogeneous Catalysis Leads the Way, *Angew. Chem. Int. Ed.* **1995,** *34*, 259-281.
35. Gugelchuk, M.; Silva, L. F.; Vasconcelos, R. S.; Quintiliano, S. A. P., Sodium Bis(2-methoxyethoxy)aluminum Hydride. In *Encyclopedia of Reagents for Organic Synthesis*, John Wiley & Sons, Ltd: **2007**.
36. Jimenez-Gonzalez, C.; Ponder, C. S.; Broxterman, Q. B.; Manley, J. B., Using the Right Green Yardstick: Why Process Mass Intensity Is Used in the Pharmaceutical Industry To Drive More Sustainable Processes, *Org. Process Res. Dev.* **2011,** *15*, 912-917.
37. Smith, A. M.; Whyman, R., Review of methods for the catalytic hydrogenation of carboxamides, *Chem. Rev.* **2014,** *114*, 5477-5510.
38. Berk, S. C.; Kreutzer, K. A.; Buchwald, S. L., A catalytic method for the reduction of esters to alcohols, *J. Am. Chem. Soc.* **1991,** *113*, 5093-5095.
39. Mimoun, H., Selective Reduction of Carbonyl Compounds by Polymethylhydrosiloxane in the Presence of Metal Hydride Catalysts, *J. Org. Chem.* **1999,** *64*, 2582-2589.
40. Adkins, H., Catalytic Hydrogenation of Esters to Alcohols. In *Org. React.*, **2011**; pp 1-27.
41. Adkins, H.; Connor, R., The Catalytic Hydrogenation of Organic Compounds over Copper Chromite, *J. Am. Chem. Soc.* **1931,** *53*, 1091-1095.
42. Depré, D.; Horváth, A.; Snissaert, W.; Bergh, L. V. D.; Dermaut, W., Implementation on Pilot-Plant Scale of the Titanocene-Catalyzed Reduction of a Lactone with Poly(methylhydrosiloxane), *Org. Process Res. Dev.* **2008,** *12*, 96-100.
43. Holladay, J. D.; Hu, J.; King, D. L.; Wang, Y., An overview of hydrogen production technologies, *Catal. Today* **2009,** *139*, 244-260.
44. Brunner, H., Hydrogenation. In *Applied Homogeneous Catalysis with Organometallic Compounds*, **1996**.

45. Ikariya, T.; Kayaki, Y., Hydrogenation of carboxylic acid derivatives with bifunctional ruthenium catalysts, *Pure Appl. Chem.* **2014,** *86*, 933-943.
46. Blanksby, S. J.; Ellison, G. B., Bond dissociation energies of organic molecules, *Acc. Chem. Res.* **2003,** *36*, 255-263.
47. Kubas, G. J., Fundamentals of H2 binding and reactivity on transition metals underlying hydrogenase function and H2 production and storage, *Chem. Rev.* **2007,** *107*, 4152-4205.
48. Stephan, D. W.; Erker, G., Frustrated Lewis pairs: metal-free hydrogen activation and more, *Angew. Chem. Int. Ed.* **2010,** *49*, 46-76.
49. Wilde, M. P. von, *Ber.* **1874,** *7*, 352-57.
50. Sabatier, P.; Senderens, J.-B., *C. R. Acad. Sci. Paris* **1897,** *124*, 1358.
51. Sabatier, P.; Senderens, J.-B., *C. R. Acad. Sci. Paris* **1901,** *132*, 210.
52. Mattson, B.; Foster, W.; Greimann, J.; Hoette, T.; Le, N.; Mirich, A.; Wankum, S.; Cabri, A.; Reichenbacher, C.; Schwanke, E., Heterogeneous Catalysis: The Horiuti–Polanyi Mechanism and Alkene Hydrogenation, *J. Chem. Educ.* **2013,** *90*, 613-619.
53. Alonso, L.; Fraga, M. J.; Juárez, M., Determination of trans

fatty acids and fatty acid profiles in margarines marketed in spain, *J. Am. Oil Chem. Soc.* **2000,** *77*, 131-136.
54. Oppenheim, J. P.; Dickerson, G. L., Adipic Acid. In *Kirk-Othmer Encyclopedia of Chemical Technology*, **2014**; pp 1-27.
55. Mitsui, T.; Rose, M. K.; Fomin, E.; Ogletree, D. F.; Salmeron, M., Dissociative hydrogen adsorption on palladium requires aggregates of three or more vacancies, *Nature* **2003,** *422*, 705-707.
56. Horiuti, I.; Polanyi, M., Exchange reactions of hydrogen on metallic catalysts, *Trans. Faraday Soc.* **1934,** *30*.
57. Lazier, W. A. Catalytic hydrogenation process, US1964000A, **1934**.
58. Giersch, W. K.; Ohloff, G., US 1989/4818747, **1989**.
59. Kreutzer, U. R., Manufacture of fatty alcohols based on natural fats and oils, *J. Am. Oil Chem. Soc.* **1984,** *61*, 343-348.
60. Pritchard, J.; Filonenko, G. A.; van Putten, R.; Hensen, E. J. M.; Pidko, E. A., Heterogeneous and homogeneous catalysis for the hydrogenation of carboxylic acid derivatives: history, advances and future directions, *Chem. Soc. Rev.* **2015,** *44*, 3808-3833.

61. Hattori, Y.; Yamamoto, K.; Kaita, J.; Matsuda, M.; Yamada, S., The development of nonchromium catalyst for fatty alcohol production, *J. Am. Oil Chem. Soc.* **2000,** *77*, 1283-1288.
62. Sauer, J.; Adkins, H., The Selective Hydrogenation of Unsaturated Esters to Unsaturated Alcohols, *J. Am. Chem. Soc.* **1937,** *59*, 1-3.
63. Tahara, K.; Nagahara, E.; Itoi, Y.; Nishiyama, S.; Tsuruya, S.; Masai, M., Liquid phase hydrogenation of carboxylic acid catalyzed by supported bimetallic Ru-Sn-alumina catalyst: effects of tin compounds in impregnation method, *J. Mol. Catal. A: Chem.* **1996,** *110*, L5-L6.
64. Halpern, J.; Harrod, J. F.; James, B. R., Homogeneous Catalytic Hydrogenation of Olefinic Compounds, *J. Am. Chem. Soc.* **1961,** *83*, 753-754.
65. Young, J.; Osborn, J.; Jardine, F.; Wilkinson, G., Hydride intermediates in homogeneous hydrogenation reactions of olefins and acetylenes using rhodium catalysts, *Chem. Commun.* **1965**, 131-132.
66. Noyori, R., Asymmetric Catalysis: Science and Opportunities (Nobel Lecture 2001), *Adv. Synth. Catal.* **2003,** *345*, 15-32.
67. Zanotti-Gerosa, A.; Hems, W.; Groarke, M.; Hancock, F., Ruthenium-Catalysed Asymmetric Reduction of Ketones, *Platinum Metals Rev.* **2005,** *49*, 158-165.
68. Blaser, H. U.; Pugin, B.; Spindler, F.; Saudan, L. A., Hydrogenation. In *Applied Homogeneous Catalysis with Organometallic Compounds*, **2017**; pp 621-690.
69. Grey, R. A.; Pez, G. P.; Wallo, A., Anionic metal hydride catalysts. 2. Application to the hydrogenation of ketones, aldehydes, carboxylic acid esters, and nitriles, *J. Am. Chem. Soc.* **1981,** *103*, 7536-7542.
70. Teunissen, H. T.; Elsevier, J. C., Homogeneous ruthenium catalyzed hydrogenation of esters to alcohols, *Chem. Commun.* **1998**, 1367-1368.
71. Colomer, I.; Chamberlain, A. E.; Haughey, M. B.; Donohoe, T. J., Hexafluoroisopropanol as a highly versatile solvent, *Nature Rev.Chem.* **2017,** *1*, 1-12.
72. Bakhmutov, V. I.; Bakhmutova, E. V.; Belkova, N. V.; Bianchini, C.; Epstein, L. M.; Masi, D.; Peruzzini, M.; Shubina, E. S.; Vorontsov, E. V.; Zanobini, F., In-depth NMR and IR study of the proton transfer equilibrium between [{(MeC(CH2PPh2)3}Ru(CO)H2] and hexafluoroisopropanol, *Can. J. Chem.* **2001,** *79*, 479-489.
73. vom Stein, T.; Meuresch, M.; Limper, D.; Schmitz, M.; Holscher, M.; Coetzee, J.; Cole-Hamilton, D. J.; Klankermayer, J.; Leitner, W., Highly versatile catalytic hydrogenation of

carboxylic and carbonic acid derivatives using a Ru-triphos complex: molecular control over selectivity and substrate scope, *J. Am. Chem. Soc.* **2014,** *136*, 13217-13225.

74. Westhues, S.; Idel, J.; Klankermayer, J., Molecular catalyst systems as key enablers for tailored polyesters and polycarbonate recycling concepts, *Sci. Adv.* **2018,** *4*, 1-8.
75. Wesselbaum, S.; Moha, V.; Meuresch, M.; Brosinski, S.; Thenert, K. M.; Kothe, J.; Stein, T. V.; Englert, U.; Holscher, M.; Klankermayer, J.; Leitner, W., Hydrogenation of carbon dioxide to methanol using a homogeneous ruthenium-Triphos catalyst: from mechanistic investigations to multiphase catalysis, *Chem. Sci.* **2015,** *6*, 693-704.
76. Pan, Y.; Luo, Z.; Xu, X.; Zhao, H.; Han, J.; Xu, L.; Fan, Q.; Xiao, J., Ru‐Catalyzed Deoxygenative Transfer Hydrogenation of Amides to Amines with Formic Acid/Triethylamine, *Adv. Synth. Catal.* **2019,** *361*, 3800-3806.
77. Cabrero-Antonino, J. R.; Alberico, E.; Drexler, H.-J.; Baumann, W.; Junge, K.; Junge, H.; Beller, M., Efficient Base-Free Hydrogenation of Amides to Alcohols and Amines Catalyzed by Well-Defined Pincer Imidazolyl–Ruthenium Complexes, *ACS Catal.* **2016,** *6*, 47-54.
78. Zhang, J.; Leitus, G.; Ben-David, Y.; Milstein, D., Facile conversion of alcohols into esters and dihydrogen catalyzed by new ruthenium complexes, *J. Am. Chem. Soc.* **2005,** *127*, 10840-10841.
79. Zhang, J.; Leitus, G.; Ben-David, Y.; Milstein, D., Efficient homogeneous catalytic hydrogenation of esters to alcohols, *Angew. Chem. Int. Ed.* **2006,** *45*, 1113-1115.
80. He, T.; Buttner, J. C.; Reynolds, E. F.; Pham, J.; Malek, J. C.; Keith, J. M.; Chianese, A. R., Dehydroalkylative Activation of CNN- and PNN-Pincer Ruthenium Catalysts for Ester Hydrogenation, *J. Am. Chem. Soc.* **2019,** *141*, 17404-17413.
81. Kar, S.; Rauch, M.; Kumar, A.; Leitus, G.; Ben-David, Y.; Milstein, D., Selective Room-Temperature Hydrogenation of Amides to Amines and Alcohols Catalyzed by a Ruthenium Pincer Complex and Mechanistic Insight, *ACS Catal.* **2020**, 5511-5515.
82. Gunanathan, C.; Milstein, D., Bond activation and catalysis by ruthenium pincer complexes, *Chem. Rev.* **2014,** *114*, 12024-12087.
83. Clarke, M. L., Recent developments in the homogeneous hydrogenation of carboxylic acid esters, *Catal. Sci. Technol.* **2012,** *2*, 2418-2423.
84. Dub, P. A.; Ikariya, T., Catalytic Reductive Transformations of Carboxylic and Carbonic Acid Derivatives Using Molecular Hydrogen, *ACS Catal.* **2012,** *2*, 1718-1741.

85. Werkmeister, S.; Junge, K.; Beller, M., Catalytic Hydrogenation of Carboxylic Acid Esters, Amides, and Nitriles with Homogeneous Catalysts, *Org. Process Res. Dev.* **2014,** *18*, 289-302.
86. Hey, D. A.; Reich, R. M.; Baratta, W.; Kühn, F. E., Current advances on ruthenium(II) N-heterocyclic carbenes in hydrogenation reactions, *Coord. Chem. Rev.* **2018,** *374*, 114-132.
87. Zhou, Y.; Khan, R.; Fan, B.; Xu, L., Ruthenium-Catalyzed Selective Reduction of Carboxylic Esters and Carboxamides, *Synth.* **2019,** *51*, 2491-2505.
88. Saudan, L.; Saudan, C. Hydrogenation of esters with Ru/bidentate ligands complexes, WO 2008/065588, **2008**.
89. Takebayashi, S.; Bergens, S. H., Facile Bifunctional Addition of Lactones and Esters at Low Temperatures. The First Intermediates in Lactone/Ester Hydrogenations, *Organometallics* **2009,** *28*, 2349-2351.
90. Carpenter, I.; Eckelmann, S. C.; Kuntz, M. T.; Fuentes, J. A.; France, M. B.; Clarke, M. L., Convenient and improved protocols for the hydrogenation of esters using Ru catalysts derived from (P,P), (P,N,N) and (P,N,O) ligands, *Dalton Trans.* **2012,** *41*, 10136-10140.
91. Kuriyama, W.; Ino, Y.; Ogata, O.; Sayo, N.; Saito, T., A Homogeneous Catalyst for Reduction of Optically Active Esters to the Corresponding Chiral Alcohols without Loss of Optical Purities, *Adv. Synth. Catal.* **2010,** *352*, 92-96.
92. Ino, Y.; Yoshida, A.; Kuriyama, W. Method for producing alcohols, EP 1 970 360, **2008**.
93. Saudan, L. A.; Saudan, C. M.; Debieux, C.; Wyss, P., Dihydrogen reduction of carboxylic esters to alcohols under the catalysis of homogeneous ruthenium complexes: high efficiency and unprecedented chemoselectivity, *Angew. Chem. Int. Ed.* **2007,** *46*, 7473-7476.
94. Geisser, R. W.; Goeke, A.; Schroeder, F. Process for the chemoselective reduction of terminally saturated carboxylic esters, WO 2013/171302, **2013**.
95. Sandoval, C. A.; Ohkuma, T.; Muniz, K.; Noyori, R., Mechanism of asymmetric hydrogenation of ketones catalyzed by BINAP/1,2-diamine-rutheniumII complexes, *J. Am. Chem. Soc.* **2003,** *125*, 13490-13503.
96. Kuriyama, W.; Ino, Y.; Ogata, O. Alcohol production method by reducing ester or lactone with hydrogen, EP 2 161 251, **2010**.
97. Kuriyama, W.; Matsumoto, T.; Ogata, O.; Ino, Y.; Aoki, K.; Tanaka, S.; Ishida, K.; Kobayashi, T.; Sayo, N.; Saito, T., Catalytic Hydrogenation of Esters. Development of an

Efficient Catalyst and Processes for Synthesising (R)-1,2-Propanediol and 2-(l-Menthoxy)ethanol, *Org. Process Res. Dev.* **2012,** *16*, 166-171.

98. Kuriyama, W.; Takaji, M.; Yasunori, I.; Ogata, O. Novel ruthenium carbonyl complexes having tridentate ligand, its production method and use, US 2011/237814, **2011**.
99. Ootsuka, T.; Imamura, M.; Ishii, A.; Ueda, K.; Mimura, S. α,α-Difluoroacetaldehyde product method, WO 2014/115801, **2014**.
100. Otsuka, T.; Ishii, A.; Dub, P. A.; Ikariya, T., Practical selective hydrogenation of alpha-fluorinated esters with bifunctional pincer-type ruthenium(II) catalysts leading to fluorinated alcohols or fluoral hemiacetals, *J. Am. Chem. Soc.* **2013,** *135*, 9600-9603.
101. Dub, P. A.; Gordon, J. C., The role of the metal-bound N–H functionality in Noyori-type molecular catalysts, *Nature Rev. Chem.* **2018,** *2*, 396-408.
102. Rammohan Rao, D.; Dwivedi, S. D.; Sreenivasulu, P.; Sahu, A.; Trinadhachari, G. N.; Sasi Kiran, S. An improved process for the preparation of Levofloxacin hemihydrate, WO 2006/048889, **2006**.
103. Derstine, B. P.; Tomlin, J. W.; Peck, C. L.; Dietz, J.-P.; Herrera, B. T.; Cardoso, F. S. P.; Paymode, D. J.; Yue, A. C.; Arduengo, A. J.; Opatz, T.; Snead, D. R.; Stringham, R. W.; McQuade, D. T.; Gupton, B. F., An Efficient Synthesis of Tenofovir (PMPA): A Key Intermediate Leading to Tenofovir-Based HIV Medicines, *Org. Process Res. Dev.* **2020,** *24*, 1420-1427.
104. Ogata, O.; Nakayama, Y.; Nara, H.; Fujiwhara, M.; Kayaki, Y., Atmospheric Hydrogenation of Esters Catalyzed by PNP-Ruthenium Complexes with an N-Heterocyclic Carbene Ligand, *Org. Lett.* **2016,** *18*, 3894-3897.
105. Fernandez-Puertas, E.; Robinson, A. J.; Robinson, H.; Sathiyalingam, S.; Stubbs, H.; Edwards, L. J., Evaluation and Screening of Spherical Pd/C for Use as a Catalyst in Pharmaceutical-Scale Continuous Hydrogenations, *Org. Process Res. Dev.* **2020,** *24*, 2147-2156.
106. Schörgenhumer, J.; Zimmermann, A.; Waser, M., SNS-Ligands for Ru-Catalyzed Homogeneous Hydrogenation and Dehydrogenation Reactions, *Org. Process Res. Dev.* **2018,** *22*, 862-870.
107. Kumar, A.; Espinosa-Jalapa, N. A.; Leitus, G.; Diskin-Posner, Y.; Avram, L.; Milstein, D., Direct Synthesis of Amides by Dehydrogenative Coupling of Amines with either Alcohols or Esters: Manganese Pincer Complex as Catalyst, *Angew. Chem. Int. Ed.* **2017,** *56*, 14992-14996.

108. Ogata, O.; Nara, H.; Matsumura, K.; Kayaki, Y., Formal Deoxygenative Hydrogenation of Lactams Using PN(H)P-Pincer Ruthenium Complexes under Nonacidic Conditions, *Org. Lett.* **2019,** *21*, 9954-9959.
109. Jankins, T. C.; Fayzullin, R. R.; Khaskin, E., Three-Component [1 + 1 + 1] Cyclopropanation with Ruthenium(II), *Organometallics* **2018,** *37*, 2609-2617.
110. Thiyagarajan, S.; Gunanathan, C., Catalytic Cross-Coupling of Secondary Alcohols, *J. Am. Chem. Soc.* **2019,** *141*, 3822-3827.
111. Ogata, O.; Nara, H.; Fujiwhara, M.; Matsumura, K.; Kayaki, Y., N-Monomethylation of Aromatic Amines with Methanol via PN(H)P-Pincer Ru Catalysts, *Org. Lett.* **2018,** *20*, 3866-3870.
112. Spasyuk, D.; Smith, S.; Gusev, D. G., Replacing phosphorus with sulfur for the efficient hydrogenation of esters, *Angew. Chem. Int. Ed.* **2013,** *52*, 2538-2542.
113. Bertoli, M.; Choualeb, A.; Lough, A. J.; Moore, B.; Spasyuk, D.; Gusev, D. G., Osmium and Ruthenium Catalysts for Dehydrogenation of Alcohols, *Organometallics* **2011,** *30*, 3479-3482.
114. Gusev, D. G., Dehydrogenative Coupling of Ethanol and Ester Hydrogenation Catalyzed by Pincer-Type YNP Complexes, *ACS Catal.* **2016,** *6*, 6967-6981.
115. Spasyuk, D.; Smith, S.; Gusev, D. G., From esters to alcohols and back with ruthenium and osmium catalysts, *Angew. Chem. Int. Ed.* **2012,** *51*, 2772-2775.
116. Spasyuk, D.; Vicent, C.; Gusev, D. G., Chemoselective hydrogenation of carbonyl compounds and acceptorless dehydrogenative coupling of alcohols, *J. Am. Chem. Soc.* **2015,** *137*, 3743-3746.
117. Goussev, D.; Spasyuk, D.; Smith, S. Catalysts based on amino-sulfide ligands for hydrogenation and dehydrogenation processes, US 2015/0202609, **2015**.
118. Zanotti-Gerosa, A.; Grainger, D.; Todd, L.; Grasa, G.; Milner, L.; Boddie, E.; Browne, L.; Egerton, I.; Wong, L., The coming of age of homogenous ester hydrogenation, *Catal. & Biocatal.* **2019,** *37*, 8-11.
119. Siesel, D. Processes for producing cycloalkylcarboxamido-pyridine benzoic acids, WO 2010/138484, **2010**.
120. Geisser, R. W.; Oetiker, J. D.; Schröder, F. Improvements in or relating to organic compounds, WO 2015/110515, **2015**.
121. Bevinakatti, H. S.; Newman, C. P.; Ellwood, S. Cyclic ethers, WO 2009/010791, **2009**.

122. Chakraborty, S.; Dai, H.; Bhattacharya, P.; Fairweather, N. T.; Gibson, M. S.; Krause, J. A.; Guan, H., Iron-based catalysts for the hydrogenation of esters to alcohols, *J. Am. Chem. Soc.* **2014,** *136*, 7869-7872.
123. Werkmeister, S.; Junge, K.; Wendt, B.; Alberico, E.; Jiao, H.; Baumann, W.; Junge, H.; Gallou, F.; Beller, M., Hydrogenation of esters to alcohols with a well-defined iron complex, *Angew. Chem. Int. Ed.* **2014,** *53*, 8722-8726.
124. Ludwig, J. R.; Schindler, C. S., Catalyst: Sustainable Catalysis, *Chem.* **2017,** *2*, 313-316.
125. ICH guideline Q3D on elemental impurities. European Medicines Agency, **2016**.
126. Risk list. British Geological Survey, **2015**.
127. Widegren, M. B.; Harkness, G. J.; Slawin, A. M. Z.; Cordes, D. B.; Clarke, M. L., A Highly Active Manganese Catalyst for Enantioselective Ketone and Ester Hydrogenation, *Angew. Chem. Int. Ed.* **2017,** *56*, 5825-5828.
128. Widegren, M. B.; Clarke, M. L., Manganese Catalyzed Hydrogenation of Enantiomerically Pure Esters, *Org. Lett.* **2018,** *20*, 2654-2658.
129. Junge, K.; Wendt, B.; Cingolani, A.; Spannenberg, A.; Wei, Z.; Jiao, H.; Beller, M., Cobalt Pincer Complexes for Catalytic Reduction of Carboxylic Acid Esters, *Chem. Eur. J.* **2018,** *24*, 1046-1052.
130. Mukherjee, A.; Milstein, D., Homogeneous Catalysis by Cobalt and Manganese Pincer Complexes, *ACS Catal.* **2018,** *8*, 11435-11469.
131. Dub, P. A.; Scott, B. L.; Gordon, J. C., Why Does Alkylation of the N-H Functionality within M/NH Bifunctional Noyori-Type Catalysts Lead to Turnover?, *J. Am. Chem. Soc.* **2017,** *139*, 1245-1260.
132. Dub, P. A.; Gordon, J. C., Metal–Ligand Bifunctional Catalysis: The "Accepted" Mechanism, the Issue of Concertedness, and the Function of the Ligand in Catalytic Cycles Involving Hydrogen Atoms, *ACS Catal.* **2017,** *7*, 6635-6655.
133. Dub, P. A.; Henson, N. J.; Martin, R. L.; Gordon, J. C., Unravelling the mechanism of the asymmetric hydrogenation of acetophenone by [RuX2(diphosphine)(1,2-diamine)] catalysts, *J. Am. Chem. Soc.* **2014,** *136*, 3505-3521.
134. Smith, N. E.; Bernskoetter, W. H.; Hazari, N., The Role of Proton Shuttles in the Reversible Activation of Hydrogen via Metal-Ligand Cooperation, *J. Am. Chem. Soc.* **2019,** *141*, 17350-17360.

135. Casey, C. P.; Johnson, J. B.; Singer, S. W.; Cui, Q., Hydrogen elimination from a hydroxycyclopentadienyl ruthenium(II) hydride: study of hydrogen activation in a ligand-metal bifunctional hydrogenation catalyst, *J. Am. Chem. Soc.* **2005,** *127*, 3100-3109.
136. Alberico, E.; Nielsen, M., Towards a methanol economy based on homogeneous catalysis: methanol to H2 and CO2 to methanol, *Chem. Commun.* **2015,** *51*, 6714-6725.
137. O'Brien, M.; Taylor, N.; Polyzos, A.; Baxendale, I. R.; Ley, S. V., Hydrogenation in flow: Homogeneous and heterogeneous catalysis using Teflon AF-2400 to effect gas–liquid contact at elevated pressure, *Chem. Sci.* **2011,** *2*.
138. Yap, S. K.; Yuan, Y.; Zheng, L.; Wong, W. K.; Yan, N.; Khan, S. A., Triphasic Segmented Flow Millireactors for Rapid Nanoparticle-Catalyzed Gas–Liquid Reactions — Hydrodynamic Studies and Reactor Modeling, *J. Flow Chem.* **2014,** *4*, 200-205.
139. Yap, S. K.; Yuan, Y.; Zheng, L.; Wong, W. K.; Zhang, J.; Yan, N.; Khan, S. A., Rapid nanoparticle-catalyzed hydrogenations in triphasic millireactors with facile catalyst recovery, *Green Chem.* **2014,** *16*, 4654-4658.
140. Khan, S. A.; Yap, S. K., US15/342686, **2015**.
141. Prieschl, M.; García-Lacuna, J.; Munday, R.; Leslie, K.; O'Kearney-McMullan, A.; Hone, C. A.; Kappe, C. O., Optimization and sustainability assessment of a continuous flow Ru-catalyzed ester hydrogenation for an important precursor of a β2-adrenergic receptor agonist, *Green Chem.* **2020,** *22*, 5762-5770.
142. Nadin, A.; Hattotuwagama, C.; Churcher, I., Lead-oriented synthesis: a new opportunity for synthetic chemistry, *Angew. Chem. Int. Ed.* **2012,** *51*, 1114-1122.
143. Nuzzo, R. G.; Haynie, S. L.; Wilson, M. E.; Whitesides, G. M., Synthesis of functional chelating diphosphines containing the bis[2-(diphenylphosphino)ethyl]amino moiety and the use of these materials in the preparation of water-soluble diphosphine complexes of transition metals, *J. Org. Chem.* **1981,** *46*, 2861-2867.
144. Lin, I. J. B.; Vasam, C. S., Preparation and application of N-heterocyclic carbene complexes of Ag(I), *Coord. Chem. Rev.* **2007,** *251*, 642-670.
145. Chen, W.; Liu, F., Synthesis and characterization of oligomeric and polymeric silver-imidazol-2-ylidene iodide complexes, *J. Organomet. Chem.* **2003,** *673*, 5-12.
146. Zhang, Y.; Chen, C.; Ghosh, S. C.; Li, Y.; Hong, S. H., Well-Defined N-Heterocyclic Carbene Based Ruthenium Catalysts for Direct Amide Synthesis from Alcohols and Amines, *Organometallics* **2010,** *29*, 1374-1378.

147. Henrion, M.; Roisnel, T.; Couturier, J.-L.; Dubois, J.-L.; Sortais, J.-B.; Darcel, C.; Carpentier, J.-F., Ruthenium complexes bearing amino-bis(phosphinite) or amino-bis(aminophosphine) ligands: Application in catalytic ester hydrogenation, *Mol. Catal.* **2017,** *432*, 15-22.
148. Nguyen, D. H.; Trivelli, X.; Capet, F.; Swesi, Y.; Favre-Réguillon, A.; Vanoye, L.; Dumeignil, F.; Gauvin, R. M., Deeper Mechanistic Insight into Ru Pincer-Mediated Acceptorless Dehydrogenative Coupling of Alcohols: Exchanges, Intermediates, and Deactivation Species, *ACS Catal.* **2018,** *8*, 4719-4734.
149. Dubey, A.; Khaskin, E., Catalytic Ester Metathesis Reaction and Its Application to Transfer Hydrogenation of Esters, *ACS Catal.* **2016,** *6*, 3998-4002.
150. Machado, R. M., *Fundamentals of Mass Transfer and Kinetics for the Hydrogenation of Nitrobenzene to Aniline*. **2007**.
151. Constable, D. J. C.; Jimenez-Gonzalez, C.; Henderson, R. K., Perspective on Solvent Use in the Pharmaceutical Industry, *Org. Process Res. Dev.* **2007,** *11*, 133-137.
152. Raymond, M. J.; Slater, C. S.; Savelski, M. J., LCA approach to the analysis of solvent waste issues in the pharmaceutical industry, *Green Chem.* **2010,** *12*.
153. Dunn, P. J., The importance of green chemistry in process research and development, *Chem. Soc. Rev.* **2012,** *41*, 1452-1461.
154. Jimnez-Gonzlez, C.; Curzons, A. D.; Constable, D. J. C.; Cunningham, V. L., Expanding GSK's Solvent Selection Guid - application of life cycle assessment to enhance solvent selections, *Clean Technol. Environ. Policy* **2005,** *7*, 42-50.
155. Alfonsi, K.; Colberg, J.; Dunn, P. J.; Fevig, T.; Jennings, S.; Johnson, T. A.; Kleine, H. P.; Knight, C.; Nagy, M. A.; Perry, D. A.; Stefaniak, M., Green chemistry tools to influence a medicinal chemistry and research chemistry based organisation, *Green Chem.* **2008,** *10*, 31-36.
156. Aycock, D. F., Solvent Applications of 2-Methyltetrahydrofuran in Organometallic and Biphasic Reactions, *Org. Process Res. Dev.* **2007,** *11*, 156-159.
157. Bornschein, C.; Werkmeister, S.; Wendt, B.; Jiao, H.; Alberico, E.; Baumann, W.; Junge, H.; Junge, K.; Beller, M., Mild and selective hydrogenation of aromatic and aliphatic (di)nitriles with a well-defined iron pincer complex, *Nat. Commun.* **2014,** *5*, 1-11.
158. Brunner, E., Solubility of hydrogen in 10 organic solvents at 298.15, 323.15, and 373.15 K, *J. Chem. Eng. Data* **1985,** *30*, 269-273.

159. Dub, P. A.; Batrice, R. J.; Gordon, J. C.; Scott, B. L.; Minko, Y.; Schmidt, J. G.; Williams, R. F., Engineering Catalysts for Selective Ester Hydrogenation, *Org. Process Res. Dev.* **2020,** *24*, 415-442.
160. Lendrem, D.; Owen, M.; Godbert, S., DOE (Design of Experiments) in Development Chemistry: Potential Obstacles, *Org. Process Res. Dev.* **2001,** *5*, 324-327.
161. Mullin, R., Design of Experiments Makes A Comeback., *Chem. Eng. News* **2013,** *91*, 25.
162. Weissman, S. A.; Anderson, N. G., Design of Experiments (DoE) and Process Optimization. A Review of Recent Publications, *Org. Process Res. Dev.* **2015,** *19*, 1605-1633.
163. Lloyd-Jones, G.; Filali, E.; Sale, D., Cleavage of tert-Butyl

Benzoates with NaH in DMF: Comments on the Mechanism and

a Simple and Safe Alternative Procedure, *Synlett* **2009,** *2009*, 205-208.
164. Le Chatelier, H. L., A general statement of the laws of chemical equilibrium, *Comp. rend.* **1884,** *99*, 786-789.
165. Budzik, B.; Li, P.; Pero, J. E.; Griffiths-Jones, C. M.; Heightman, T. D.; Willems, D. M. G.; Weelford, A. J. 3-Carboxylic acid pyrroles as NRF2 regulators, WO 2018/109641, **2018**.
166. Halbert, S. M.; Thompson, S. K.; Veber, D. F. Protease inhibitors, US 5998470, **1999**.
167. Pu, Y.-M.; Ku, Y.-Y.; Grieme, T.; Black, L. A.; Bhatia, A. V.; Cowart, M., An Expedient and Multikilogram Synthesis of a Naphthalenoid H3Antagonist, *Org. Process Res. Dev.* **2007,** *11*, 1004-1009.
168. Davidson, A. H.; Moffat, D. F. C.; Day, F. A.; Donald, A. D. G. HDAC inhibitors, WO 2008/040934, **2008**.
169. Sisko, J.; Mans, D.; Yin, H. Process for preparing pyrano-[2,3-C]pyridine derivatives, WO 2012/012391, **2012**.
170. Simon, E., *Liebigs Ann.* **1839,** *31*, 263.
171. Lavanya, R., Sulphonamides: a pharmaceutical review, *Int. J. of Pharma. Sci. Inv.* **2017,** *6*, 1-3.
172. Collins, K. D.; Glorius, F., A robustness screen for the rapid assessment of chemical reactions, *Nature Chem.* **2013,** *5*, 597-601.
173. Gasgnier, M., *J. Mater. Sci.* **2001,** *20*, 1259-1262.
174. Blackmond, D. G., Kinetic Profiling of Catalytic Organic Reactions as a Mechanistic Tool, *J. Am. Chem. Soc.* **2015,** *137*, 10852-10866.

175. Seki, T.; Nakajo, T.; Onaka, M., The Tishchenko Reaction: A Classic and Practical Tool for Ester Synthesis, *Chem. Lett.* **2006,** *35*, 824-829.
176. Wheeler, P.; Phillips, J. H.; Pederson, R. L., Scalable Methods for the Removal of Ruthenium Impurities from Metathesis Reaction Mixtures, *Org. Process Res. Dev.* **2016,** *20*, 1182-1190.
177. Widdowson, K. L. Tricyclic nitrogen containing compounds for treating neisseria gonorrhoea infection, WO 2016/027249, **2016**.
178. Parikh, J. R.; Doering, W. v. E., Sulfur trioxide in the oxidation of alcohols by dimethyl sulfoxide, *J. Am. Chem. Soc.* **1967,** *89*, 5505-5507.
179. Machado, R. M.; Heier, K. R.; Broekhuis, R. R., Developments in hydrogenation technology for fine-chemical and pharmaceutical applications, *Current Opinion in Drug Discovery and Development* **2001,** *4*, 745-755.
180. Ogata, O.; Nara, H.; Nakayama, Y. Ruthenium complex, method for producing same, and use of same, US 2017/0044196, **2017**.
181. Nahm, S.; Weinreb, S. M., N-methoxy-n-methylamides as effective acylating agents, *Tetrahedron Lett.* **1981,** *22*, 3815-3818.
182. Beeler, A. B., Introduction: Photochemistry in Organic Synthesis, *Chem. Rev.* **2016,** *116*, 9629-9630.
183. Zhou, Q. Q.; Zou, Y. Q.; Lu, L. Q.; Xiao, W. J., Visible-Light-Induced Organic Photochemical Reactions through Energy-Transfer Pathways, *Angew. Chem. Int. Ed.* **2019,** *58*, 1586-1604.
184. Prier, C. K.; Rankic, D. A.; MacMillan, D. W., Visible light photoredox catalysis with transition metal complexes: applications in organic synthesis, *Chem. Rev.* **2013,** *113*, 5322-5363.
185. Crisenza, G. E. M.; Melchiorre, P., Chemistry glows green with photoredox catalysis, *Nature. Commun.* **2020,** *11*, 803.
186. Sambiagio, C.; Noël, T., Flow Photochemistry: Shine Some Light on Those Tubes!, *Trends in Chem.* **2020,** *2*, 92-106.
187. Bonfield, H. E.; Knauber, T.; Levesque, F.; Moschetta, E. G.; Susanne, F.; Edwards, L. J., Photons as a 21st century reagent, *Nat. Commun.* **2020,** *11*, 1-4.
188. Bonfield, H. E.; Williams, J. D.; Ooi, W. X.; Leach, S. G.; Kerr, W. J.; Edwards, L. J., A Detailed Study of Irradiation Requirements Towards an Efficient Photochemical Wohl-Ziegler Procedure in Flow, *ChemPhotoChem* **2018,** *2*, 938-944.

189. Bonfield, H. E.; Mercer, K.; Diaz‐Rodriguez, A.; Cook, G. C.; McKay, B. S. J.; Slade, P.; Taylor, G. M.; Ooi, W. X.; Williams, J. D.; Roberts, J. P. M.; Murphy, J. A.; Schmermund, L.; Kroutil, W.; Mielke, T.; Cartwright, J.; Grogan, G.; Edwards, L. J., The Right Light: De Novo Design of a Robust Modular Photochemical Reactor for Optimum Batch and Flow Chemistry, *ChemPhotoChem* **2019,** *4*, 45-51.
190. Harper, K. C.; Moschetta, E. G.; Bordawekar, S. V.; Wittenberger, S. J., A Laser Driven Flow Chemistry Platform for Scaling Photochemical Reactions with Visible Light, *ACS Cent. Sci.* **2019,** *5*, 109-115.
191. Day, J. I.; Teegardin, K.; Weaver, J.; Chan, J., Advances in Photocatalysis: A Microreview of Visible Light Mediated Ruthenium and Iridium Catalyzed Organic Transformations, *Org. Process Res. Dev.* **2016,** *20*, 1156-1163.
192. Corcoran, E. B.; McMullen, J. P.; Levesque, F.; Wismer, M. K.; Naber, J. R., Photon Equivalents as a Parameter for Scaling Photoredox Reactions in Flow: Translation of Photocatalytic C-N Cross-Coupling from Lab Scale to Multikilogram Scale, *Angew. Chem. Int. Ed.* **2020,** *59*, 11964-11968.
193. Sezen-Edmonds, M.; Tabora, J. E.; Cohen, B. M.; Zaretsky, S.; Simmons, E. M.; Sherwood, T. C.; Ramirez, A., Predicting Performance of Photochemical Transformations for Scaling Up in Different Platforms by Combining High-Throughput Experimentation with Computational Modeling, *Org. Process Res. Dev.* **2020,** *24*, 2128-2138.
194. Yang, C.; Li, R.; Zhang, K. A. I.; Lin, W.; Landfester, K.; Wang, X., Heterogeneous photoredox flow chemistry for the scalable organosynthesis of fine chemicals, *Nat. Commun.* **2020,** *11*, 1239.
195. Bauta, W. E., Benzyl Bromide. In *Encyclopedia of Reagents for Organic Synthesis*, **2001**.
196. Procopiou, P. A.; Barrett, V. J.; Bevan, N. J.; Biggadike, K.; Box, P. C.; Butchers, P. R.; Coe, D. M.; Conroy, R.; Emmons, A.; Ford, A. J.; Holmes, D. S.; Horsley, H.; Kerr, F.; Li-Kwai-Cheung, A. M.; Looker, B. E.; Mann, I. S.; McLay, I. M.; Morrison, V. S.; Mutch, P. J.; Smith, C. E.; Tomlin, P., Synthesis and structure-activity relationships of long-acting beta2 adrenergic receptor agonists incorporating metabolic inactivation: an antedrug approach, *J. Med. Chem.* **2010,** *53*, 4522-30.
197. Ochen, A.; Whitten, R.; Aylott, H. E.; Ruffell, K.; Williams, G. D.; Slater, F.; Roberts, A.; Evans, P.; Steves, J. E.; Sanganee, M. J., Development of a Large-Scale Copper(I)/TEMPO-Catalyzed Aerobic Alcohol Oxidation for the Synthesis of LSD1 Inhibitor GSK2879552, *Organometallics* **2018,** *38*, 176-184.

198. Hayler, J. D.; Howie, S. L. B.; Giles, R. G.; Negus, A.; Oxley, P. W.; Walsgrove, T. C.; Whiter, M., Development of Large-Scale Syntheses of Ropinirole in the Pursuit of a Manufacturing Process, *Org. Process Res. Dev.* **1998,** *2*, 3-9.
199. Hayler, J. D.; Howie, S. L. B.; Giles, R. G.; Negus, A.; Oxley, P. W.; Walsgrove, T. C.; Walsh, S. E.; Dagger, R. E.; Fortunak, J. M.; Mastrocola, A., Some synthetic approaches to ropinirole (sk&f 101468-a): A potent dopamine receptor agonist, *J. Heterocycl. Chem.* **1995,** *32*, 875-882.
200. Mirguet, O.; Gosmini, R.; Toum, J.; Clement, C. A.; Barnathan, M.; Brusq, J. M.; Mordaunt, J. E.; Grimes, R. M.; Crowe, M.; Pineau, O.; Ajakane, M.; Daugan, A.; Jeffrey, P.; Cutler, L.; Haynes, A. C.; Smithers, N. N.; Chung, C. W.; Bamborough, P.; Uings, I. J.; Lewis, A.; Witherington, J.; Parr, N.; Prinjha, R. K.; Nicodeme, E., Discovery of epigenetic regulator I-BET762: lead optimization to afford a clinical candidate inhibitor of the BET bromodomains, *J. Med. Chem.* **2013,** *56*, 7501-7515.
201. Corcoran, E. B.; Pirnot, M. T.; Lin, S.; Dreher, S. D.; DiRocco, D. A.; Davies, I. W.; Buchwald, S. L.; MacMillan, D. W., Aryl amination using ligand-free Ni(II) salts and photoredox catalysis, *Science* **2016,** *353*, 279-283.
202. Romero, N. A.; Margrey, K. A.; Tay, N. E.; Nicewicz, D. A., Site-selective arene C-H amination via photoredox catalysis, *Science* **2015,** *349*, 1326-1330.
203. Ohkubo, K.; Mizushima, K.; Iwata, R.; Fukuzumi, S., Selective photocatalytic aerobic bromination with hydrogen bromide via an electron-transfer state of 9-mesityl-10-methylacridinium ion, *Chem. Sci.* **2011,** *2*.
204. Romero, N. A.; Nicewicz, D. A., Organic Photoredox Catalysis, *Chem. Rev.* **2016,** *116*, 10075-10166.
205. Crisenza, G. E. M.; Mazzarella, D.; Melchiorre, P., Synthetic Methods Driven by the Photoactivity of Electron Donor-Acceptor Complexes, *J. Am. Chem. Soc.* **2020,** *142*, 5461-5476.
206. El-Kady, M.; Afify, A.; El-Hashash, M.; Kassab, E., Some reactions with 5,6-benzo-4-(p-bromobenzoyl)-3,4-dihydrocoumarin, *Pol. J. Chem.* **1982,** *56*, 1387.
207. Kokkes, M. W.; Stufkens, D. J.; Oskam, A., Photochemistry of metal-metal-bonded complexes, *Inorg. Chem.* **1985,** *24*, 2934-2942.
208. Islam, S. D.-M.; Ito, O., Solvent effects on rates of photochemical reactions of rose bengal triplet state studied by nanosecond laser photolysis, *J. Photochem. Photobio. A: Chem.* **1999,** *123*, 53-59.

209. Kimpe, N. D., Bromoacetone. In *Encyclopedia of Reagents for Organic Synthesis*, **2001**.
210. Konya, K. G.; Paul, T.; Lin, S.; Lusztyk, J.; Ingold, K. U., Laser Flash Photolysis Studies on the First Superoxide Thermal Source. First Direct Measurements of the Rates of Solvent-Assisted 1,2-Hydrogen Atom Shifts and a Proposed New Mechanism for This Unusual Rearrangement1, *J. Am. Chem. Soc.* **2000,** *122*, 7518-7527.
211. Otake, Y.; Williams, J. D.; Rincón, J. A.; de Frutos, O.; Mateos, C.; Kappe, C. O., Photochemical benzylic bromination in continuous flow using BrCCl3 and its application to telescoped p-methoxybenzyl protection, *Org. Biomol. Chem.* **2019,** *17*, 1384-1388.
212. Frisch, M. J.; Trucks, G. W.; Schlegel, H. B.; Scuseria, G. E.; Robb, M. A.; Cheeseman, J. R.; Scalmani, G.; Barone, V.; Petersson, G. A.; Nakatsuji, H.; Li, X.; Caricato, M.; Marenich, A. V.; Bloino, J.; Janesko, B. G.; Gomperts, R.; Mennucci, B.; Hratchian, H. P.; Ortiz, J. V.; Izmaylov, A. F.; Sonnenberg, J. L.; Williams; Ding, F.; Lipparini, F.; Egidi, F.; Goings, J.; Peng, B.; Petrone, A.; Henderson, T.; Ranasinghe, D.; Zakrzewski, V. G.; Gao, J.; Rega, N.; Zheng, G.; Liang, W.; Hada, M.; Ehara, M.; Toyota, K.; Fukuda, R.; Hasegawa, J.; Ishida, M.; Nakajima, T.; Honda, Y.; Kitao, O.; Nakai, H.; Vreven, T.; Throssell, K.; Montgomery Jr., J. A.; Peralta, J. E.; Ogliaro, F.; Bearpark, M. J.; Heyd, J. J.; Brothers, E. N.; Kudin, K. N.; Staroverov, V. N.; Keith, T. A.; Kobayashi, R.; Normand, J.; Raghavachari, K.; Rendell, A. P.; Burant, J. C.; Iyengar, S. S.; Tomasi, J.; Cossi, M.; Millam, J. M.; Klene, M.; Adamo, C.; Cammi, R.; Ochterski, J. W.; Martin, R. L.; Morokuma, K.; Farkas, O.; Foresman, J. B.; Fox, D. J. *Gaussian 16 Rev. C.01*, Wallingford, CT, **2016**.
213. Marenich, A. V.; Cramer, C. J.; Truhlar, D. G., Universal solvation model based on solute electron density and on a continuum model of the solvent defined by the bulk dielectric constant and atomic surface tensions, *J. Phys. Chem. B* **2009,** *113*, 6378-6396.
214. Nuzzi, A.; Fiasella, A.; Ortega, J. A.; Pagliuca, C.; Ponzano, S.; Pizzirani, D.; Bertozzi, S. M.; Ottonello, G.; Tarozzo, G.; Reggiani, A.; Bandiera, T.; Bertozzi, F.; Piomelli, D., Potent alpha-amino-beta-lactam carbamic acid ester as NAAA inhibitors. Synthesis and structure-activity relationship (SAR) studies, *Eur. J. Med. Chem.* **2016,** *111*, 138-159.
215. Tamizmani, M.; Sivasankar, C., Synthesis, characterization and catalytic application of some novel PNP-Ni(II) complexes: Regio-selective [2+2+2] cycloaddition reaction of alkyne, *J. Organomet. Chem.* **2017,** *845*, 82-89.
216. Soobramoney, L.; Bala, M. D.; Friedrich, H. B., Coordination chemistry of Co complexes containing tridentate SNS ligands and their application as catalysts for the oxidation of n-octane, *Dalton Trans.* **2014,** *43*, 15968-15978.

217. Murai, N.; Yonaga, M.; Tanaka, K., Palladium-catalyzed direct hydroxymethylation of aryl halides and triflates with potassium acetoxymethyltrifluoroborate, *Org. Lett.* **2012,** *14*, 1278-1281.
218. Doi, R.; Kikushima, K.; Ohashi, M.; Ogoshi, S., Synthesis, characterization, and unique catalytic activities of a fluorinated nickel enolate, *J. Am. Chem. Soc.* **2015,** *137*, 3276-82.
219. Nishimoto, Y.; Babu, S. A.; Yasuda, M.; Baba, A., Esters as acylating reagent in a Friedel-Crafts reaction: indium tribromide catalyzed acylation of arenes using dimethylchlorosilane, *J. Org. Chem.* **2008,** *73*, 9465-9468.
220. Wang, R.; Tang, Y.; Xu, M.; Meng, C.; Li, F., Transfer Hydrogenation of Aldehydes and Ketones with Isopropanol under Neutral Conditions Catalyzed by a Metal-Ligand Bifunctional Catalyst [Cp*Ir(2,2'-bpyO)(H2O)], *J. Org. Chem.* **2018,** *83*, 2274-2281.
221. Nguyen, T. V. Q.; Yoo, W.-J.; Kobayashi, S., Chelating Bis(1,2,3-triazol-5-ylidene) Rhodium Complexes: Versatile Catalysts for Hydrosilylation Reactions, *Adv. Synth. Catal.* **2016,** *358*, 452-458.
222. Bartwal, G.; Saroha, M.; Khurana, J. M., Nickel boride mediated chemoselective deprotection of 1,1-diacetates to aldehydes and deprotection with concomitant reduction to alcohols at ambient temperature, *Synth. Commun.* **2017,** *48*, 97-103.
223. Fuentes, J. A.; Smith, S. M.; Scharbert, M. T.; Carpenter, I.; Cordes, D. B.; Slawin, A. M.; Clarke, M. L., On the Functional Group Tolerance of Ester Hydrogenation and Polyester Depolymerisation Catalysed by Ruthenium Complexes of Tridentate Aminophosphine Ligands, *Chem. Eur. J.* **2015,** *21*, 10851-10860.
224. Zheng, J.; Elangovan, S.; Valyaev, D. A.; Brousses, R.; César, V.; Sortais, J.-B.; Darcel, C.; Lugan, N.; Lavigne, G., Hydrosilylation of Aldehydes and Ketones Catalyzed by Half-Sandwich Manganese(I) N-Heterocyclic Carbene Complexes, *Adv. Synth. Catal.* **2014,** *356*, 1093-1097.
225. Plank, T. N.; Drake, J. L.; Kim, D. K.; Funk, T. W., Air-Stable, Nitrile-Ligated (Cyclopentadienone)iron Dicarbonyl Compounds as Transfer Reduction and Oxidation Catalysts, *Adv. Synth. Catal.* **2012,** *354*, 597-601.
226. Bhunia, S. K.; Das, P.; Nandi, S.; Jana, R., Carboxylation of Aryl Triflates with CO2 Merging Palladium and Visible-Light-Photoredox Catalysts, *Org. Lett.* **2019,** *21*, 4632-4637.
227. Chen, M.; Ichikawa, S.; Buchwald, S. L., Rapid and efficient copper-catalyzed Finkelstein reaction of (hetero)aromatics under continuous-flow conditions, *Angew. Chem. Int. Ed.* **2015,** *54*, 263-266.

228. Ulm, F.; Poblador-Bahamonde, A. I.; Choppin, S.; Bellemin-Laponnaz, S.; Chetcuti, M. J.; Achard, T.; Ritleng, V., Synthesis, characterization, and catalytic application in aldehyde hydrosilylation of half-sandwich nickel complexes bearing (kappa(1)-C)- and hemilabile (kappa(2)-C,S)-thioether-functionalised NHC ligands, *Dalton Trans.* **2018,** *47*, 17134-17145.
229. Liu, X.; Xia, Q.; Zhang, Y.; Chen, C.; Chen, W., Cu-NHC-TEMPO catalyzed aerobic oxidation of primary alcohols to aldehydes, *J. Org. Chem.* **2013,** *78*, 8531-8536.
230. Bürgstein, M. R.; Berberich, H.; Roesky, P. W., Homoleptic Lanthanide Amides as Homogeneous Catalysts for Alkyne Hydroamination and the Tishchenko Reaction, *Chem. Eur. J.* **2001,** *7*, 3078-3085.
231. Wekesa, F. S.; Arias-Ugarte, R.; Kong, L.; Sumner, Z.; McGovern, G. P.; Findlater, M., Iron-Catalyzed Hydrosilylation of Aldehydes and Ketones under Solvent-Free Conditions, *Organometallics* **2015,** *34*, 5051-5056.
232. Lu, W.; Zhao, M.; Li, M., Visible-Light-Driven Oxidative Mono- and Dibromination of Benzylic- sp3 C–H Bonds with Potassium Bromide/Oxone at Room Temperature, *Synth.* **2018,** *50*, 4933-4939.

APPENDIX

Crystals of Ru(PNP)Cl_2(NHC) (**1.51**) suitable for X-ray diffraction were obtained by allowing slow diffusion of heptane into a solution of the complex dissolved in DCM under a nitrogen atmosphere.

Crystal data and structure refinement.

Identification code	Ru_J	
Empirical formula	C13 H27 Cl2 N3 Ru S2	
Formula weight	461.46	
Temperature	123(2) K	
Wavelength	1.54184 Å	
Crystal system	Triclinic	
Space group	P -1	
Unit cell dimensions	a = 8.2226(5) Å	a= 86.646(7)°.
	b = 15.1643(13) Å	b= 75.959(5)°.
	c = 15.9494(11) Å	g = 78.548(6)°.
Volume	1890.8(2) $Å^3$	
Z	4	
Density (calculated)	1.621 Mg/m^3	
Absorption coefficient	11.345 mm^{-1}	
F(000)	944	
Crystal size	0.39 x 0.27 x 0.18 mm^3	
Theta range for data collection	7.033 to 73.354°.	
Index ranges	-10<=h<=8, -18<=k<=17, -19<=l<=18	
Reflections collected	13328	
Independent reflections	7382 [R(int) = 0.0323]	
Completeness to theta = 70.000°	99.6 %	
Absorption correction	Analytical	
Max. and min. transmission	0.332 and 0.115	
Refinement method	Full-matrix least-squares on F^2	
Data / restraints / parameters	7382 / 0 / 393	
Goodness-of-fit on F^2	1.122	
Final R indices [I>2sigma(I)]	R1 = 0.0460, wR2 = 0.1358	
R indices (all data)	R1 = 0.0502, wR2 = 0.1409	
Extinction coefficient	n/a	
Largest diff. peak and hole	1.946 and -1.610 e.$Å^{-3}$	

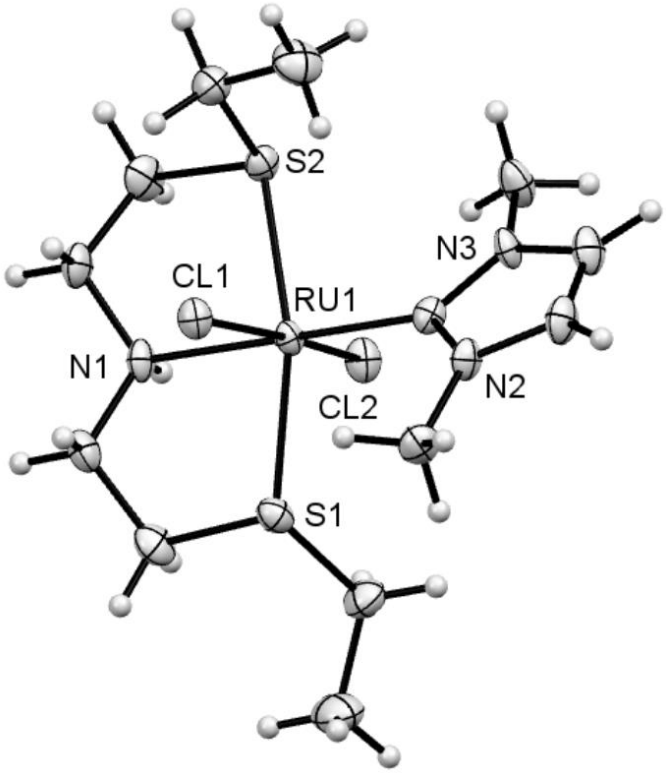

Figure 77 *ORTEP diagram of Ru(diEtSNS)Cl$_2$(NHC) (**1.51**).*

The ANOVA (analysis of variance) tables shown below are another output from the software which gives a test of the overall statistical significance of variables on responses. In general, parameters with a p-value prob > F of less than 0.05 are considered to be statistically significant. The software analysis initially assumes the responses will vary linearly between the maximum and minimum values for each parameter. The centre-points, in addition to providing information about natural variability also give an indication as to whether or not this linearity holds true. Due to the size of the design, a test for curvature was performed in each case.

Certain models built by the software were shown to have a high “lack of fit”. This was as a consequence of values becoming less variable as they approach 100% or 0%, the theoretical maximum and minimum attainable values respectively. This violates one of the parametric assumptions made by the software, namely that variability of the response is the same regardless of the response size. This issue was solved by applying a “logit” transformation to the input data.

Source	Sum of Squares	df	Mean Square	F-Value	p-value Prob > F	
Model	15971.25	3	5323.75	36.74	< 0.0001	*significant*
A-Base Quantity	12769.00	1	12769.00	88.11	< 0.0001	
B-Hydrogen Pressure	2500.00	1	2500.00	17.25	0.0008	
D-Reaction Temperature	702.25	1	702.25	4.85	0.0438	
Curvature	4805.00	1	4805.00	33.16	< 0.0001	
Residual	2173.75	15	144.92			
Lack of Fit	2155.75	12	179.65	29.94	0.0086	*significant*
Pure Error	18.00	3	6.00			
Predicted R^2				0.7870		
Adjusted R^2				0.8562		

Table 37 *ANOVA table for formation of product adjusted for curvature (scoping experimental design).*

Source	Sum of Squares	df	Mean Square	F Value	p-value Prob > F	
Model	103.69	3	34.56	17.14	< 0.0001	*significant*
A-Base Quantity	*33.06*	*1*	*33.06*	*16.39*	*0.0010*	
C-Concentration	*60.06*	*1*	*60.06*	*29.78*	*< 0.0001*	
AC	*10.56*	*1*	*10.56*	*5.24*	*0.0370*	
Curvature	7.81	1	7.81	3.87	0.0678	
Residual	30.25	15	2.02			
Lack of Fit	*28.25*	*12*	*2.35*	*3.53*	*0.1634*	*not significant*
Pure Error	*2.00*	*3*	*0.67*			
Predicted R^2				0.5985		
Adjusted R^2				0.7290		

Table 38 *ANOVA table for formation of hydrolysis side-product adjusted for curvature (scoping experimental design).*

Source	Sum of Squares	df	Mean Square	F Value	p-value Prob > F	
Model	2.20	2	1.10	11.36	0.0009	*significant*
A-Base Quantity	*0.40*	*1*	*0.40*	*4.14*	*0.0587*	
C-Concentration	*1.80*	*1*	*1.80*	*18.57*	*0.0005*	
Curvature	0.39	1	0.39	4.05	0.0614	
Residual	1.55	16	0.097			
Lack of Fit	*1.50*	*13*	*0.12*	*7.65*	*0.0599*	*not significant*
Pure Error	*0.045*	*3*	*0.015*			
Predicted R^2					0.3708	
Adjusted R^2					0.5351	

Table 39 *ANOVA table for formation of product adjusted for curvature (robustness experimental design).*

Source	Sum of Squares	df	Mean Square	F Value	p-value Prob > F	
Model	119.21	2	59.61	23.53	< 0.0001	*significant*
A-Base Quantity	*43.44*	*1*	*43.44*	*17.15*	*0.0008*	
C-Concentration	*75.77*	*1*	*75.77*	*29.91*	*< 0.0001*	
Curvature	0.51	1	0.51	0.20	0.6586	
Residual	40.53	16	2.53			
Lack of Fit	*38.69*	*13*	*2.98*	*4.84*	*0.1099*	*not significant*
Pure Error	*1.84*	*3*	*0.61*			
Predicted R^2					0.6126	
Adjusted R^2					0.7146	

Table 40 *ANOVA table for formation of hydrolysis side-product (robustness experimental design).*

Source	Sum of Squares	df	Mean Square	F Value	p-value Prob > F	
Model	51.70	2	25.85	16.68	0.0001	*significant*
C-Concentration	*8.63*	*1*	*8.63*	*5.57*	*0.0313*	
D-Reaction Temperature	*43.07*	*1*	*43.07*	*27.78*	*< 0.0001*	
Curvature	5.91	1	5.91	3.81	0.0685	
Residual	24.80	16	1.55			
Lack of Fit	*24.80*	*13*	*1.91*			
Pure Error	*0.000*	*3*	*0.000*			

Predicted R^2	0.5089
Adjusted R^2	0.6353

Table 41 *ANOVA table for time taken for reaction to go to completion (robustness experimental design).*

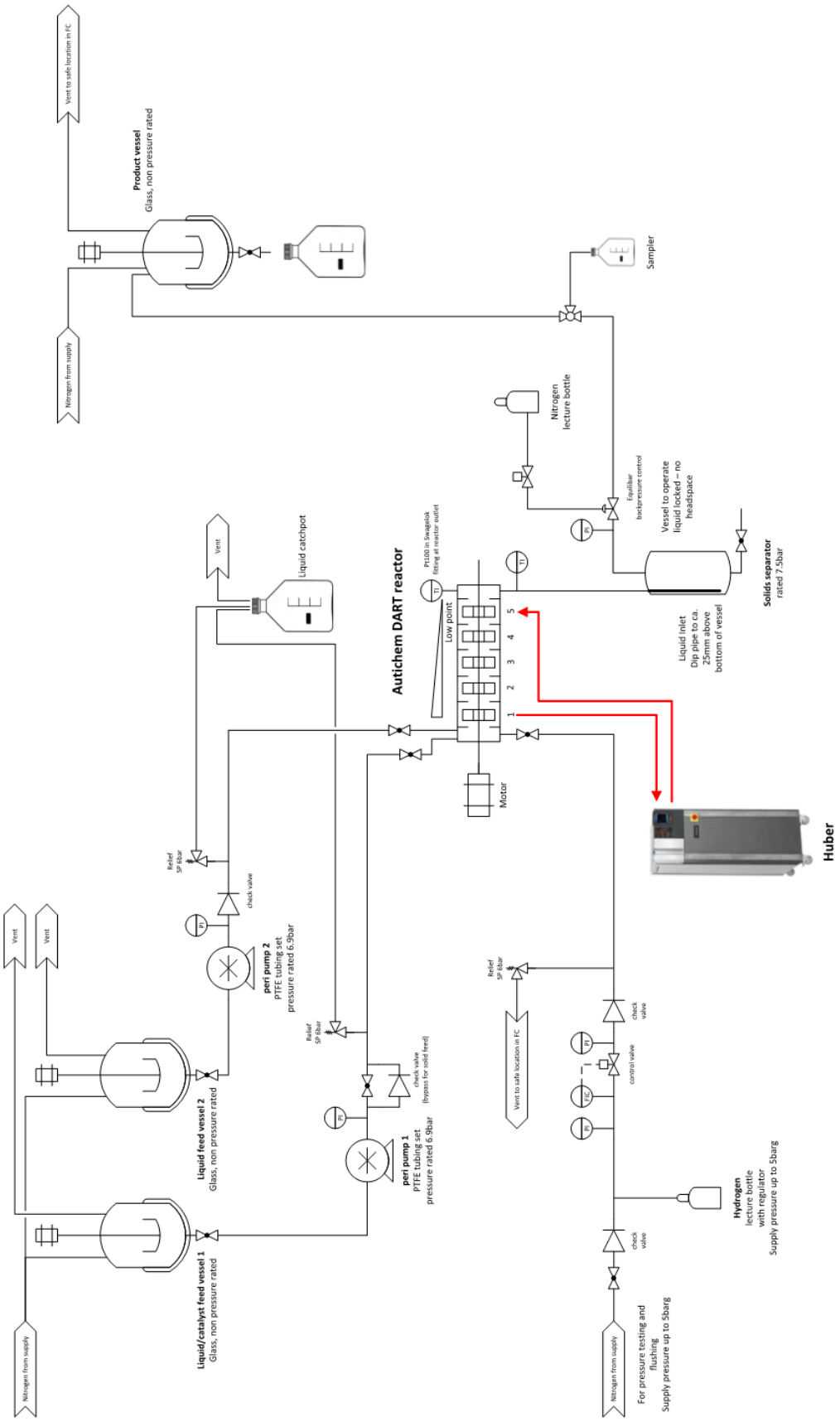

Figure 78 More detailed schematic of CSTR flow rig.